

# **Investigating the relationship between Ambra1, Autophagy and Cell proliferation in Melanoma**

**By Milad Ibrahim**

A thesis submitted in fulfilment of the  
requirements of the University of  
Sunderland for the degree of Doctor of  
Philosophy



**UNIVERSITY OF SUNDERLAND**

Faculty of Health Sciences & Wellbeing

February 2021

## **Abstract**

Activating molecule in Beclin1-regulated autophagy1 (Ambra1) protein discovered in 2007 is an essential regulator in autophagy; it is also involved in the development of the nervous system, regulating normal cell survival, and, proliferation. Its role in autophagy has been extensively studied. However; its role in cell proliferation is less understood. Ambra1 has been related to proliferative disorders like cancer but, the underlying mechanisms by which Ambra1 can regulate cell proliferation in normal and pathologic conditions remain largely unclear. Melanoma is the most deadly type of skin cancers and, there is a continuous need to develop early biomarkers as well as treatments to improve the survivability of patients.

This study explores the role of Ambra1 in different cellular processes including cell proliferation with a focus on Melanoma. The research was designed to use a systems based “omics” approach to investigate novel roles of Ambra1. An interactomic approach was carried on to identify novel Ambra1 protein binding partners using yeast two-hybrid assays and Ambra1 differentially expressing A375 melanoma cell lines were utilized for cell proliferation assays, proteomics, metabolomics and transcriptomics approaches to investigate the impacts of Ambra1 overexpression and knockdown on different cellular processes..

Yeast two-hybrid assays performed in this study identified novel Ambra1 binding partners. Analyses of these interactors provide evidence for new roles for Ambra1 in different cellular processes. Additional analysis, with data from a recent large scale interactome screening project suggests that Ambra is a key component of a larger network of proteins than previous evidence suggests. Results from the cell proliferation assays, proteomic, metabolomic and transcriptomic analyses suggest that Ambra1 overexpression in nutrient rich media has little additional effect on proliferation or any other pathways. Transcriptomic analysis of the knock-down of Ambra1 however, was shown to result in significant dysregulation of a significant number of transcripts. This appears to have identified a number of novel roles for Ambra 1 in a range of cellular pathways; some of these are hallmarks of cancer signaling including, cell cycle, angiogenesis, tissue growth factor, axon guidance and Wnt signaling. The work shows that the Ambra1 knockdown appears to upregulate metastatic genes/proteins and supports previous studies demonstrating that the loss of Ambra1 is associated with poor prognosis in melanoma.

## **Acknowledgments**

I would like to thank my supervisor, Dr Noel Carter for his continued support, advice and, guidance throughout the PhD and without whom I would not have had the opportunity to take part in such research, I would like to thank him also for sharing his expertise with me which developed my practical skills and knowledge, I also would like to appreciate his support during hard times in this research, on a personal level I really appreciate his good character and his leading skills and spirit of challenge.

I would also like to thank my second supervisor, Dr Jane Armstrong for her advice and support throughout this research.

I would like to show appreciation for the technical staff at the Molecular Biology laboratories at the University of Sunderland and specially, Dr Linda Henry for their continuous help and support throughout this research.

Personally I would like to thank God, my Lord Jesus Christ for his provision, guidance and, faithfulness in this journey. I would also like to acknowledge someone very dear to me who is there for me always and supports me through the whole journey, my wife Hanan, I love you and you mean the world to me. It is with your support that I was able to accomplish this.

# Lists of figures and tables

## List of figures

Figure 1.1: Melanoma skin cancer incidence trends over time.....	2
Figure 1.2: Scheme of the epidermis structure.....	4
Figure 1.3: Simplified scheme of the melanin synthesis in melanocytes during melanogenesis. ....	5
Figure 1.4: Stages of histopathologic progression in melanocyte transformation. ....	8
Figure 1.5: Melanoma classification according to tumor size from cancer research UK. ....	10
Figure 1.6: A schematic representation of driver gene mutations in melanoma. ....	26
Figure 1.7: The three different types of autophagy. ....	31
Figure 1.8: Morphology of macroautophagy.....	34
Figure 1.9: Autophagy role in cancer.....	37
Figure 1.10: Overview of Ambra1 protein structure and binding sites .....	42
Figure 2.1: Transcriptome analysis suite software. ....	72
Figure 2.2 General String analysis legends .....	73
Figure 3.1: graphical representation of SRB assay comparing the proliferation rate of rAmbra to rBgal cell lines over time. ....	77
Figure 3.2: graphical representation of SRB assays comparing the proliferation rate of rAmbra to rBgal from four different passages.....	78
Figure 3.3: graphical representation of SRB assay comparing the proliferation rate of ShAmb to ShCon cell lines over time. ....	80
Figure 3.4: graphical representation of SRB assay comparing the proliferation rate of ShAmb to ShCon cell lines over time after extended period of no antibiotic selection....	81
Figure 3.5: Incucyte live cell imaging comparing the proliferation rates of the different A375 cell lines over time. Growth curves are blotted by Incucyte software, phase object confluence percent (Y-Axis) against time in hours (X-Axis) .....	83
Figure 3.6: Incucyte live cell imaging comparing the proliferation rates of the different A375 cell lines over time after extended period of no antibiotic selection .....	84
Figure 3.7: Western blot analysis of Ambra1 overexpression model. ....	86

Figure 3.8: Western blot analysis of $\beta$ -galactosidase protein in the overexpression model. .....	87
Figure 3.9: Western blot analysis of Ambra1 Knockdown model.....	89
Figure 3.10: Western blot analysis of Ambra1 Knockdown model after extended period of no antibiotic selection. ....	90
Figure 4.1: The yeast Two Hybrid principle.....	100
Figure 4.2: Yeast two-hybrid work flow. ....	103
Figure 4.3: Map of the DNA-binding domain vector pGBKT7.....	105
Figure 4.4: In-silico digest of the Ambra ORF using NEBcutter tool.....	106
Figure 4.5: PCR primer design to enable the cloning of Ambra1 into the vector pGBKT7. .....	107
Figure 4.6: unsuccessful Ambra1 PCR reaction.....	108
Figure 4.7: Ambra Control primers PCR amplification. ....	109
Figure 4.8: unsuccessful Ambra1 PCR reaction temperature gradient. ....	110
Figure 4.9: unsuccessful Ambra1 amplification using the (Full2) set of primers. ....	111
Figure 4.10: Ambra1 PCR amplification using an ORF clone.....	113
Figure 4.11: Ambra1 PCR amplification and purification. ....	114
Figure 4.12: colony PCR of transformed bacteria to screen for Ambra1 inserts .....	115
Figure 4.13: Restriction analysis of recombinant plasmids to screen for Ambra1 insert in the DNA-BD pGBKT7 using EcoR I and Nde I. ....	116
Figure 4.14: Blunt-end Ambra1 cDNA amplification using Q5 polymerase.....	118
Figure 4.15: Restriction analysis of recombinant TOPO vector to screen for Ambra1 inserts using EcoR I and Nde I showing no inserts. ....	119
Figure 4.16: TOPO vector control PCR Product and restriction digestion analysis for successful cloning of the amplified insert into the TOPO vector. ....	120
Figure 4.17: PCR amplification of PP2CA cDNA using Iproof and Q5 DNA polymerases	122
Figure 4.18: Restriction analysis of recombinant plasmids to screen for PP2CA inserts in pGBKT7.....	123
Figure 4.19: Restriction digestion analysis of recombinant Zero blunt TOPO cloning vector to screen for PP2CA clones .....	124
Figure 4.20: Restriction digestion analysis of recombinant pGBKT7 to screen for PP2CA inserts.....	125

Figure 4.21: Restriction digestion analysis of PP2CA clones in the Y2H bait vector pGBKT7.....	126
Figure 4.22: Restriction digestion analysis of recombinant plasmids to screen for Ambra1 inserts after using EcoR I alone as a restriction enzyme. ....	127
Figure 4.23: A representative diagram of In-Fusion HD cloning technique.....	128
Figure 4.24: Multi-step restriction digestion analysis of pGBKT7 with Nde I followed by EcoR I .....	129
Figure 4.25: Restriction digestion analysis of Ambra1 clones in the Y2H bait vector pGBKT7.....	130
Figure 4.26: Ambra cloning verification by sequencing using T7 sequencing primer....	131
Figure 4.27: yeast two hybrid strains growth and maintenance.....	132
Figure 4.28: Yeast Two Hybrid control experiments .....	134
Figure 4.29: screening of pGBKT7-Ambra1 for auto-activation test. ....	136
Figure 4.30: screening of pGBKT7-PP2CA for auto-activation test.....	137
Figure 4.31: Yeast-two Hybrid screening of Ambra. ....	139
Figure 4.32: Yeast two hybrid screening of PP2CA. ....	140
Figure 4.33: pGADt7-Rec map showing ampicillin resistance sequence .....	142
Figure 4.34: restriction digestion analysis of recombinant plasmids with an insert confirmed to be an Ambra interactor.....	144
Figure 4.35: STRING protein analysis for Ambra1 identified binding partners.....	146
Figure 4.36: String protein network analysis showing the interaction between AGO3 and MYC from curated databases .....	147
Figure 4.37: analysis of plasmids isolated from PP2CA Y2H mating.....	148
Figure 4.38: STRING protein analysis for PP2CA identified binding partners. ....	150
Figure 4.39: A representative diagram of Ambra1 novel roles identified by yeast two hybrid assays .....	159
Figure 5.1 E-coli standard protein sample separation using 2D electrophoresis.....	169
Figure 5.2: Optimized E-coli standard protein sample separation using 2D electrophoresis .....	169
Figure 5.3: 2D electrophoresis of protein samples on 5-8 11cm IEF strip at 25K volt-hours .....	171

Figure 5.4: 2d-Electrophoresis of rAmbra and rBGal 11 cm 5-8 IEF strips at 40K volt-hours .....	172
Figure 5.5: 2d-Electrophoresis of rAmbra and rBGal 17 cm 5-8 IEF strips.....	173
Figure 5.5 2D-Electrophoresis and stain free blots of rAmbra and rBgal.....	175
Figure 5.6: Total ion chromatograms obtained from rAmbra metabolites GC-MS. ....	177
Figure 5.7: MS analysis of peaks from TIC representative example .....	179
Figure 5.8: MS total ion chromatograms for metabolites extracted and derivatised using MSTFA.....	181
Figure 5.9: MS total ion chromatograms for metabolites extracted and derivatised using BSTFA .....	182
Figure 5.10: Total Ion Chromatogram (TIC) of a 20 amino acids standard solution .....	184
Figure 6.1: Microarray work flow.....	192
Figure 6.2: Quality analysis of total RNA using Bio-Rad electrophoresis station. ....	194
Figure 6.3: analysis results of the differentially expressed genes in two different datasets showing up and down regulated genes in each dataset. ....	196
Figure 6.4: PCA mapping of the Ambra1 overexpression model microarray dataset. ....	198
Figure 6.5: PCA mapping of the Ambra1 knockdown model microarray dataset. ....	199
Figure 6.6: Combined PCA Mapping of the overexpression and knockdown models microarrays datasets .....	200
Figure 6.7 volcano plots analysis.....	202
Figure 6.8: Hierarchical clustering Heatmaps of the microarrays overexpression and knockdown datasets.....	204
Figure: 6.9: STRING analysis of the 81 differentially expressed genes resulting from Ambra1 knockdown. ....	209
Figure 6.10: Western blot analysis of WNT5A from Ambra1 knockdown model .....	213
Figure 6.11: Western blot analysis of FLT1 from Ambra1 knockdown model.....	214
Figure 6.12 STRING protein analyses showing the interaction between NAA11 and cyclin dependent kinases .....	217
Figure 6.13 STRING protein analysis of TRIM63.....	218
Figure 6.14: string analysis of selected differentially expressed genes.....	220
Figure 7.1: The generation of functional diversity at different molecular levels.....	238

Figure 7.2: key pathways identified by Ambra1 transcriptome, proteome and interactome analyses .....	239
Figure 7.3: BioPlex database analysis of Ambra1 binding partners. ....	245
Figure 7.4: Gene ontology enrichment analysis of BioPlex Ambra1 binding partners ...	246
Figure 7.5: String protein network analyses of Ambra1 protein binding partners .....	247
Figure 7.6: Gene ontology biological process enrichment analysis of Ambra1 binding partners .....	248

## List of tables

Table 2.1: chemicals, reagents and kits used in the research .....	51
Table 2.2: Primers used and their sequences.....	54
Table 2.3: Western blots antibodies and dilutions .....	55
Table 2.4: homemade buffers and their constituents .....	56
Table 2.5: transformed plasmids in different yeast strains .....	61
Table 2.6: PCR protocols.....	64
Table 2.7: protein concentration and rehydration buffer volume used for each IEF strip.	68
Table 2.8: protocols used for focusing IPG strips.....	68
Table 3.1: modified A375 melanoma cells used and the method of modification.....	75
Table 4.1: Mating efficiencies and number of screened clones for Ambra1 and PP2CA yeast-two hybrid screening.....	138
Table 4.2 Ambra1 binding partners identified by yeast two hybrid mating assay. ....	145
Table 4.3 PP2CA binding partners identified by yeast two hybrid mating assay .....	149
Table 5.1: mass spectrometry identified metabolites for rAmbra.....	178
Table 6.1: RNA integrity numbers for RNA extractions used for microarrays data analyses. ....	195
Table 6.2 datasets analyzed from the HUGENE_2.0 microarray for comparing Ambra1 effect on transcriptome .....	195
Table 6.3: Differentially expressed genes comparing rAmbra to rBgal. ....	205
Table 6.4: genes differential expression in the ShAmb cells compared to the ShCon cells .....	206



<b>Table 6.5: KEGG pathway showing top five pathways affected by Ambra1 knockdown.</b>	<b>210</b>
<b>Table 6.6: GO biological processes showing top biological processes affected by Ambra1 knockdown. ....</b>	<b>211</b>
<b>Table 6.7: FLT1 and WNT5A microarrays and western blot analyses differential expression fold change as a result of Ambra1 knockdown. ....</b>	<b>215</b>
<b>Table 6.8: VEGF related genes differential expression in the Knockdown model .....</b>	<b>219</b>
<b>Table 6.9: melanoma progression related genes identified to be differentially expressed upon Ambra1 knockdown .....</b>	<b>221</b>
<b>Table 6.10: differentially expressed semaphorins as a result of Ambra1 knock-down...</b>	<b>230</b>

## Abbreviations

AD	Activating domain
AGO3	Protein argonaute-3
AJCC	American Joint Committee on Cancer
Ambra1	Activating molecule in beclin1-regulated autophagy
ANK	Ankyrin
ANKRD	Ankyrin repeat domain
BANCR	BRAF-activated non-protein coding RNA
BARKOR	Beclin-1-associated autophagy-related key regulator
BCLN1	Beciln1
BCL2	BCL2 Apoptosis Regulator
BRAF	proto-oncogene B-Raf
BSA	Bovine Serum Albumin
CDH	Cadherin
CDK	Cyclin dependent kinases
CK	casein kinase
DBD	DNA Binding Domain
DDB	DNA Binding Protein
DDO	Double Dropout
DDT	Dithiothreitol
DLC	Dynein Light Chain
DMEM	Dulbecco's Modified Eagle Medium
DSTN	Dextrin
EGFR	Epidermal Growth Factor Receptor
FDR	False Discovery Rate
FLT1-VEGFR	Vascular Endothelial Growth Factor Receptor-1
FZD	Frizzled Receptors
GAPDH	Glyceraldehyde 3-Phosphate Dehydrogenase
GHR	Growth Hormone Receptor
HCQ	Hydroxychloroquine
HGF	Hepatocyte Growth Factor
HRP	Horseradish Peroxidase
IDP	Intrinsically Disordered Protein
IEF	Iso-Electric Focusing
IGFBP	Insulin like Growth Factor Binding Protein
INHBA	Inhibin Beta A
IPG	Immobiline DryStrip gels
KDR-VEGFR-2	Vascular Endothelial growth factor receptor-2
MAPK	Mitogen-activated protein kinase
MITF	Microphthalmia Transcription Factor
MSTFA	N-Trimethylsilyl-N-methyl trifluoroacetamide
mTOR	Mammalian Target of Rapamycin
NAA	N(Alpha)-Acetyltransferase
NRP	Neuropillin
ORF	Open Reading Frame
PAS	Pre-Autophagosomal Structures
PBS	Phosphate-Buffered Saline

<b>PCA</b>	<b>Principal components analysis</b>
<b>PDGF</b>	<b>Platelet Derived Growth Factor</b>
<b>PDGFR</b>	<b>Platelet Derived Growth Factor Receptor</b>
<b>PEG</b>	<b>Polyethylene Glycol</b>
<b>PLXN</b>	<b>Plexin</b>
<b>PP2CA</b>	<b>Protein Phosphatase 2AC</b>
<b>PTEN</b>	<b>Phosphatase and Tensin homologue</b>
<b>PVDF</b>	<b>Polyvinylidene Difluoride</b>
<b>QDO</b>	<b>Quadropole Dropout</b>
<b>RISC</b>	<b>RNA-Induced Silencing Complex</b>
<b>RNF</b>	<b>Ring Finger Protein</b>
<b>ROS</b>	<b>Reactive Oxygen Species</b>
<b>SDS</b>	<b>Sodium Dodecyl Sulfate</b>

# ***Table of Contents***

<b>Abstract</b>	<b>2</b>
<b>Acknowledgments</b>	<b>3</b>
<b>Lists of figures and tables</b>	<b>4</b>
<b>Abbreviations</b>	<b>10</b>
<b>Chapter 1- Introduction</b>	<b>1</b>
<b>1.1 Melanogenesis</b> .....	<b>4</b>
<b>1.2 Melanoma</b> .....	<b>7</b>
<b>1.3 Cell signaling pathways</b> .....	<b>12</b>
1.3.1 Cyclin dependent kinases (CDKs)	13
1.3.2 Epidermal growth factor receptor (EGFR) signaling pathway	15
1.3.3 Transforming growth factor beta (TGF- $\beta$ ) signaling pathways	17
1.3.4 WNT signaling pathway	18
1.3.5 RAS/RAf/MAPK pathway	19
1.3.6 E2F protein and the Retinoblastoma protein (pRb)	21
1.3.7 The mTOR and the AMPK signaling pathway	22
1.3.8 The DNA damage response	24
<b>1.4 Gene mutations in melanoma</b> .....	<b>25</b>
<b>1.5 Autophagy</b> .....	<b>29</b>
<b>1.6 Ambra1</b> .....	<b>39</b>
1.6.1 Structure	39
1.6.2 The role of Ambra1 in Autophagy	43

1.6.3 The role of Ambra1 in apoptosis	45
1.6.4 The role of Ambra1 in Development	46
1.6.5 The role of Ambra1 in cell proliferation	47
1.6.6 Ambra1 in cancer and other pathologies	48
<b>1.7 Aims of the study.....</b>	<b>49</b>
<b>Chapter 2- Materials and methods</b>	<b>50</b>
<b>2.1 Materials .....</b>	<b>51</b>
2.1.1 Chemicals, reagents and kits	51
2.1.2 Match maker yeast two hybrid system from Clontech Co.	53
2.1.3 Restriction enzymes	53
2.1.4 Primers	54
2.1.5 Cell lines	55
2.1.6 Antibodies	55
2.1.7 Buffers	56
<b>2.2 Methods.....</b>	<b>57</b>
2.2.1 Tissue culture	57
2.2.2 Protein extraction and quantification	58
2.2.3 SRB Cell proliferation assays	59
2.2.4 Western blot analysis	60
2.2.5 Y2H	61
2.2.6 Y2H Control experiments	62
2.2.7 cDNA synthesis and PCR amplification:	63

2.2.8 Gel excision and DNA extraction	65
2.2.9 DNA digestion, Ligation, Plasmid extraction from E. coli and transformation into yeast cells	66
2.2.10 2d Gel electrophoresis	68
2.2.11 Metabolomics	70
2.2.12 RNA extraction and quality analysis	71
2.2.13 Gene expression analysis by microarray	71
2.2.14 Differential expression data analysis	71
2.2.15 Microarray data functional analysis	73
<b>Chapter 3- cell line characterization</b>	<b>74</b>
3.1 A375 melanoma cell lines .....	75
3.2 Cell lines growth curves .....	75
3.2.1 SRB analysis of rAmbra versus rBgal	76
3.2.2 SRB analysis of ShAmb versus ShCon	79
3.2.3 Incucyte live cell imaging of the four cell lines	82
3.3 Western blot analysis of the cell line models.....	85
3.4 Discussion .....	91
<b>Chapter 4- Ambra1 protein binding partners</b>	<b>96</b>
4.1 Introduction.....	97
4.2: Yeast two Hybrid work flow .....	102
4.3 Results.....	104
4.3.1 Amplifying Ambra1 by PCR	104
4.3.2 Cloning Ambra1 into the DNA-binding domain vector	115

4.3.3: Yeast two hybrid mating	132
4.3.4: protein binding partners identified by Y2H	142
<b>4.4 Discussion .....</b>	<b>151</b>
<b>Chapter 5- Development of methods for the proteomic and metabolomics analysis of Ambra1 overexpression</b>	<b>165</b>
<b>5.1 Introduction:.....</b>	<b>166</b>
<b>5.2 Results.....</b>	<b>168</b>
5.2.1 2D gel electrophoresis	168
5.2.2 GC-MS metabolomics studies:	176
<b>5.3 Discussion: .....</b>	<b>185</b>
<b>Chapter 6- Transcriptomic analysis of differential Ambra1 expression</b>	<b>189</b>
<b>6.1 INTRODUCTION: .....</b>	<b>190</b>
<b>6.2 Microarrays analysis workflow</b>	<b>192</b>
<b>6.3 Results</b>	<b>193</b>
6.3.1 RNA quality analysis	193
6.3.2 Differential expression analysis of the microarray results	195
6.3.3 Differential expression functional analysis of the microarray results:	208
6.3.4 Western blot analysis to confirm differential genes overexpression	212
6.3.5 Further analyses	216
<b>6.4. Discussion .....</b>	<b>222</b>
<b>Chapter 7- Final discussion</b>	<b>236</b>
<b>7.1 prelude to final discussion .....</b>	<b>237</b>

<b>7.2 Ambra1 role in cell proliferation.....</b>	<b>240</b>
7.2.1 Ambra1 role in melanoma cells proliferation rate	240
7.2.2 Ambra1 interacts with cell cycle components	241
7.2.3 Ambra role in embryogenesis	243
<b>7.3 Ambra1 novel protein binding partners in this and other recent studies.....</b>	<b>244</b>
<b>7.4 Ambra1 role in different cellular processes .....</b>	<b>251</b>
7.4.1 Ambra1 role in angiogenesis	251
7.4.2 Ambra role in Wnt signaling	252
7.4.3 Ambra1 role in axon guidance	254
7.4.5 Ambra1 role in RAS signaling pathway	255
7.4.6 Ambra1 role in (TGF- $\beta$ ) signaling pathways	256
<b>7.5 Limitations of the study .....</b>	<b>257</b>
<b>7.6 final remarks .....</b>	<b>258</b>
<b>Chapter 8- Appendices</b>	<b>259</b>
<b>Appendix 1: full list of differentially expressed genes resulting from Ambra1 overexpression (P&lt;0.05).....</b>	<b>260</b>
<b>Appendix 2: full list of differentially expressed genes resulting from Ambra1 Knockdown (P&lt;0.05).....</b>	<b>262</b>
<b>Appendix 3: Ambra binding partners identified in this study, by BioPlex data bases and reported in literature.....</b>	<b>268</b>
<b>Chapter 9- References</b>	<b>270</b>



## ***Chapter 1- Introduction***

Cancer is the second cause of death globally according to the world health organization (WHO) which estimated 9.6 million deaths in 2018 (WHO 2020). In UK Melanoma was the fifth most common cancer in 2016. According to cancer research UK (Cancer research UK 2020) around 44 people are diagnosed with melanoma everyday accounting for around 16,000 new patients every year and more than 6 deaths per day. The melanoma rate in UK has also increased by around 50% over the last three decades (Figure1.1).

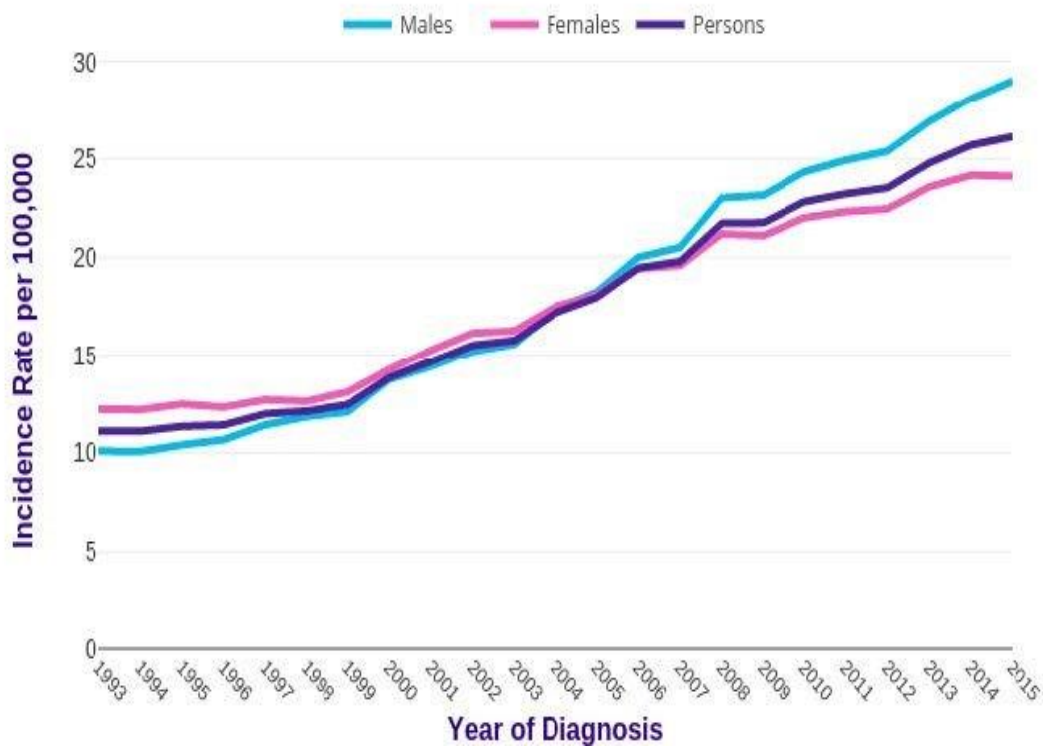


**Figure 1.1: Melanoma skin cancer incidence trends over time.** Melanoma Skin Cancer, European Age-Standardized Incidence Rates, UK, 1993-2015 Cancer Research UK (MelanomaUK 2018).

Melanoma is the most deadly type of skin cancer (Karimkhani et al., 2017), Whilst easily diagnosed at an early stage due to neoplasm being visible through the production of melanin pigments, melanoma remains one of the most therapy-resistant and aggressive cancers despite efforts to develop different therapies (Tsao et al., 2012). Survival rates for 5 years after being diagnosed with melanoma are highly dependent on the stage of the disease. In UK survival rate after 5 years is 90% of newly diagnosed patients at stage one falling dramatically to 30-40% for late stages melanoma.

## 1.1 Melanogenesis

Skin is exposed to high levels of ultraviolet (UV) radiation on daily basis. The primary purpose of the melanogenesis is to reduce the damaging effects of UV-radiation which is known to be a major cause of DNA damage and cancer development (Rastogi et al., 2010)

Melanogenesis is the production of the photo-protective melanin pigment always by melanocytes which are dendritic cells of the neuroectoderm, located in the basal layer of the epidermis known as the stratum germinativum (Bonaventure et al., 2013) (Figure 1.2). The precursor cells of the melanocytes (melanoblasts) are unpigmented cells originating from embryonic neural crest cells (Sviderskaya et al., 2001)

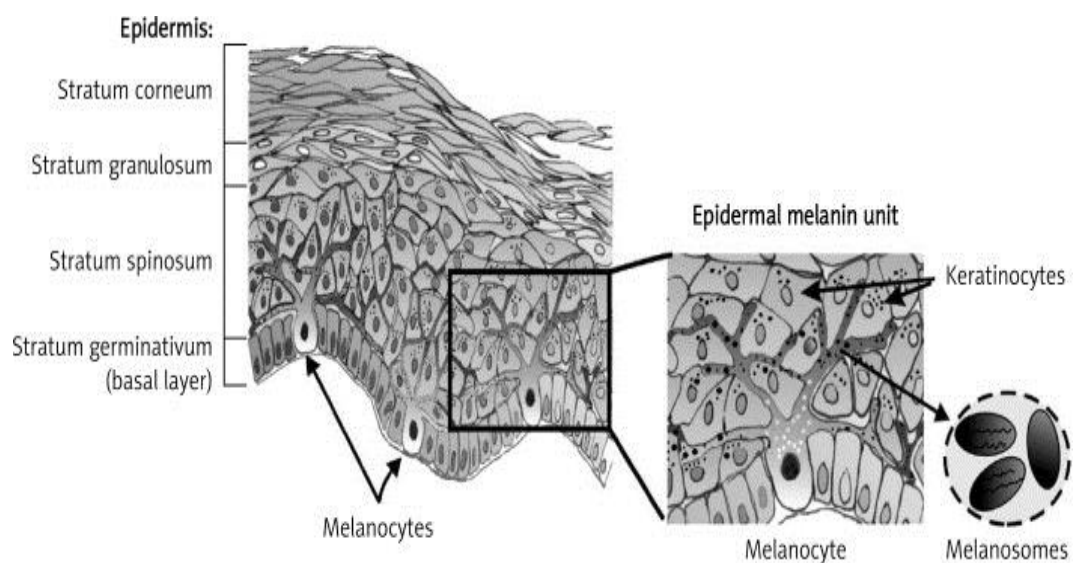


**Figure 1.2: Scheme of the epidermis structure.** Melanocyte reside between the basal layer cells and through dendritic processes communicates with about 30-40 keratinocytes in the epidermal melanin unit. Melanocyte synthesizes melanins in melanosomes transported into keratinocytes to protect them from UV radiation (taken from Cichorek et al., 2013).

There are several steps involved in the life cycle of melanocytes and can be listed as: migration and proliferation of melanoblasts, differentiation into melanocytes, maturation of melanocytes, transport of mature melanosomes (which are the melanin producing organelle in the melanocytes) to keratinocytes and cell death (Cichorek et al., 2013). There are two major types of melanin pheomelanin and eumelanin. The productions of these types depend on the availability of substrates and the function of melanogenesis enzymes (Figure 1.3).

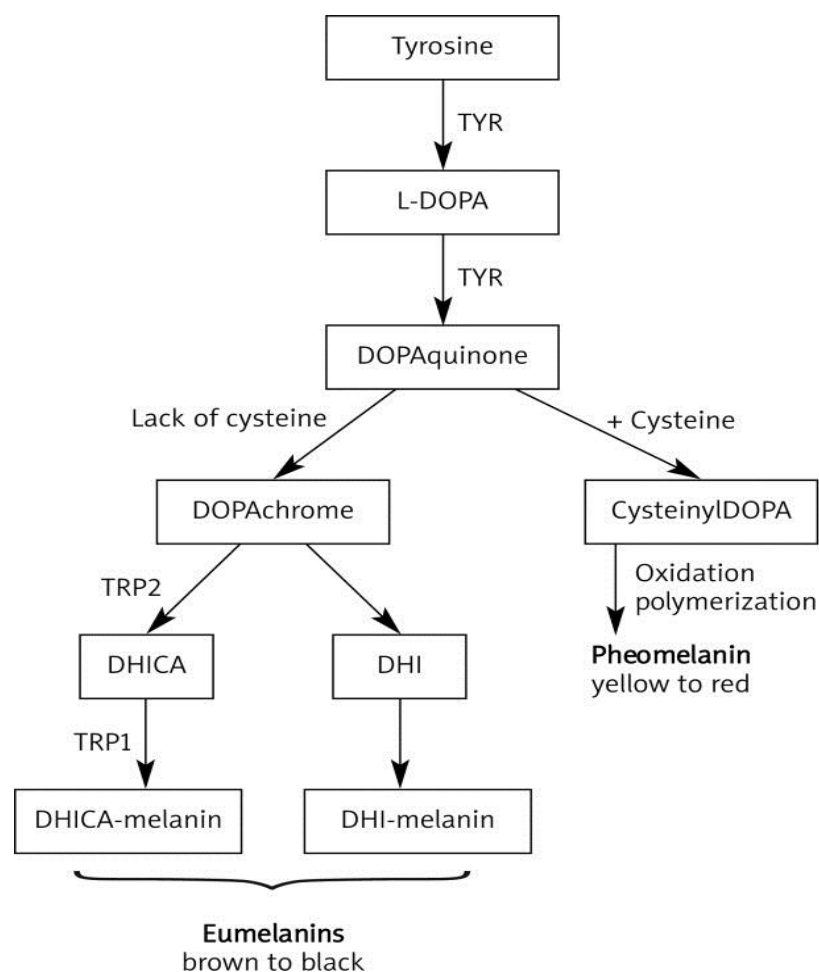


**Figure 1.3: Simplified scheme of the melanin synthesis in melanocytes during melanogenesis.** Tyrosine under influence of the basic enzymes such as tyrosinase (TYR), tyrosine- related protein 1 (TYRP1) and 2 (TYRP2) changes into a polymer of melanin, a mixture of pigments named eumelanin (black-brown) and pheomelanin (yellow-red) (taken from Cichorek et al., 2013)

The melanocyte proliferation and differentiation is under the control of the receptor tyrosine kinase c-Kit and the basic helix-loop-helix leucine zipper transcription factor microphthalmia transcription factor (MITF). C-Kit activation leads to the activation of RAS/RAF signaling and post translational modifications of MITF which is responsible for activating genes involved in pigment production such as TYR, TRP-1 and TRP-2 and melanocyte survival such as Bcl-2 and is modified by mitogen-activated protein kinase (MAPK) phosphorylation (Kormos et al., 2011)

After the melanosomes are produced they migrate to the keratinocytes via dendritic extensions using protease-activated receptor-1 (PAR2) which is a trans-membrane receptor where they primarily function as a defense against UV-radiation (Haass and Herlyn, 2005) there are many keratinocyte-to-melanocyte signaling pathways that can be activated upon the exposure of keratinocytes to UV-radiation which leads to increased number of melanosomes exported to adjacent keratinocytes (Boissy, 2003). Keratinocytes can also respond to UV-radiation by increasing the amount of melanin pigment produced from the melanosomes.

Melanosomes are positioned and located around the nucleus more to the sun exposed side where they primarily act to protect DNA against UV-radiation exposure by scavenging reactive oxygen species (ROS) (Felix et al., 1978).

A benign naevus, more commonly known as a mole is formed when hyper-proliferative atypical melanocytes are clustered together after they escape their normal regulation by the surrounding keratinocytes, this is often happens by a mutation in the RAS/RAF signaling pathway (Davies et al., 2002).

## **1.2 Melanoma**

Evidence currently available on cells of origin of melanoma and mechanisms of tumor initiation is conflicting. Melanocytes and stem cells are both reported to be the origin of melanoma. Recently a team led by Harvard Medical School researchers at Boston Children's Hospital has, for the first time, visualized the origins of melanoma from the first affected cell and watched its spread in a live animal. This team has shown that mature pigment-producing melanocytes can be taken back into a stem-cell like state after oncogenes activation (Kaufman et al., 2016). Another recent study has proved that melanocytes stem cells are not the origin of melanoma but mature melanocytes (Köhler et al., 2017). However; there are other studies that suggest that stem cells are the origin of melanoma (Moon et al., 2017).

Cutaneous melanoma arises from the malignant transformation of melanocytes derived from either previously normal looking skin or from melanocytic naevi (benign lesions composed of a concentrated amount of melanocytes) (Figure1.4).

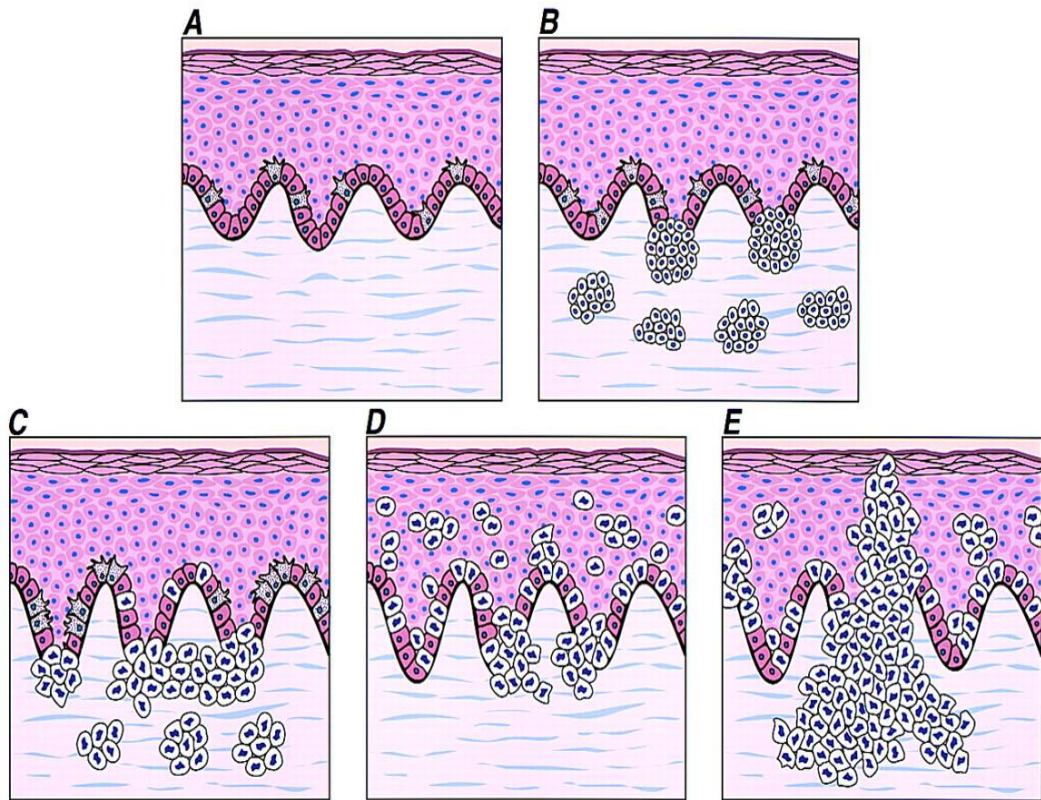
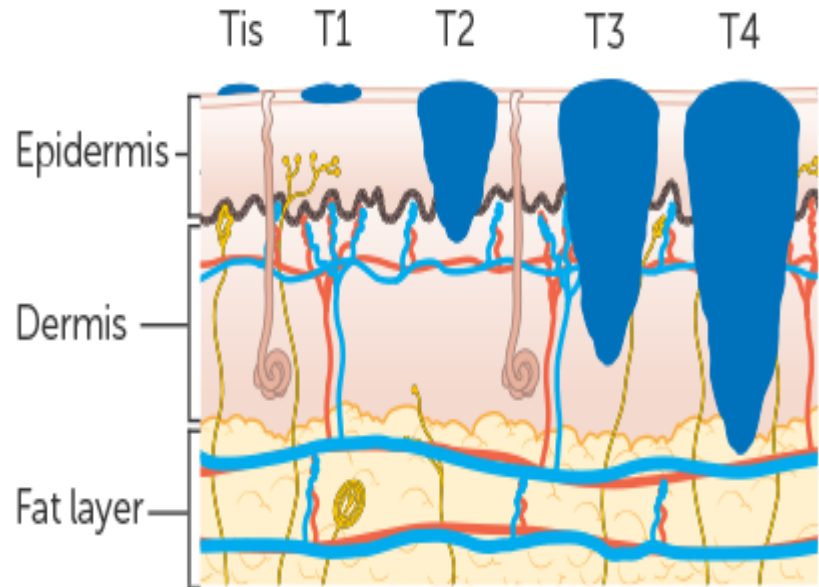


**Figure 1.4: Stages of histopathologic progression in melanocyte transformation.** (A) Normal skin. Note the even distribution of dendritic melanocytes throughout the basal layer. (B) Benign proliferation of melanocytes. Nevoid melanocytes are organized into uniform nests in a compound nevus. (C) Melanocyte dysplasia. Note the irregular and bridging nests consisting of large atypical melanocytes in a dysplastic nevus. (D) In situ melanoma, radial growth phase (RGP). Note the single cells in upper layer of the epidermis (pagetoid spread). (E) Malignant melanoma, vertical growth phase (VGP) (taken from Chin et al., 1998).



The American Joint Committee on Cancer (AJCC) clinical staging of melanoma is based on thickness of the lesion and evaluation of its spread to lymph nodes and different tissues in the body also known as The TNM (Tumor, Node, Metastases). It classifies melanoma into stages 0-4 where stage 0 means the lesion is in situ in the epidermis and is not spreading to deeper layers whereas an invasive lesions that have spread into other body tissues is classified as stage 4 (“Stages and types | Melanoma skin cancer | Cancer Research UK,”) (Figure1.5). A very recent study has managed to make a paradigm shift in the prognostication and stratification of the American Joint Committee on Cancer stage I melanomas by defining epidermal Ambra1/Loricrin loss as a biomarker for higher risk melanomas (Ellis et al., 2019).



Cancer Research UK

**Figure 1.5: Melanoma classification according to tumor size from cancer research UK.** Tis means the melanoma cells are only in the very top layer of the skin surface. It is called melanoma in situ. T0 means no melanoma cells can be seen where the melanoma started (primary site). T1 means the melanoma is 1 mm thick or less. It is split into T1a and T1b. T1a means the melanoma is less than 0.8 mm thick and the skin over the tumor does not look broken under the microscope (not ulcerated). T1b means either: the melanoma is less than 0.8 mm thick but is ulcerated or the melanoma is between 0.8 mm and 1.0 mm and may or may not be ulcerated. T2 means the melanoma is between 1 mm and 2 mm thick. T3 means the melanoma is between 2 mm and 4 mm thick. T4 means the melanoma is more than 4 mm thick.

Cancer cells show alteration in the balance between cell proliferation and apoptosis. Cell proliferation is controlled by multiple complex signaling pathways. These pathways control cellular proliferation, differentiation, cell growth arrest and apoptosis to maintain tissue homeostasis (Heichman and Roberts, 1994).

Multiple mutations in these signaling pathways lead to the development of cancer. Hence; the study of cell proliferation and growth and their respective pathway is crucial to understand uncontrolled cell proliferation in cancer.

### **1.3 Cell signaling pathways**

Eukaryotic cell division involves four sequential phases: G1, S, G2 and M (mitosis). The major events of the cell cycle occur in S and M phase. Where; in S phase chromosome duplication takes place to produce an identical copy of the cell DNA. While in M phase copied chromosomes are distributed into two daughter nuclei and cytoplasmic division takes place generating two daughter cells (CHAFFEY, 2003).

The G1 and G2 phases are gap phases between the S and the M phase. They are as simple as a gap period between the two main cell cycle phases to allow enough time for the cell to grow, and monitor the internal and external environment to assure that conditions are suitable for the cell to divide (Molecular cell biology, 2008).

In multicellular organisms differentiated cells usually exit the active cell cycle during G1 phase and enter G0 phase, where they remain metabolically active for days or years performing their specified functions (Duronio and Xiong, 2013).

Unlike unicellular organisms which grow and divide depending on the availability of nutrients. Multicellular organisms require an extracellular signal to promote cell cycle and cell division. These signals are termed “mitogens”, and there are more than 50 proteins that are identified as mitogens. Most of these proteins have a broad specificity (Duronio and Xiong, 2013). One of the first to be identified was platelet derived growth factor (PDGF) which can stimulate different types of cells to divide (Hannink and Donoghue, 1989). On the other hand; there are some mitogens that show narrow specificity like erythropoietin that stimulates the proliferation of red blood cells precursors (Krantz, 1991).

### **1.3.1 Cyclin dependent kinases (CDKs)**

G1 phase is of a specific importance as it is the restriction point for cell proliferation. Restriction point means that the cell will continue to divide after this point regardless of the presence or the removal of the external signals that promoted cell division from the start (Pardee, 1974). Cyclin-dependent kinases (CDKs) are Central components of the cell-cycle control. The activities of these kinases rise and fall as the cell progresses through the cycle, leading to cyclical changes in the phosphorylation of intracellular proteins that start and regulate the major events of the cell cycle (Morgan, 1995) CDKs levels are constant in the simple cell cycle. However, their activity is mainly controlled by cyclins which are proteins that undergo a cycle of synthesis and degradation in each cell cycle. This change in the cyclin protein levels result in the cyclic activation of CDKs, which subsequently triggers cell cycle events (Koepp et al., 1999). On the other hand; CDK inhibitors (CKIs) like p16, p21 and p27 act as brakes to deactivate the kinase activity of CDK/cyclin complexes to stop the cell cycle under favorable conditions (Elledge and Harper, 1994).

CDKs have no protein kinase activity unless they are tightly bound to a cyclin. There are four different types of cyclins: G1 cyclins (D), G1/S cyclins (E), S-cyclins (A) and M-cyclins (B), they are defined by the stage of the cell cycle at which they bind CDKs (Molecular cell biology, 2008). D cyclins start accumulating at mid-G1, while cyclin E appears later, just prior to the G1/S transition. Cyclin A is involved in S-phase and lastly Cyclin B is essential in mitosis (Koepp et al., 1999).

The hallmark of cancer is uncontrolled cell proliferation. Cancer is able to interfere with the normal cell cycle signaling pathway by the mutation of several genes that are responsible for encoding proteins that activates cell cycle either

by over-activating proteins promoting cell proliferation or deactivating proteins suppressing it (Sherr, 1996). An example of these mutations is the overexpression of cyclin D1 which is common in many human cancers. Specific mutations lead to the inactivation of INK4a gene in melanoma which encodes p15 (INK4b), p18 (INK4c), and p19 (INK4d) proteins that inhibits CDK4 or CDK6 (Hall and Peters, 1996). CDKN1A, CDKN2A, and CDKN2B are proposed to be mutated in melanoma (Soto et al., 2005) and also CDK2, CDK1, and CDK5 are reported to be overexpressed in primary and metastatic melanoma (Abdullah et al., 2011).

### **1.3.2 Epidermal growth factor receptor (EGFR) signaling pathway**

EGFR belongs to the ErbB family of receptor tyrosine kinase (RTK). This family also includes ErbB-2, ErbB-3 and ErbB-4 proteins. These four proteins are trans-membrane receptors that possess an extracellular ligand-binding domain. Signals are often transmitted to other family members when an external signal hits one of these receptors. Receptors of this family are activated by binding to EGF produced from either the same cells possessing the ErbB receptors or surrounding cells (Yarden and Sliwkowski, 2001). Growth factors that act on ErbB can be classified into three groups. The first group acts specifically on the EGFR, it includes EGF, TGF- $\alpha$  and amphiregulin. The second group acts on both EGFR and ErbB-4, it includes heparin-binding growth factor and betacellulin, lastly the third group acts on either ErbB-4 only or ErbB-3 and ErbB-4, it includes neuregulins (Normanno et al., 2006). An indirect activation of these receptors can also take place by cytokines like growth hormone and prolactin.

Activation of ErbB receptors induces the formation of receptor homo- or heterodimers, and subsequent activation of the intrinsic tyrosine kinase domain within these receptors leading to phosphorylation of specific tyrosine residues within the cytoplasmic tail of the ErbB (Olayioye et al., 2000). In turn these residues activate proteins containing Src homology 2 (SH2) and phosphotyrosine binding (PTB) domains which leads to the activation of intracellular signaling pathways like activating: Shc, Grb7, Grb2, Crk, Nck, the phospholipase C $\gamma$  (PLC $\gamma$ ), the intracellular kinases Src and PI3K proteins, RAS/RAF/MAPC pathway and the protein tyrosine phosphatases SHP1 and SHP2 and the Cbl E3 ubiquitin ligase (Normanno et al., 2006). All these activated proteins and pathways promote cell cycle.

ErbB receptors are over expressed in the majority of human carcinomas. EGFR protein overexpression occurs in different tumor types. In some cases EGFR overexpression is independent of EGFR gene mutations. Literature lacks enough data to assess the role of EGFR signaling pathway in Melanoma. However, few studies suggest that overexpression of this pathway is accompanied with worse prognosis (Dimova and Dyson, 2005) and more recently an inhibitor of this pathway in combination with an inhibitor of MET (hepatocyte growth factor receptor) decreased melanoma cells invasive abilities (Simiczyjew et al., 2019).



### **1.3.3 Transforming growth factor beta (TGF- $\beta$ ) signaling pathways**

TGF- $\beta$  receptor plays an important role in tissue homeostasis. It is also a trans-membrane receptor and it is a serine/threonine kinase. The function of TGF- $\beta$  is opposite to the EGFR. When this receptor is activated it phosphorylates Smads proteins in the cytoplasm which subsequently migrate to the nucleus and turn on specific target genes. One of the most important genes that can be activated through this pathway is P21 which is a CDK inhibitor. This pathway signaling end result is arresting cell cycle and promoting cell entry to G0 (Massagué et al., 2000; Uttamsingh et al., 2007).

The role of TGF- $\beta$  in cancer is dual. In some types of cancer TGF- $\beta$  components can act as tumor suppressor. Down regulations in this pathway are reported in different types of human cancers. However; TGF- $\beta$  in other cases is overexpressed in Cancer cells which deactivate the tumor-suppressive arm of the TGF- $\beta$  pathway. In the last case TGF- $\beta$  act as a tumor-derived immune-suppressor, an inducer of tumor mitogens and a promoter of carcinoma invasion in other types of cancer including melanoma (Massagué, 2008; Neel et al., 2012).

### **1.3.4 WNT signaling pathway**

The WNT is a signaling pathway in metazoan animals. WNT proteins are analogue mitogens to EGF. They are involved in the regulation of cell proliferation, cell motility, cell polarity, organogenesis, cell fate and stem cells renewals (Logan and Nusse, 2004).

These proteins activation induces intracellular signal pathways either by the canonical (WNT/ $\beta$ -catenin) dependent pathway or the non-canonical  $\beta$ -catenin independent pathway. The first pathway occurs when WNT proteins bind to Frizzled receptors which are cell surface receptors that upon activation they interrupt a  $\beta$ -catenin destruction complex. This complex includes Axin, adenomatosis polyposis coli (APC), protein phosphatase 2A (PP2A), glycogen synthase kinase 3 (GSK3) and casein kinase 1 $\alpha$  (CK1 $\alpha$ ). The resultant elevated  $\beta$ -catenin phosphorylates the cyclin D promoter thus promoting cell cycle (Komiya and Habas, 2008).

Downregulation of APC is the most frequent mutation in this pathway in cancer. Mutations of the Wnt pathway are observed in melanoma specifically during invasion (Kaur et al., 2016). Moreover, therapies targeting the activation of  $\beta$ -catenin in melanoma show improvement in prognosis (Polakis, 2012).

### **1.3.5 RAS/RAf/MAPK pathway**

Mitogens act on the G1 phase to control the rate of cell division, by activating CDKs thus promoting the cell cycle to proceed to S phase. This occurs by interacting with cell-surface protein kinase receptors like the epidermal growth factor receptor (EGFR) and the platelet-derived growth factor receptor (PDGFR) to trigger multiple signaling pathways like small GTPase RAS which is one of the major signaling pathways (Duronio and Xiong, 2013). Activating this pathway leads to the activation of Mitogen-activated protein kinases (MAPK) cascade which subsequently lead to an increase in the production of gene regulatory proteins. Like MYC (Kelly et al., 1983). MYC promotes cell cycle entry by different mechanisms, one of which is over-expressing genes encoding D-cyclins; another is increasing cell growth genes like telomerase reverse transcriptase (TERT). The increase of D cyclins promotes the G1-Cdk activity which subsequently activates E2F proteins.

There is evidence that c-Myc can regulate cellular metabolism. Several lines of evidence suggest that oncogenic amplification of c-Myc directly alters glucose metabolism and also regulates specialized biosynthetic activities required for successful cell division. Oncogenic c-Myc promotes increased aerobic glycolysis through the constitutive elevation of LDH-A (Osthus et al., 2000; Shim et al., 1997), as well as expression of enzymes involved in nucleotide and amino acid metabolism (Gordan et al., 2007).

Many of the genes that were identified as oncogenes in this pathway are mutant versions of the genes that encode components that control the mitogenic signaling pathways; For instance a mutation of a single amino acid in RAS causes constant stimulation of RAS-dependent signaling pathways by permanently over-activating RAS protein (Downward, 2003). Another example

is the MYC protein where cells proliferate excessively if the MYC is mutated and overexpressed (Beroukhim et al., 2010).

In human cancer cells RAS is one of the most frequently mutated oncogenes. K-RAS which is the frequent mutant of RAS appears in 72-90% of pancreatic cancer (Dergham et al., 1997). K-RAS plays a key role in the alteration of this pathway by RAS gene amplification or activation of the pathway even when the oncogenic mutations are not active. Other mutations in this pathway include the somatic B-RAF which is the most common mutation in malignant melanoma in (Davies et al., 2002; Cheng et al., 2018).

MAPK is rarely activated in the absence of K-RAS or B-RAF and is only seen in less than 50% in human low-grade ovarian serous carcinomas (Hsu et al., 2004).

MYC is also one of the most highly amplified oncogenes in human cancer (Beroukhim et al., 2010; Dang, 2012) its knock-down in cancer cell lines usually decreases cancer cells proliferation and sometimes induces apoptosis (Cappellen et al., 2007). Not all of the molecular functions of MYC are clear. However; its main studied molecular functions indicates that MYC plays an important role in cell proliferation, differentiation and tumorigenesis (Conacci-Sorrell et al., 2014).

### **1.3.6 E2F protein and the Retinoblastoma protein (pRb)**

E2f proteins are a group of gene regulatory factors that promotes the encoding of G1-S cyclins, S-cyclins which regulates the G1/S transition and promotes S-phase entry this is by far the most studied function of the E2F proteins (Nevins, 1998). Other roles of these proteins include the regulation of DNA replication during the cell cycle. However, it is still unclear if they exert this effect directly on DNA or if it happens only in response to certain conditions like DNA damage, recently E2F role in links between cell cycle checkpoint and DNA damage repair has been explored (Wang et al., 2018). These proteins are also found to be involved in: the regulation of mitosis and apoptosis, DNA repair and finally cell differentiation (Dimova and Dyson, 2005).

Retinoblastoma pathway is the primary control of the restriction point in mammalian cells. In the absence of mitogens Retinoblastoma protein (pRB) inhibits the E2F-stimulated gene expression thus inhibiting cell proliferation (Weinberg, 1995). Active G1-Cdk phosphorylates Rb proteins reducing their binding to E2F and promoting cell cycle (Hinds et al., 1992).

Mutations of Rb pathway occurs in nearly all human cancers (Knudsen and Wang, 2010). Studies have shown that the E2F proteins can act as both oncogenes and tumor suppressor genes. Although deregulation of E2F proteins in cancer has been reported in many studies; there are other studies that illustrate that mutations in the E2F genes can result in tumor suppression (Massagué, 2008). Literature also suggests that it is not possible to fully understand the role of this pathway in cancer unless the cellular functions of this pathway in controlling normal cell cycle in are fully studied and understood (Chen et al., 2009).

### **1.3.7 The mTOR and the AMPK signaling pathway**

Mammalian target of rapamycin (mTOR) kinase is a conserved serine/threonine protein kinase that belongs to the phosphoinositide 3-kinase (PI3K)-related protein kinase (PIKK) family. It plays an essential role in regulating cell growth and cell cycle progression in response to cellular signals. mTOR assembles into two distinct structural and functional complexes: mTORC1 which is characterized by its RAPTOR subunit and is sensitive to rapamycin and, mTORC2 which is characterized by a RICTOR subunit instead of the RAPTOR subunit and it is rapamycin insensitive (Yang et al., 2013). While mTORC1 regulates cell growth and metabolism, mTORC2 instead controls proliferation and survival (Saxton and Sabatini, 2017).

mTORC1 activity is regulated by 4 different signals: growth factors, energy status, oxygen and amino acids. Growth factors include: insulin, insulin like growth factor 1 (IGF-1), EGF, TGF, hepatocyte growth factor (HGF), vascular endothelial growth factor (VEGF) and platelet-derived growth factor (PDGF), growth factors mTORC1 activation is mediated by Phosphatidylinositol 3 kinase (PI3K)-Akt pathway. Energy status signals are transmitted to mTOR through AMP-activated protein kinase (AMPK), decreased energy activates AMPK which can either directly inhibit mTORC1 as it phosphorylates RAPTOR or indirectly by the phosphorylation of tuberous sclerosis complex 2 (TSC2) which in turn deactivates small RAS-related GTPase Rheb (Ras homolog enriched in brain) resulting in the reduction of mTORC1 activity. Hypoxia also triggers the AMPK leading to the same effect on mTORC1. Amino acids that can regulate mTORC1 include leucine and rag proteins. However; the understanding of this particular signaling effect on mTOR remains unclear (Laplane and Sabatini, 2009; Saxton and Sabatini, 2017).

Stress and inflammation can also regulate the activity of the mTORC1. Activated mTOR phosphorylates different proteins that promote ribosome biogenesis, translation and lipids and nucleotides synthesis and it suppress autophagy (Tan et al., 2014)

There are a large number of tumor suppressor genes and proto oncogenes involved in the mTOR pathway. Different types of cancers show mutations in this pathway specifically in the two mTOR upstream effectors: PI3K/Akt pathway as well as the Ras/Raf/Mek/Erk (MAPK) pathway, in fact mTOR pathway controls most hallmarks of cancer like cell cycle, metabolism and genomic instability (Tan et al., 2014; Tian et al., 2019), mTOR is hyper activated in a high percentage of cancers (Saxton and Sabatini, 2017).

### ***1.3.8 The DNA damage response***

Not only mitogens can control cell proliferation signaling pathway, but also other intracellular and extracellular effects. DNA damage is one of the most important intracellular influences to arrest cell cycle (Broustas and Lieberman, 2014). Activating this pathway indirectly activates the gene regulatory protein p53 by initiating a signaling pathway that starts by activating either ATM or ATR protein kinases which leads to the phosphorylation of Chk1 and Chk2 kinases and subsequent phosphorylation and activation of p53 which stimulates the encoding of CKI p21 protein and finally resulting in either cell cycle arrest for the damaged DNA to be repaired or apoptosis (El-Deiry et al., 1993; Xiong et al., 1993, Hafner et al., 2019). Mutations in the genes encoding p53 or the ones encoding p53 activating proteins are very common in cancer (Beer et al., 2004; Perri et al., 2016; Serrano et al., 1997).



### ***1.4 Gene mutations in melanoma***

The understanding of different pathways involved in melanoma is crucial as there is a continuous need for identifying new potential therapeutic targets especially with metastatic melanoma being resistant to almost all available therapies. There are far many mutations observed in Melanoma. However; there are few gene mutations that can be considered as driver mutations in this type of skin cancer (Figure 1.6).

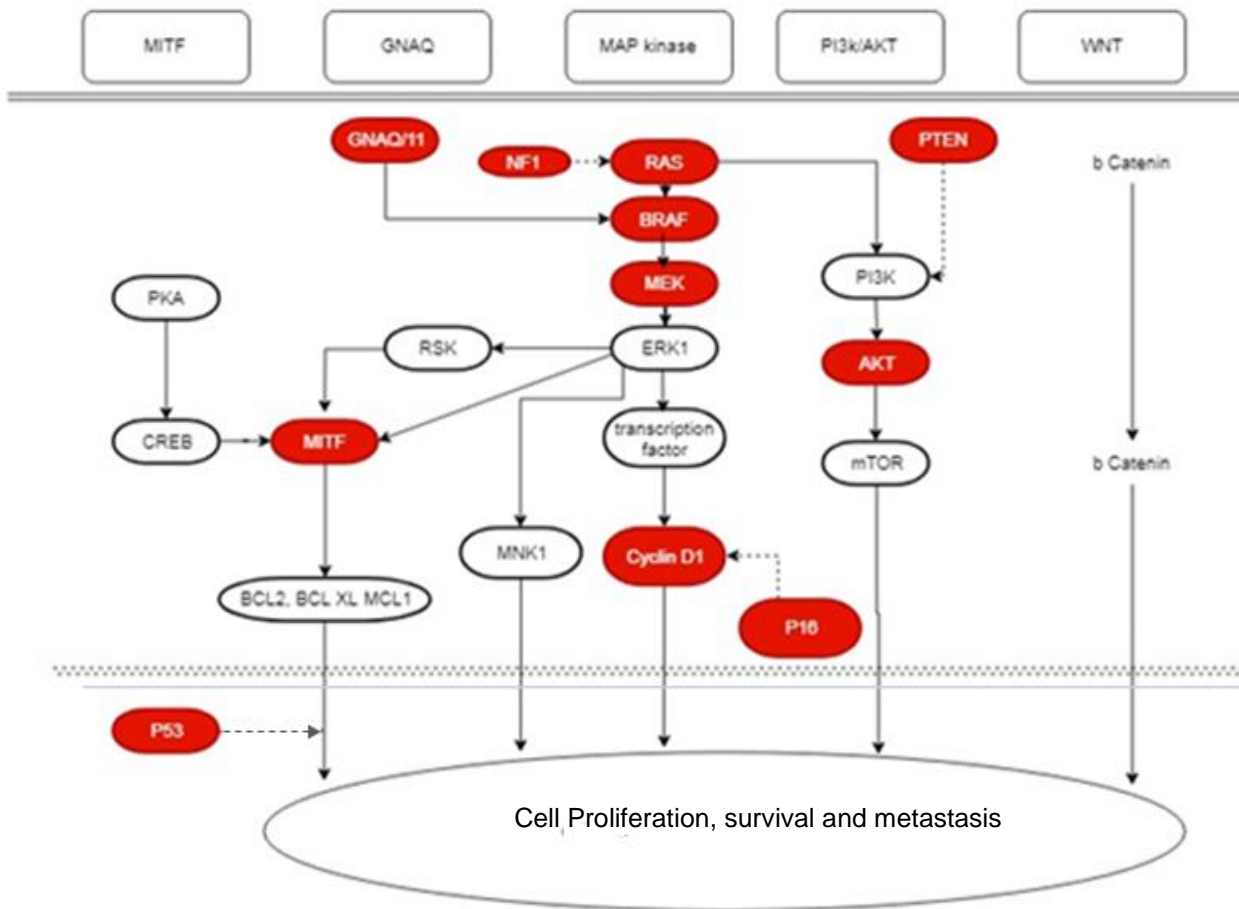


**Figure 1.6: A schematic representation of driver gene mutations in melanoma.** Identified driver mutated genes are colored in red. Arrows represent activation while dotted arrows represent inhibition of target genes.

Mitogen-activated protein kinase (MAPK) pathway is very complex and its constitutive activation leads to regulating several genes expression involved in cell proliferation and survival by the phosphorylation of ERK1 which results in phosphorylating nuclear transcription factors like ETS, ELK-1 and MYC, it also regulates apoptosis by regulating the post-translational phosphorylation of molecules like BCL2, MCL1 (Dhillon et al., 2007). This constitutive activation is reported in different cancers and particularly in melanomas, where the mutation rates for B-RAf is 50-70% and NRAS is 15-30%, MEK is also one of the identified mutants in this pathway, moreover, ERK1 mutation has been identified recently in therapeutic-resistance reoccurring tumors (Jaiswal et al., 2018). MAPK pathway can also activate PI3K/AKT pathway which is crucial in the development of melanoma. Mutations in this pathway include the tumor suppressor PTEN which shows inhibitory effect on this pathway and is mutated in 20-30% of melanomas (Kwong and Davies, 2013). The loss of PTEN activity in BRAF mutated melanoma results in increased tumor invasiveness and metastasis. Mammalian target of rapamycin (mTOR) is one of the downstream targets of the PI3K/AKT pathway, mTOR activation leads to increased cell proliferation and survival. There is evidence that the mTOR is of specific importance in the development of the malignancy of melanoma (Karbowiczek et al., 2008); in fact one study suggests that the mutation of the two major oncogenes in melanoma BRAF and PTEN while blocking the mTOR can prevent cancer cells from progressing to malignancy (Souroullas and Sharpless, 2015). AKT can also control cellular energy and glucose metabolism by the phosphorylation and inhibition protein phosphatase 2A (PP2A) glycogen synthase kinase-3 (GSK3), phospho-diesterase-3B, and Raf-1 (Khan et al., 2013). One of the most deleted lesions or inactivated by mutations in

melanomas is the locus encoding the cyclin dependent kinase 2A (CDKN2A) inhibitors p16<sup>INK4A</sup> which promotes cell cycle arrest at the G<sub>1</sub>-S checkpoint and p14<sup>ARF</sup> which is a positive regulator of the most inactivated tumor suppressor gene in all cancers P53 (Paluncic et al., 2016).

Microphthalmia-associated transcription factor (MITF) is a melanocyte specific transcription factor amplified in 20-30% of melanomas and is able to control different biological processes like proliferation, differentiation as well as apoptosis. It is important to highlight that MITF mutation in melanoma has only been found in a small subset of melanomas. However, being a downstream target of the MAPK pathway contributes for its activation in most cases. MITF is also controlled by the Wnt/ $\beta$ -catenin pathway which role is not fully clear in melanoma yet but mutation in this pathway is observed more in non-melanoma cancers (Hartman and Czyz, 2015). However, non- canonical Wnt signaling is of a specific importance in melanoma as it is involved in melanoma invasiveness, this role is mediated by Wnt5A (Kaur et al., 2016)

Being a target in other types of cancer; there is a growing body of research that considers the mTOR as a potential therapeutic target in melanoma, this is challenging as the gene mutations of mTOR in melanoma are distributed making it hard to target (Wu et al., 2018).

## **1.5 Autophagy**

Autophagy is the process of up-taking proteins and organelles into lysosomes and/or vacuoles for degradation and it is evolutionary conserved in eukaryotes. The word autophagy is the Greek for “automated self-eating” and its role is to balance sources of energy and remove mis-folded and aggregated proteins, clear damaged cell organelles like mitochondria and finally eliminating intracellular pathogens (Glick et al., 2010).

Autophagy roles are essential for a normal cell survival; it is involved in lifespan extension, cellular differentiation and development (Yorimitsu and Klionsky, 2005). Under physiological conditions, autophagy maintains normal turnover of cellular components by signaling network that ensures quality control of cellular components and maintains cell homeostasis. Whereas; in pathological settings such as DNA damage, hypoxia and starvation autophagy act as a key pro survival response and its activation mediates defense against extracellular insults and pathogens (Behrends et al., 2010; Rubinsztein et al., 2012). Moreover; autophagy and cell growth are mirror images of one another. If cell growth is defined as the process of mass accumulation through the net uptake and conversion of nutrients into macromolecules, autophagy can be considered to act in opposition to these biosynthetic processes through the catabolic breakdown of biomolecules. Under normal conditions cells have the ability to increase their mass in the presence of permissive factors such as nutrients and hormonal signals. This cellular growth requires enormous energy and it takes place in embryos and juveniles during development as well as in adults whose sizes are in steady states, damaged cells are replaced by the growth of differentiated and stem cells. Whereas; in pathological conditions like DNA

damage and stress cells start a defensive mechanism to deal with the stress and among those mechanisms is autophagy (Neufeld, 2012).

The current model for the role of autophagy in cancer is that in the early stages autophagy suppresses tumor development by limiting oxidative stress and genomic instability, whereas in advanced stages, tumors may trigger autophagy to survive metabolic stress (Galluzzi et al., 2015). Cytotoxic events often induce autophagy; it is unclear if this is an effort for cellular preservation or a death mechanism (Mizushima, 2007). It is very challenging to resolve the role of autophagy in cancer, as in most cases cancer cells will utilize a defective autophagy (Aita et al., 1999; Liang et al., 1999; Mathew et al., 2007).

Factors controlling autophagy are: the status of cellular energy, nutrients and amino acids, and growth factors such as insulin (Behrends et al., 2010).

Autophagy can be classified into three types (Boya et al., 2013): macro-autophagy, micro-autophagy, and chaperone-mediated autophagy (Figure 1.7). In macro-autophagy; the autophagosome is a double-lipid bilayer that engulfs the cytoplasmic proteins, and then fuses with the lysosome where degradation occurs (Behrends et al., 2010). Micro-autophagy is different as it involves the uptake of the cytoplasmic components directly by the lysosome through invagination of the lysosomal membrane (Mizushima, 2007). However, the common feature of both mechanisms is that they can engulf large cytoplasmic components. In chaperone-mediated autophagy, lysosomal-associated membrane protein 2A (LAMP-2A) recognises targeted proteins after the association of these proteins with the chaperone proteins facilitating their unfolding and degradation (Saftig et al., 2008).

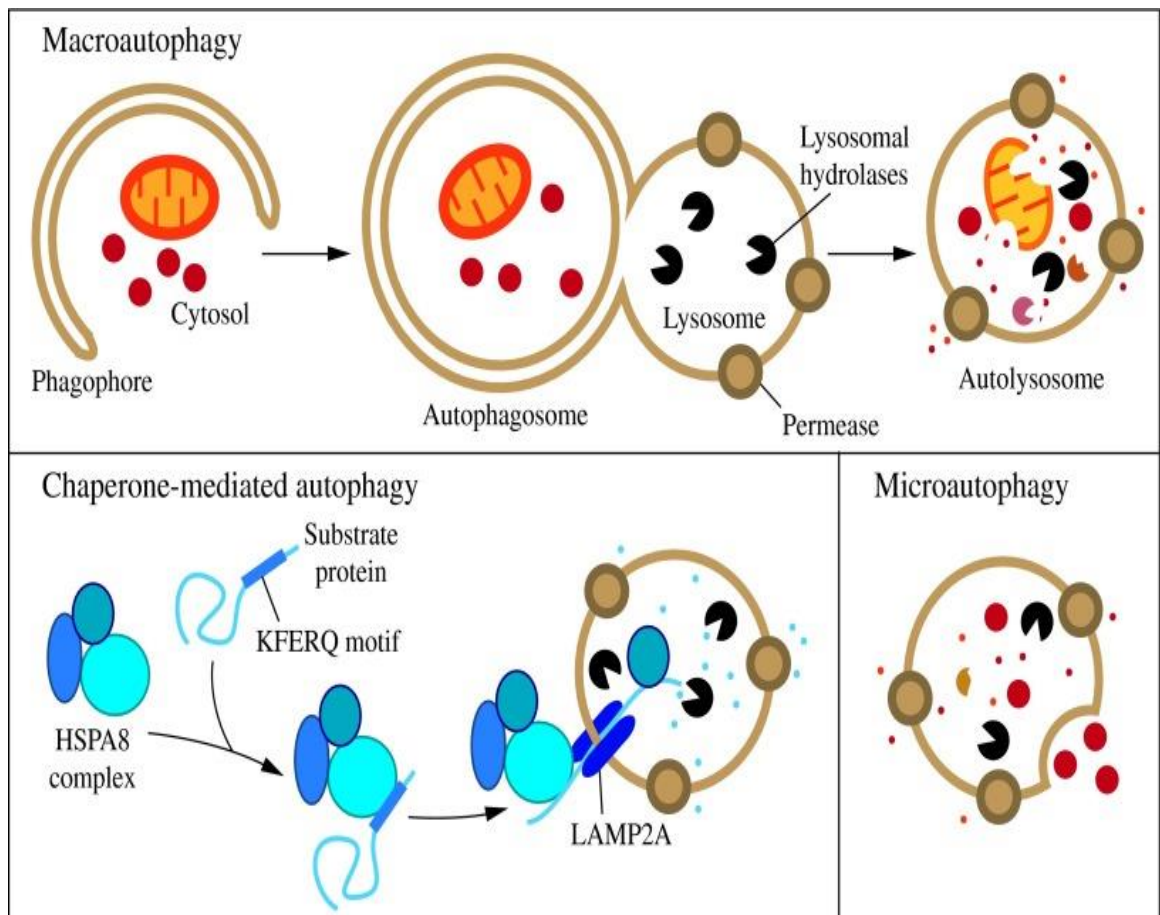


**Figure 1.7: The three different types of autophagy.** Macro-autophagy where an autophagosome is formed, Micro-autophagy where lysosomes directly engulf cytoplasmic components and Chaperone-mediated autophagy where a mediator facilitates the degradation process (Parzych and Klionsky, 2014).

Macro-autophagy (which will be subsequently referred as autophagy) is a complex process that involves the interaction of various proteins and domains and there are around 32 so-called autophagy-related (ATG) genes. The process is very complex and can be classified into: initiation and nucleation, elongation and completion.

Initiation and nucleation start with the *de novo* synthesis of autophagosome from a precursor phagophore, the source of this phagophore membrane was unclear until one study suggested that endoplasmic reticulum(ER) contributes for phagophore formation (Axe et al., 2008). Other studies reported additional membrane sources for phagophore formation such as plasma membrane (Nair et al., 2011), mitochondria (Hailey et al., 2010), Golgi complex (van der Vaart et al., 2010), ER–mitochondria contact sites (Hamasaki et al., 2013), ER exit sites (Graef et al., 2013), and recycling endosomes (Puri et al., 2013). This step requires the activation of class-III phosphoinositide 3-kinase (PI3K), Vps34 which is a specific macromolecule complex for autophagy and contains beclin1, Atg14 and Vps15 and finally it involves Atg5, Atg12 and Atg16 proteins along with focal adhesion kinase (FAK) which is newly identified to be involved in autophagy (Hara et al., 2008).

The second step is autophagosome elongation where the membrane expands and it is called a phagophore. This phagophore expands and bends to form a spherical autophagosome which starts to surround the target cargo. This step involves two ubiquitylation-like reactions where in the first one; Atg5 and Atg12 are conjugated onto (pre-autophagosomal structures)-assembly sites (PAS) in a reaction that requires Atg7 [ubiquitin-activating-enzyme (E1)-like] and Atg10 [ubiquitin-conjugating-enzyme (E2)-like] and are dissociated after phagosome formation, this process is positively regulated by the small GTPase Rab5



(Ravikumar et al., 2008) and it depends on Vps34 function and activity. While in the second ubiquitylation-like reaction which requires the activities of Atg7 (E1-like) and Atg3 (E2-like) (Mizushima et al., 2004); the microtubule associated protein 1 light chain 3 (MAP1-LC3; also known as Atg8 and LC3) conjugates to the lipid phosphatidylethanolamine (PE), where the cleavage of C-terminus of LC3 by Atg4 forms cytosolic LC3-I, which conjugates covalently with PE to form membrane associated LC3-II, which is the only known protein that associates specifically with autophagosomes and not with other vesicular structures (Kabeya et al., 2000). It also can remain associated with phagosomes after fusion with lysosomes and finally recycled as LC3-I (Scherz-Shouval et al., 2007).

The completion step is that the phagophore completely surround its target cargo to form a double membrane autophagosome which is finally fused with the lysosomes clustered around the Microtubule-organization system (MTOC). The fusion of the autophagosomes with the lysosomes product in mammalian cells is referred as autolysosome. The contents of the autolysosome are degraded and the products are part transported to the cytoplasm. An alternative route in mammals is that the autophagosome may fuse to an endosome before the final fusion with the lysosome. In this case the fusion product of the autophagosome and the endosome is termed amphisomes (Figure 1.8) (Parzych and Klionsky, 2014).

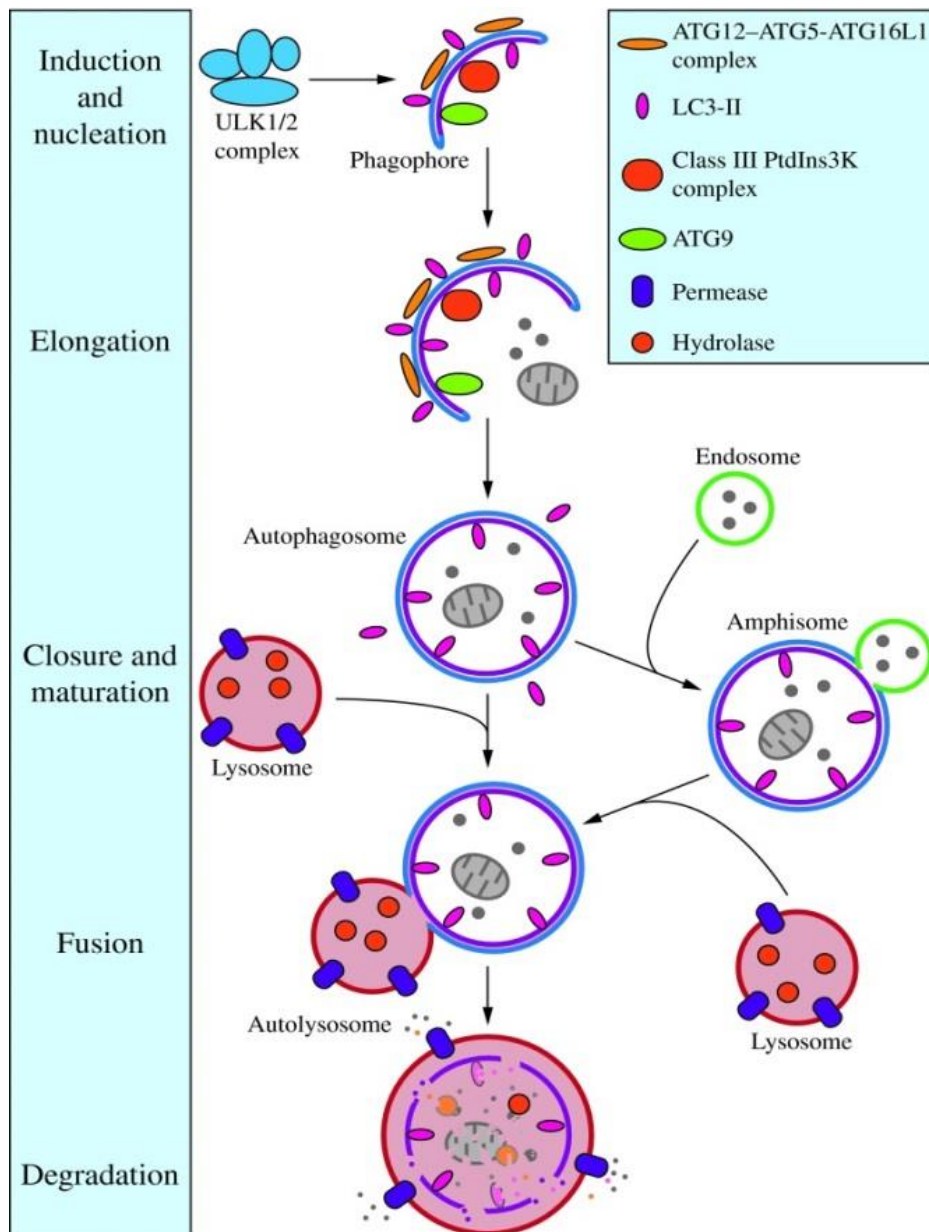


**Figure 1.8: Morphology of macroautophagy.** Nucleation of the phagophore occurs following induction by the ULK1/2 complex. Elongation of the phagophore is aided by the ATG12-ATG5-ATG16L1 complex, the class III PtdIns3K complex, LC3-II, and ATG9. Eventually, the expanding membrane closes around its cargo to form an autophagosome and LC3-II is cleaved from the outer membrane of this structure. The outer membrane of the autophagosome will then fuse with the lysosomal membrane to form an autolysosome. In some instances, the autophagosome may fuse with an endosome, forming an amphisome, before fusing with the lysosome. The contents of the autolysosome are then degraded and exported back into the cytoplasm for reuse by the cell (Parzych and Klionsky, 2014).

Autophagosome formation is controlled by two distinct signals; the first is mammalian target of rapamycin (mTOR) dependent pathway which has a central role in controlling both cell growth and autophagy. The activation of mTOR deactivates autophagy. For example starvation induced autophagy is activated due to the inhibition of mTOR in starvation conditions. mTOR can also be deactivated by the effect of drugs such as rapamycin (Rubinsztein et al., 2007). Mammalian Atg13, ULK1 and ULK2 are identified as direct targets of mTOR, where Atg13 binds to ULK1 and ULK2 (ULK1/2) and mediates their interaction with FIP200. This complex is associated with mTOR under nutrient rich conditions, while under starvation conditions mTOR is inhibited and dissociated from this complex leading to partial dephosphorylation of Atg13 and ULK1/2, which leads to activation of autophagy by phosphorylation of FIP200 by ULK1/2 (Hosokawa et al., 2009). Other signaling molecules that regulate mTOR pathway include; insulin or insulin-like growth factor, activation of adenosine-monophosphate-activated protein kinase (AMPK) which inhibits mTOR pathway. A commonly mutated gene in human cancer; p53 is reported to have a dual opposite effect on autophagy. Studies report that p53 can activate autophagy by activating AMPK or up-regulating phosphatase and tensin homologue (PTEN) and Tsc1. However, other studies report that the same effect can also be achieved by the chemical inhibition of p53 (Levine and Abrams, 2008). Finally, recent discoveries in the regulation of starvation induced autophagy revealed many pathways that can deactivate autophagy, like the binding of apoptosis-related proteins B-cell lymphoma 2 (Bcl2) or basal-cell lymphoma-extra-large (Bcl-XL) to beclin 1 (Atg6) (Ravikumar et al., 2009), moreover, several other beclin1 binding partners can activate beclin1 such as activating molecule in beclin-1-regulated autophagy (Ambra1), Rab5, ultraviolet-

radiation resistance-associated gene (UVRAG) and beclin-1-associated autophagy-related key regulator (BARKOR) (Ravikumar et al., 2009).

The second autophagy controlling signal is mTOR independent pathway which was discovered recently (Sarkar et al., 2005) and it up-regulates autophagy by the inhibition of inositol monophosphatase (IMPase), thus reduces free inositol and myoinositol-1,4,5-triphosphate (IP3) levels (Sarkar et al., 2005), further investigations in this pathway revealed that it is also controlled by intracellular calcium ions and cyclic AMP (cAMP) (Williams et al., 2008) , where elevated intracellular levels of cAMP inhibit autophagy.

It is widely agreed that the current model of autophagy in cancer is that in the early stages of cancer autophagy tend to protect the cells against cancer invasion. Hence; cancer development requires the downregulation of autophagy. Conversely, the upregulation of autophagy in a developed cancer is favored to the tumor and can help metastasis and therapy resistance (White, 2015) (Yang et al., 2011) (Figure 1.9)

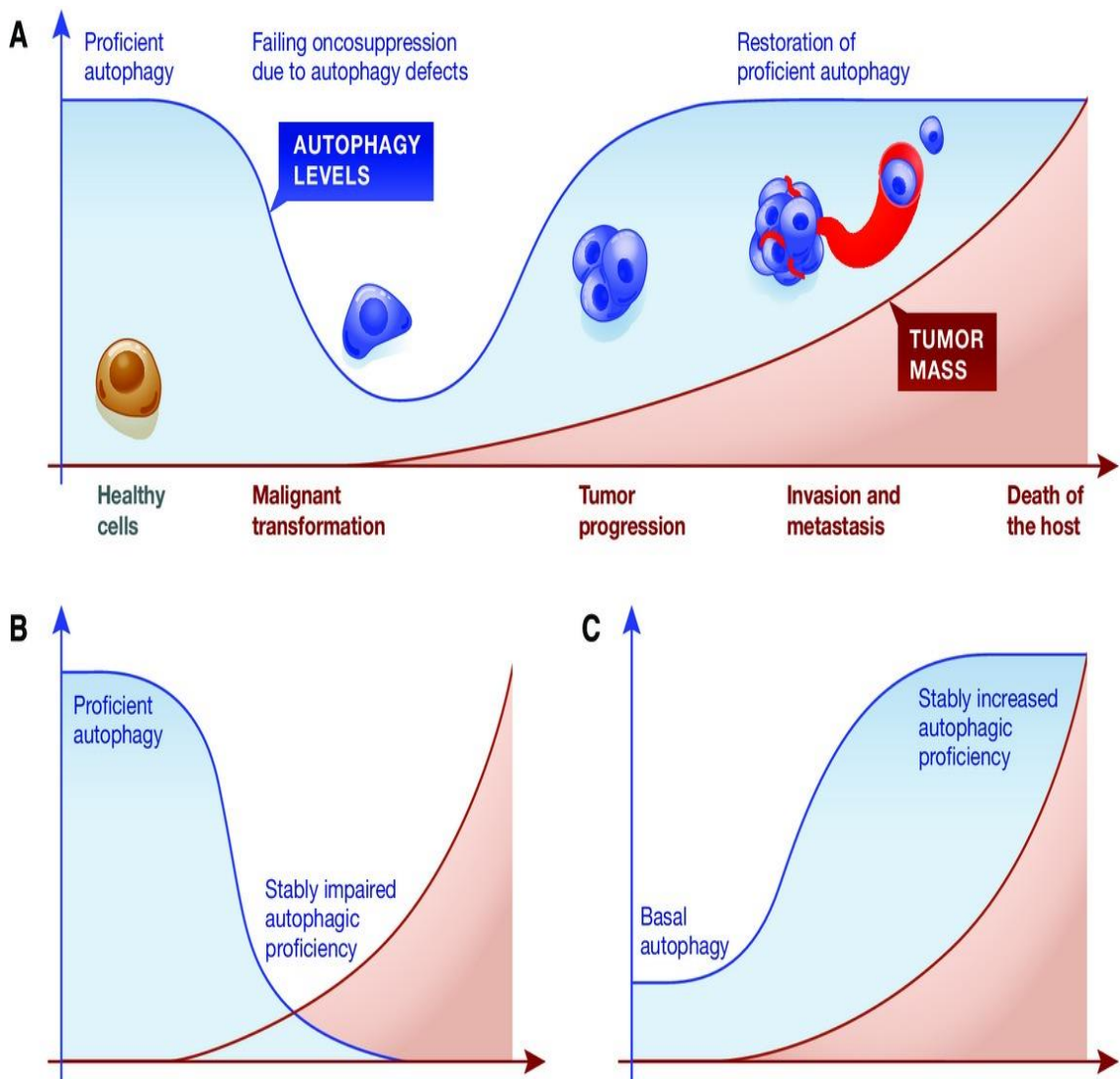


**Figure 1.9: Autophagy role in cancer** (A) Healthy cells appear to be protected from malignant transformation by proficient autophagic responses. Conversely, autophagy promotes tumor progression and therapy resistance in a variety of models. Thus, the transition of a healthy cell toward a metastatic and therapy-insensitive neoplasm may involve a temporary (but not a stable) loss in autophagy competence. The mechanisms underlying the restoration of proficient autophagic responses after malignant transformation remain to be elucidated. (B, C) In specific settings, oncogenesis and tumor progression may rely on a permanent loss (B) or gain (C) of autophagic proficiency (Galluzzi et al., 2015).

The protective role of autophagy against cancer development is clearly related to the molecular processes of autophagy discussed before. The downregulation of autophagy through one of the autophagy related genes is common in different cancer developments and is reported in different studies for example, BCLN1 loss is associated with the development of different types of cancer (Qu et al., 2003)

Ambra1 is an essential component of the autophagy machinery and this study will focus on its different roles and cellular functions.

## **1.6 Ambra1**

Ambra1 (activating molecule in beclin1 regulated autophagy) is protein that regulates autophagy and development of the nervous system (Fimia et al., 2007). Since its discovery in 2007 advances have been made to study the structure, cellular functions and pathological conditions involved with this protein. Here we review recent advances in these discoveries.

### **1.6.1 Structure**

Ambra1 is a large protein of 1300 amino acids bearing three WD40 domains at its amino terminus, proline-and- serine rich domains and dynein binding domains. Its molecular mass is ~130 kDa, it has no apparent orthologs in lower eukaryotes (Fimia et al., 2007). The WD40 repeats in a protein fold into a  $\beta$ -propeller shape of a seven blades, they are involved in different cellular process in which they can act as a platform for the interaction between one protein and another or one protein (Xu and Min, 2011). The proline-and-serine rich domains are of specific importance in Ambra1 binding partners. However; not all the functions of these domains have been identified.

Being an intrinsically disordered protein (IDP); Ambra1 shows high plasticity which makes it an excellent scaffold-molecule candidate that coordinates autophagy with several intracellular processes (Mei et al., 2014).

IDPs are those proteins that are characterized by regions of presumed intrinsic disorder (IDRs) (Uversky and Dunker, 2010) and can undergo a range of conformational changes to form different interaction surfaces that complement different proteins. It means that IDP is a protein of high protein-protein interaction capability and is involved in multiple cellular interactions which is the case in Ambra1 protein (Cianfanelli et al., 2015).

The gene that encodes Ambra1 is located on chromosome 11 in humans and on mouse chromosome 2 and it comprises 18–19 exons, some of which are predicted or have been shown to undergo alternative splicing, giving rise to at least six transcript variants (Cianfanelli et al., 2015). In zebrafish; Ambra1 gene is composed of 19 exons and encodes two paralogues Ambra1a and Ambra1b which are both essential and do not compensate for each other during development (Benato et al., 2013). The difference in the number and the length of exons corresponds to the Ambra1 C-terminal identity while the N-terminal identity of Ambra1 is highly conserved

Ambra1 interactions sites have been identified in previous studies, with some interactions occur at the proline-and-serine rich domains and others at the WD 40 domains (Figure1.10) for example:

- Beclin1 (BCLN1) binds to Ambra Serine-rich domain (Fimia et al., 2007).
- Dynein light chain1 (DLC1) also termed DYLL1 binds to Ambra1 at its c-terminus (AA 1056 to AA 1094) (Di Bartolomeo et al., 2010).
- Cullin 4 adaptor Damage Specific DNA Binding Protein 1 (DDB1) binds to Ambra1 at its WD40 domains resulting in Ambra1 sharp degradation (Antonioli et al., 2014).
- Cullin 5 substrate Elongin B binds to the C-terminal part of Ambra1 (Antonioli et al., 2014)
- Protein phosphatase 2AC (PP2CA) binds to the proline-rich region of Ambra1 as well as its C-terminal region (Cianfanelli et al., 2015)
- TNF receptor-associated factor 6 (TRAF6) binds to Ambra1 at its Serine rich region (Nazio et al., 2013).



- BCL2 Apoptosis Regulator (BCL2) binds Ambra1 at its C-terminus and N-terminus (Strappazzon et al., 2011).
- LC3-interacting region (LIR) near Ambra1 C-terminus binds LC3 (Strappazzon et al., 2015).
- TRIM32 preferentially associates with the C-terminal part of Ambra1 (Rienzo et al., 2019).

Ambra1 is cleaved by Caspases and Calpains; an event that is required to induce apoptosis, Caspases are responsible for Ambra1 cleavage at D482 site. While Calpains can completely degrade Ambra1 (Pagliarini et al., 2012).

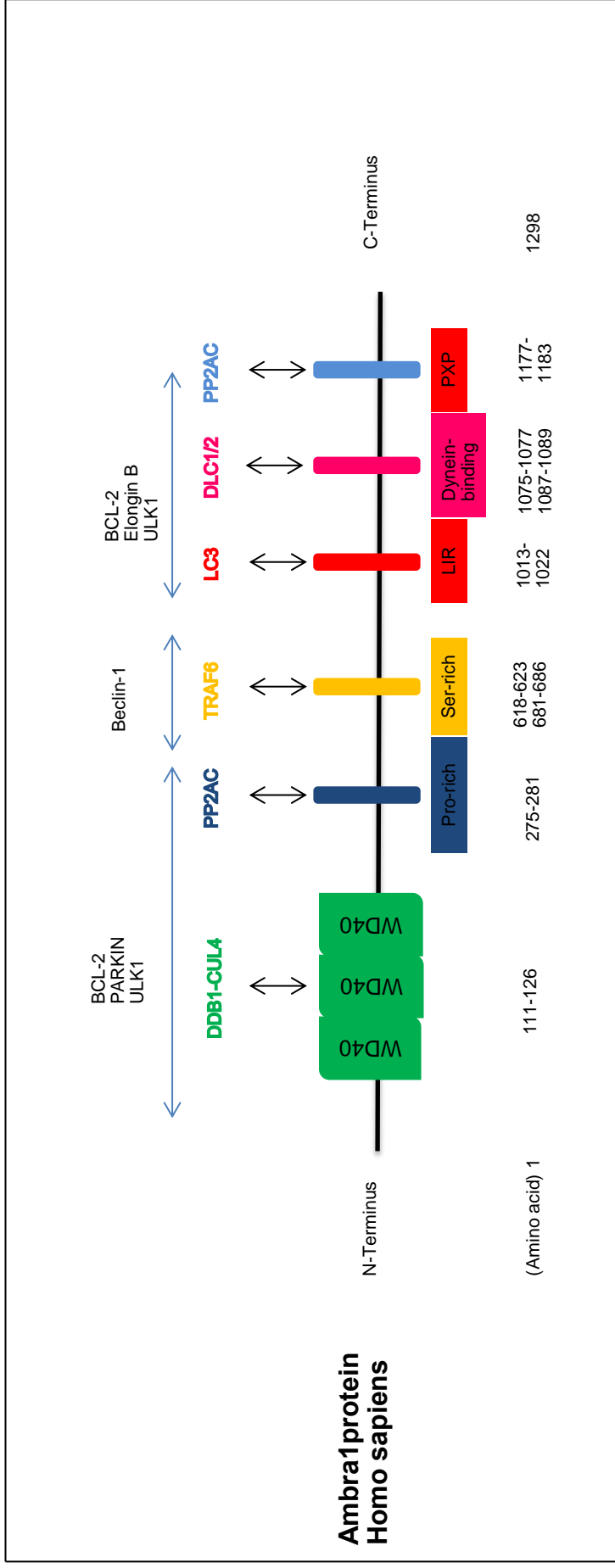


**Figure 1.10: Overview of Ambra1 protein structure and binding sites.** The black line represents the length of the Ambra1 protein, perpendicular colored blocks represent key functional domains with their amino acid positions shown below. Some of the key known protein binding regions are shown as double headed blue arrows with the interacting proteins for those regions indicated above. This diagram was adapted from Cianfanelli *et. al* (2015).

### **1.6.2 The role of Ambra1 in Autophagy**

Ambra-1 can bind to beclin1 upon autophagic stimuli; promoting its binding to Vps34 to induce autophagy. Conversely, down regulation of Ambra-1 leads to a remarkable decrease in rapamycin and starvation-induced autophagy (Kang et al., 2011).

Under normal growth conditions Ambra1 is phosphorylated at ser52 and inhibited by mTOR and is bound to the dynein light chains (DLC1 and DLC2) of the dynein motor complex together with Beclin-1 and PI3KIII. Upon autophagic stimuli the ULK1-mediated phosphorylation releases Ambra1 from the dynein complex. Ambra1 is then translocated together with Beclin-1 and PI3KIII to the endoplasmic reticulum where the autophagosome formation starts (Di Bartolomeo et al., 2010). Ambra1 regulates ULK1 activity and stability suggesting that it has a boarder rule in executing autophagy, it was demonstrated that Ambra enhances the signaling capacity of ULK1 by promoting its self-association by the ubiquitylation of the latter through Lys-63-linked ubiquitin chains, this action is mediated by E3 ligase TNF receptor associated factor 6 (TRAF6) (Nazio et al., 2013).

There is a growing body to look at Ambra1 role in autophagy; recent studies have proposed different Ambra1 interactions that can regulate autophagy. An example of these interactions is that between Ambra1 and cullin E3 ubiquitin ligases. This interaction is essential for autophagy activation (Antonioli et al., 2014); on the other hand; there are interactions that are essential to terminate autophagy. An example is the ubiquitylation of Ambra1 at lys45 with Lys48-linked ubiquitin chains by a complex compromising ring finger protein 2 (RNF2) (Xia et al., 2014). Another example is the ubiquitylation and degradation of Ambra1 by the cullin-4–DDB1 complex (Antonioli et al., 2014)

Ambra1 plays an important role in a selective form of autophagy termed mitophagy in which the defective mitochondria are selectively degraded by autophagy (Ding and Yin, 2012). Early discovery showed one mechanism by which Ambra1 regulates mitophagy through the interaction between Ambra1 and PARKIN (PARKIN mediated mitophagy) (Van Humbeeck et al., 2011). However, a recent study has identified another mechanism in which Ambra1 regulates mitophagy by binding the autophagosome adapter LC3 through a LIR (LC3 interacting region) motif (Strappazzon et al., 2015). The later study proved that Ambra1 can regulate mitophagy by the later mechanism independent of the PARKIN mediated mitophagy indicating that Ambra1 is essential for regulating mitophagy via different cellular mechanisms.

### ***1.6.3 The role of Ambra1 in apoptosis***

Apoptosis is programmed cell death that takes place in normal cell turnover, proper development and embryonic development (Elmore, 2007).

Recent studies suggest that Ambra1 shows an inhibitory effect on the apoptosis process and favors autophagic cell survival, Ambra1 must be cleaved during apoptosis to prevent pro-survival autophagy (Pagliarini et al., 2012), therefore it can control the conversion between both processes to determine the resulting cell survival or death (Fimia et al., 2013; Gu et al., 2014). High number of Apoptotic cells is observed in Ambra1 deficient mice (Fimia et al., 2007).

#### ***1.6.4 The role of Ambra1 in Development***

Ambra1 appears to have a crucial role in embryogenesis, specifically in the development of nervous system. It is highly expressed in the central nervous system particularly in the neuroepithelium, spinal cord, dorsal root ganglia, neural retina and encephalic vesicles (Fimia et al., 2007; Vázquez et al., 2012). Ambra-1 functional deficiency in mouse embryos leads to severe neural tube defects associated with autophagy impairment, accumulation of ubiquitinated proteins, unbalanced cell proliferation, and excessive apoptotic cell death (Kang et al., 2011). In the context of development Ambra1 deficiency leads to abnormal skeletal muscle morphology in mice and zebrafish (Skobo et al., 2014). Most recently Ambra1 has been reported to Control regulatory T-Cell differentiation and homeostasis upstream of the FOXO3-FOXP3 axis and its loss worsens multiple sclerosis in a mouse model (Becher et al., 2018)

### ***1.6.5 The role of Ambra1 in cell proliferation***

Ambra1 loss is associated with hyper-proliferative, non-developed cells (Benato et al., 2013) it is also associated with higher mRNA levels of cyclins A and B (Cianfanelli et al., 2015) the latter study has shown a mechanism by which Ambra1 can contribute to the control of cell proliferation which is the facilitation of the proto-oncogene c-Myc. degradation by binding to the catalytic subunit of the serine/threonine-protein phosphatase 2A (PP2A) resulting in the dephosphorylation of c-Myc. (Cianfanelli et al., 2015) the role of Myc. In cell proliferation is discussed in section 1.2.5. However; literature lacks any other data about the mechanism by which Ambra1 can control cell proliferation despite the fact that literature is full of evidence that this particular gene is of a great importance in cell proliferation and in cancer.

To study the role of Ambra1 in cell proliferation it is important to consider the mTOR signaling pathway in the context of cell proliferation (1.2.7) mTOR is responsible for the phosphorylation of Ambra1 at Ser52 to maintain the latter inactivity under normal growth conditions.

### **1.6.6 Ambra1 in cancer and other pathologies**

Ambra1 is associated with different pathological conditions like Schizophrenia (Rietschel et al., 2011), autism (Dere et al., 2014) and neurodegenerative CNS disorders like Alzheimer's disease (Sepe et al., 2014) and most importantly in cancer. The role of Ambra1 in cancer is dynamic and seems to be very important during different cancer stages. For instance; in support of Ambra1 pro-survival role, a very recent study has managed to make a paradigm shift in the prognostication and stratification of the American Joint Committee on Cancer stage I melanomas by defining epidermal Ambra1/Loricrin loss as a biomarker for higher risk melanomas (Ellis et al., 2019). Furthermore; studies have shown the protective role of Ambra1 against cancer cells. Ambra1 deficient mice show more spontaneous tumorigenesis compared to controls and, it is mutated in endometrial, colorectal and urinary tract neoplasms (Cianfanelli et al., 2015). The role of Ambra1 in late stage cancer especially after metastasis is still under exploring and only few studies reported the role of Ambra1 in developed cancers, its role seems to be more of a protective role that helps cancer cells survive and even resist therapeutic agents. A recent study has shown that in late stage breast cancer, the higher Ambra1 levels; the higher the resistance to epirubicin treatment (Sun et al., 2018). Another study reported Ambra1 to desensitize human prostate cancer cells to cisplatin. This role is mediated by the ability of Ambra1 to activate autophagy and cell survival (Liu et al., 2019). Finally a study has related the role of Ambra in the cross talk between autophagy and apoptosis to its role in cancer cell survival as it contributes to shifting the cells towards autophagy rather than apoptosis, this study proved the pro survival role of Ambra in colorectal SW620 cell lines (Gu et al., 2014).



## **1.7 Aims of the study**

It is clear that the unusual nature of intrinsic disordered proteins suggest that Ambra1 may play a dynamic role in a whole range of cellular processes. Ambra 1 is increasingly identified as having a role in an increasing range of pathologies. It's deficiency in early stage melanoma appears to be a strong candidate as a biomarker in for example. Understanding the mechanism by which this protein acts on the cell may provide leads for identifying potential therapeutic targets against proliferative disorders. This study will focus on identifying novel functions of Ambra1 using a range of "omics" technologies.

The specific aims are:

- To determine if Ambra1 plays a role in regulating cellular proliferation.
- Identify novel binding partners of Ambra-1 using a Yeast two-Hybrid approach.
- Use a range of "omics" techniques to identify novel roles in cellular pathways affected by Ambra1 using cell lines that differentially express Ambra1.

## ***Chapter 2- Materials and methods***

## 2.1 Materials

### 2.1.1 Chemicals, reagents and kits

**Table 2.1: chemicals, reagents and kits used in the research**

<b>Chemicals, reagents and kits</b>	<b>supplier</b>
Match maker yeast two hybrid system	Takara (Clontech) Bio Europe SAS (France)
Easy yeast isolation kit	Takara (Clontech) Bio Europe SAS (France)
Universal human normalized mate and plate library in Y187 strain	Takara (Clontech) Bio Europe SAS (France)
T4 DNA ligase	Thermo-Fisher (Cramlington, UK)
Instant sticky-end ligase master mix	New England Bio-labs (Hitchin, UK)
Electro-ligase	New England Bio-labs (Hitchin, UK)
In fusion cloning kit	Takara (Clontech) Bio Europe SAS (France)
Zero blunt topo PCR cloning kit	Thermo-Fisher (Cramlington, UK)
Perfectly blunt cloning kits	Novagen
Superscript III first-strand synthesis system fo RT-PCR	Thermo-Fisher (Cramlington, UK)
High-capacity cDNA reverse transcription kits for 200 reactions (Applied biosystems)	Thermo-Fisher (Cramlington, UK)
Gel Extraction Kit (50)	Qiagen technologies (Manchester, UK)
plasmid plus midi kit	Qiagen technologies (Manchester, UK)
Chemical Competent <i>E-coli</i> DH5- $\alpha$ strain	Thermo-Fisher (Cramlington, UK)
One Shot TOP10 chemically-competent Cells	Thermo-Fisher (Cramlington, UK)
One Shot TOP10 Electro-competent Cells	Thermo-Fisher (Cramlington, UK)
MAX Efficiency stbl2 competent cells	Thermo-Fisher (Cramlington, UK)
Stellar chemically competent cells	Takara (Clontech) Bio Europe SAS (France)
Immomix master mix	Bioline (Nottingham, UK)
Iproof™ High-fidelity PCR kit	Bio-Rad (Perth, UK)
Q5 DNA polymerase	Bioline
Ampicillin	Labtech (Heathfield, UK)
Kanamycin sulfate	Labtech (Heathfield, UK)
Bio-sera High or low Dulbecco's Modified Eagle Medium (DMEM)	Thermo-Fisher (Cramlington, UK)
10% Foetal Bovine serum	Gibco/ Thermo-Fisher (Cramlington, UK)
primocin	Invivogen UK
L-glutamine	Lab-tech (Heathfield, UK)
TRIzol reagent (Ambion)	Thermo-Fisher (Cramlington,UK)
RNAse Away (Ambion)	Thermo-Fisher (Cramlington,UK)
RNAsecure (Ambion)	Thermo-Fisher (Cramlington,UK)

10X Tris Glycine SDS (TGS) buffer	Sigma-Aldrich (Poole, UK)
4X Laemmli Sample Buffer	Bio-Rad (Perth,UK)
2-Mercaptoethanol	Bio-Rad (Perth,UK)
Precision Plus Protein™ All Blue Standards	Bio-Rad (Perth,UK)
Precision Plus Protein™ unstained standards	Bio-Rad (Perth,UK)
Mini-PROTAEN® TGX Stain-Free™ gels	Bio-Rad (Perth,UK)
Trans-Blot® Turbo™ PVDF Transfer Pack	Bio-Rad (Perth,UK)
Trans-Blot® Turbo™ LF PVDF Transfer pack	Bio-Rad (Perth,UK)
Clarity™ Western ECL Blotting Substrate	Bio-Rad (Perth,UK)
GelRed™ Nucleic Acid Stain	Thermo-Fisher (Cramlington,UK)
HyperLadder IKB™	Thermo-Fisher (Cramlington,UK)
Bradford Reagent	Expedion
BSA protein standard	Bio-Rad (Perth,UK)
3-10 IEF 11cm strips	Bio-Rad (Perth,UK)
3-10 IEF 17cm strips	Bio-Rad (Perth,UK)
5-8 11 cm strips	Bio-Rad (Perth,UK)
5-8 IEF 17cm strips	Bio-Rad (Perth,UK)
Ready prep 2D-clean up kit	Bio-Rad (Perth,UK)
Ready prep 2D starter kit	Bio-Rad (Perth,UK)
Ready prep 2D starter kit rehydration/sample buffer	Bio-Rad (Perth,UK)
Criterion TGX Stain-Free™ gels	Bio-Rad (Perth,UK)
Trichloroacetic acid	Sigma-Aldrich (Poole, UK)
DDT	Thermo-Fisher (Cramlington,UK)
Iodocetamide	Sigma-Aldrich (Poole, UK)
100% Glycerol	Bio-Rad (Perth,UK)
20% SDS solution	Bio-Rad (Perth,UK)
1.5M Tris Hcl Ph 8.0	Bio-Rad (Perth,UK)
8M Urea	Sigma-Aldrich (Poole, UK)
Tween 20	Bio-Rad (Perth,UK)
10X cell lysis buffer	Abcam (Cambridge, UK)
Absolute ethanol	Sigma-Aldrich (Poole, UK)
HPLC-grade methanol	Sigma-Aldrich (Poole, UK)
Isopropanol (2-propanol)	Sigma-Aldrich (Poole, UK)
Glacial acetic acid	Sigma-Aldrich (Poole, UK)
Sodium thiosulphate	Sigma-Aldrich (Poole, UK)
Hydrochloric acid	Sigma-Aldrich (Poole, UK)
Anhydrous sodium acetate	Sigma-Aldrich (Poole, UK)
Silver nitrate	Sigma-Aldrich (Poole, UK)
Anhydrous sodium carbonate	Sigma-Aldrich (Poole, UK)
Formaldehyde	Sigma-Aldrich (Poole, UK)
EDTA-Na <sub>2</sub>	Sigma-Aldrich (Poole, UK)
Acetone	Sigma-Aldrich (Poole, UK)
Coomassie brilliant blue G250	Sigma-Aldrich (Poole, UK)
Ortho-phosphoric acid	Sigma-Aldrich (Poole, UK)
Ammonium sulfate	Sigma-Aldrich (Poole, UK)
SRB stain	Sigma-Aldrich (Poole, UK)
Methoxyhydrochloride	Sigma-Aldrich (Poole, UK)
Pyridine	Sigma-Aldrich (Poole, UK)
MSTFA	Sigma-Aldrich (Poole, UK)
BSTFA	Sigma-Aldrich (Poole, UK)

### **2.1.2 Match maker yeast two hybrid system from Clontech Co.**

- 0.5 ml solutions of Y2H gold and Y187 yeast strains.
- pGBKT7 DNA-BD cloning vector.
- PGADT7 AD cloning vector.
- pGBKT7-53 Control Vector.
- pGADT7-T Control Vector.
- pGBT9 (positive control plasmid).
- pGBKT7-Lam Control Vector.
- Cultural media pouches of: YPDA, SD-Trp, SD-Leu, SD-Trp-Leu, SD-Trp-Leu-His and SD-Trp-Leu-His-Ade.
- YPD plus Liquid Medium.
- 50% Polyethylene glycol (PEG)
- 1 M LiAc (10X).
- 10X TE Buffer.
- X- $\alpha$ -gal.
- Aurobasidin A.

### **2.1.3 Restriction enzymes**

All restriction enzymes were from Thermo-fisher (Cramlington,UK):

- *Bam*H I
- *Eco*R I
- *Nde* I

### 2.1.4 Primers

All primers (table 2.2) were purchased from Integrated DNA Technologies, re-suspended in sterile TE buffer to give a final concentration of 100 nM solutions and were then diluted 100x in TE to make a 100µM stock.

**Table 2.2: Primers used and their sequences**

Primer name	sequence
Ambra1 Fcon	5'- TGC CAC AAT CTC CTG ACC TT -3'
Ambra1 Rcon	5'- TCG CTG TGT CTG GTT AAA TT -3'
Ambra1 Ffull (full)	5'- CCC CAT ATG AG GTT GTC CCA GAA AAG AAT GC -3'
Ambra1 Rfull (full)	5'- CCG AAT TCC TAC CTG TTC CGT GGT TCT CCC CT -3'
AMBRA FullF2 (new)	5'-CCC CAT ATG AAG GTT GTC CCA GAA AAG A -3'
AMBRA FullR2 (new)	5'- CCG AAT TCC TAC CTG TTC CGT GGT TCT CC -3'
AMBRA LongR (long)	5'- CCG AAT TCC TAC CTG TTC CGT GGT TCT CCC C -3'
AMBRA LongFnde (long)	5'- CCC CAT ATG AAG GTT GTC CCA GAA AAG AAT GCT -3'
AMBRA LongFeco (long)	5' CCC GAA TTC ATG AAG GTT GTC CCA AAG AAT GCT -3'
AMBRA FusionF	5'- AGG AGG ACC TGC ATA TGA AGG TTG TCC CAG AAA AGA ATG CC -3'
AMBRA FusionR	5' GCC TCC ATG GCC ATA CTA CCT GTT CCG TGG TTC TCC C-3'
PP2CA F	5'- CGC CAT ATG GAC GAG AAG GTG TTC ACC -3'
PP2CA R	5'- CGC GAA TTC TTA CAG GAA GTA GTC TGG GGT ACG-3'
PP2CA F_Eco	5'- CGC GAA TTC ATG GAC GAG AAG GTG TTC ACC -3'
PP2CA R_Bam	5'- CGC GGA TCC TTA CAG GAA GTA GTC TGG GGT ACG -3'

### 2.1.5 Cell lines

Four stably transfected A375 melanoma cell lines were utilized in this study and are detailed in section 3.0

### 2.1.6 Antibodies

**Table 2.3: Western blots antibodies and dilutions**

<b>Primary antibody</b>	<b>Supplier</b>	<b>Dilution</b>
Mouse antihuman GAPDH4	Abcam (Cambridge, UK)	1:10,000
Rabbit anti human Ambra1 antibody	SDIX (Oxfordshire, UK)	1:10,000
Chicken anti-beta-Galactosidase	Sigma-aldrich (Poole, UK)	1:5,000
Mouse monoclonal to VEGF receptor 1 (ab9540)	Abcam (Cambridge, UK)	1:500
Rabbit monoclonal to Wnt5a-C-terminal	Abcam(Cambridge, UK)	1:2,000
<b>Secondary antibody</b>		
Goat anti rabbit IgG	Vector Labs (Peterborough, UK)	1:10,000
Goat anti mouse IgG	Vector Labs (Peterborough, UK)	1:10,000
Goat anti-chicken IGY (ab97135)	Abcam (Cambridge, UK)	1:10,000
Goat anti mouse IgG alexa flour plus 448	Thermo-Fisher (Cramlington,UK)	1:500
Goat anti mouse IgG star bright blue 250	Bio-rad (Perth,UK)	1:500

## 2.1.7 Buffers

**Table 2.4: homemade buffers and their constituents**

<b>Buffer</b>	<b>constituents</b>
TAE	(40mM Tris, 20mM acetic acid, 1mM EDTA pH 8.0)
Tris-buffered saline (TBS)	(150mM NaCl, 50mM Tris, pH 7.6)
TBS-tween (TBST)	(TBS, pH 7.6 with 0.05% Tween 20)
2d equilibration buffer 1	8M Urea, 20%SDS, 14.5M Tris Hcl, Glycerol, milliQH <sub>2</sub> O, DDT
2d equilibration buffer 2	8M Urea, 20%SDS, 14.5M Tris Hcl, Glycerol, milliQH <sub>2</sub> O, Iodocetamide
Fixation solution for 2D gels	Ethanol (40% VV <sup>-1</sup> ), glacial acetic acid (10% VV <sup>-1</sup> ) and milliQH <sub>2</sub> O
Colloidal coomassie staining solution	Coomassie Brilliant Blue G250 (0.1% WV <sup>-1</sup> ), ortho-phosphoric acid (2% WV <sup>-1</sup> ), ammonium sulfate (10% WV <sup>-1</sup> ) and methanol
Sensitizing solution for silver staining of 2D gels	Ethanol (30% VV <sup>-1</sup> ), sodium thiosulphate (0.01M), sodium acetate (0.8M) and milliQH <sub>2</sub> O
Silver reaction solution for 2D gels	Silver nitrate (0.015M), milliQH <sub>2</sub> O
Developing solution for silver staining of 2D gels	Sodium carbonate (0.25M), Formaldehyde (0.075% VV <sup>-1</sup> ) and milliQH <sub>2</sub> O
Stopping solution for silver staining of 2d gels	EDTA (0.5M) and milliQH <sub>2</sub> O



## **2.2 Methods**

### **2.2.1 Tissue culture**

Cells were cultured and routinely passaged to be maintained in the exponential phase in either high or low Dulbecco's Modified Eagle Medium (DMEM) (Biosera). The media was supplemented with 10% Foetal Bovine serum (Gibco), 100 µg/ml primocin (Invivogen) and 300 µg/ml L-glutamine (Lab-tech). Cells were grown at 37°C in a 5% CO<sub>2</sub> humidified atmosphere.

Transfection maintenance was performed by adding antibiotics to the media. The overexpression strains were maintained using G418 at a concentration of 2 µg ml<sup>-1</sup> and the knock-down cell lines were maintained using puromycin at a concentration of 2 µg ml<sup>-1</sup>. Antibiotics were omitted 24 to 72 hours before protein extraction, metabolites extraction, RNA extraction and SRB assays.

### **2.2.2 Protein extraction and quantification**

Cells were seeded at a concentration of  $5 \times 10^5$  to a 6-well plate and grown at 37°C, and maintained in the exponential phase. Cells were then washed twice with PBS and harvested with 200  $\mu$ l 1x cell lysis buffer and sonicated for 3x10 seconds to disrupt cell wall. Lysates were stored at -80°C and used for downstream analysis.

Protein quantification was performed using BSA as a standard and Bradford reagent according to the manufacturer's instructions in a 96-well plate and absorbance measured at 595nm using a plate reader

### **2.2.3 SRB Cell proliferation assays**

Cell proliferation assays were performed using Sulforhodamide B (SRB) to monitor the growth of the different cell lines over time. Cells were seeded in a concentration of 1500 cell per well at a volume of 200  $\mu$ l. cells were fixed by incubating at 4°C for 1 hour with 50% trichloroacetic acid (TCA) at 24, 48 and 72 hours intervals. The cells were then stained with 100  $\mu$ l 0.4% SRB stained prepared in 1% acetic acid and incubated for 30 minutes. The plates were washed with 1% acetic acid 5 times and incubated at 60°C to dry for 2 hours. The stain was solubilized using 100  $\mu$ l 10mM tris (PH 10.5) and absorbance was read at 570nm.

To plot the data the absorbance reading from a single well was converted to an arbitrary value of 100% growth within each cell line from one of the absorbance readings at 24 hours. Within each cell line (for example rBgal) the other absorbance values were converted to an arbitrary % in order to calculate the mean and standard deviation for the growth at each time point. Setting the baseline value within each cell line enabled comparisons to be made irrespective of the absolute starting number of cells in each well. Statistical significance was performed by Mann-Whitney U-test.

#### **2.2.4 Western blot analysis**

Proteins were denatured with SDS buffer at 95°C for 5 minutes, and 25µg of this lysates were resolved by 12% polyacrylamide gel (Bio-Rad) electrophoresis and transferred to polyvinylidene difluoride (PVDF) or low fluorescence polyvinylidene difluoride (LF PVDF) membranes (Bio-Rad). PVDF membranes were blocked in Immobilon® Block-Chemiluminescent Blocker (CB) (Merck) for 1 hour at room temperature, while LF PVDF membranes were blocked by incubating over-night at 4°C with TBS containing 5% milk. Membranes were then incubated with primary antibodies overnight at 4°C with shaking, washed 3x10 minutes with TBST and incubated with secondary antibodies for 1 hour at room temperature (see table 2.3 for concentrations) followed by another 3x10 minutes wash, PVDF membranes were then incubated with 2 ml freshly prepared (1:1) mixture of peroxide reagent and luminol/enhancer reagent supplied from Bio-Rad for chemiluminescent detection of HRP activity of the conjugated secondary antibody. However; this step was omitted for LF PVDF membranes. The membranes were then analyzed by the ChemiDoc™ Imaging System (Bio-Rad, UK) for protein band detection.

### **2.2.5 Y2H**

Yeast strains were maintained by streaking at least once every 4 weeks on fresh YPDA plates, incubated at 30°C for 3 to 5 days then stored at 4°C. Only fresh grown colonies were used for transformations. Plates were prepared by adding each media pouch content to 500 ml deionized water then autoclaving, left to cool to 50°C then X- $\alpha$ -gal and/or antibiotics were added before pouring the plates.

Yeast transformation, positive and negative control experiments were performed as stated by Yeast-Two Hybrid System manufacturer (Clontech Laboratories).

All yeast transformations performed are shown in table 2.5.

**Table 2.5: transformed plasmids in different yeast strains**

Y2H gold	Y187 strain
pGBKT7-53 Control Vector	pGADT7-T Control Vector
pGBKT7-Lam Control Vector	
pGBKT7-Ambra1	
pGBKT7-PP2CA	

All isolated plasmids were sequenced using a t7 promoter at Source Bio-science limited

### **2.2.6 Y2H Control experiments**

Yeast transformation, positive and negative control experiments were performed as stated by Yeast-Two Hybrid System manufacturer (Clontech Laboratories) a positive control mating was performed by mating Y2H gold strain fused with murine p53 and Y187 yeast strain fused with SV40 large T-antigen. On the other hand a negative control experiment was performed by mating Y2h gold yeast stain fused with lamin and Y187 yeast strain fused with SV40 large T-antigen.

### ***2.2.7 cDNA synthesis and PCR amplification:***

Different cDNAs were prepared using oligo and random primers by PCR using RNA extracted from U-937 (ATCC® CRL-1593.2™) and A-375 (ATCC® CRL-1619™) cell lines. An ORF clone with Ambra1 sequence was purchased to be used as a PCR template.

PCR reactions were performed on Bio-Rad T100 thermal cycle. PCR reactions were performed using 10 x Immomix master mixes (Bio-Rad), Q5 polymerase (Bio-labs), and proof-reading polymerase was later used (Iproof Bio-Rad). Different PCR protocols were used with different polymerases and are shown in table 2.6.

**Table 2.6: PCR protocols**

**(A) PCR protocol for the amplification of Ambra1 and PP2CA full lengths ORFs a using Immomix and Q5 polymerase**

Temperature	95°C	95°C	64°C	72°C	Repeat	72°C	12°C
Duration (minutes)	3:00	0:30	0:30	1:30	45x	5:00	∞

**(B) PCR protocol for the amplification of Ambra1 full length using Iproof polymerase**

Temperature	98°C	98°C	66.6°C	72°C	Repeat	72°C	12°C
Duration (minutes)	3:00	0:30	0:30	1:30	45x	5:00	∞

**(C) PCR protocol for the amplification of PP2CA full length using Iproof polymerase**

Temperature	95°C	95°C	63°C	72°C	Repeat	72°C	12°C
Duration (minutes)	3:00	0:30	0:30	1:00	45x	5:00	∞

Colony PCR was performed by re-suspending a single colony into 100µl sterile water and using 1µl as a DNA template for the PCR amplification, all other PCR reaction reagents and specifications remains as above.

All of the PCR products were made ready for gel electrophoresis by adding an appropriate amount of 4x loading dye to each reaction mixture, then tested on 1% Agarose in TAE buffer using gel red as indicator and Hyperladder 1Kb as a reference, electrophoresis were made on Bio-rad power Pac basic at 100 volts and ran for 45 minutes to 1 hour.



### **2.2.8 Gel excision and DNA extraction**

DNA fragments were extracted from gels using QIAquick® Gel Extraction Kit (Qiagen technologies). The DNA fragment was excised from the agarose gel with a sterile scalpel, gel slices were weighed in colorless tubes, the protocol was performed according to the manufacturer's instructions. DNA was eluted in 50µL Buffer EB (10 mM Tris-Cl, pH 8.5). DNA concentrations were quantified on the Nano drop light spectrophotometer

### **2.2.9 DNA digestion, Ligation, Plasmid extraction from *E. coli* and transformation into yeast cells**

Plasmids were transformed to competent *E. coli* (DH5- $\alpha$  strain) by adding 50  $\mu$ l of *E. coli* to 100 ng of DNA and left on ice for 30 minutes, the mixture was heat shocked at 42°C for 20 seconds, then transferred back to ice for 5 minutes. 950  $\mu$ l of nutrient broth were added and the mixture was shaken at 37° C for 1 hour and 200  $\mu$ ls of each sample were plated on Agar plates contained Ampicillin (100 $\mu$ gml<sup>-1</sup>) for the ampicillin resistant vectors and on Agar plates contained kanamycin (50 $\mu$ gml<sup>-1</sup>) for kanamycin resistant vectors. Plasmids were transformed into the yeast strains according to the manufacture specifications (Clontech).

*E. coli* containing plasmids were regrown to facilitate the isolation of the plasmids by adding one colony of the grown bacteria of each plasmid to 250 ml growth media (15 gm. Tryptophan, 5 g. Yeast, 5 g. NaCl and made up to 1 L with water) and 250  $\mu$ l of antibiotic (either ampicillin or kanamycin) and incubated for 5 hours at 37 °C then shacked overnight.

Plasmids were extracted from *E. coli* using plasmid plus midi kit (QIAGEN technologies) according to manufacturer's instructions. DNA was eluted by adding 200  $\mu$ l of EB buffer and centrifuged for 1 minute. DNA concentration of each plasmid was measured on Nano drop light spectrophotometer (Thermo Scientific).

All of the PCR products and plasmids were digested for gel electrophoresis by adding 200 ng DNA to 1  $\mu$ l of the restriction enzymes, 2  $\mu$ l 10x fast digest buffer and making it up with water to 20  $\mu$ l. A gel of 0.7% w/v of agarose in TAE buffer was prepared and 10  $\mu$ l of gel green indicator were added. Finally 4  $\mu$ l of 6x loading solution were added to each 20  $\mu$ l digest, mixed and 20  $\mu$ l of the

mixture were loaded on the agarose gel with 5  $\mu$ l of Hyperladder IKB (Bioline) indicator as a reference.

All ligation reactions were made at a vector to insert ratio of 1:5, the appropriate ligase was added to the reaction mixture and incubated overnight at room temperature.

### 2.2.10 2d Gel electrophoresis

Total protein was precipitated by either using 2d clean-up kit (Bio-Rad, UK) or by adding a 1:1 volume of 100% acetic acid to the protein lysate solution and incubated at 4°C for 10 minutes. Proteins were pelleted by centrifugation at 15000 RPM for 10 minutes, washed twice with ice-cold acetone and the pellets were re-suspended in a freshly reconstituted rehydration buffer (Bio-Rad). The amount and the final volume of protein used to rehydrate the IEF strips are shown in table 2.7.

**Table 2.7: protein concentration and rehydration buffer volume used for each IEF strip.**

IEF strip	Rehydration buffer volume	Final protein concentration	application
11cm (3-10 or 5-8)	200 µl	200 µg	Coomassie G-250
11cm (3-10 or 5-8)	200 µl	50 µg	Silver stain
17cm (3-10 or 5-8)	300 µl	300 µg	Coomassie G-250
17cm (3-10 or 5-8)	300 µl	50 µg	Silver stain

Strips were covered by mineral oil and left overnight for rehydration. Rehydrated strips were then transferred to an IEF focusing tray and loaded to IEF cell. Different protocols used are in table 2.8.

**Table 2.8: protocols used for focusing IPG strips**

IEF strip PH 3-10 or 5-8	Desalting step (2,000 volts for 2 hours followed by wicks replacement)	Focusing protocol			
		End voltage	Volt-hours	Ramp	Temperature
11cm recommended protocol	No	8,000	20-35,000	Rapid	20°C
11cm optimized protocol	Yes	8,000	40,000	Rapid	20°C
17cm recommended protocol	No	10,000	40-60,000	Rapid	20°C
17cm optimized protocol	yes	10,000	60,000	Rapid	20°C

After focusing strips were equilibrated for 15 minutes with 5mls equilibration buffer1 containing DDT (2% W/V) followed by 5mls equilibration buffer 2 containing iodoacetamide (2.5% W/V). Strips were then loaded onto TGX stain free gels (Bio-Rad) and ran on Bio-Rad power Pac at 200V for 1 hour. Gels were imaged on a ChemiDoc™ Imaging System (Bio-Rad, UK). Gels were fixed by incubation with fixation solution on an orbital shaker for 30 minutes followed by overnight incubation with shaking at 4°C. gels were washed with milliQH<sub>2</sub>O for 2x10 minutes.

All staining steps were performed on an orbital shaker at room temperature.

#### ***2.2.10.1 Colloidal Coomassie G-250 stain***

Gels were stained overnight with a freshly prepared mixture of colloidal Coomassie dye stock solution and methanol (80:20% V/V). Gels were finally de-stained with milliQH<sub>2</sub>O until background became clear.

#### ***2.2.10.2 Silver stain***

Gels were treated with sensitizing solution for 30 minutes followed by 3x5 minutes washes with milliQH<sub>2</sub>O. Gels were then reacted with silver nitrate solution and washed 2x 1 minute. For the developing step gels were incubated with the developing solution and visually monitored for 2-10 minutes until clear brownish protein bands were observed. The reaction was then stopped by incubating the gels with EDTA for 10 minutes. Finally the gels were washed 3x5 minutes with milliQH<sub>2</sub>O.

### **2.2.11 Metabolomics**

Cells were seeded at a concentration of  $5 \times 10^5$  to a 6-well plate and grown at  $37^\circ\text{C}$ , and maintained in the exponential phase. Cells were then washed once with PBS and harvested with 1 ml HPLC grade methanol, several freeze/thaw cycles were applied to the extracts and these extracts were dried on LABCONCO CentriVap. Samples were then reacted with 100  $\mu\text{l}$  of methoxy hydrochloride in pyridine ( $20 \text{ mg ml}^{-1}$ ) and incubated for 2 hours at room temperature followed by an overnight reaction with 200  $\mu\text{l}$  of either-N-Methyl-N-(trimethylsilyl) trifluoroacetamide (MSTFA) or N,O-bis(trimethylsilyl)trifluoroacetamide (BSTFA) for derivatization. Samples were then loaded onto GC-MS column.

### ***2.2.12 RNA extraction and quality analysis***

Total RNA was extracted from each cell line using Trizol reagent (Thermo-Fisher, catalogue number 15596026) according to the manufacturer's instructions and the precipitated RNA was re-suspended in 200  $\mu$ l 1xRNA secure reagent (Ambion).

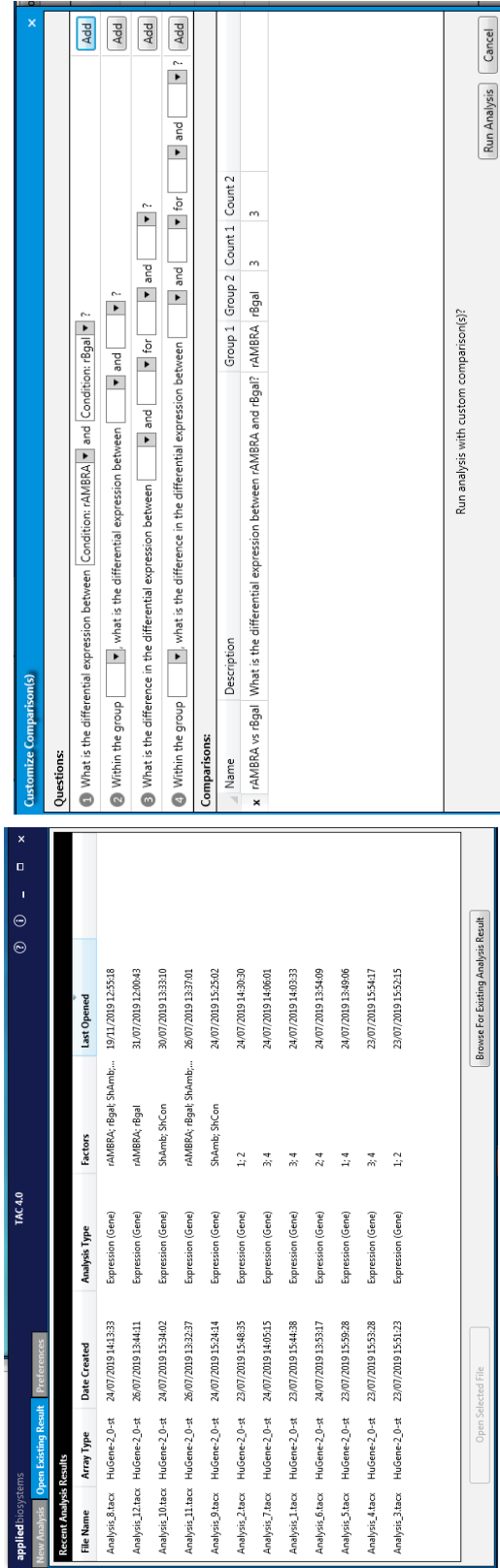
RNA quality analysis was performed using Experion™ RNA StdSens and HighSens Analysis Kits from Bio-Rad following instructions from the manufacturer.

### ***2.2.13 Gene expression analysis by microarray***

The analysis was performed by Source bio-Science. Three biological replicates from each cell line at a concentration of 120  $\text{ng } \mu\text{l}^{-1}$  were hybridized on GeneChip™ Human Gene 2.0 ST.

### ***2.2.14 Differential expression data analysis***

The microarray data was normalized and analyzed using Transcriptome analysis suite (TAC version 4.0.1) (Thermo-fisher) (Figure 2.1). Ebayes Anova method was used and the analysis was set to gene-Level Fold Change < -2 or > 2 and P-Value < 0.05.



### Analysis 8

Data Created: 24/07/2019 14:13:33  
 Array Type: HuGene-2\_0-st  
 Analysis Type: Expression (Gene)  
 Analysis Version: version 1  
 Summarization Method: Gene Level - RMA  
 Genome Version: hg19 (Homo sapiens)  
 Annotation: HuGene-2\_0-st-v1.na36.hg19.transcript.csv  
 Condition (Comparison): rAMBRA; rBgal; ShAmb; ShCon

#### Expression Analysis Settings:

- Gene-Level Fold Change < -2 or > 2
- Gene-Level P-value < 0.05
- Anova Method: ebayes

Comparison	Group 1	Group 2	Count 1	Count 2	Up	Down
rAMBRA vs ShCon	rAMBRA	ShCon	3	3	81	102
ShAmb vs ShCon	ShAmb	ShCon	3	3	255	104
rAMBRA vs rBgal	rAMBRA	rBgal	3	3	63	45
rAMBRA vs ShAmb	rAMBRA	ShAmb	3	3	44	120

**Figure 2.1: Transcriptome analysis suite software. Screenshots showing different stages of**

analysis performed using TAC software to analyze the microarray data.



### 2.2.15 Microarray data functional analysis

Functional analysis of the differentially expressed genes was performed using STRING protein-protein interaction tool, KEGG pathways tool and GO biological process tool. Fisher's exact tests were performed and only results of FDR  $P < 0.05$  were considered.

A general legend that applies to all string analysis in this research is shown in figure 2.2.

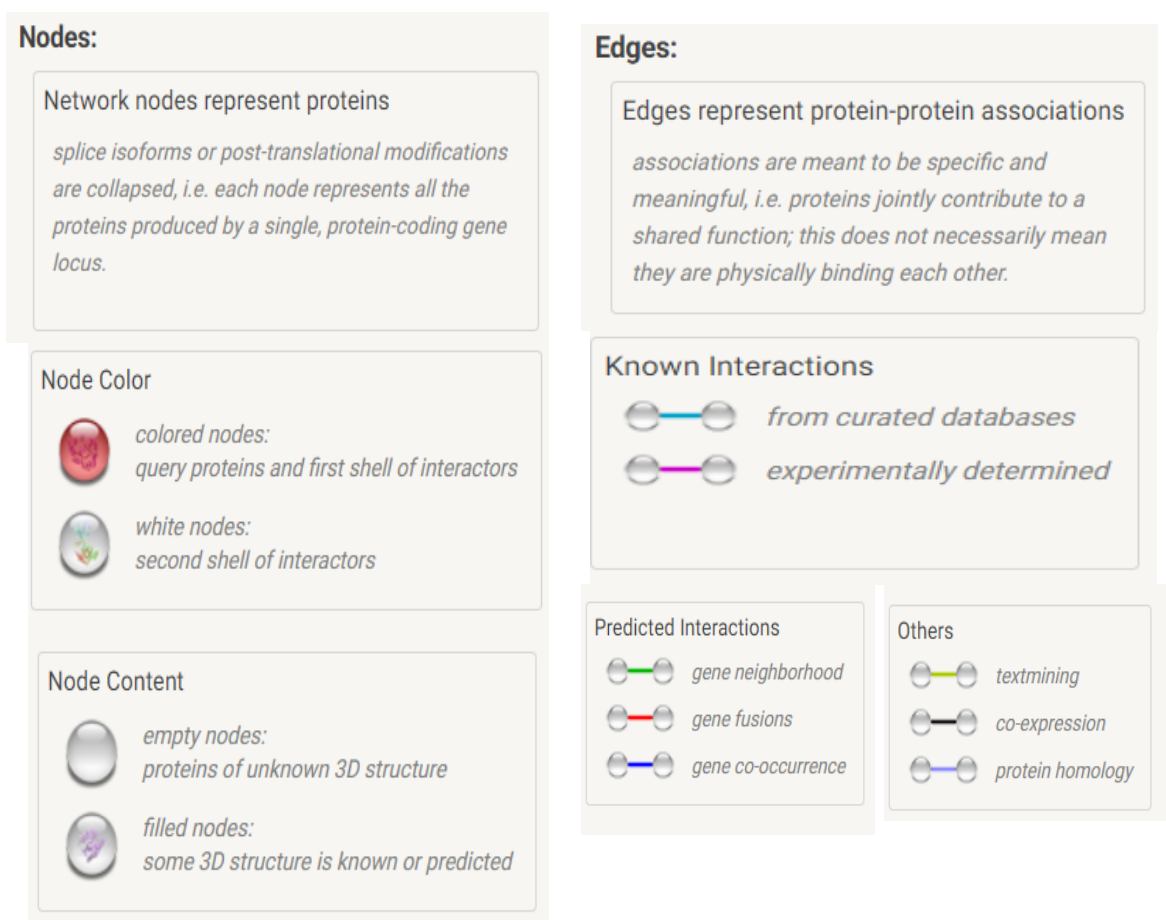


Figure 2.2 General String analysis legends

## ***Chapter 3- cell line characterization***

### **3.1 A375 melanoma cell lines**

Four stably transfected A375 melanoma cell lines were provided by Dr Corazzari (University of Piemonte Orientale, Novara) and Prof Lovat (University of Newcastle, UK) to be utilized for this study. Overexpression of Ambra1 and its matching control,  $\beta$ -galactosidase was performed by retroviral infection (Pagliarini et al., 2012). While knockdown of Ambra1 was performed by lentiviral infection that expresses a shRNA construct targeted to AMBRA1 and the control cell line expressed a scrambled shRNA control (Armstrong et al., 2015). Cell lines names used in this study are shown in Table 3.1.

**Table 3.1: modified A375 melanoma cells used and the method of modification**

A375 cells modification	Referred as	Method of stable transfection
Overexpressing Ambra1	rAmbra	Retrovirus overexpression
Overexpressing $\beta$ -galactosidase	rBgal	Retrovirus overexpression
Ambra1 knockdown	ShAmb	lentivirus infection
Ambra1 knockdown matched control	ShCon	lentivirus infection

### **3.2 Cell lines growth curves**

Initially Sulforhodamine B (SRB) assays were performed to study the effect of Ambra1 overexpression and knockdown on the proliferation rates of the four cell lines; in an attempt to answer one of the main initial hypothesis question “Does Ambra1 have a role in cancer cell proliferation?”. SRB assays was the only reliable and, inexpensive approach available at the start of the project. Towards the end of the project the faculty acquired a live cell imager, the Incucyte (Sartorius), which allows the acquisition of true proliferation rates by live cell counting rather than using an indirect measurement.

### **3.2.1 SRB analysis of rAmbra versus rBgal**

The overexpression model was analyzed by SRB to monitor the effect of Ambra1 overexpression on the A375 melanoma cell lines proliferation rate. Growth curves of rAmbra against the matching control rBgal were generated and statistically analyzed (Figures 3.1). A large number of assays (n=10) were performed using different passages aiming at generating a conclusion of the effect of Ambra1 overexpression on the proliferation rate. Results sometimes showed that rAmbra grew faster than rBgal and sometimes; the opposite was observed and also some other times; proliferation rates were observed to be similar for both cell lines. In conclusion data generated from 10 biological replicates was non-reproducible; some of these data are collected to show the different outcomes of SRB assays (Figure 3.2).

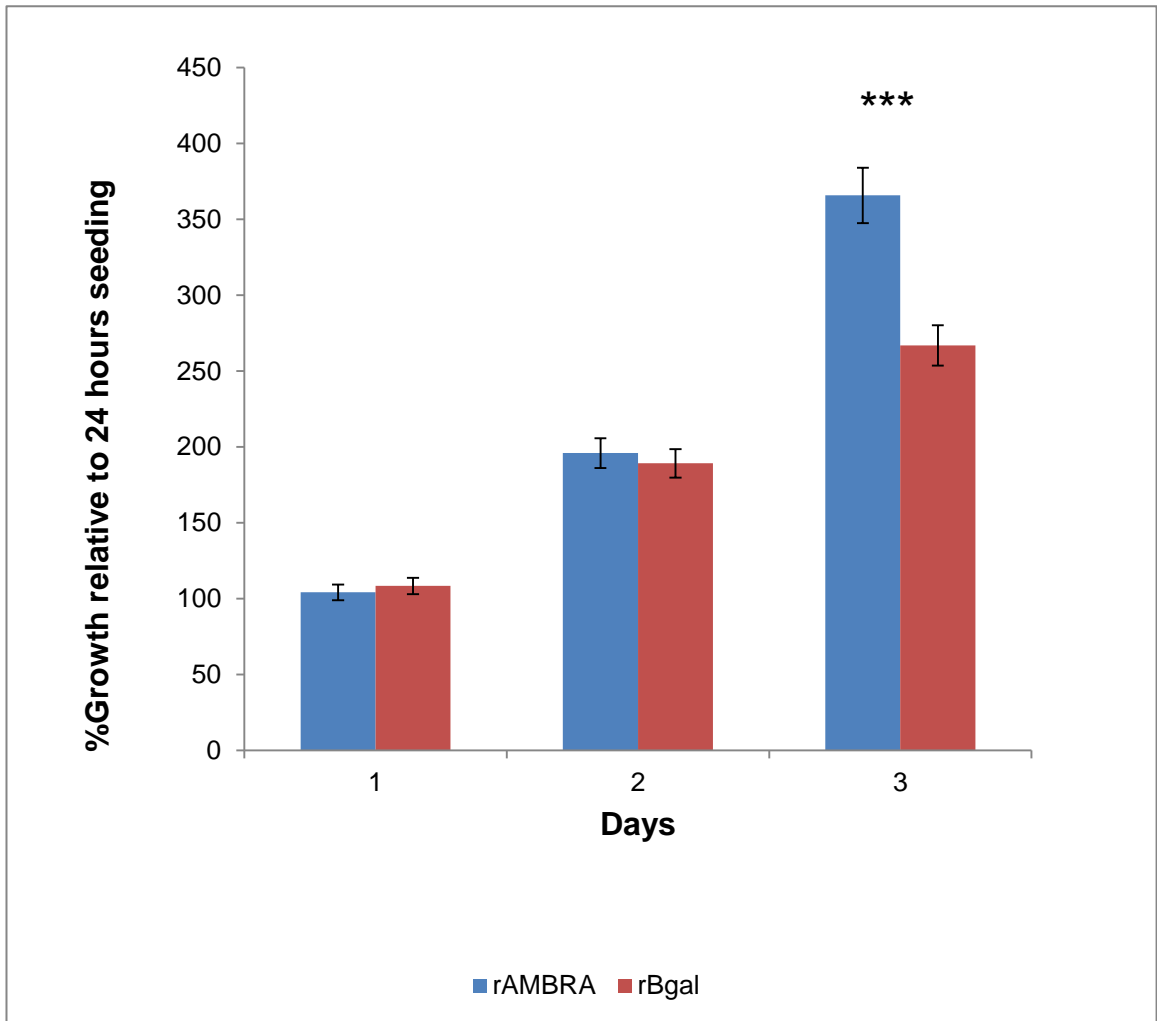


**Figure 3.1: graphical representation of SRB assay comparing the proliferation rate of rAmbra to rBgal cell lines over time.** Bar chart showing the % growth of the two cell lines after 2 and 3 days relative to cells counts at 24 hours from seeding, error bars represents +/- SD, n=48. Statistical analysis was performed by Mann-Whitney U-test, \*\*\*p<0.001 comparing the mean value of the %growth after 3 days to 1 day for each cell line, blue bars rAmbra, red bars rBgal.

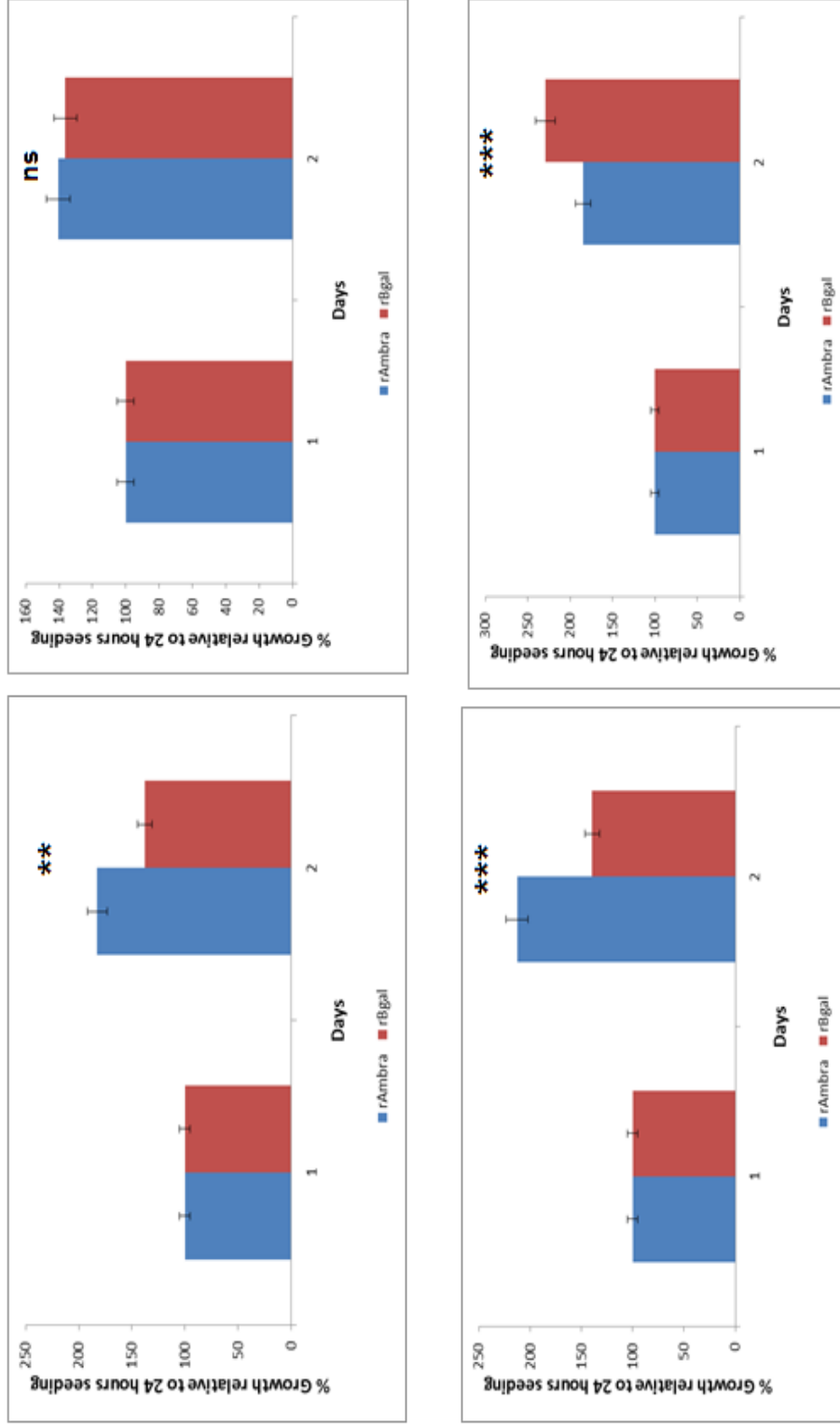


**Figure 3.2: graphical representation of SRB assays comparing the proliferation rate of rAmbra to rBgal from four different passages.** Bar charts showing the % growth of the two cell lines after 2 days relative to cells counts at 1 day from seeding, error bars represents +/- SD, n=48. Statistical analysis was performed by Mann-Whitney U-test, comparing the mean value of the %growth after 2 days to 1 day for each cell line, ns= non-significant, \*P<0.05, \*\*p<0.01, \*\*\*p<0.001 blue bars rAmbra, red bars rBgal

### **3.2.2 SRB analysis of ShAmb versus ShCon**

The knockdown model was also analyzed by the same technique to assess the proliferation rate of ShAmb against its matching control ShCon. SRB assays for Ambra1 knockdowns were performed 24 hours after selection antibiotic removal (Figure 3.3). Growth curves were generated and statistically analyzed. ShAmb proliferation rate was significantly slower than ShCon. SRB assays were repeated after extended period of growing both cell lines without antibiotic selection. Growth curves were generated and statistically analyzed (Figure 3.4). Difference in the proliferation rate between both cell lines was much smaller compared to the previous run which indicates that the effect of Ambra1 knockdown on the proliferation rate started to diminish compared to the ShCon.

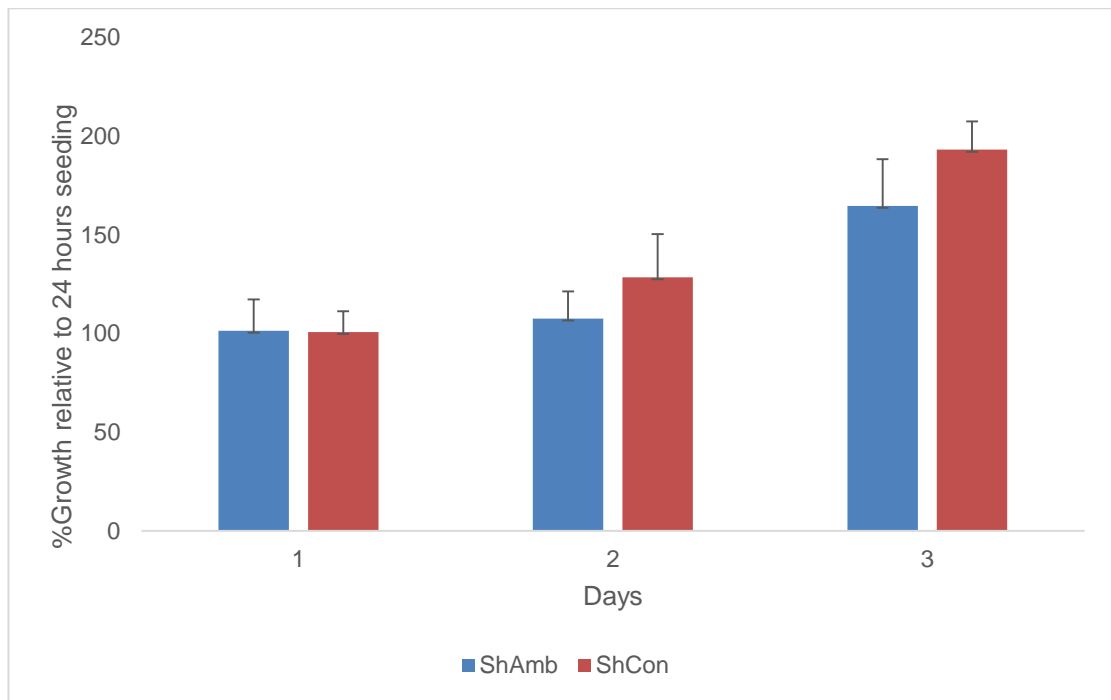


**Figure 3.3: graphical representation of SRB assay comparing the proliferation rate of ShAmb to ShCon cell lines over time.** Bar chart showing the % growth of the two cell lines after 2 and 3 days relative to cells counts at 24 hours from seeding, error bars represents +/- SD, n=48. Statistical analysis was performed by Mann-Whitney U-test, \*\*\*p<0.001 comparing the mean value of the %growth after 3 days to 1 day for each cell line, blue bars ShAmb, red bars ShCon.



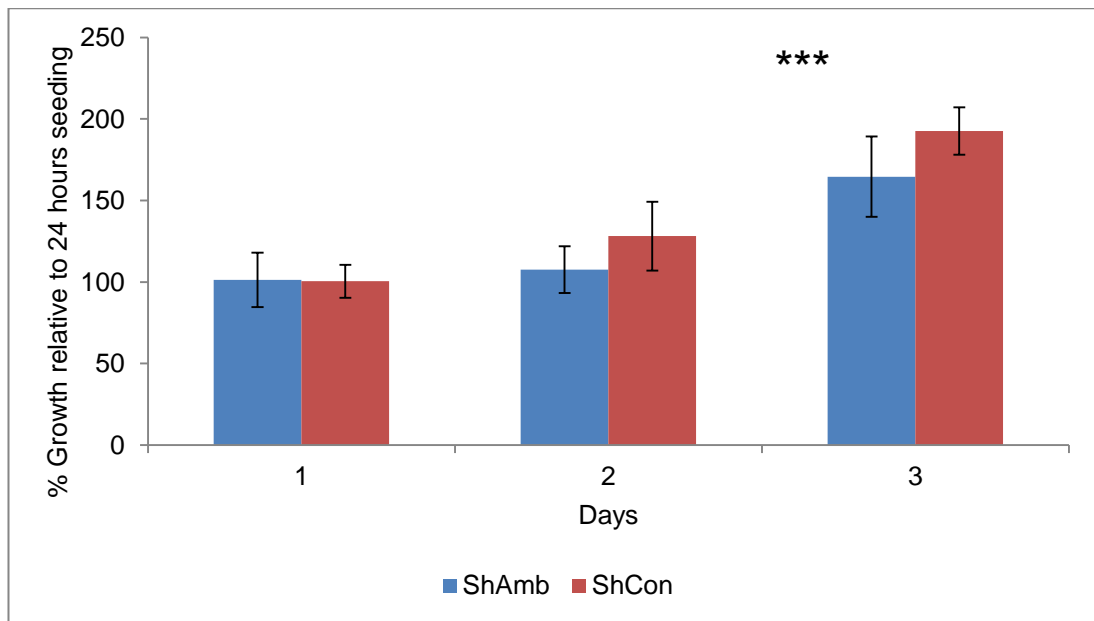


**Figure 3.4: graphical representation of SRB assay comparing the proliferation rate of ShAmb to ShCon cell lines over time after extended period of no antibiotic selection.** Bar chart showing the % growth of the two cell lines after 2 and 3 days relative to cells counts at 24 hours from seeding, error bars represents +/- SD, n=48. Statistical analysis was performed by Mann-Whitney U-test, \*\*\*p<0.001 comparing the mean value of the %growth after 3 days to 1 day for each cell line, blue bars ShAmb, red bars ShCon.

The reproducibility of the SRB assays after running 10 biological replicates was very limited, and it did not generate solid data regarding the effect of the change in Ambra1 expression on proliferation rates of the cell lines. Data generated from comparing rAmbra against rBgal was highly variable. ShAmb proliferation rate were mostly consistent to be slower than ShCon. However; a different technique to assess the effect of the expression of Ambra1 on the proliferation rate was required.

### ***3.2.3 Incucyte live cell imaging of the four cell lines***

Live cell imaging technique was performed later on to compare the proliferation rate of the four cell lines using Incucyte. Cells were seeded at the same densities (1500cell/well in 200µl) and, loaded to the Incucyte with or without antibiotic selection and, live images to monitor the growth were taken for up to a week starting from 24 hours after seeding. Growth curves were generated by the Incucyte software (Figure 3.5). Comparing growth curves generated for rAmbra and rBgal showed no difference in the proliferation rate for the overexpression of Ambra1. On the other hand; growth curves showed a distinguishable decrease in the proliferation rate of the ShAmb to all the three different cell lines. The proliferation rate of the ShAmb cell lines did not show a difference in the presence (Red) or the absence (purple) of the selection antibiotic for up to 72 hours. However; after 72 hours an outgrowth of the cells without an antibiotic selection was observed. To further demonstrate the effect of antibiotic selection on ShAmb proliferation rate; cells were grown for more than two weeks without antibiotic selection and proliferation rate was monitored (Figure 3.6). The complete removal of the antibiotic selection for extended periods of time leads to a no-difference in the proliferation rate of the ShAmb cell lines (Light blue) compared to the three other cell lines.

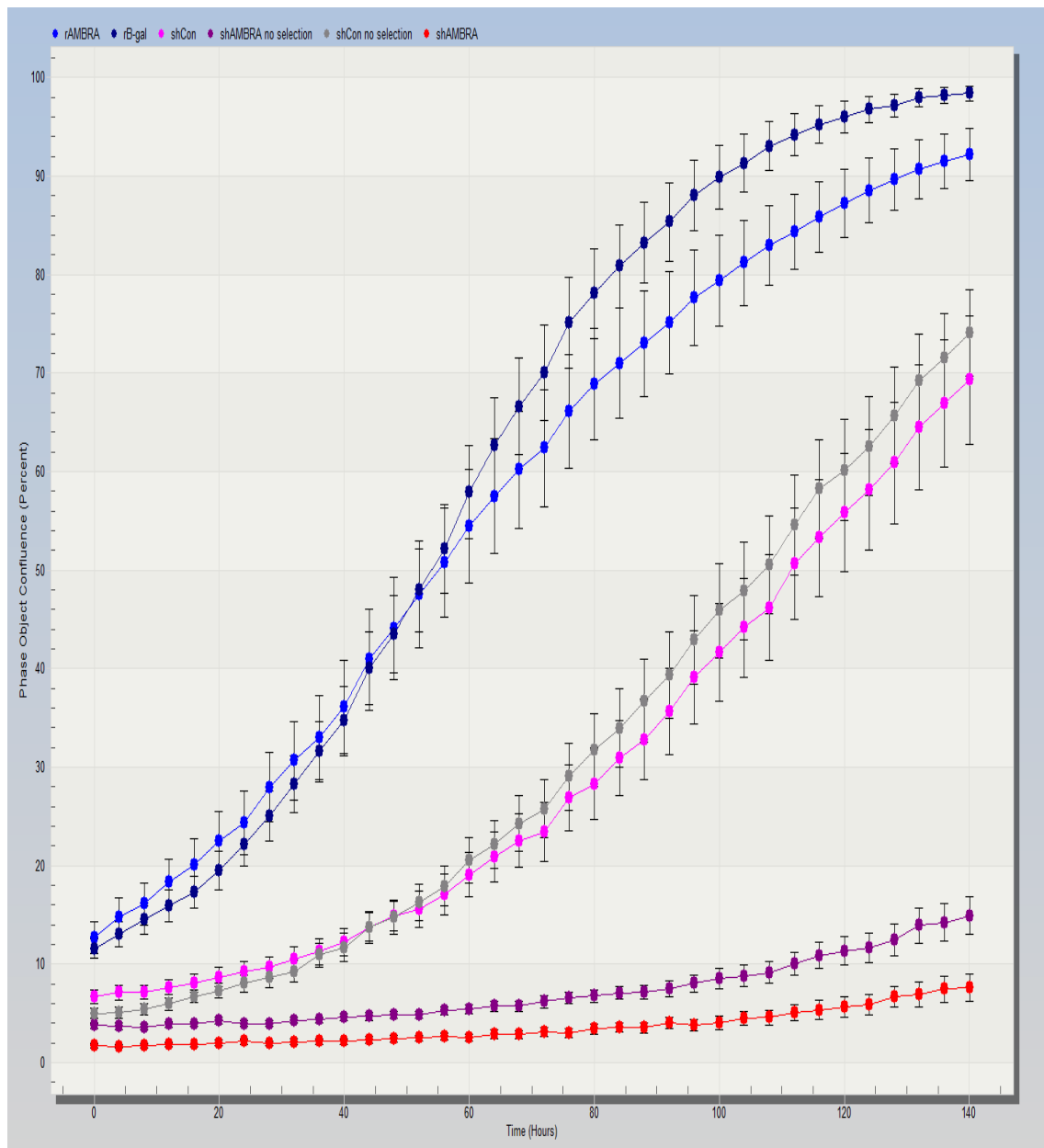


**Figure 3.5: Incucyte live cell imaging comparing the proliferation rates of the different A375 cell lines over time.** Growth curves are blotted by Incucyte software, phase object confluence percent (Y-Axis) against time in hours (X-Axis). Cells were seeded at the same densities (1500 cells/well, n= 24), and the knockdown model was seeded with and without antibiotic selection. The curves show that there is a slower proliferation rate of ShAmb compared to rAmbra, rBgal and ShCon. This effect of Ambra1 knockdown on the proliferation rate starts and continues to decrease after approximately 72 hours of growth, light blue rAmbra, dark blue rBgal, pink ShCon, grey ShCon no antibiotic selection, red ShAmb and, purple ShAmb no antibiotic selection.

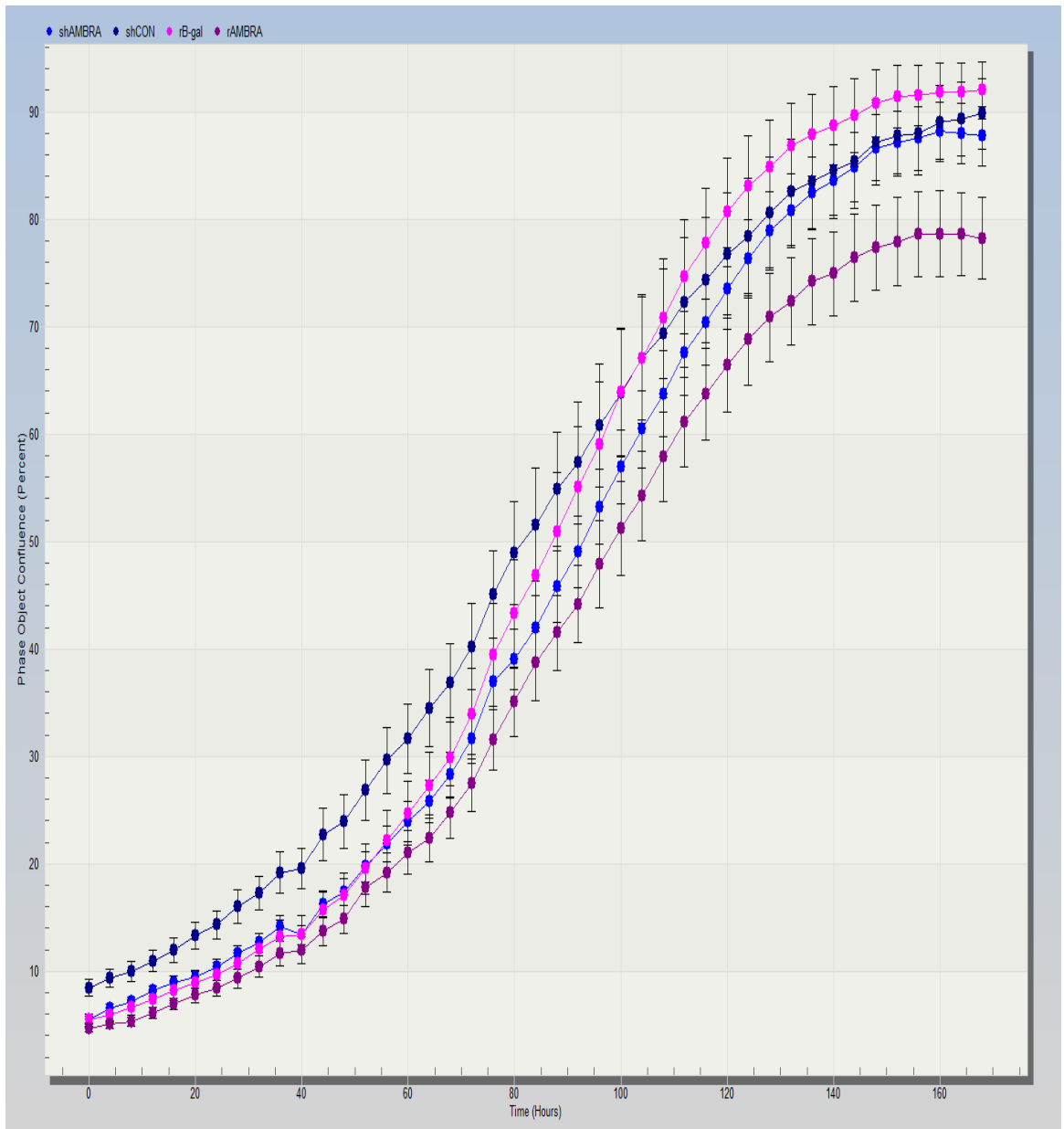
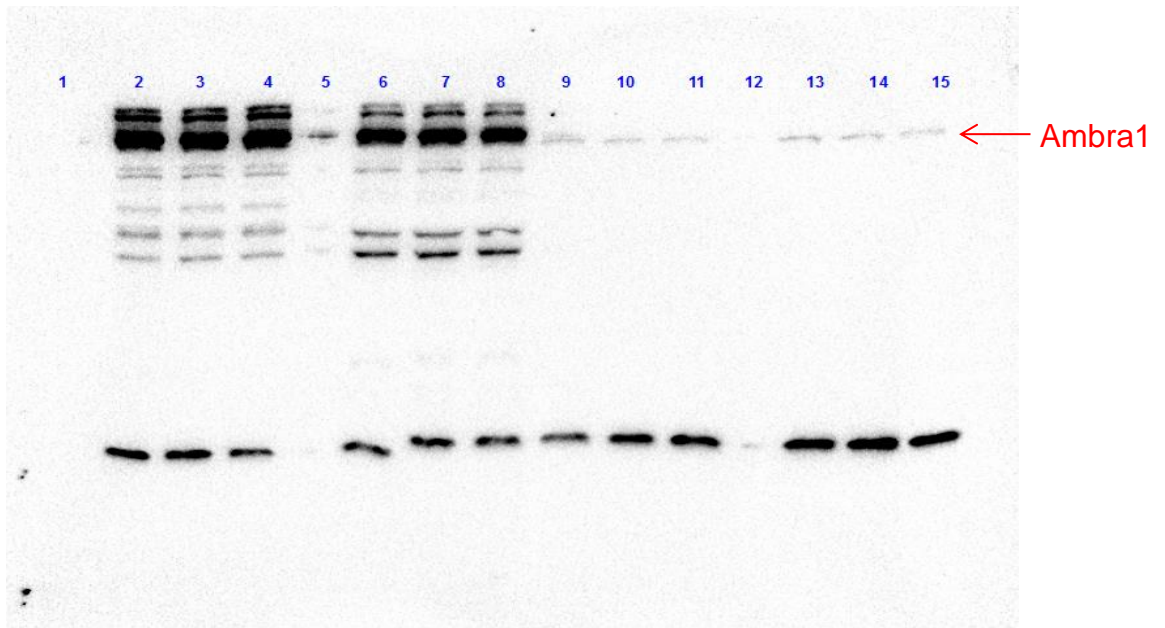


**Figure 3.6: Incucyte live cell imaging comparing the proliferation rates of the different A375 cell lines over time after extended period of no antibiotic selection.** Growth curves are blotted by Incucyte software, phase object confluence percent (Y-Axis) against time in hours (X-Axis). Curves show that there is almost no difference in the proliferation rate of the four cell lines when seeded at nearly the same density (n=24) upon the removal of antibiotic selection for weeks, purple rAmbra, pink rBgal, dark blue ShCon and light blue ShAmb.

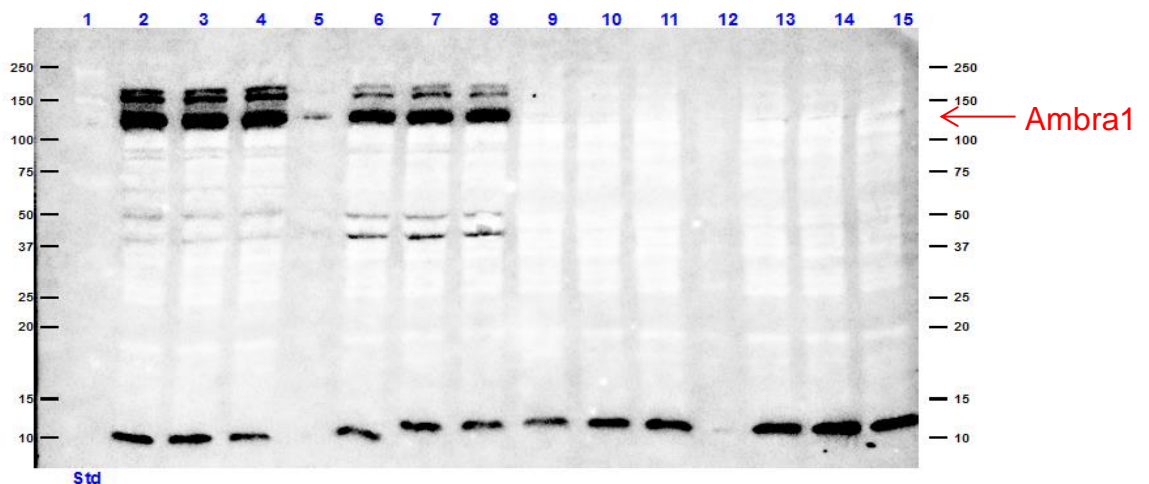
### **3.3 Western blot analysis of the cell line models**

Both the overexpression and the knockdown expression of Ambra1 were assessed in cell lines to confirm the phenotypic effect of the modifications. Western blot (WB) analyses were used to confirm the overexpression and the knockdown of Ambra1 in all cell lines. Ambra1 overexpression was confirmed in the rAmbra cell lines by WB analysis (Figure 3.7). The analysis showed a clear band for Ambra1 at ~130kD in the rAmbra cell lines and, these bands were very faint in the rBgal matching control cells, other bands were observed for rAmbra cell lines only at ~150kDa, ~90 kDa, 50 kDa and 30 kDa. A band is observed in both cell lines at ~10 kDa, these extra bands are discussed in details (5.3). A merged image of the western blot overlaid on a stain free image of the PVDF membrane showing total protein is also shown to demonstrate equal loading in each lane. The weak band intensities of the Ambra1 in rBgal cell lines indicates that endogenous Ambra1 levels are low and hence; its detection is challenging.

$\beta$ -galactosidase overexpression was also confirmed by WB (Figure 3.8) and a band was observed in the rBgal cells only at ~116kDa. The stain free TGX gel image merged with the western blot demonstrates slight difference in protein loading in each lane. However; this technical error should not affect the results as the concentration of total protein is higher in rAmbra yet no bands for  $\beta$ -gal were observed.



(A)



(B)

**Figure 3.7: Western blot analysis of Ambra1 overexpression model.** (A) Western blot analysis showing Ambra1 overexpression in the transfected melanoma cell lines (rAmbra) compared to the matching control overexpressing B-Galactosidase (rBgal). Lanes 2 to 4 and lanes 6 to 8 are technical replicates of different rAmbra extracts from two different passages. Lanes 9 to 11 and lanes 13 to 15 are technical replicates of different rBgal extracts from two different passages. Ambra1 is observed at ~130 KDa for rAmbra cell lines as well as four bands at ~150, 90, 50 and 37 KDa. A cross reactive protein is showing bands at ~10 KDa in both cell lines. Ambra1 band at ~130 kDa is also observed for rBgal cells. (B) A merged image of the western blot overlaid on a stain free image of the PVDF membrane showing total protein to demonstrate equal loading in each lane.

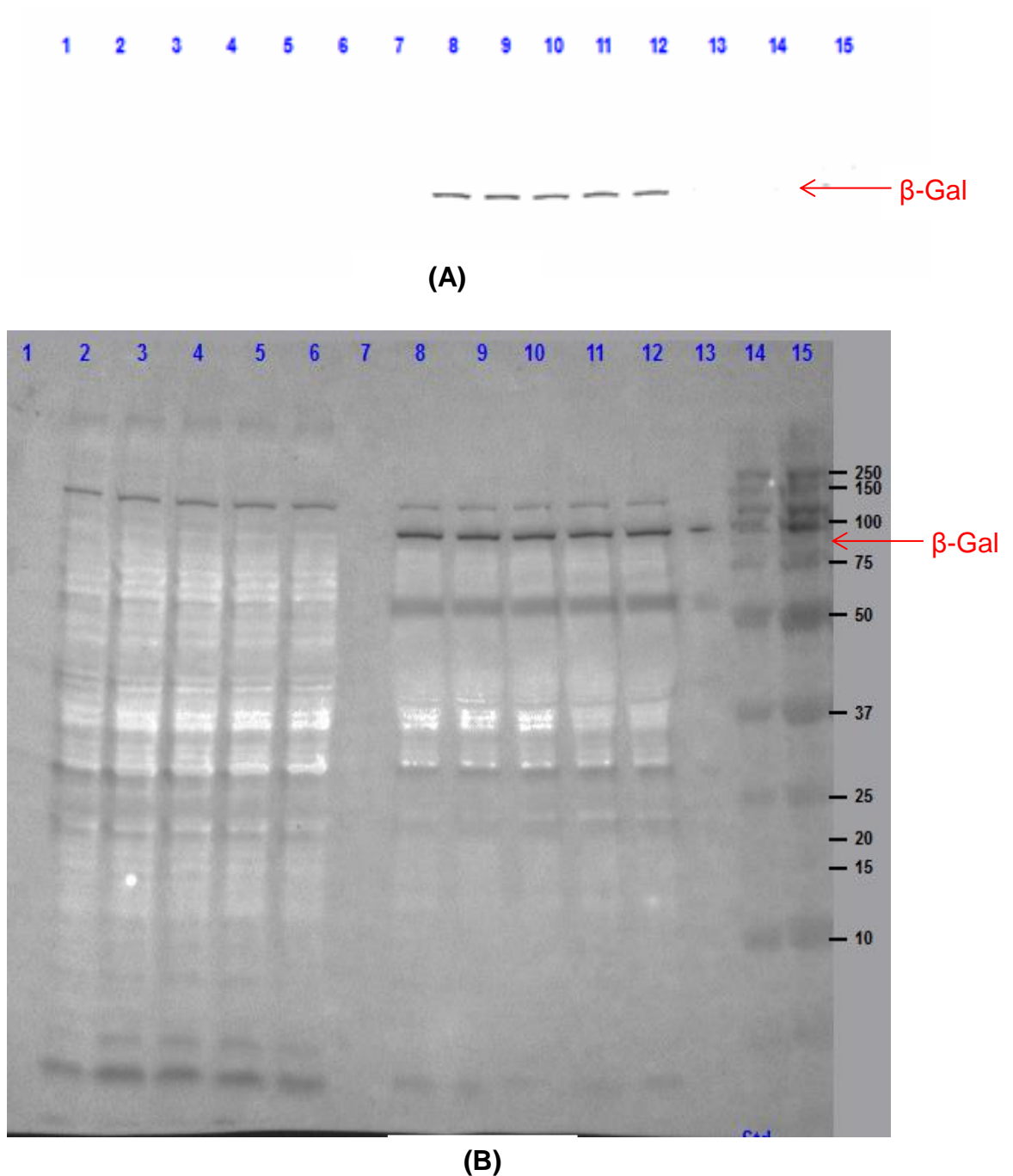
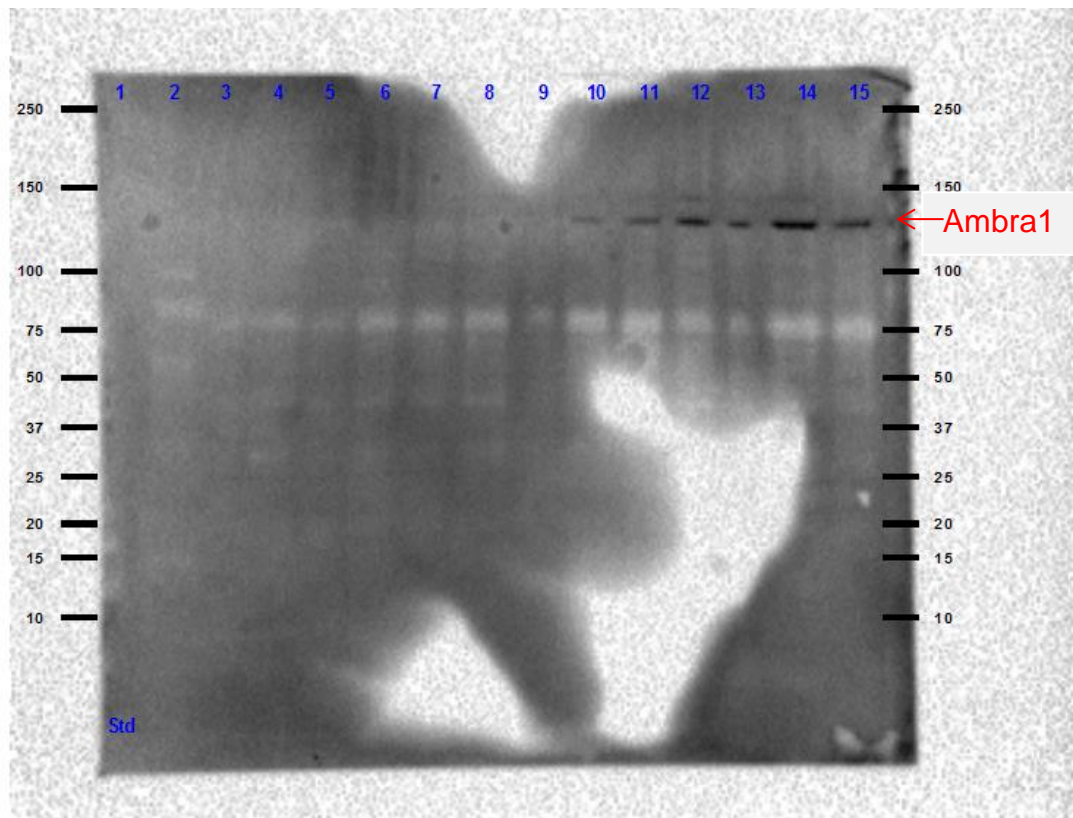


**Figure 3.8: Western blot analysis of  $\beta$ -galactosidase protein in the overexpression model.** (A) Lanes 2 to 3 and lanes 4 to 6 are technical replicates of rAmbra protein extracts from two different passages. Lanes 8 to 9 and lanes 10 to 12 are technical replicates of rBgal of protein extracts from two different passages. A band for  $\beta$ -galactosidase can be observed at ~116kDa for rBgal cell lines only. (B) A merged image of the western blot overlaid on a stain free TGX gel image of showing total protein to demonstrate loading in each lane.

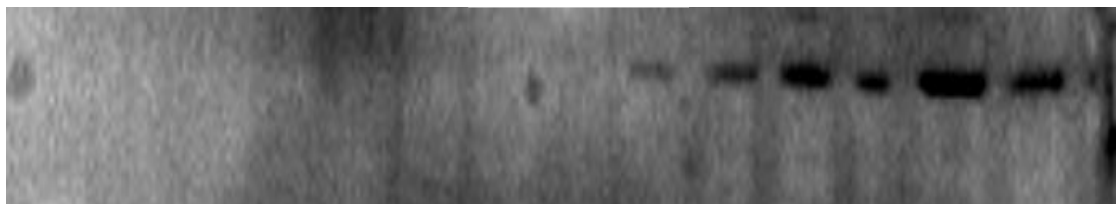
Ambra1 knockdown was also confirmed by western blot analysis in the knock down model (Figure 3.9). However; detecting a band for Ambra1 at such low levels of endogenous expression, as well as; even lower levels in the knockdown cells was challenging and images generated were not of a good quality. A band was observed for Ambra1 at~130KDa in the ShCon cell lines and not in the ShAmb cell lines which confirms the knockdown of Ambra1 in the ShAmb cell lines.

ShAmb cells behaved differently to the three other cell lines in terms of proliferation rate and morphology; an effect that was gradually diminished upon the release of the selection antibiotic. A western blot analysis was performed after extended period of no antibiotic selection to monitor the level of Ambra1 in the ShAmb (Figure 3.10), under no antibiotic selection ShAmb cells were able to compensate for the shRNA mediated knockdown of Ambra1 to levels comparable to ShCon. The image for the TGX-stain free gel used shows slight difference of total protein loaded in each lane. These differences match with the band intensities on the western blot.



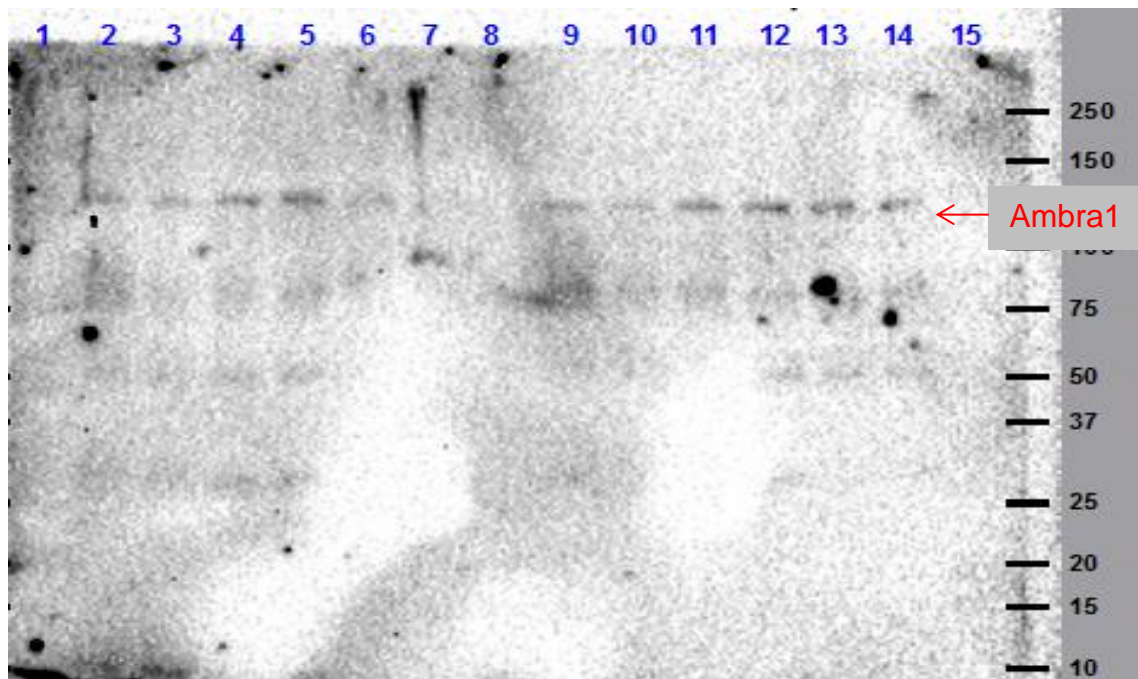


(A)

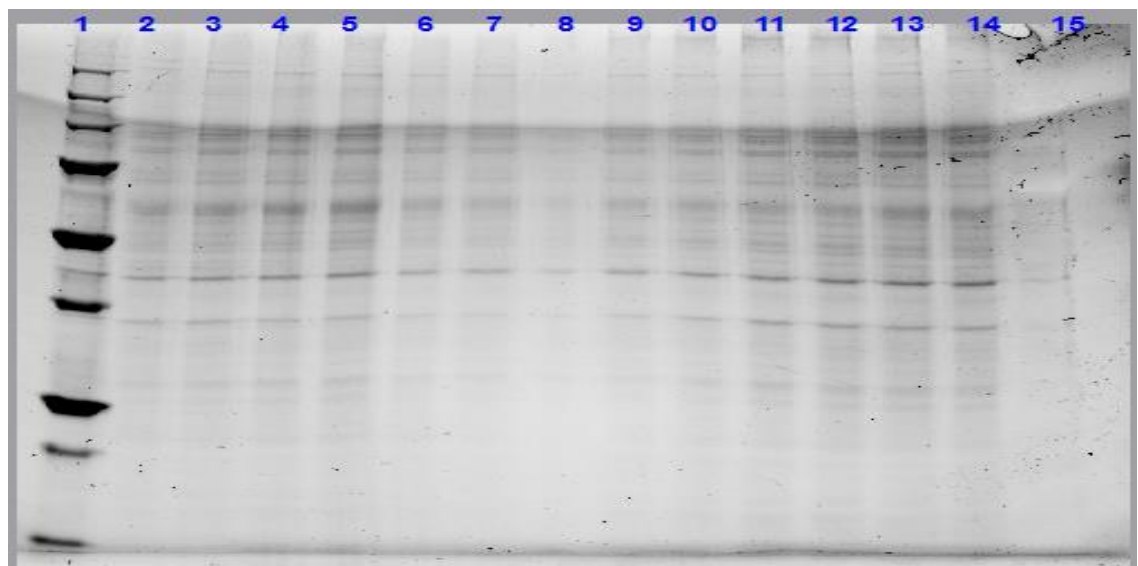


(B)

**Figure 3.9: Western blot analysis of Ambra1 Knockdown model.** (A) Western blot analysis showing Ambra1 knockdown in the transfected melanoma cell lines ShAmb compared to the matching control ShCon. Lanes (3 and 4), (5 and 6) and (7 and 8) are technical replicates of biological ShAmb extracts from three different passages. Lanes (10 and 11), (12 and 13) and (14 and 15) are technical replicates of biological ShCon extracts from three different passages. A band can be observed at ~130 KDa for ShCon cell lines and not for the ShAmb. (B) Cropped image from A different exposure showing clearer highlighting the bands for Ambra1 in the ShCon cell lines compared to the ShAmb knockdown cells.



(A)



(B)

**Figure 3.10: Western blot analysis of Ambra1 Knockdown model after extended period of no antibiotic selection.** (A) Western blot analysis showing Ambra1 re-expression in the ShAmb compared to the matching control ShCon. Lanes (2 and 3), (4 and 5) and (6 and 7) are technical replicates of biological ShAmb extracts from three different passages. Lanes (9 and 10), (11 and 12) and (13 and 14) are technical replicates of biological ShCon extracts from three different passages. A band can be observed at ~130 KDa for both cell lines. (B) TGX gel used showing total protein to demonstrate loading in each lane.

### **3.4 Discussion**

Sulforhodamide B (SRB) assays were developed to measure drug-induced cytotoxicity and cell proliferation. Its principle is based on the ability of the protein dye Sulforhodamide B to bind electrostatically and pH dependent on protein basic amino acid residues of trichloroacetic acid-fixed cells. Under mild acidic conditions it binds to and under mild basic conditions it can be extracted from cells and solubilized for measurement. Results of the SRB assay were linear with cell number and cellular protein measured at cellular densities ranging from 1 to 200% of confluence. It performed similarly compared to other cytotoxicity assays such as MTT or clonogenic assay. This assay is reliable, reproducible and inexpensive approach to study these effects on proliferation rate (Orellana and Kasinski, 2016). A different study compared to MTT assays to three different cell enumeration assays, one of which was SRB, showed superiority of SRB over MTT assays in terms of variability of results (van Tonder et al., 2015). Generally speaking there is a limitation in all colorimetric assays including SRB, as none of these assays are able to directly count the number of viable cells but rather; the viability of the cells based on protein binding ability of the dye used. Specific limitations to SRB assays include: complicated procedures and, manual handling of the cells especially during repeated washing and drying steps which can be a source of technical variance (Aslantürk, 2018).

Using SRB assays to study the proliferation rate of the cell lines was based on the reported reliability of this technique. However, data generated from SRB was mostly irreproducible (n=10). The difference between rAmbra and rBgal was highly variable. In some cases the proliferation rate of rAmbra was significantly higher while, in other cases it was significantly lower. Five different

cell passages were tried and data was constantly variable. However, the reproducibility of SRB assays cannot be judged based on this experiment as the variability in the results might be well due to the lack of a direct effect of Ambra1 overexpression on the proliferation rate of the transfected melanoma cell lines rather than the technique used. With all of the colorimetric assays for measuring proliferation, such as SRB, the assay is indirect and metabolic differences can significantly affect results. Metabolic differences could arise due to different passage numbers and variations in initial cell density. These assays do not actually measure directly the number of cells.

These drawbacks of SRB assays were overcome by the use of Incucyte live cell imaging which is a semi-automated microscopy based system that captures cell growth inside an incubator by the production of time-lapse images. Numbers of cells are calculated based by training the software to recognize cells and the confluency on the surface of the plastic ware is calculated. Growth rates produced are therefore based upon actual cell counts. The use of live cell imaging confirmed that there is no discernable difference in the proliferation rate of rAmbra1 compared to rBgal when seeded at the same density in a rich media (DMEM) with high glucose.

However, the ShAmb cell line viability was noticeably different to the ShCon matching control and to the rAmbra and rBgal cell lines. ShAmb cells tended to grow much slower compared to the three other transfected cell lines when seeded at the same density. It took almost double the time compared to other cell lines to reach a confluency of 70-80%. ShAmb cells also looked different and not as healthy under the microscope, the morphology tended to be distorted with spiky protrusions at the edge of the cell membrane. These differences appeared to diminish gradually after the removal of the selection

antibiotic and growth rate began to match that of the other three cell lines. Incucyte live cell images showed that there is a distinguishable decrease in the proliferation rate of the ShAmb compared to all the three different cell lines; with the antibiotic selection and initially after the antibiotic selection removal. SRB assays were much more consistent in demonstrating slower proliferation rate than ShCon where the effects are more marked. Western blot analysis after an extended time of no antibiotic selection showed that ShAmb cells had Ambra1 expression that had returned to normal levels.

Unpublished data generated by the Lovat laboratory, Newcastle University (Jane Armstrong, *pers. Comm.*) showed that cell proliferation in primary cells can be increased by the transient Ambra1 knockdown (siRNA). However, some cells become non-viable upon stable knockdown of Ambra1 by shRNA. In this study, it is clear that the knockdown of Ambra1 is highly unfavorable to the cells and results in decreased proliferation rates. The effect of Ambra1 knockdown on the proliferation rate of the ShAmb cell lines starts to gradually diminish after approximately 72 hours of selection antibiotic removal, and that this effect was completely lost after around two weeks of no selection. Coupled with the western blot data it appears that the cells appear to eject the shAmbra construct resulting in an outgrowth of more rapidly dividing “wild type” A375 cells that express Ambra1 at normal levels. Often the ShAmb cells could be rescued by reapplying the selection where initially 80-90% of cells were killed by selection (results not shown) supporting the theory that without selection there is a strong biological drive to restore “normal” levels of Ambra1 in the cells. This suggests that the complete loss of Ambra1 could be lethal in a full genetic knockout.

The roles of Myc, mTORC1 and, Ambra1 in cell proliferation have been discussed (1.3.5, 1.3.7 and 1.6.5). It is clear that in non-tumor cells mTORC1

has the opposite effect to Ambra1 on cell proliferation, mTORC1 is an upstream effector of Ambra1 and, signaling between mTORC1 and Ambra1 is not limited to cell proliferation, it extends to nearly all Ambra mediated roles as Ambra1 is primarily inhibited by mTORC1 under normal conditions (Nazio and Cecconi, 2013), and upon cellular signals that inhibit mTORC1 like nutrient deprivation Ambra1 is activated by dephosphorylation and is released from the dynein motor complex (Di Bartolomeo et al., 2010). Ambra1 activation reduces cell proliferation by enhancing the activity of the catalytic subunit PP2CA leading to the de-phosphorylation and degradation of the proto-oncogene c-Myc (Cianfanelli et al., 2015). However, growth curves generated in this study show that in the melanoma A375 cell lines and under nutrient rich conditions Ambra1 overexpression does not inhibit cell proliferation and, Ambra1 knockdown dramatically decrease cell proliferation, which is the exact opposite of Ambra1 reported role in normal cells, Ambra1 levels in late stage metastatic melanomas is yet to be explored. However, its loss in stage I melanomas identifies high-risk tumor subsets, this was identified by monitoring Ambra1 levels in epidermis overlaying primary melanomas, the same group of researchers demonstrated the ability of Ambra1 to regulate keratinocytes differentiation (Ellis et al., 2019). In summary, they have demonstrated that Ambra1 levels are decreased in the proliferative compartment of the epidermis and elevated in the differentiating compartment.

mTORC1 is a very complex signaling pathways, its role is fundamental in coordinating anabolic and catabolic processes, deregulation of mTORC1 is reported in a vast majority of human cancers, in melanoma mTORC1 constitutive activation is essential for metastasis (1.4), unlike normal cells, in cancer the activation of mTORC1 does not necessarily lead to autophagy

inhibition (Paquette et al., 2018), in fact there are studies that reported autophagy over activation in late stage melanomas, to the extent that autophagy inhibitors to treat melanoma are in clinical trials (Ndoye and Weeraratna, 2016). What is already known about mTORC1 and autophagy in melanomas may give an explanation to the effect of Ambra1 differential expression on the proliferation rates of the melanoma A375 cell lines, Ambra1 may be overexpressed in metastatic melanoma to an extent that further overexpression of this gene appear to not have an effect on the proliferation rate, on the other hand, Ambra1 knockdown appear to decrease the metastatic melanoma proliferation rate, whether this effect is mediated by autophagy which is essential for cell survivals in the case of metastatic cancers, or a different mechanism is a question that require an answer to fully understand this role.

As the project progressed it was clear that the overexpression of Ambra1 in media that is not nutrient limiting did not appear to significantly play a direct role in cellular proliferation as a consequence the role of the Ambra1 knockdown effects became the focus of the transcriptomic analysis (Chapter 6).

## ***Chapter 4- Ambra1 protein binding partners***



## **4.1 Introduction**

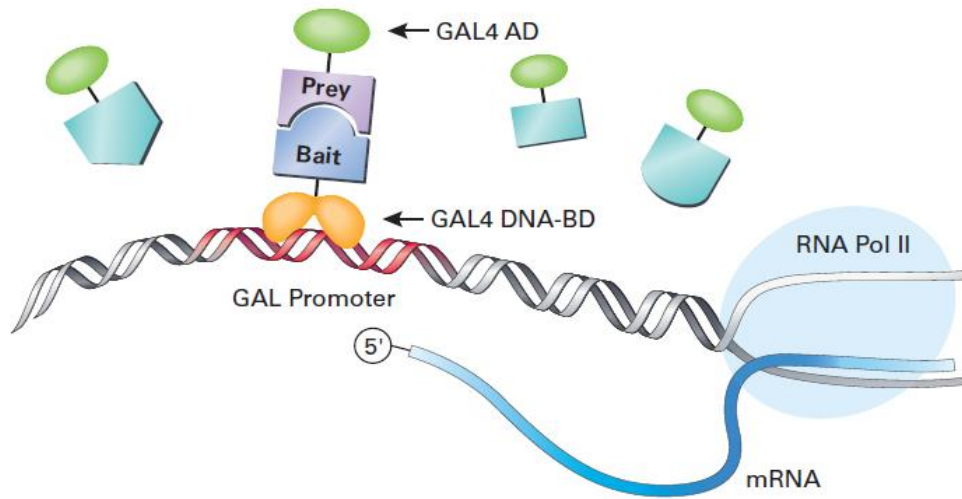
The physical interaction between proteins or other molecules determines their biological activity (Alberts et al., 2002). The detection of such interactions is of an importance in understanding the organization and the function of the proteome. The Ambra1 protein contains a number of WD 40 domains (Cianfanelli et al., 2015) and, is part of a group of proteins referred to as intrinsically disordered proteins (IDPs). IDPs appear to have a very fluid structure which appears to increase the number of specific protein-protein interactions they can engage in and may make them hubs for protein interaction complexes (Csizmok et al., 2016). This makes the study of protein-protein interactions with Ambra1 particularly intriguing to identify its potential for regulating and connecting different biological processes. Many biochemical techniques have been employed to detect protein-protein interaction such as co-immunoprecipitation (Co-IP), affinity purification and co-purification; however, these methods have limitations, perhaps the most important is that these techniques require *in-vitro* handling of protein, unlike Y2H which preserves the native surroundings in which the interaction takes place and is monitored. (Brückner et al., 2009).

In 1989 Stanley Fields and Ok-kyu Song reported a novel technique for *in-vivo* study of protein-protein interactions by using the yeast *Saccharomyces cerevisiae* and they applied this technique to test for protein-protein interaction between SNF1 and SNF4 proteins known to interact with each other (Fields and Song, 1989). This technique is called “Yeast-two-hybrid” and it utilizes the properties of a transcription factor called GAL4. GAL4 binds to a specific sequence on DNA known as the upstream activation domain (UAS). GAL4 is relatively simple and consists of just two functional domains that are at distinct

ends of the protein: The: N-terminal domain which is DNA binding domain (DBD) and C-terminal which is transcription activation domain (AD) (Keegan et al., 1986). Functional GAL4 activation requires the two domains to be within close proximity of each other. The principle of the assay is the two domains are split into two individual proteins that have no natural affinity. Fusion proteins with the domains are then constructed containing two potential naturally binding proteins or domains to reconstitute a functionally active GAL4. Generally, the protein of interest is attached to GAL4 DBD which is called the “Bait” and is typically assayed against a library of proteins translationally fused to the GAL4 AD referred to as “Prey” (Figure 4.1A). When bait and prey protein interact, the GAL4 activates transcription and by testing for the expressed proteins, interaction can be detected (Chien et al., 1991). The Matchmaker Gold Yeast Two-Hybrid System (Clontech) was used in this study. It is one of the most advanced systems due to a combination of a new yeast strain (Y2H Gold), stringent reporters, easy-to-use libraries and, high-level expression vectors. This system requires the activation of four reporter genes under the control of three distinct Gal4-responsive promoters (Figure 4.1B) to detect protein interactions:

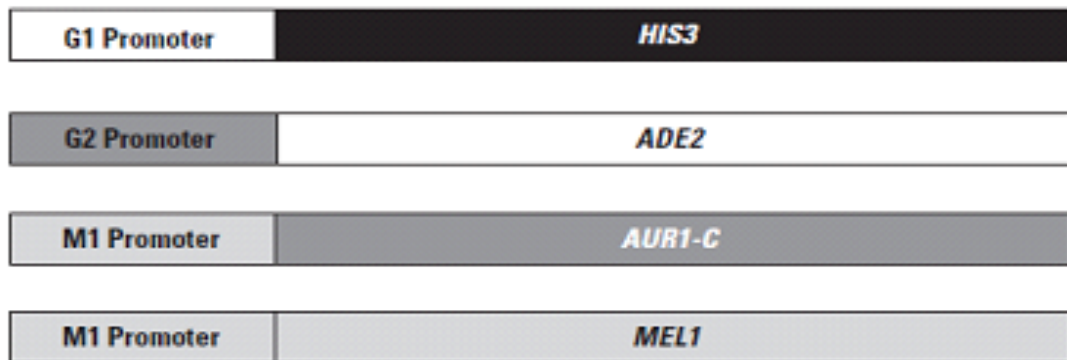
- ***AUR1-C***: A dominant mutant version of the *AUR1* gene that encodes the enzyme inositol phosphoryl ceramide synthase. *AUR1-C* is expressed in Y2HGold Yeast Strain in response to protein-protein interactions that bring the GAL4 transcriptional activation and DNA binding domains into close proximity. In *Saccharomyces cerevisiae*, its expression confers strong resistance (AbAr) to the otherwise highly toxic drug Aureobasidin A.

- **HIS3:** Y2HGold is unable to synthesize histidine and is therefore unable to grow on media that lack this essential amino acid. When bait and prey proteins interact, Gal4-responsive *His3* expression permits cells to biosynthesize histidine and grow on –His minimal medium.
- **ADE2:** Y2HGold is also unable to grow on minimal media that does not contain adenine. However, when two proteins interact, *Ade2* expression is activated, allowing these cells to grow on –Ade minimal medium.
- **MEL:** *MEL-1* encodes  $\alpha$ -galactosidase, an enzyme occurring naturally in many yeast strains. As a result of two-hybrid interactions,  $\alpha$ -galactosidase (*MEL1*) is expressed and secreted by the yeast cells. Yeast colonies that express Mel1 turn blue in the presence of the chromogenic substrate X-a-Gal.

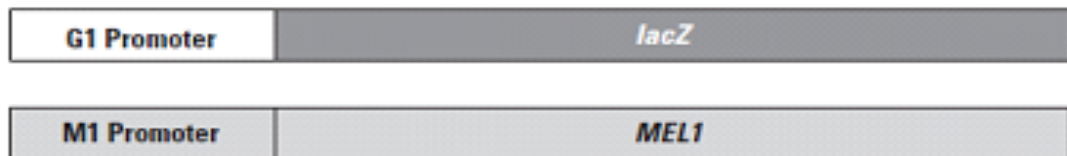


(A)

#### Y2H gold (Mating Partner) reporter gene constructs



#### Y187 (Library Host Strain) reporter gene constructs



(B)

**Figure 4.1: The yeast Two Hybrid principle.** (A) Two proteins are expressed separately, one (a bait protein) fused to the Gal4 DNA-binding domain (BD) and the other (a prey protein) fused to the Gal4 transcriptional activation domain (AD). In Y2HGold Yeast Strain, activation of the reporters (*AUR1-C*, *ADE2*, *HIS3*, and *MEL1*) only occurs in a cell that contains proteins which interact and bind to the Gal4-responsive promoter. (B) In Y2HGold, the *HIS3*, *ADE2*, and *MEL1/AUR1-C* reporter genes are under the control of three completely heterologous Gal4-responsive promoter elements—G1, G2, and M1, respectively. The protein-binding sites within the promoters are different, although each is related to the 17-mer consensus sequence recognized by Gal4 (Figures adapted from Clontech Laboratories).

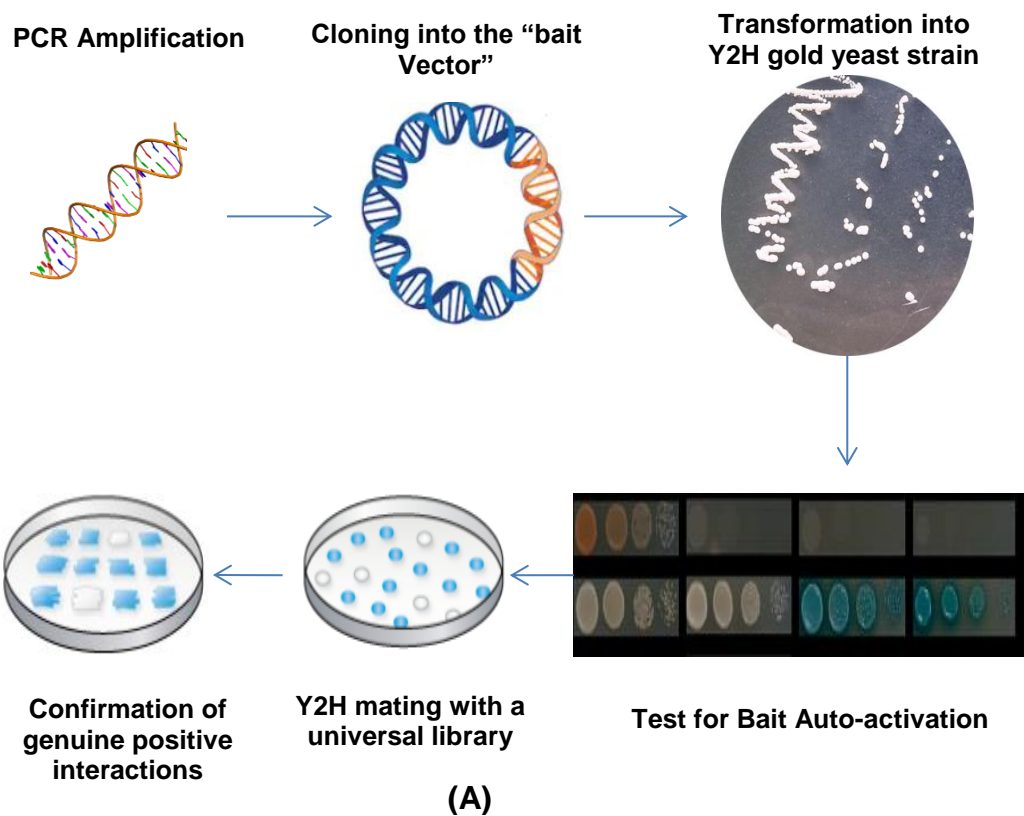
The aim of this part of the study was to apply the Y2H assay to investigate potential Ambra1 protein-protein interactions using the full length Ambra1 complementary DNA encoding 1298 amino acids; Uniprot isoform 1 ID: Q9C0C7-1 (<https://www.uniprot.org/uniprot/Q9C0C7>). The use of the Y2H assay to screen for binding partners of Ambra1 had been previously reported prior to this study commencing. A cDNA encoding the first 667 amino acids of the human Ambra1 cDNA ORF was used as bait and screened against a human brain cDNA library from this, Ambra1-BECLIN1 interaction was reported in this study and confirmed by co-immunoprecipitation (Fimia et al., 2007). Later on the same team published the use of the same approach to identify Ambra1 interaction with PP2CA (Cianfanelli et al., 2015). Another yeast two hybrid assay was performed by cloning the C-terminal region (aa 533–1,269) cDNA of Ambra1, this study identified the interaction between Ambra1 and DLC1 (Di Bartolomeo et al., 2010). However, screening of the full length Ambra1 against a universal protein library using this technique has not been reported.

## **4.2: Yeast two Hybrid work flow**

The Y2H assay is a multi-step process that can be classified into:

1. Amplifying the gene of interest by PCR.
2. Cloning the gene of interest into the DNA binding domain (DNA-BD) (pGBKT7).
3. Transforming the recombinant pGBKT7 into Y2H gold yeast strain.
4. Testing for the gene of interest (Bait) auto-activation of the reporter genes.
5. Mating transformed Y2H gold strain with a normalized universal mate and plate library cloned in Y187 yeast strain.
6. Positive interactions between the assayed bait and different preys are plated on X- $\alpha$ -gal and Aureobasidin highly strict plates (SD/–Ade/–His/–Leu/–Trp), which allows the growth of selected genuine positive interactions only that can activate the four reporter genes (*AUR1-C*, *HIS3*, *ADE2* and, *MEL1*).
7. Isolation and rescuing plasmids of positive interactions
8. Sequencing the picked up preys to identify the interactor proteins of the tested bait.

A summary of the workflow can be seen in Figure 4.2.



Ambra1 was amplified by PCR and initial trials to clone it into the desired vector was unsuccessful, different approaches were applied to address possible issues.

PP2CA control experiments were performed and issues in cloning Ambra1 were identified to be mainly the selected restriction enzymes with traditional digestion and sticky end ligation.

Ambra1 was cloned into the desired vector by using fusion cloning technique.

Both Ambra1 and PP2CA passed auto-activation tests and, Yeast two hybrid matings were performed. Novel binding partners were identified for both Ambra1 and PP2CA.

(B)

**Figure 4.2: Yeast two-hybrid work flow.** (A) General Y2H workflow design for this study. (B) Summary of Ambra1 and PP2CA control experiment Y2H work flow. Arrows represent proceeding to the following step.

## **4.3 Results**

### **4.3.1 Amplifying Ambra1 by PCR**

#### **4.3.1.1 Ambra1 primers design**

The initial step of performing the Y2H was to design the primers to amplify Ambra1 by PCR. The DNA-BD vector has the restriction sites: *Nde* I, *Nco* I, *sfi* I, *EcoR* I, *Sma* I/*Xma* I, *Bam*H I, *Sal* I and *Pst* I (Figure 4.3). The Ambra1 cDNA sequence is ~4Kb. An *in-silico* digest of Ambra1 ORF using NEBcutter showed that of the enzymes sites available in the vector that most resulted in cuts within the ORF (Figure 4.4). These enzymes include : *Bam*H I, *Nco* I, *Pst* I and *Sal* I the primers were therefore designed with the restriction sites: *EcoR* I and *Nde* I. An initial set of Ambra1 primers was designed to have *Nde* I restriction site on the forward and *EcoR* I restriction site on the reverse primers. Primers were termed Ambra1Ffull and Ambra1Rfull respectively (Figure 4.5)



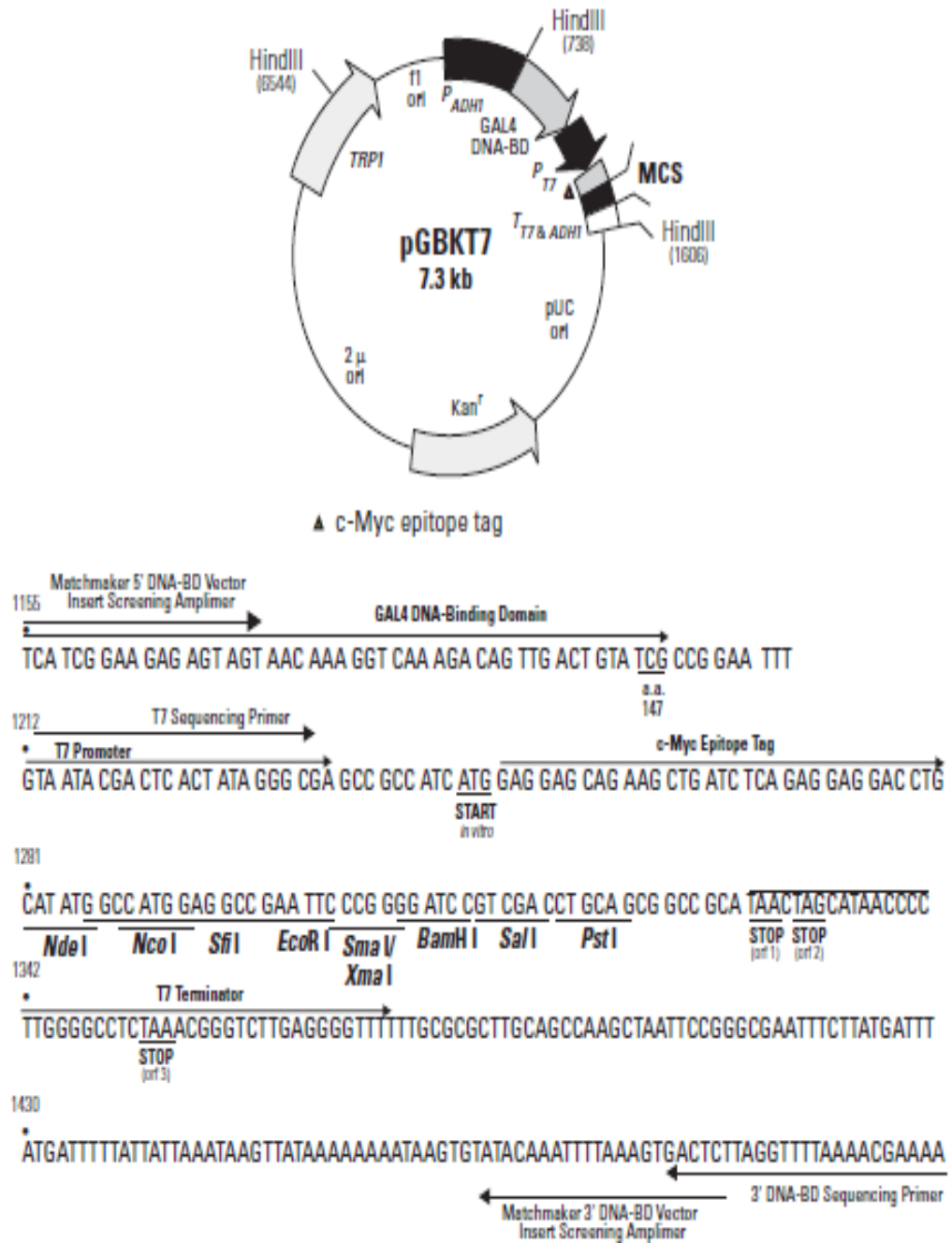
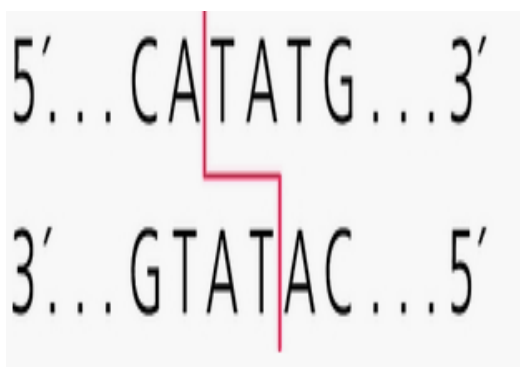


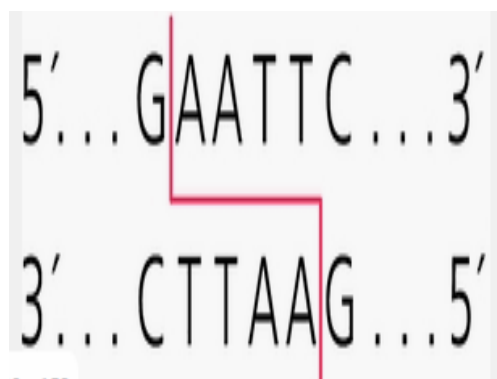
**Figure 4.3: Map of the DNA-binding domain vector pGBKT7.** The map shows the Fusion cloning region of the vector and the multiple cloning sites are in bold (image from Clontech laboratories).



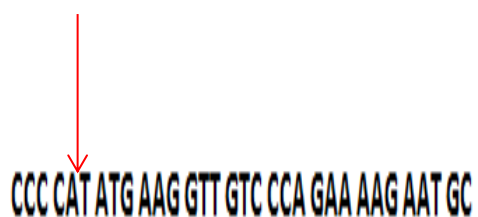
***Nde* I restriction site**



***EcoR* I restriction site**



**Ambra forward primer with *Nde* I site**



**Ambra reverse primer with *EcoR* I site**

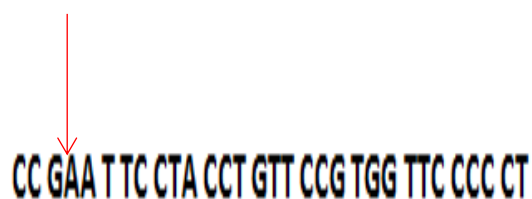


**Figure 4.5: PCR primer design to enable the cloning of Ambra1 into the vector pGBKT7.** Ambra primers were designed as to have *Nde* I restriction site on the forward and *EcoR* I restriction site on the reverse primers. The design of the primers would enable Ambra1 to be cloned as a translational fusion with the DNA binding domain Image showing the *Nde* I and *EcoR* I unique restriction site and sequence of primers designed.

#### 4.3.1.2 Ambra1 PCR amplification

For the amplification of Ambra1 using PCR, forward and reverse primers at a concentration of 0.2 $\mu$ M, 100 ng cDNA synthesized from RNA extracted from U-937 (ATCC® CRL-1593.2™) or A-375 (ATCC® CRL-1619™) cell lines were used as DNA templates and ImmoMix<sup>R</sup> (IMMOLASE™ DNA Polymerase from Bio-Line) as a DNA polymerase. At this stage the PCR reactions were unsuccessful and no bands for Ambra1 were observed (Figure 4.6).

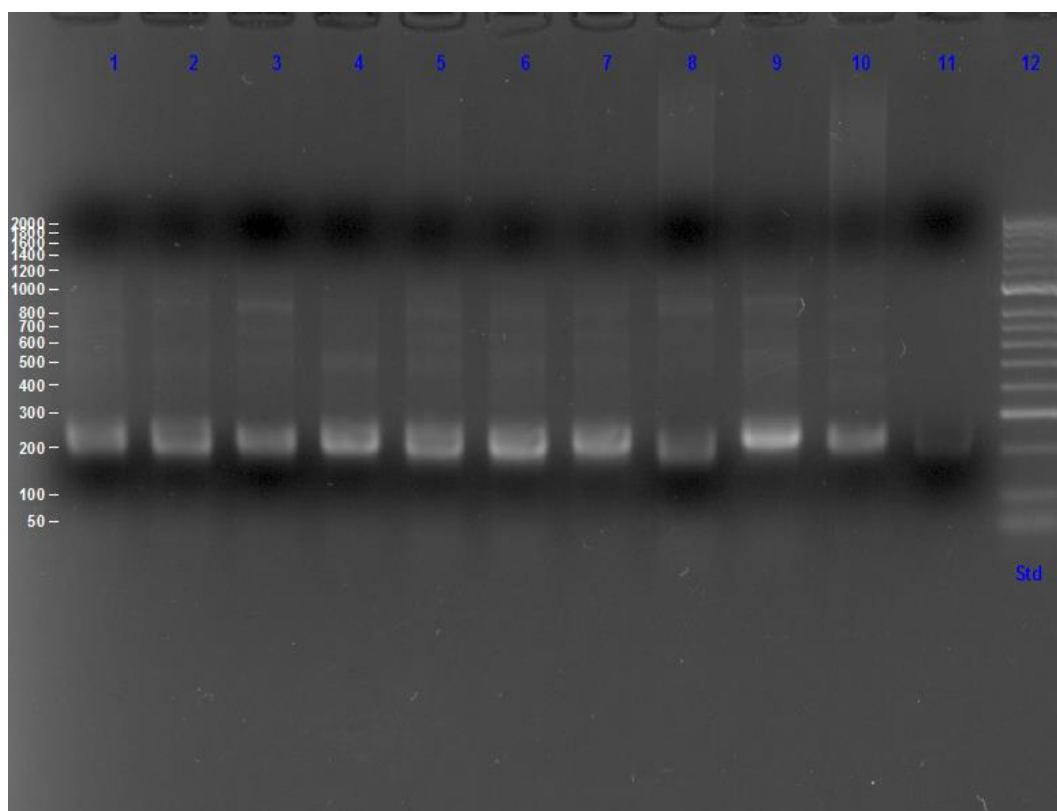


**Figure 4.6: unsuccessful Ambra1 PCR reaction.** Lanes 1 to 10 are replicates of Ambra1 PCR reactions. Lane 12 is Hyperladder 50bp. No bands observed for Ambra1 cDNA at~4Kb.

Since Ambra1 amplification was not achievable; a set of control primers were designed to amplify an internal sequence of ~500bp. of Ambra1 cDNA (Ambra1Fcon: TGC CAC AAT CTC CTG ACC TT. Ambra1Rcon: TCG CTG GGT CTG GGT AAA TT). This step was to help identify the presence of sufficient DNA template in the cDNA synthesized from the two cell lines mentioned above used for the PCR reaction. Amplifying this cDNA sequence was successful using cDNA from U-937 cell line and a band was observed at~500bp as expected (Figure 4.7) after this step only cDNA from the U-937 cell line was used as a template for PCR reactions.

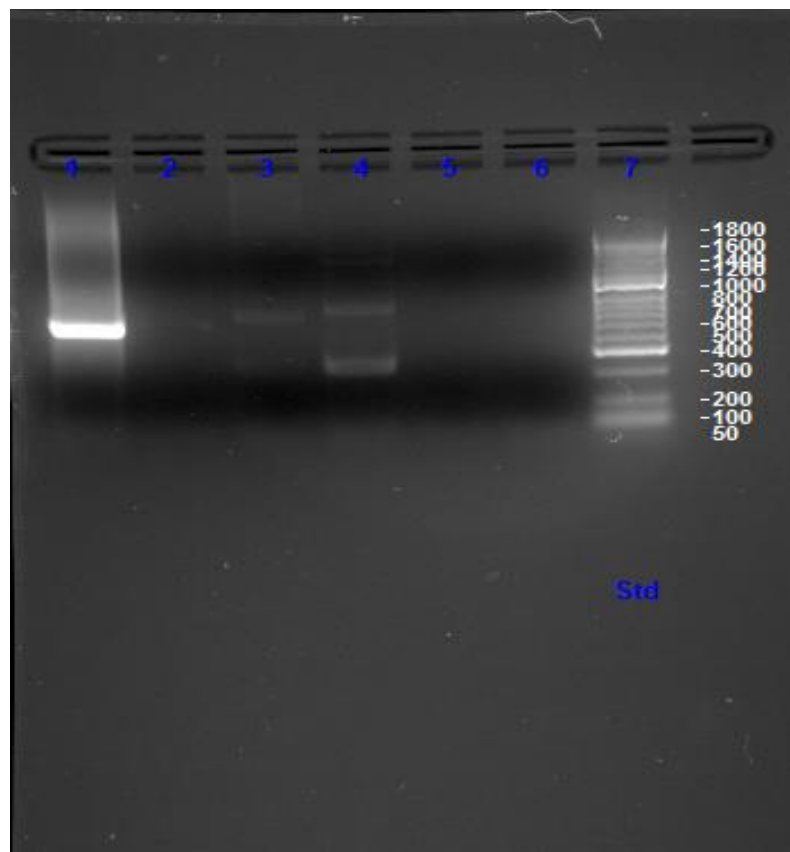


**Figure 4.7: Ambra Control primers PCR amplification.** Lanes 1 and 2 are Ambra control primers using cDNA extracted from U-937 and A375 respectively. A band can be observed at ~500bp for amplification of Ambra1 internal sequence. Lanes 3 and 4 are two replicates using Ambra full length primers using cDNA from U-937 cell line. Lanes 5 and 6 are replicates using Ambra full length primers using cDNA from A375 cell line. No bands at~4Kbp for Ambra can be observed in lanes 2 to 6. Lane 7 is Hyperladder 50bp.

Upon identifying the presence of the DNA template in the cDNA library; PCR reaction was optimized to amplify the Ambra1 full cDNA sequence. First approach was to try optimizing the annealing temperature. A temperature gradient was set up at temperatures of 60°C and 64°C as the lowest and the highest annealing temperature respectively. . However, amplification was still not achieved (Figure 4.8).

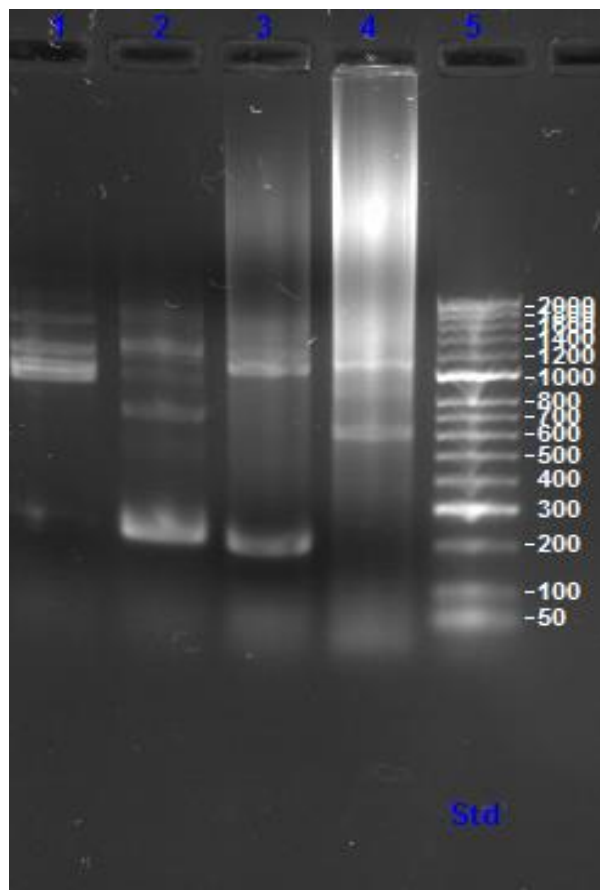


**Figure 4.8: unsuccessful Ambra1 PCR reaction temperature gradient.** Lanes 1 to 4 are temperature gradient PCR reactions from 60°C to 64°C for the annealing step. Lane 5 is Hyperladder 50bp. No bands can be observed at ~4kbp for Ambra.

Since an internal fragment of Ambra1 cDNA was amplified by control primers; the second approach to optimize PCR reactions was to design a new set of full length primers. The primers (Ambra1Ffull2 and Ambra1Rfull2) were designed with four base pairs less than the original primers (Ambra1Ffull and Ambra1Rfull) (2.1.4.). However, mis-amplification was observed upon using these primers and no bands were observed for full length Ambra1 (Figure 4.9)

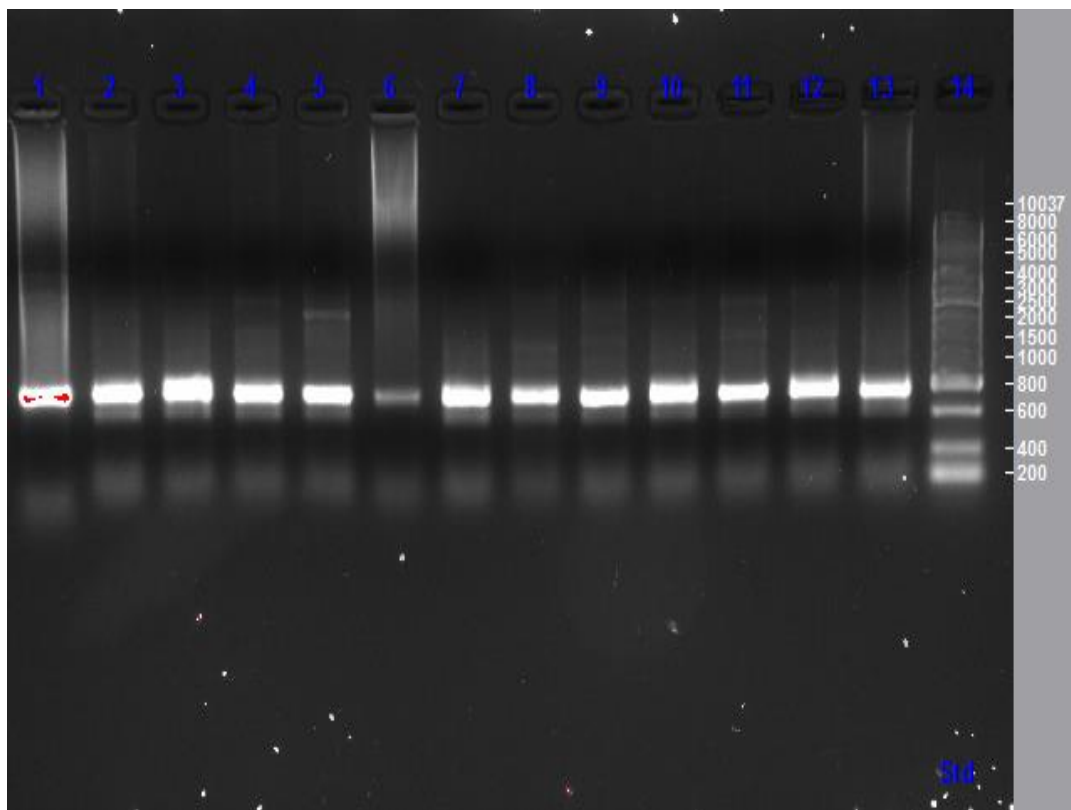


**Figure 4.9: unsuccessful Ambra1 amplification using the (Full2) set of primers.** Lanes 1 to 13 are thirteen PCR replicates performed for the amplification of Ambra1 showing no bands near the right size (~4kb). Lane 14 is hyper ladder 1kb.

Successful amplification of an internal sequence of Ambra1 Using the control primers suggested that the cDNA synthesized did not have the full length of Ambra1 ORF and therefore, the final step to optimize the PCR reaction was to purchase an Ambra1 open reading frame (ORF) clone (ORF plasmid clone name: IRATp97OC125D Source Bio-Science). The clone was previously sequence verified and this ORF clone was subsequently used as a template for all Ambra1 amplifications as well as a new set of primers AMBRA LongR and AMBRA LongF (2.1.4). PCR reactions were performed using Immomix master mix and 20ng and 100ng concentrations of Ambra1 ORF were tested. A band was observed for Ambra1 at ~4kbp upon using 20ng of the DNA template (Figure 4.10A).

A proof reading polymerase was subsequently used (IPROOF, Bio-Rad) to ensure fidelity of the amplified product to amplify Ambra1 using the 20 ng optimum DNA template concentration (2.2.4), and the annealing temperature for Ambra1 was set to 66.6°C after running a temperature gradient PCR between 65°C and 67°C (Figure 4.10B). Reproducibility of Ambra1 PCR amplification was achieved; all PCR products were purified by gel excision technique (Figure 4.11). Ambra1 amplified cDNA was verified by sequencing.



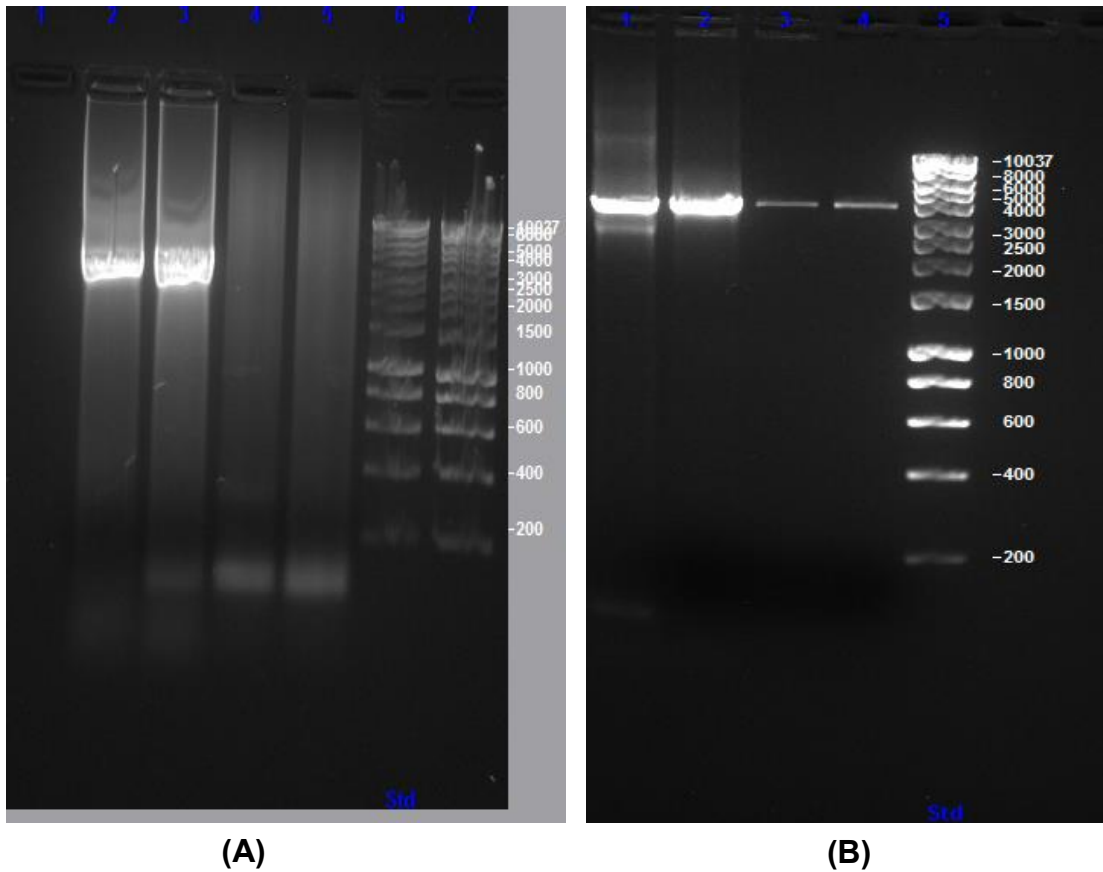


**Figure 4.10: Ambra1 PCR amplification using an ORF clone.** (A) PCR amplification using Immomix master mix. Lanes 2 and 3 are technical replicates of PCR reaction using 20ng of DNA template showing a band at ~4Kbp. Lanes 4 and 5 are technical replicates of PCR reaction using 100ng of DNA template showing no amplification. Lanes 6 and 7 are Hyperladder 1Kb (B) PCR amplification using a proof reading polymerase (Iproof). Lanes 1 to 4 are annealing temperature gradient PCR products of Ambra1 from 65°C to 67°C. A band is observed in all 4 lanes at ~4kbp with the highest annealing temperature showing the best DNA quality. Lane 5 is Hyperladder 1Kb.

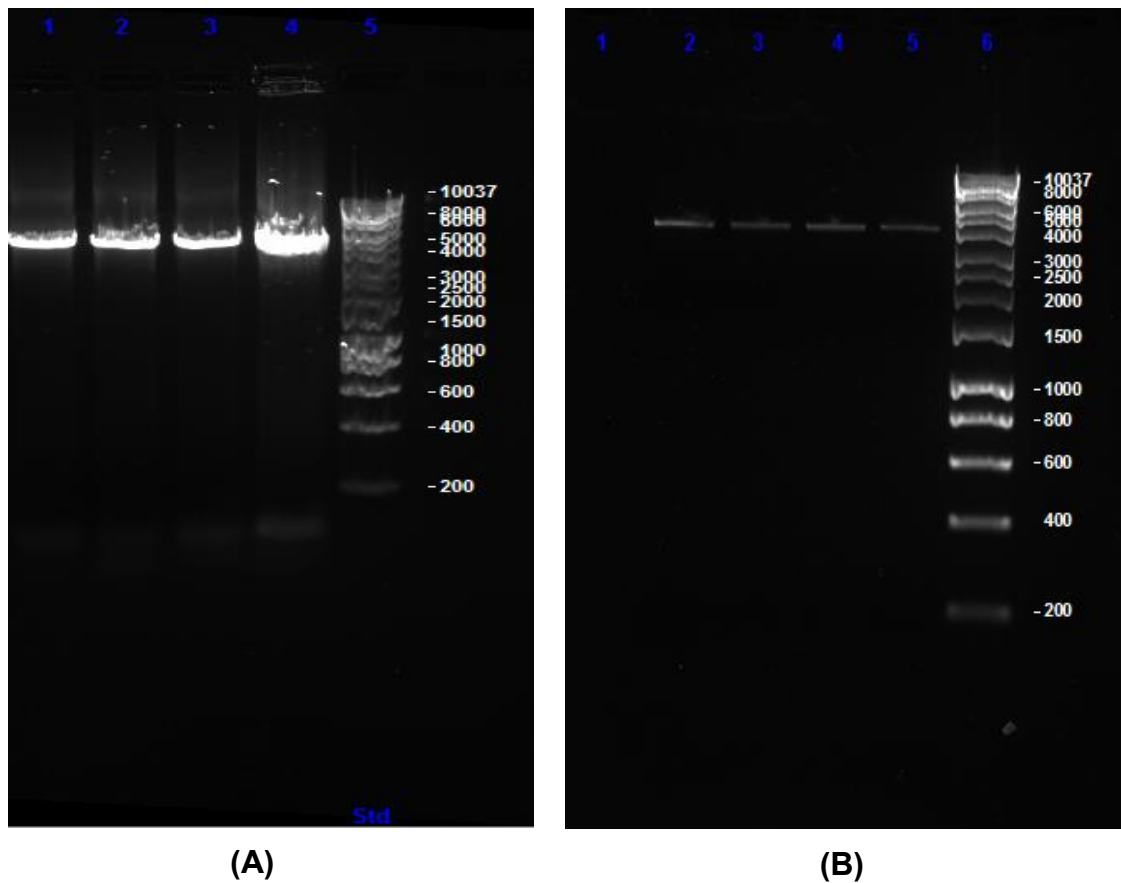


**Figure 4.11: Ambra1 PCR amplification and purification.** PCR amplification was optimized using Iproof reading polymerase and DNA was purified by gel excision technique. (A) Electrophoresis of PCR products. Lanes 1 to 4 are four technical replicates of Ambra1 PCR products using Iproof polymerase. Bands are observed at ~4Kbp in all lanes. Lane 5 is Hyperladder 1kb. (B) Electrophoresis of purified PCR bands by gel excision technique. Lanes 2 to 5 are 4 technical replicates. Bands can be observed at ~4Kbp in all lanes. Lane 6 is Hyperladder 1Kb.

### 4.3.2 Cloning Ambra1 into the DNA-binding domain vector

#### 4.3.2.1: cloning Ambra1 using sticky end ligation

Ambra1 PCR products and the DNA-binding domain plasmid (PGBkT7) were digested with *EcoR I* and *Nde I*, ligated and transformed to *DH5α E-coli* transformations were selected for on kanamycin-agar plates (2.2.6). Initially no colonies were observed at all and after repeating the same step few times; few colonies were observed on the selection media plates. testing for inserts were either performed by colony PCR (Figure 4.12) or by isolation of plasmids from colonies followed by digestion and analysis on agarose gel (Figure 4.13). In all cases no recombinant Ambra1 clones were isolated.

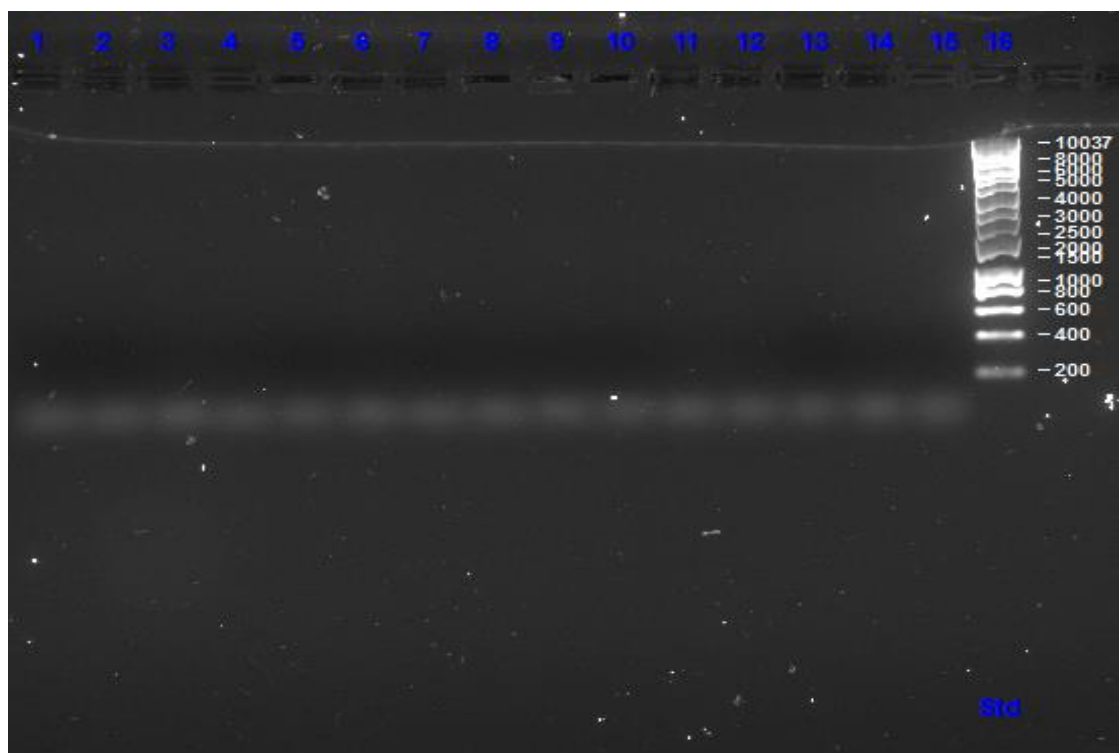


**Figure 4.12: colony PCR of transformed bacteria to screen for Ambra1 inserts.** Lanes 1 to 15 are different colony PCR products and no bands for Ambra1 can be observed at ~4kbp. Lane 16 is Hyper Ladder 1Kb.

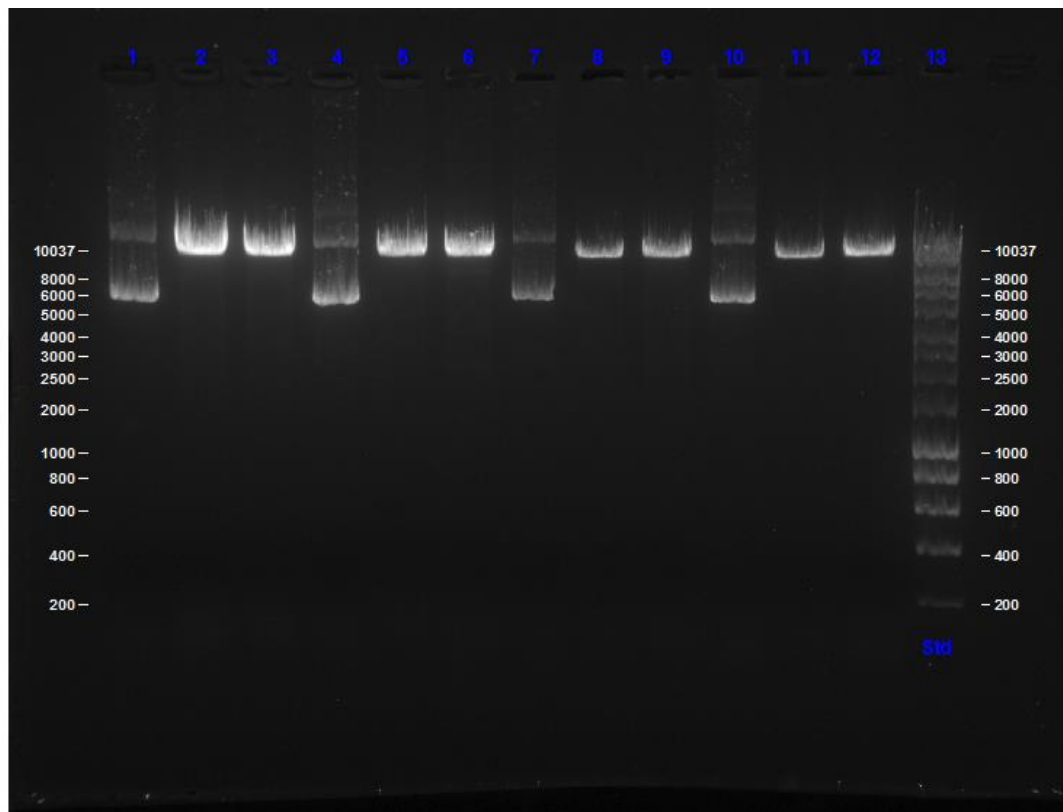


**Figure 4.13: Restriction analysis of recombinant plasmids to screen for Ambra1 insert in the DNA-BD pGBKT7 using *EcoR* I and *Nde* I.** Lanes 1, 4, 7 and 10 are undigested plasmids. Lanes 2, 5, 8 and 11 are single *EcoR* I plasmid digests showing linear plasmids. Lanes 3, 6, 9 and 12 are double *EcoR* I and *Nde* I plasmid digests showing linear plasmids and no inserts. Lane 13 is Hyper Ladder 1Kb.

#### **4.3.2.2: cloning Ambra1 using zero blunt TOPO vector**

Traditional digestion and sticky end ligation approaches appeared not to be a viable approach to clone Ambra1. Two possible issues were to address at this point. Firstly, the use of *Nde* I restriction enzyme at the end of a linear ORF produced by PCR as it has been reported that *Nde* I can show weak digestion efficiency. Secondly, cloning a large ~4Kbp ORF fragment into a relatively large ~7.3kbp plasmid creates a very large construct which can be quite difficult to transform. Alternatives to overcome these issues were explored and, control experiments as well as different approaches were designed. Attempts to clone a control ORF of the gene PP2CA (fragment size ~927 bp); Uniprot isoform 1 ID: P67775-1 <https://www.uniprot.org/uniprot/P67775> indicated similar issues using *Nde* I when digesting linear PCR products; so ways to avoid this were essential. One option was to try cloning the insert into a relatively smaller general purpose cloning vector and then sub-cloning. Therefore, the first approach was switching to blunt end cloning into a Zero blunt TOPO cloning vector. TOPO vector is ~3.5 Kbp and it was chosen as it offers the ability to clone blunt ended PCR products by Topoisomerase I and, without the use of restriction enzymes. The use of restriction enzymes to digest Ambra1 cDNA from a TOPO circular vector rather than a linear PCR product may have enhanced the efficiency of digestion and allow sub-cloning the digested Ambra1 cDNA into the desired pGBKT7 plasmid.

In order to perform blunt end cloning using the TOPO vector; the use of proofreading polymerase is required to produce blunt-end PCR products. Ambra1 cDNA was amplified using Q5® High-Fidelity DNA Polymerase (2.2.4) (Figure 4.14), incubated with TOPO vector and transformed to *StbI2 E-coli* cells

which were recommended by the manufacturer. No cloning was observed upon the analysis of the transformed colonies (Figure 4.15).

A control experiment was performed simultaneously as recommended by the TOPO vector supplier (Thermo-Fisher Scientific), and a PCR fragment of 800BP was amplified to be used as a control and was successfully transformed into the TOPO vector (Figure 4.16).

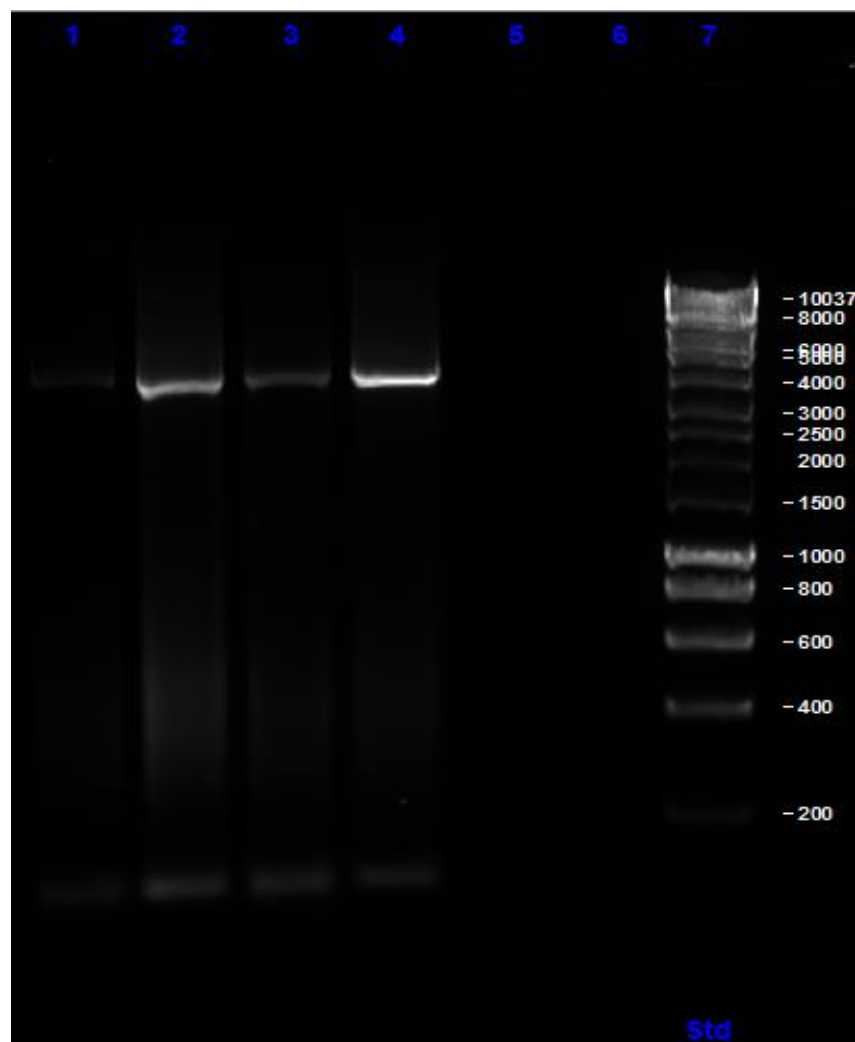


**Figure 4.14: Blunt-end Ambra1 cDNA amplification using Q5 polymerase.** Lanes 1 to 4 are four technical replicates of Ambra1 PCR products showing bands at~4kbp. Lane 5 is Hyper Ladder 1Kb marker.

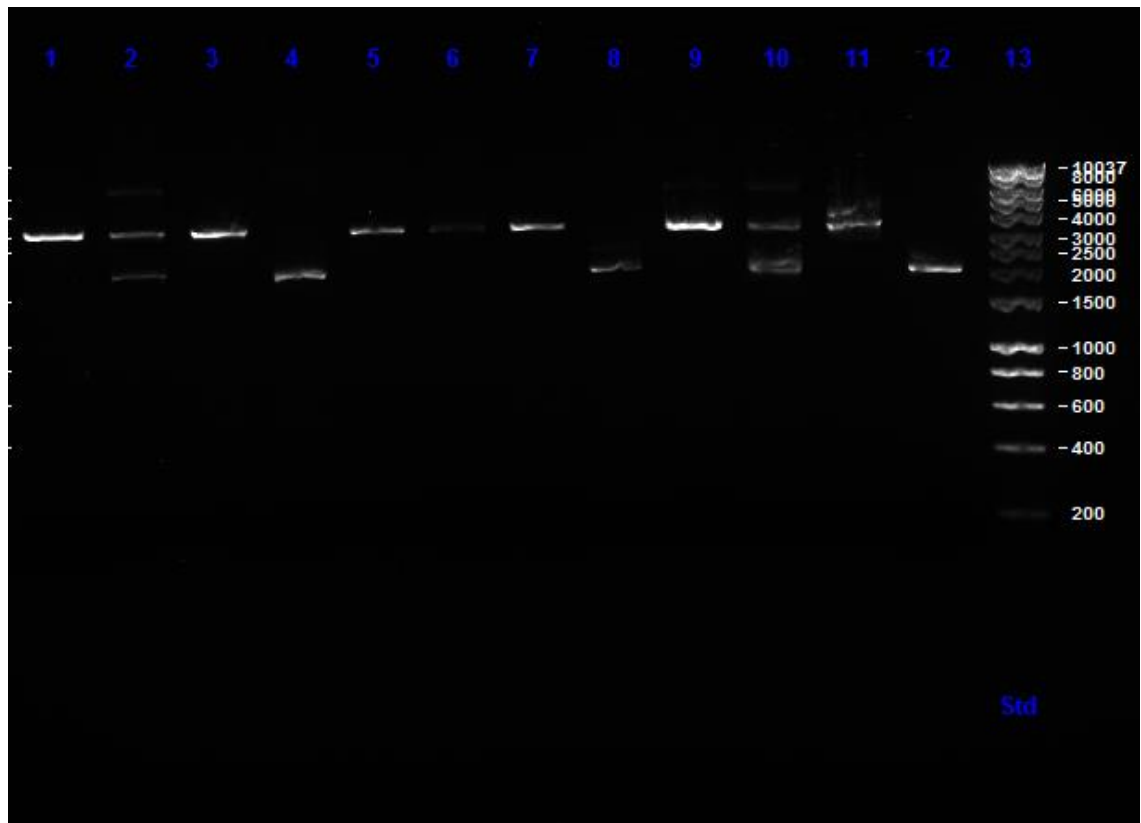


**Figure 4.15: Restriction analysis of recombinant TOPO vector to screen for Ambra1 inserts using EcoR I and Nde I showing no inserts.** These are 3 biological replicates. Lanes 1, 5 and 9 are undigested plasmids. Lanes 2, 6 and 10 are single *EcoR I* digests. Lanes 3, 7 and 11 are single *Nde I* digests. Lanes 4, 8 and 12 are *EcoR I* and *Nde I* double digests. No Ambra1 cDNA bands were observed at ~4kbp. Lane 13 is Hyperladder 1kb.

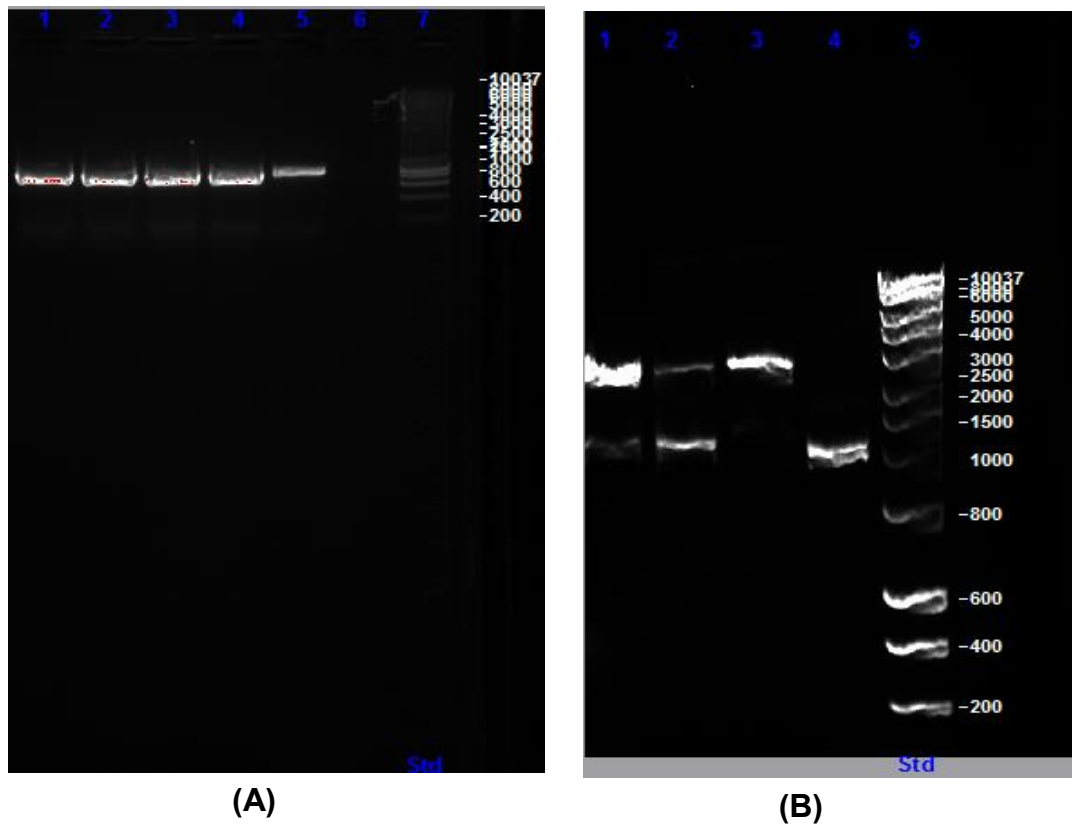


**Figure 4.16: TOPO vector control PCR Product and restriction digestion analysis for successful cloning of the amplified insert into the TOPO vector.** (A) Electrophoresis of control inserts PCR amplification. Lanes 1 to 5 are technical replicates and bands can be observed at ~800 bp in all lanes. Lane 7 is Hyperladder 1Kb. (B) Electrophoresis of isolated and digested TOPO plasmid with control insert. Lanes 1 to 4 are four biological replicates of *EcoR I* and *Nde I* double digests of extracted plasmids. Two bands can be observed at ~3.5Kbp for the TOPO vector and at ~1Kbp for the control insert in lanes 1 and 2. Lane 5 is Hyperladder 1Kb.



#### **4.3.2.3: cloning Ambra1 using Electro-transformation**

The use of a general purpose relatively smaller TOPO vector to overcome the issue of cloning Ambra1 did not result in cloning Ambra1 and there was a need for a different approach to try and overcome the relatively large pGBKT7-Ambra1 plasmid. Thinking was then shifted towards questioning the ability of traditional chemical-transformations to transform such a relatively large plasmid and therefore; Electro- transformation was applied to the transformation of the ligated vector. The electro-transformation was just another approach that was not sufficient to clone the ORF Ambra1 into pGBKT7. At this point the concern for the vector size was minimized as if it was the real challenge then one of the two approaches used to overcome the size would have resulted in successful cloning.

#### **4.3.2.4: Designing a control experiment using PP2CA**

A control experiment was performed after the unsuccessful cloning of Ambra1 cDNA using the previously mentioned approaches. Attempting cloning of PP2CA, a known binding partner of Ambra1, was ideal as it could also be a useful control for the Y2H screening. A recent study has reported and confirmed by the yeast two hybrid assay the interaction of Ambra1 with PP2CA.

PP2CA primers were designed with *Nde* I and *Eco*R I restriction sites similar to the Ambra1 primers (PP2CA F, PP2CA R 2.1.4). The same approaches were repeated using PP2CA amplified with these primers. PCR amplification of PP2CA from cDNA was successful (Figure 4.17) and the product gel purified. However, attempts to clone *Nde* I/*Eco*R I digested PP2CA PCR product into pGBKT7 using traditional sticky end ligation was unsuccessful (Figure 4.18).

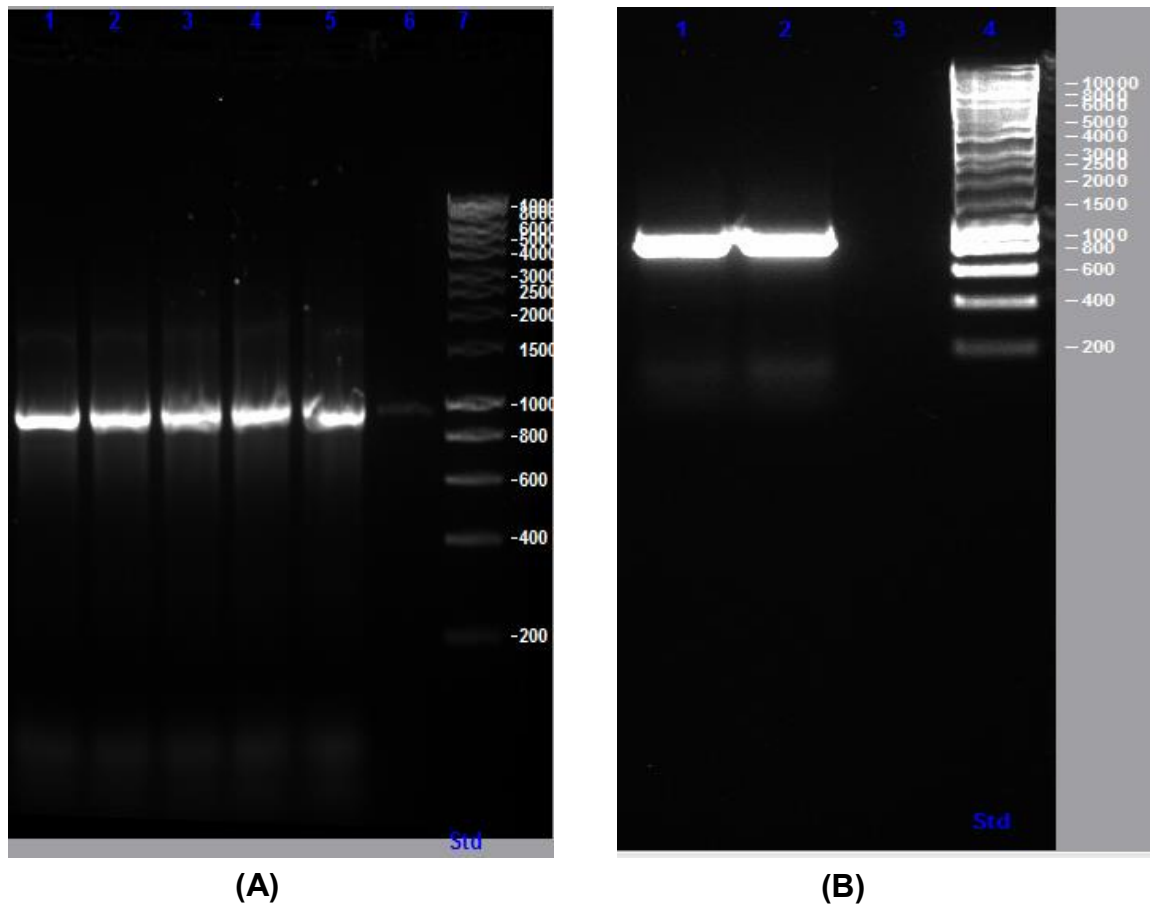


**Figure 4.17: PCR amplification of PP2CA cDNA using Iproof and Q5 DNA polymerases.** (A) Electrophoresis of Iproof PP2CA PCR products. Lanes 1 to 5 are technical replicates of PCR reaction. A band is observed in all lanes at ~1Kbp. Lane 7 is Hyperladder 1Kb. (B) Electrophoresis of Q5 polymerase PP2CA PCR products. Lanes 1 and 2 are technical replicates of PCR reaction. A band is observed in both lanes at ~1Kbp. Lane 4 is Hyperladder 1Kb.

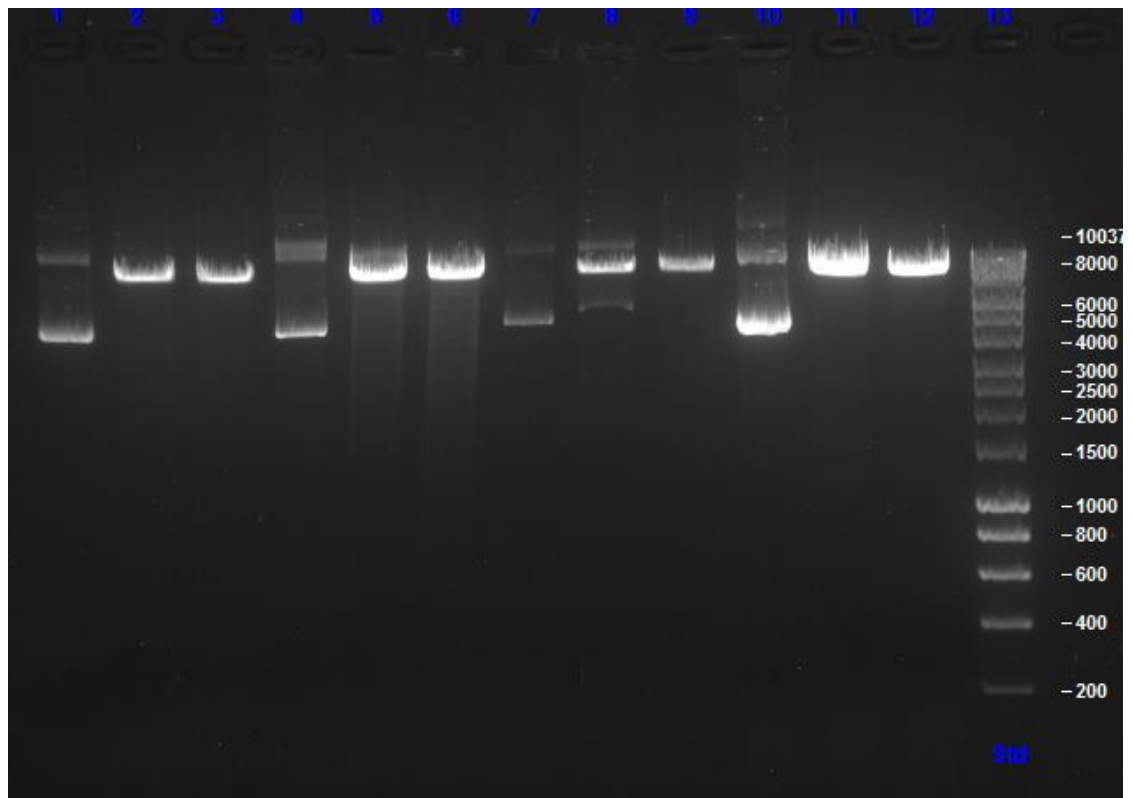


**Figure 4.18: Restriction analysis of recombinant plasmids to screen for PP2CA inserts in pGBKT7.** Lanes 1, 4, 7 and 10 are undigested plasmids. Lanes 2, 5, 8 and 11 are *EcoR I* digests showing a linear plasmid at ~8Kbp. Lanes 3, 6, 9 and 12 are double *EcoR I* and *Nde I* digests showing a linear plasmid at ~8kbp no inserts are observed at ~1kbp. Lane 13 is Hyperladder 1Kb.

The second PP2CA control experiment was blunt end cloning using zero blunt Topo vector rather than sticky end ligation. Unlike Ambra1; PP2CA was successfully cloned into the TOPO vector and analysing the recombinant TOPO vector released the PP2CA insert at ~1kbp (Figure 4.19). However, sub-cloning of *Nde* I/*EcoR* I digested PP2CA fragment from the TOPO vector into the *Nde* I/*EcoR* I digested pGBKT7 was unsuccessful (Figure 4.20). It appeared that the digestion of pGBKT7 was not digesting well with *Nde* I (4.4) since the generation of the PP2CA fragment from the TOPO vector meant that a *Nde* I site must be generated at the 5' end of the PP2CA fragment.

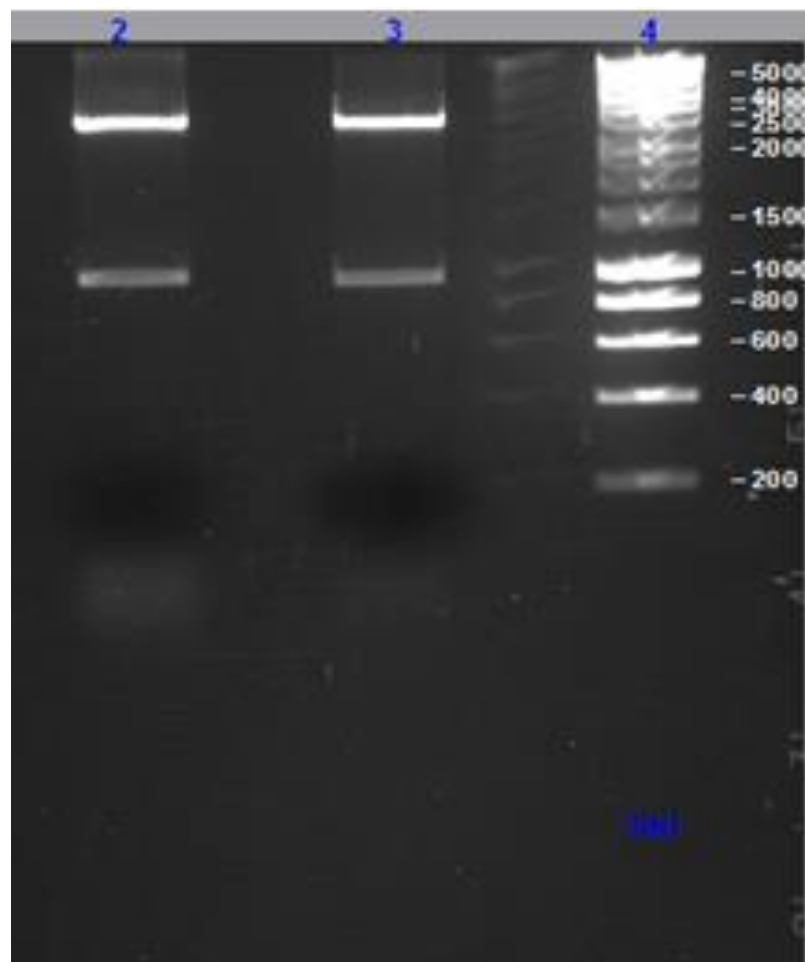


**Figure 4.19: Restriction digestion analysis of recombinant Zero blunt TOPO cloning vector to screen for PP2CA clones.** Lanes 2 and 3 are two replicates of *EcoR* I and *Nde* I digests PP2CA clones, linear plasmid band is observed at ~3.5Kbp. A linear ORF PP2CA can be observed at ~1Kbp. Lane 4 is Hyperladder 1Kb.

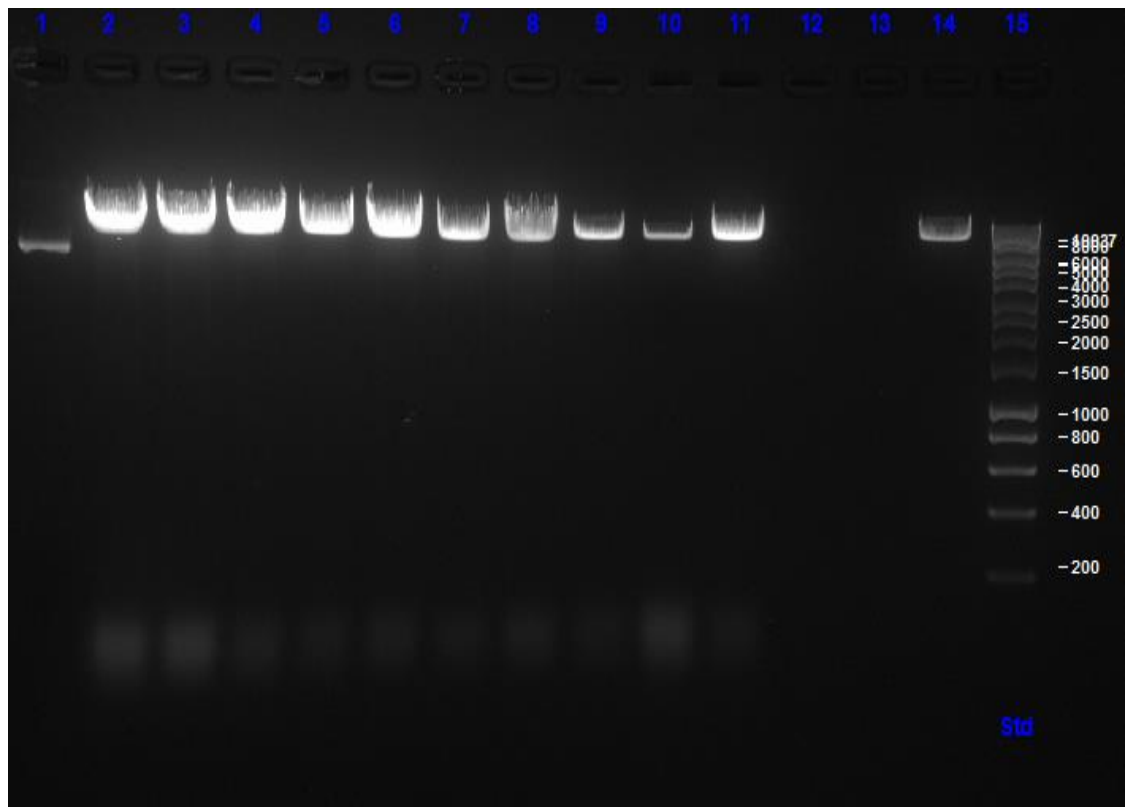


**Figure 4.20: Restriction digestion analysis of recombinant pGBKT7 to screen for PP2CA inserts.** Lanes 1 to 14 are fourteen biological replicates of *EcoRI* and *NdeI* double digests of plasmids extracted from transformed *DH5 $\alpha$*  after PP2CA was sub-cloned from Zero blunt topo vector into pGBKT7. Linear plasmid bands can be observed at ~8kbp but no bands are observed for PP2CA insert at ~1kbp, lane 15 is Hyperladder 1Kb.

A greater choice of restriction sites available for PP2CA meant that *BamH* I was chosen to replace the *Nde* I site on new PP2CA primers to generate an *EcoR* I / *BamH* I fragment. The forward primer (PP2CA F\_Eco) was designed with *EcoR* I restriction site and the reverse primer (PP2CA R\_Bam) was designed with *BamH* I restriction site (2.1.4). Repeating the sticky end ligation of PP2CA with pGBKT7 resulted in the successful cloning of PP2CA (Figure 4.21) Recombinant clones were verified by sequencing

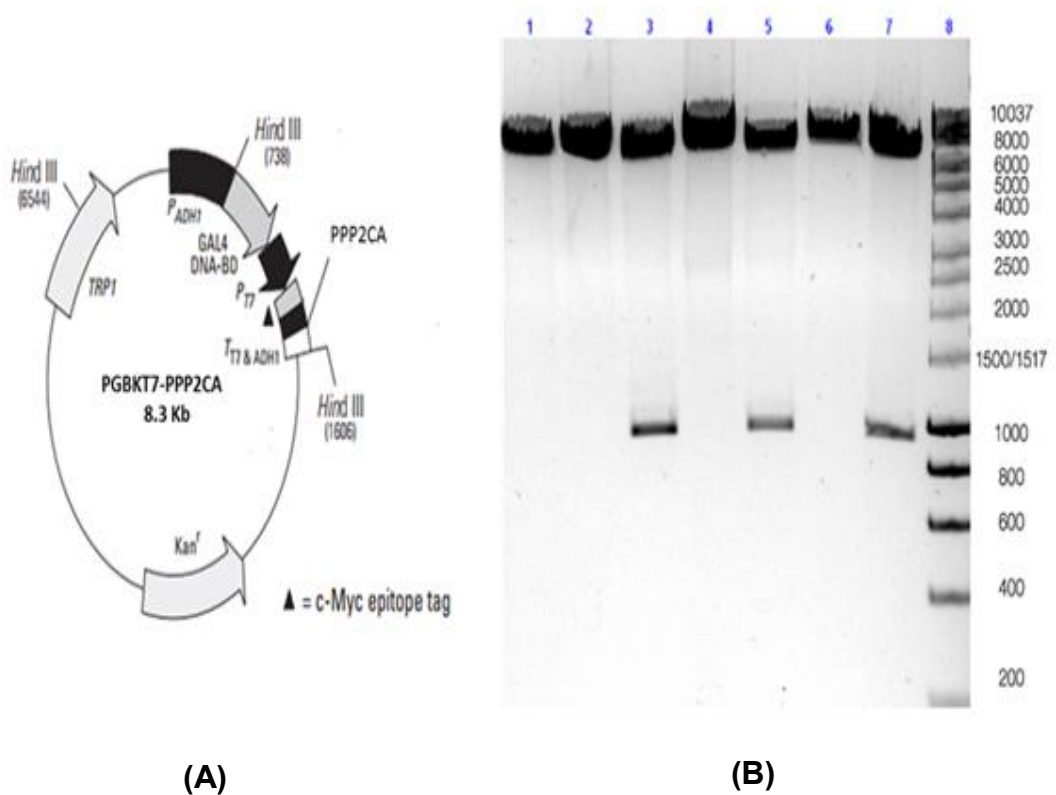


**Figure 4.21: Restriction digestion analysis of PP2CA clones in the Y2H bait vector pGBKT7.** (A) Recombinant plasmid. (B) Lanes 1,4 and 6 are *EcoR* I digests of 3 different PP2CA clones, linear band is observed at ~9Kbp. lane 2 is a *BamH* I digest, linear band is observed at ~9Kbp. Lanes 3,5 and 7 are double digests using *EcoR* I and *BamH* I showing a linear plasmid at ~8Kbp and the ORF PP2CA at ~1Kbp.

#### 4.3.2.5: Ambra1 cloning using *EcoR* I-*EcoR* I restriction sites

Successful cloning of PP2CA into pGBKT7 using *EcoR* I and *Bam*H I confirmed that the real challenge was the use of the *Nde* I. The available alternative to *Nde* I that can be used on Ambra1 cDNA sequence was *EcoR* I. a new forward primer was designed with the sequence of *EcoR* I restriction site replacing the *Nde* I site (AMBRA LongFeco 2.1.4), in attempt to clone Ambra1 cDNA with *EcoR* I restriction sites on both ends. PCR amplification was performed and cloning procedures into pGBKT7 were repeated, an insert was observed at ~4Kbp on the restriction analysis (Figure 4.22). However; sequencing this insert showed that it is not Ambra1 cDNA.

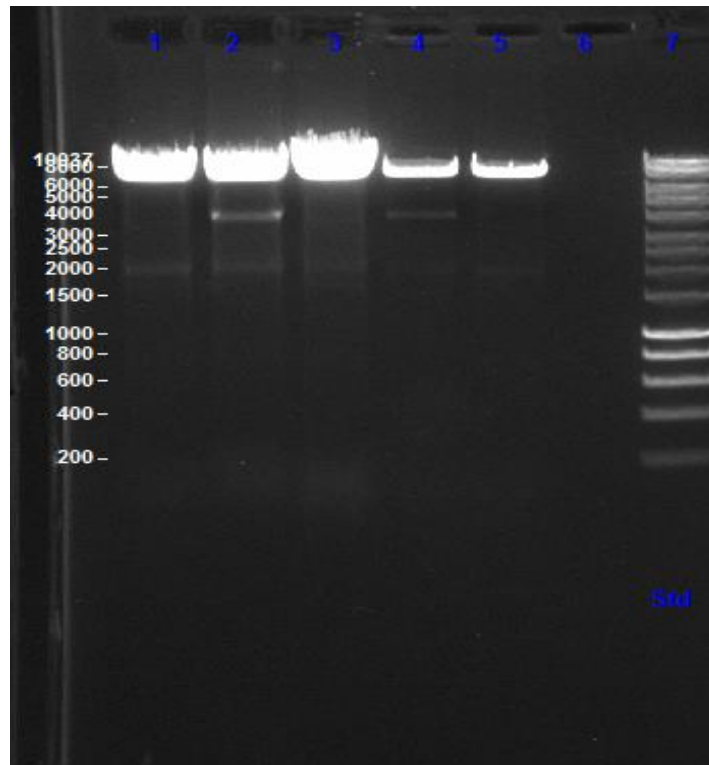


**Figure 4.22: Restriction digestion analysis of recombinant plasmids to screen for Ambra1 inserts after using *EcoR* I alone as a restriction enzyme.** Lanes 1 to 5 are biological replicates of plasmids digested with *EcoR* I to test for cloning Ambra1 into pGBKT7. Linear plasmid bands at ~8Kbp can be observed in all lanes. A possible Ambra1 band at ~4Kbp can be observed in lanes 2 and 4.

#### 4.3.2.6: *Ambra1* cloning using Fusion technique

An alternative to traditional sticky end and blunt end ligations was chosen to attempt to clone *Ambra1*. The previous control experiments demonstrated that the use of *Nde* I needed to be avoided.

In-Fusion HD Cloning can be used for fast, directional cloning of one or more fragments of DNA into any vector. The cornerstone of In-Fusion cloning technology is an In-Fusion Enzyme, which promotes single cross over recombination events between homologous DNA fragments (e.g., PCR-generated inserts and linearized vectors) with an overlap of only 15-bp. These 15-bp overlaps can be engineered into the 5'-end of primers used for the amplification of the desired sequences (Figure 4.23).

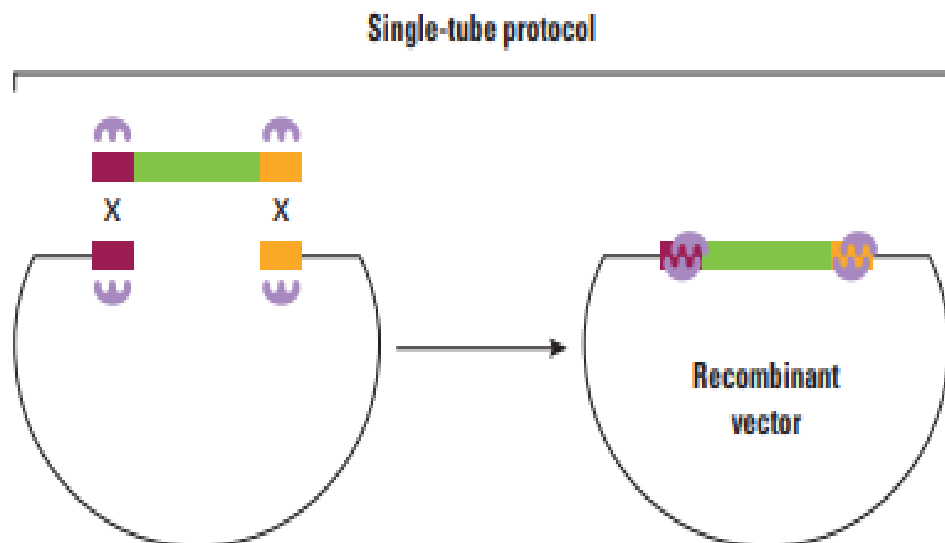


**Figure 4.23: A representative diagram of In-Fusion HD cloning technique.** DNA fragment is colored in green and the yellow and purple colors represent the 15 bp overlaps that are ligated to generate a recombinant vector (Image from Clontech Laboratories, Inc.)



New primers were designed to have the 15-bp overhangs that will overlap with *Nde I*/*EcoR I* digested pGBKT7 (AMBRA FusionF, AMBRA FusionR 2.1.4). The digestion of pGBKT7 was performed on two steps where the first step was to digest with *Nde I* and running the digested plasmid on an agarose gel to test for the linearity and be sure that *Nde I* has cut the plasmid, the second step was to add *EcoR I* as it is more efficient in cutting the plasmid (Figure 4.24).

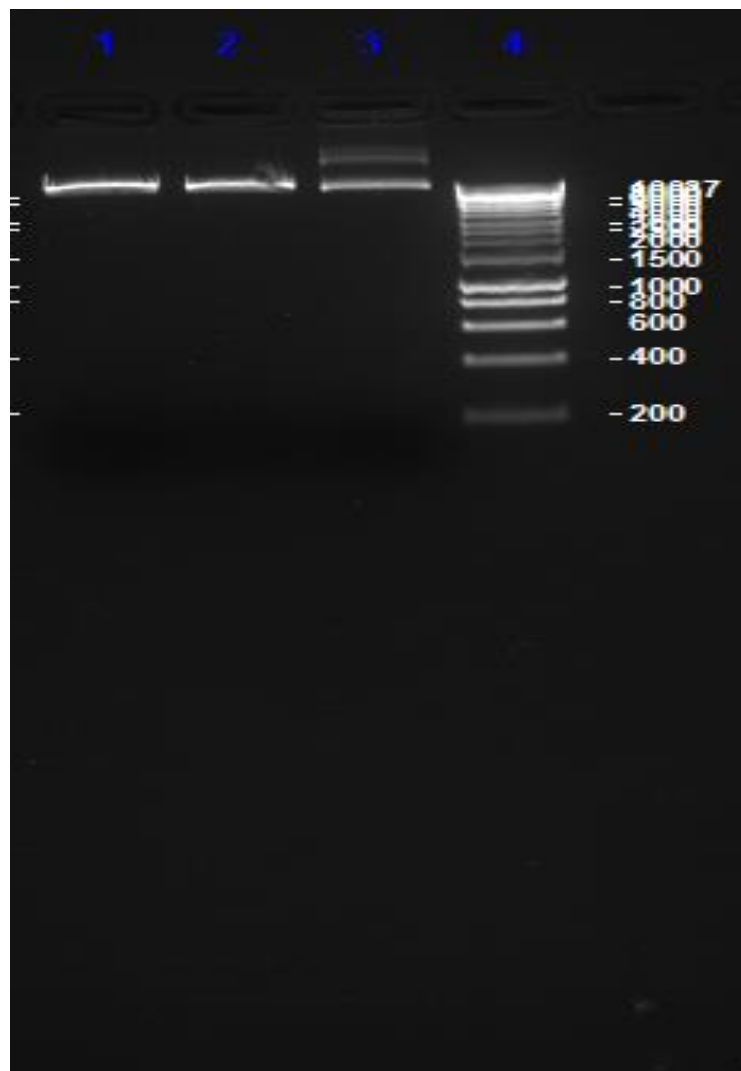


**Figure 4.24: Multi-step restriction digestion analysis of pGBKT7 with *Nde I* followed by *EcoR I*.** Lane 1 is a single digest of pGBKT7 using *Nde I* alone. Lane 2 is a double digest of pGBKT7 after adding *EcoR I* to the *Nde I* digested pGBKT7. Lane 3 is intact plasmid. Linear bands can be observed at ~8Kbp in wells 1 and 2 showing digested plasmid. Lane 4 is Hyperladder 1Kb.

In-fusion HD cloning approach was performed according to manufacturer's specifications and the cloning of the full length Ambra1 gene was successful. Cloning was confirmed by restriction analysis of isolated recombinant vector (Figure 4.25) and verified by sequencing (~800 bases at each end) using a T7 sequencing primer (Figure 4.26).

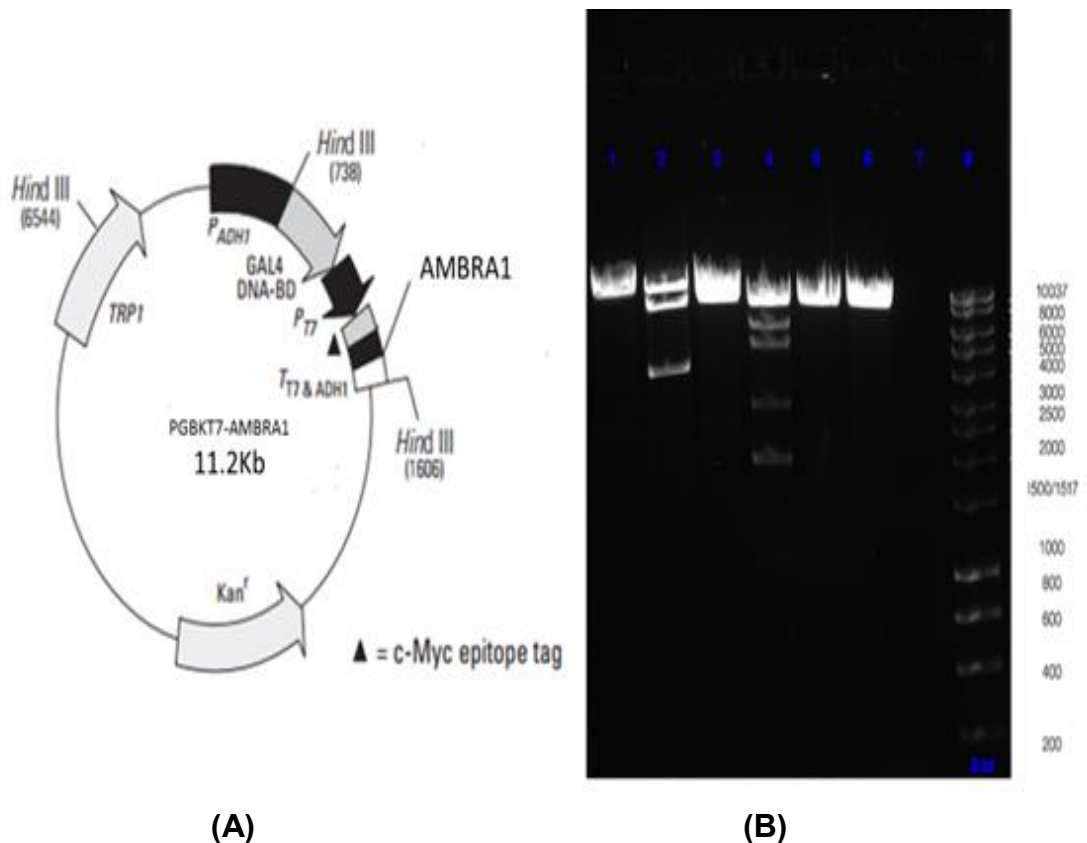
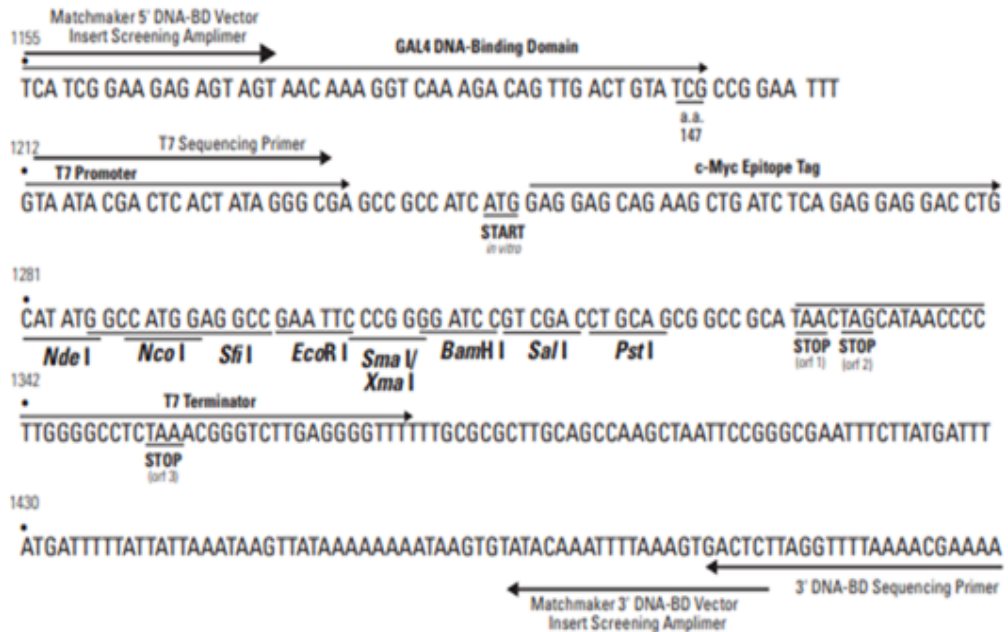


**Figure 4.25: Restriction digestion analysis of Ambra1 clones in the Y2H bait vector pGBKT7.** (A) Recombinant plasmid. (B) Lanes 1, 3 and 6 are *Eco* R1 digests of 3 different Ambra1 clones, linear band is observed at ~11Kbp. lanes 2, 4 and 6 are double digests using *Eco* R1 and *Nde* I. In lane 2 a linear plasmid at ~8Kbp and the ORF Ambra1 at ~4Kbp are observed. In the same lane a linear single digested plasmid is showing a band at ~11Kbp which indicates partial digestion of the plasmid.



CTGATCTCAGAGGAGGACCTGCATATGAAGGTTGTCCCAGAAAAGAA  
 pGBKt7 vector sequence └┬┘ AMBRA 1 sequence  
*Nde* I restriction site-in frame

(A)

Homo sapiens autophagy/beclin-1 regulator 1, mRNA (cDNA clone MGC:33725 IMAGE:5296472), complete cds  
 Sequence ID: [BC045609.1](#) Length: 5057 Number of Matches: 1

Range 1: 361 to 1492 [GenBank](#) [Graphics](#) [Next Match](#) [Previous Match](#)

Score	Expect	Identities	Gaps	Strand
2039 bits(2260)	0.0	1131/1132(99%)	0/1132(0%)	Plus/Plus
Query 1	ATGAAGGTTGTCCCAGAAAAGAATGCTGTCCGGATACTCTGGGGGCGAGAACGGGGTGCT	60		
Sbjct 361	ATGAAGGTTGTCCCAGAAAAGAATGCTGTCCGGATACTCTGGGGGCGAGAACGGGGTGCT	420		
Query 61	CGGGCCATGGGAGCTCAGCGGCTTCTGCAGGAGCTGGTAGAGGATAAAACCGGTGGATG	120		
Sbjct 421	CGGGCCATGGGAGCTCAGCGGCTTCTGCAGGAGCTGGTAGAGGATAAAACCGGTGGATG	480		
Query 121	AAATGGGAGGGCAAGAGAGTAGAACTGCCGGATAGTCCACGCTCTACCTTCTATTGGCC	180		
Sbjct 481	AAATGGGAGGGCAAGAGAGTAGAACTGCCGGATAGTCCACGCTCTACCTTCTATTGGCC	540		

(B)

**Figure 4.26: Ambra cloning verification by sequencing using T7 sequencing primer.** (A) Recombinant vector sequence showing Ambra cloned in frame. The red nucleotides represent pGBKT7 sequence and black nucleotides represent Ambra sequence. (B) Blast nucleotide analysis of the sequence verified showing it is a match of Ambra sequence (~800 bases at each end).

### **4.3.3: Yeast two hybrid mating**

#### **4.3.3.1: yeast strains maintenance**

Yeast strains Y2H gold and Y187 were grown and maintained on YPDA plates (Figure 4.27).

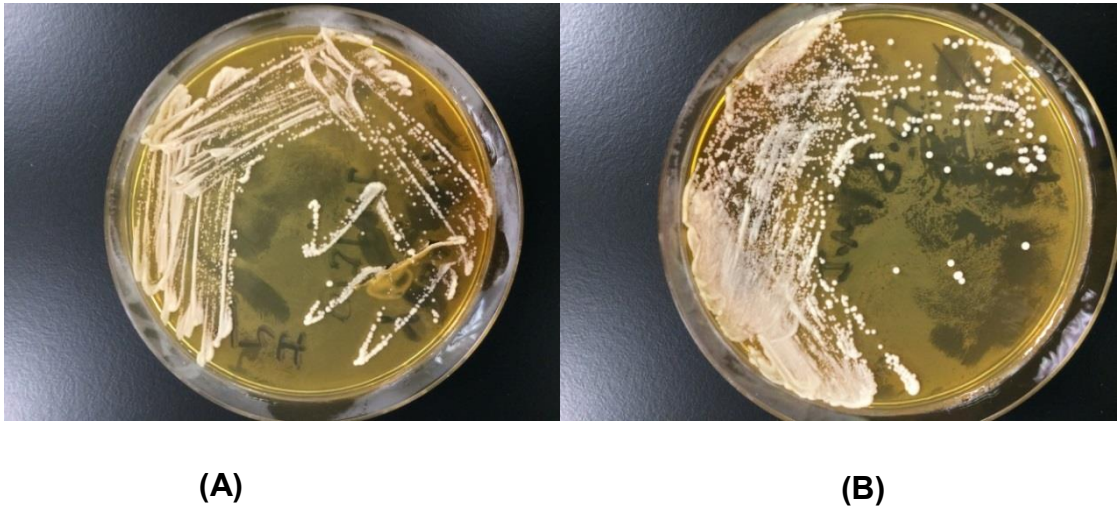


**Figure 4.27: yeast two hybrid strains growth and maintenance. (A) Y2H gold. (B) Y187.**

#### **4.3.3.2: yeast-two Hybrid control experiments**

Control experiments were performed as specified by manufacturer. The positive control experiment is an interaction between pGBKT7-53 (murine p53 protein cloned into pGBKT7) transformed into Y2H gold strain and pGADT7-T (SV40 large T-antigen cloned into pGADT7) transformed into Y187 strain. While the negative control involved a mating between pGBKT7-Lam (lamin protein cloned into pGBKT7) transformed to Y2H gold strain and pGADT7-T. for both positive and negative controls white colonies should grow on the –Leu-Trp plates but only a positive protein-protein interaction should result in blue colonies growing on the –Leu-Trp/X/Aba as four reports are required to detect a positive interaction (Figure 4.28).

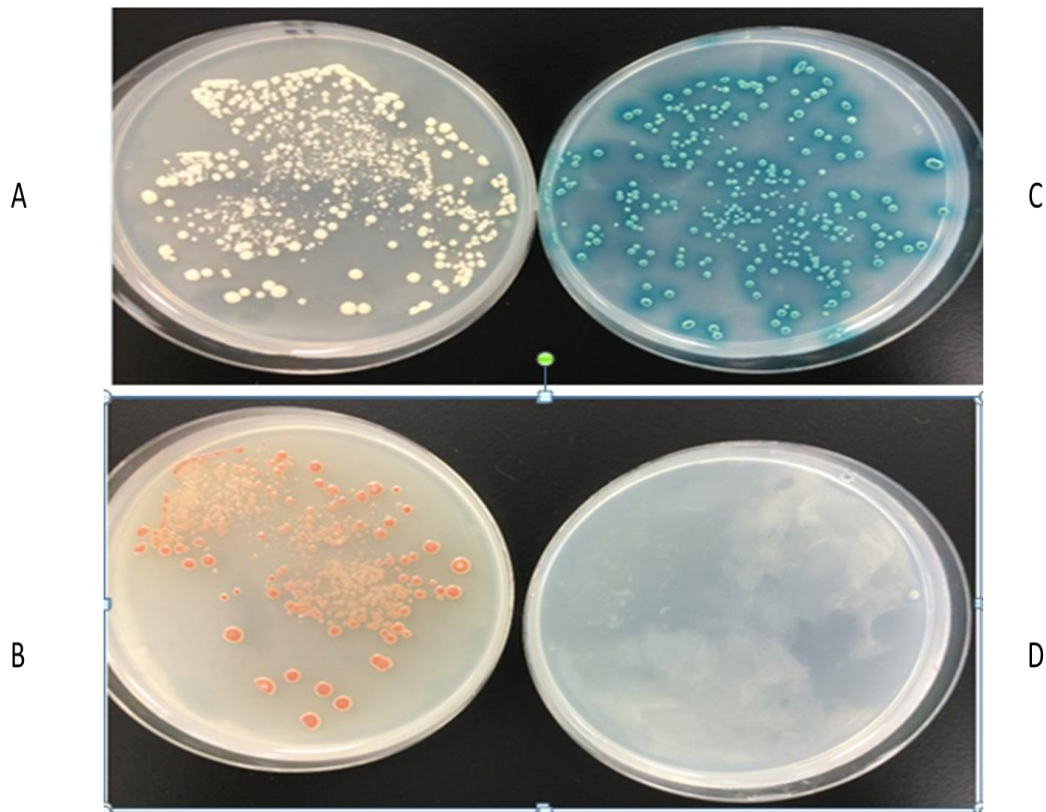


**Figure 4.28: Yeast Two Hybrid control experiments.** (A) -Leu-Trp plate showing colonies growing for positive control experiment (B) -Leu -Trp plate showing similar growth of the negative control experiment to the positive control. (C) blue colonies for positive control experiment on -Leu-Trp/X/Aba plates confirming an interaction between the candidate proteins (D) negative control plate showing no growth for the negative control experiment on -Leu-Trp/X/Aba plate.

#### **4.3.3.3: Ambra1 and PP2CA auto-activation tests**

The next step after cloning Ambra1 and PP2CA into pGBKT7 was the transformation of these recombinant vectors into the target Y2H gold strain and testing the insert for auto-activation of the reporter genes. The Transformations were performed according to the manufacturer's instructions. The auto-activation tests were performed by plating the transformed yeast on single dropout plates (SD-Trp), single dropout plates in the presence of X- $\alpha$ -gal (SD-Trp/X $\alpha$ ) and single dropout plates in the presence of X- $\alpha$ -gal and Aurobasidin antibiotic (SD-Trp/X $\alpha$ /Aba). Transformed Y2H gold strain with recombinant vector should show growth on the SD-Trp plates as tryptophan is expressed by the vector. Colonies should also grow on the SD-Trp/X $\alpha$  but without activation of X- $\alpha$ -gal *i.e.* no blue colonies should be observed. Finally no colonies should grow on SD-Trp/X $\alpha$ /Aba. If the colonies turn blue on the SD-Trp/X $\alpha$  or show any growth on the SD-Trp/X $\alpha$ /Aba it means that the tested bait activates the reporter genes and is not suitable for pursuing the Y2H mating as the results will be mostly false positives.

Ambra1 clone did not show any auto-activation of the reporter genes (Figure 4.29). Neither did PP2CA clone (Figure 4.30).



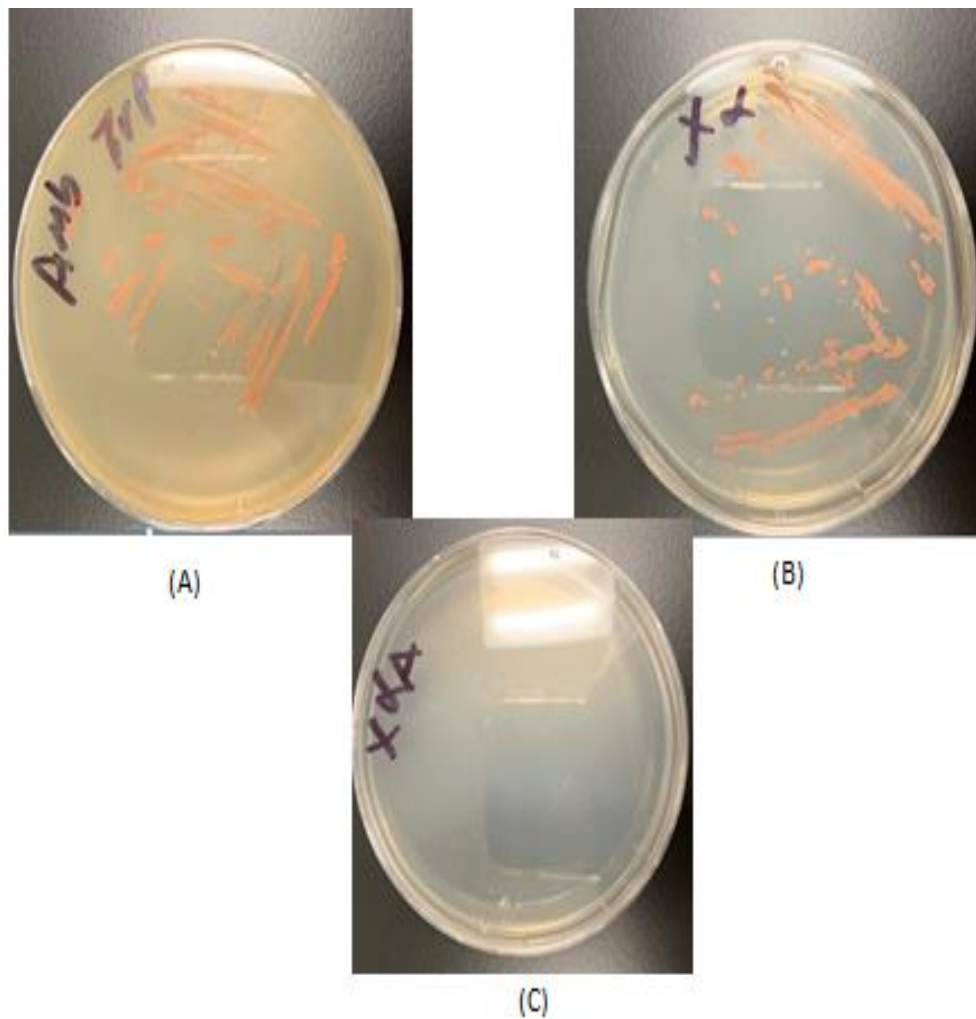


**Figure 4.29: screening of pGBKT7-Ambra1 for auto-activation test.** Colonies of Y2H gold yeast strain transformed with Ambra1-pGBKT7 plasmid is grown on three different media plates to perform the auto-activation test. (A) SD-Trp plate showing colonies growing in the absence of tryptophan. (B) SD-Trp/X $\alpha$  plate showing colonies growing in the absence of tryptophan and not activating X $\alpha$ -Gal as the colonies have the same color as plate (A). (C) SD-Trp/X $\alpha$ /Aba plate showing no colonies growing in the presence of Aureobasidin A.



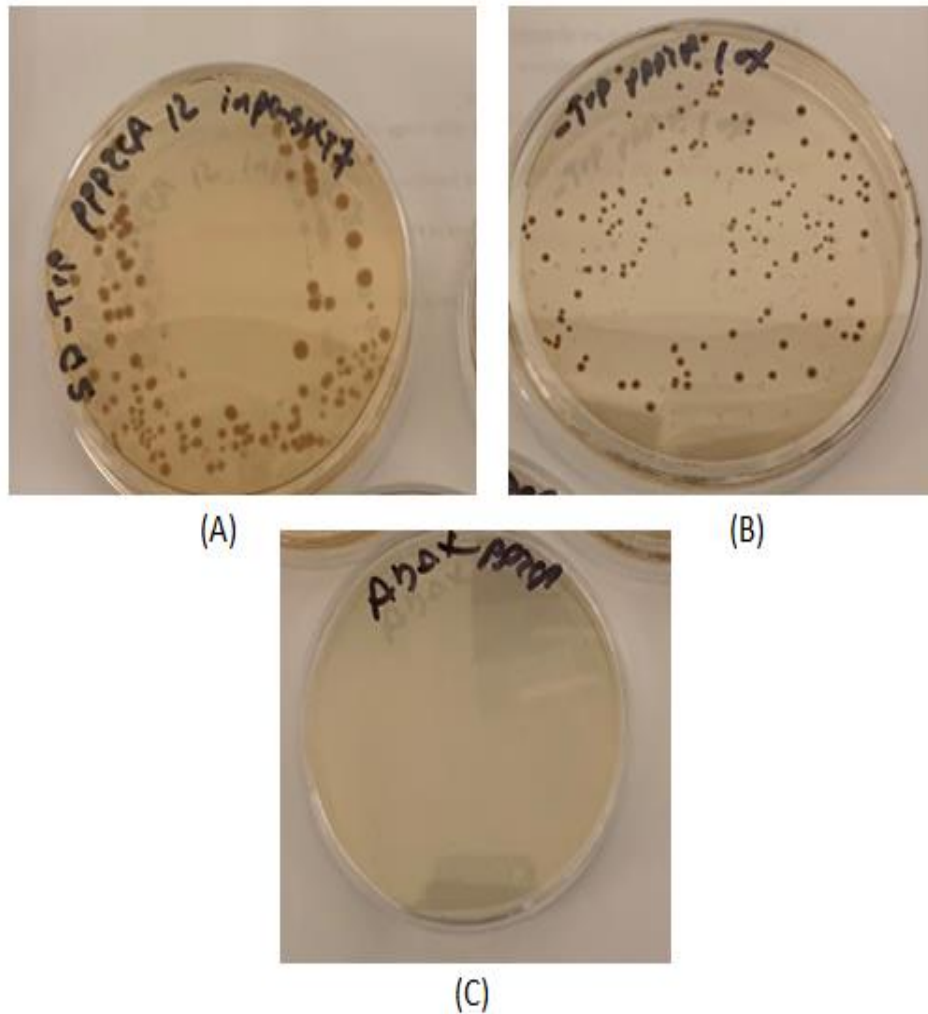


**Figure 4.30: screening of pGBKT7-PP2CA for auto-activation test.** Colonies of Y2H gold yeast strain transformed with PP2CA -pGBKT7 plasmid is grown on three different media plates to perform the auto-activation test. (A) SD-Trp plate showing colonies growing in the absence of tryptophan. (B) SD-Trp/X $\alpha$  plate showing colonies growing in the absence of tryptophan and not activating X $\alpha$ -Gal as the colonies have the same color as plate (A). (C) SD-Trp/X $\alpha$ /Aba plate showing no colonies growing in the presence of Aureobasidin A.

#### **4.3.3.4: yeast-two Hybrid mating**

Since the two tested candidates Ambra1 and PP2CA did not show any toxicity and passed auto-activation tests of the reporter genes, the transformed yeast gold strains with Ambra1-pGBKT7 vector and PP2CA-pGBKT7 were mated with a normalized universal mate and plate libraries according to manufacturer's specifications. Different concentrations of the mated culture were plated on SD/-Trp, SD/-Leu and SD/-Leu/-Trp (DDO) to calculate the mating efficiency and the number of colonies screened. The rest of the mated cultures were plated on DDO/X/A plates. All plates were incubated at 30°C for 3 days. Ambra1 mating resulted in distinguishable greenish-blue colonies indicating positive Ambra1 interactors (Figure 4.31); and so did PP2CA mating (Figure 4.32). Mating efficiency is calculated using the limiting partner; which is of the lower viability (either the bait or the prey). Ambra1 and PP2CA were the limiting partners in each individual mating; and hence; mating efficiencies were calculated using the baits. Number of colonies screened is calculated from the DDO plates. Mating efficiencies and number of colonies screened for both cDNAs are shown in table 4.1.

**Table 4.1: Mating efficiencies and number of screened clones for Ambra1 and PP2CA yeast-two hybrid screening.**

	<b>Manufacturer's recommendation</b>	<b>Ambra1</b>	<b>PP2CA</b>
<b>Mating efficiency</b>	>2%	20%	4.56%
<b>Number of colonies screened</b>	At least 1 million colonies	57,000,000	1,560,000

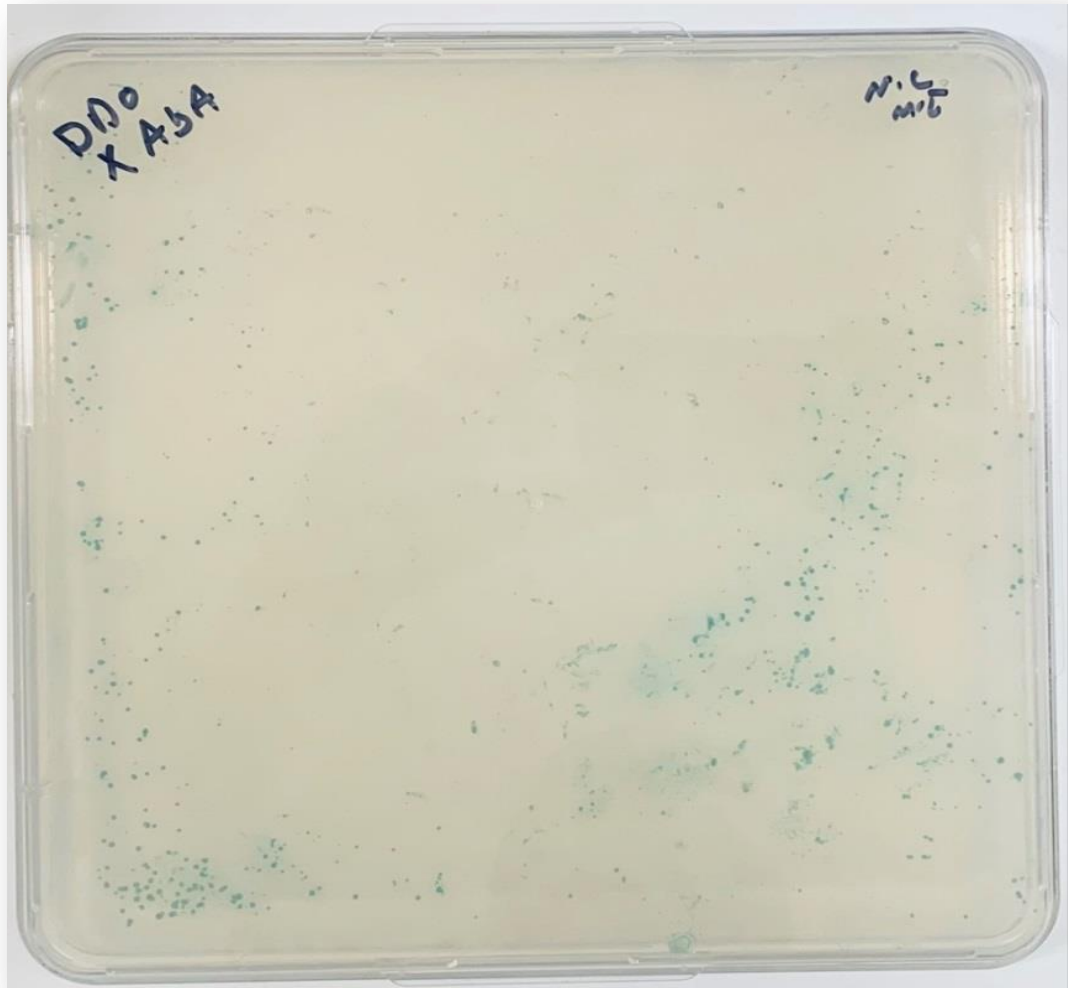


**Figure 4.31: Yeast-two Hybrid screening of Ambra.** Successful mating of Y2H gold strain transformed with pGBKT7-Ambra with Y187 strain transformed with universal mate and plate library. Greenish-blue colonies on these –Leu-Trp/X/Aba plates are positive protein-protein interactions.

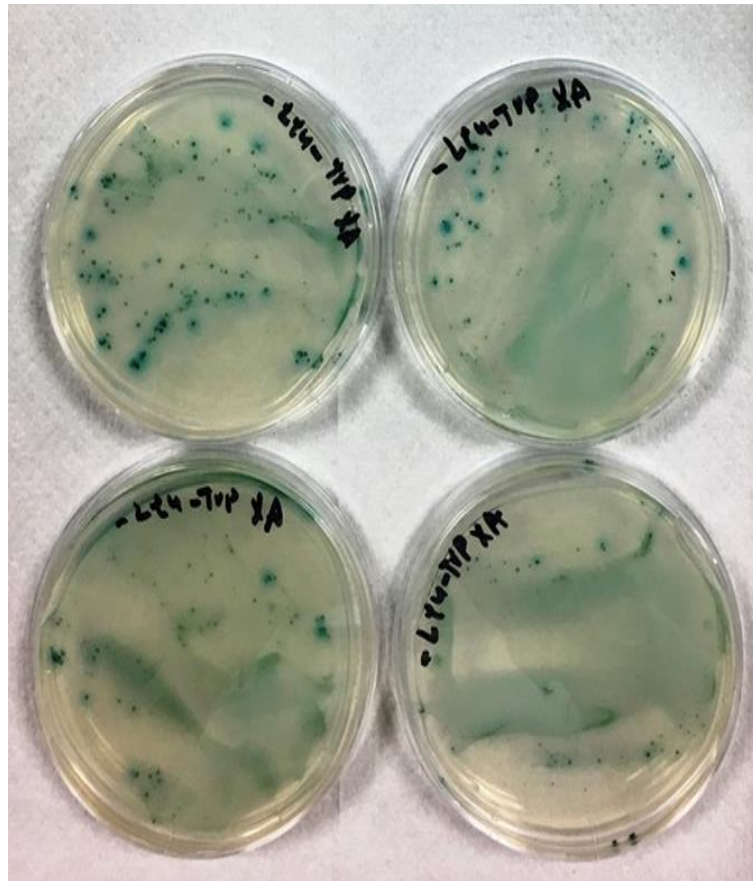


**Figure 4.32: Yeast two hybrid screening of PP2CA.** Successful mating of Y2H gold strain transformed with pGBKT7-PP2CA with Y187 strain transformed with universal mate and plate library. Greenish-blue colonies on these –Leu-Trp/X/Aba shows a positive protein-protein interaction.

#### **4.3.3.5: Confirmation of genuine positive interactions**

A final step to eliminate false positive interactions and confirm genuine positive interactions after successful Y2H mating was performed by streaking greenish-blue grown colonies from the DDO plates from Ambra1 and PP2CA matings on the highly strict quadrupole drop-out plates (QDO/X- $\alpha$ Gal/ABA). Only greenish-blue colonies grown on the QDO plates are genuine positive interactions and were further analyzed to identify the interacting binding partners.

#### 4.3.4: protein binding partners identified by Y2H

The colonies growing on the QDO plates and showing a greenish-blue color are mated colonies that contain the “Bait” plasmid tested as well as the unknown picked up “Prey”. In order to isolate the prey’s plasmids of interest simply they were selected for by extracting the plasmids from the grown yeast according to Manufacturer’s specifications, transforming the isolated plasmids into *E-coli* and finally growing the transformed bacteria on Ampicillin plates. This step allows the growth of bacteria that is only transformed with plasmids containing preys as the preys are on pGADT7-RecAB which contains ampicillin resistance sequence (Figure 4.33).

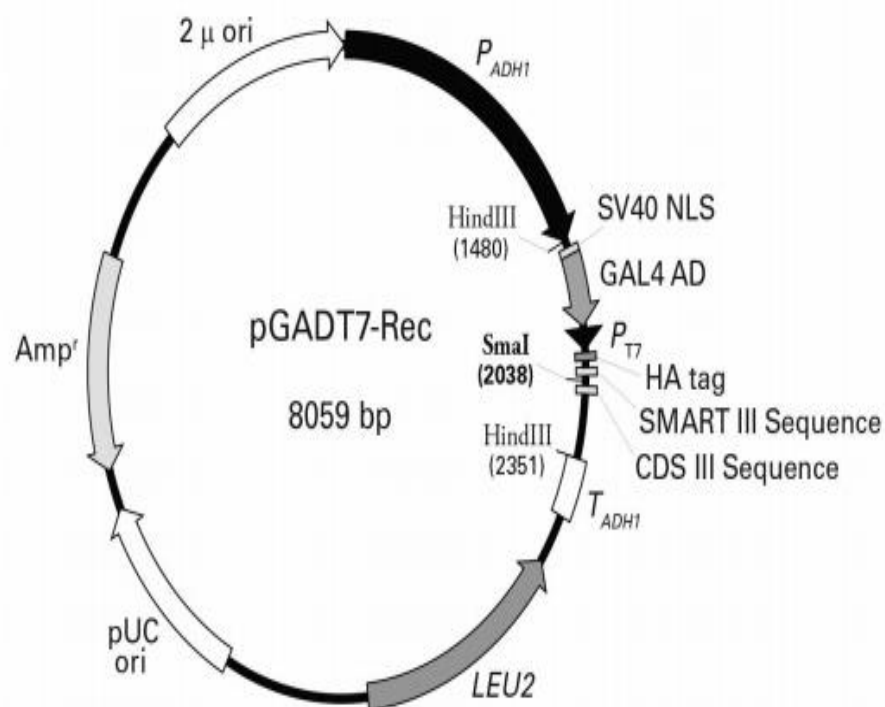


**Figure 4.33: pGADt7-Rec map showing ampicillin resistance sequence.**  
(Image from ClonTech).

#### **4.3.4.1: Ambra1 interactor's analysis**

Preys recombinant vectors from Ambra1 mating were extracted from bacteria grown on Ampicillin plates. A sample of isolated vectors was digested using *BamH I* and *EcoR I* to verify there is a vector with a possible insert (Figure 4.34). Recombinant vectors were sequenced using a T7 sequence primer (source Bio-Science) and compared to databases (NCBI, ensemble) to identify interactor's cDNA. Nearly all sequenced cDNAs were identified more than once in the analysis (Table 4.2).

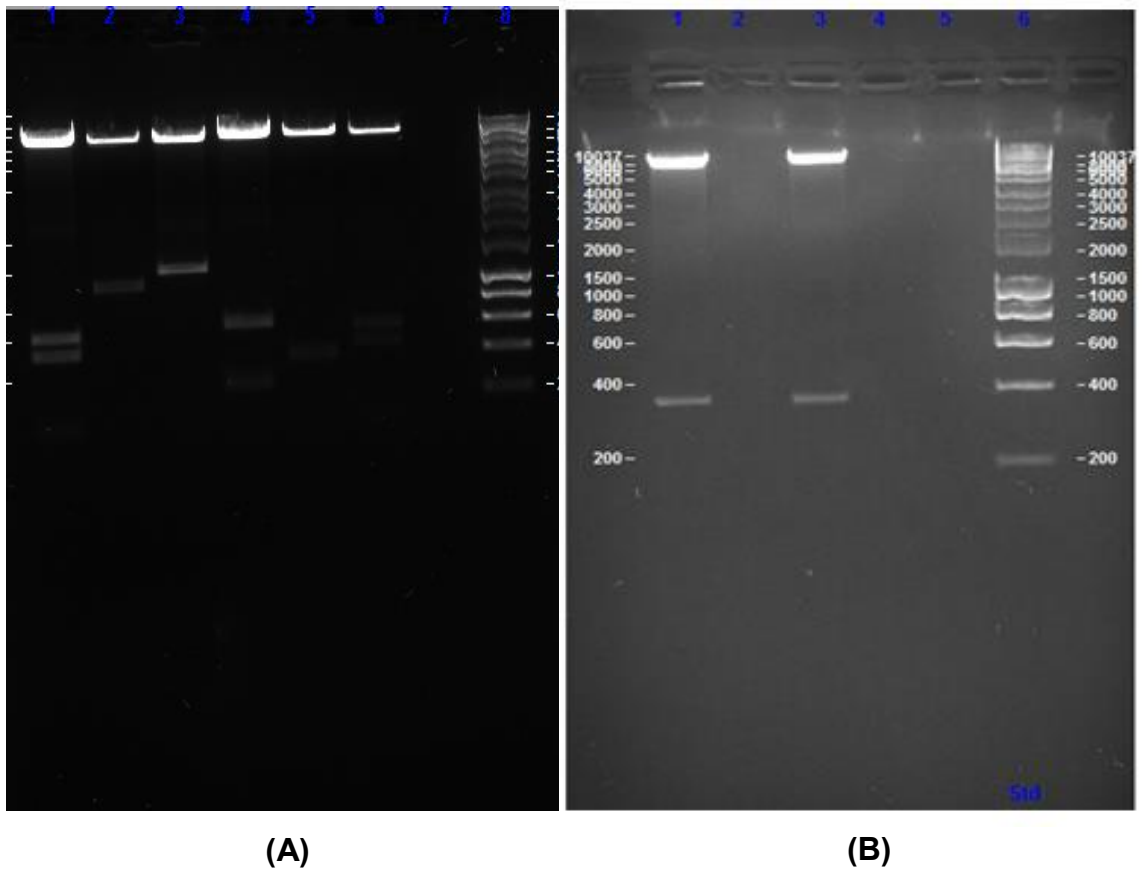


**Figure 4.34: restriction digestion analysis of recombinant plasmids with an insert confirmed to be an Ambra interactor.** (A) Lanes 1 to 6 are six different plasmids of Ambra interactors digested with *Bam*H I and *Eco*R I. Lane 8 is Hyperladder 1Kb. (B) Lanes 1 and 3 are two different samples digested with *Bam*H I and *Eco*R I. Lane 6 is Hyperladder 1Kb.



**Table 4.2 Ambra1 binding partners identified by yeast two hybrid mating assay.** Numbers of identified clones for each protein are shown in brackets

Ambra1 binding partners gene symbol	Protein name and number of identified clones	Selected cellular function by Uniprot
AGO3	Protein argonaute-3 (1)	Required for RNA-mediated gene silencing (RNAi). Binds to short RNAs such as microRNAs (miRNAs) and represses the translation of mRNAs which are complementary to them.
Ankyrin-3	ANK3 (2)	May participate in the maintenance/targeting of ion channels and cell adhesion molecules at the nodes of Ranvier and axonal initial segments
ANKRD7	Ankyrin repeat domain-containing protein 7 (2)	
DSTN	Destrin (6)	Actin-depolymerizing protein. Severs actin filaments (F-actin) and binds to actin monomers (G-actin). Acts in a pH-independent manner.
Human DNA sequence from clone RP4-789D17 on chromosome 1p34.1-34.3, complete sequence	Unnamed protein (3)	
STX7	Syntaxin-7 (2)	May be involved in protein trafficking from the plasma membrane to the early endosome (EE) as well as in homotypic fusion of endocytic organelles. Mediates the endocytic trafficking from early endosomes to late endosomes and lysosomes.
TMED7	Transmembrane emp24 domain-containing protein 7 (3)	Potential role in vesicular protein trafficking, mainly in the early secretory pathway. Appears to play a role in the biosynthesis of secreted cargo including processing and post-translational modifications.

These identified proteins were analyzed using STRING protein interactions tool to scan for any previously reported Ambra1 binding partners (Figure 4.35).

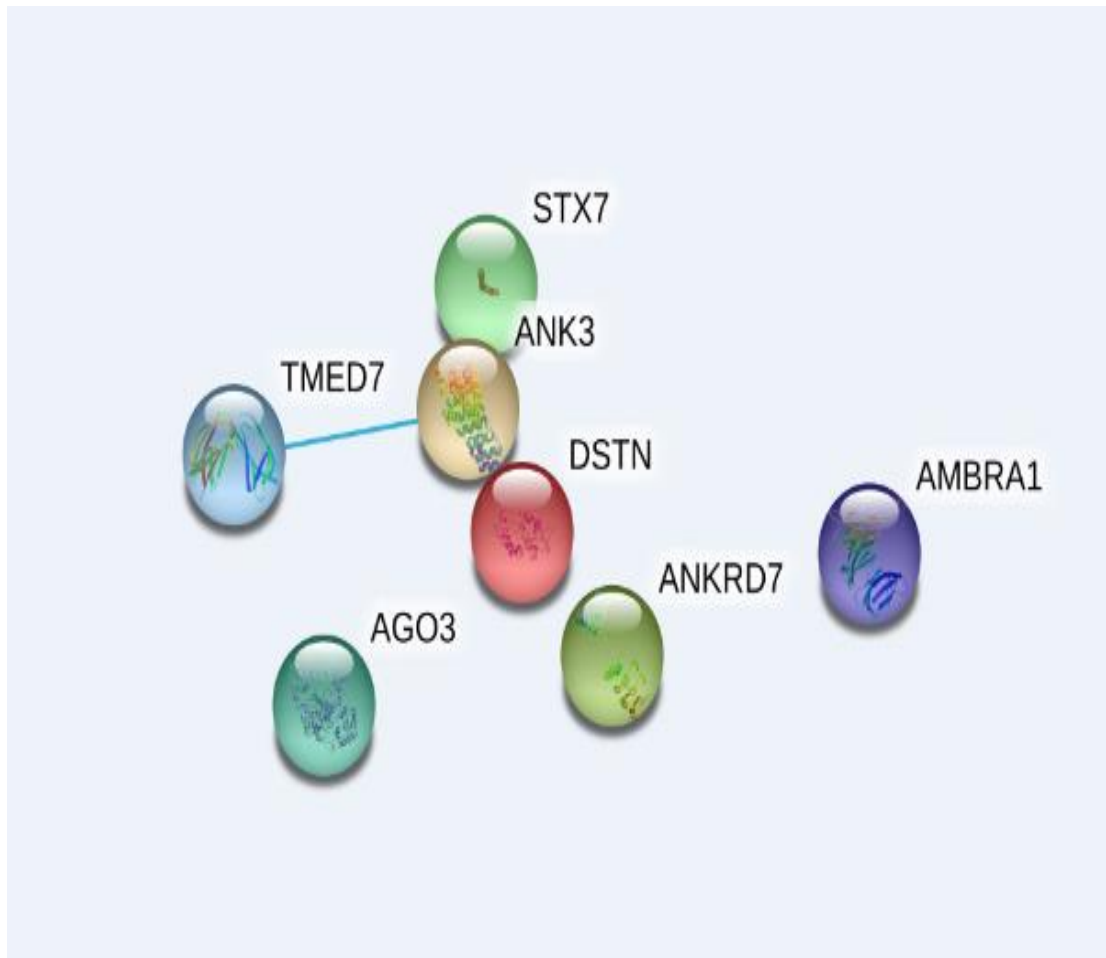


**Figure 4.35: STRING protein analysis for Ambra1 identified binding partners.** The analysis shows that none of the identified Ambra1 binding partners have been reported prior to this study. Colored nodes represent proteins, lines represent interactions and, light blue color represents interactions from curated databases

String analysis of each individual protein was performed to screen for potential pathways that these identified proteins can interact. One of this proteins; AGO3 is of a specific importance as it interacts MYC directly and indirectly via PTEN and TFDP1 (Figure 4.36).

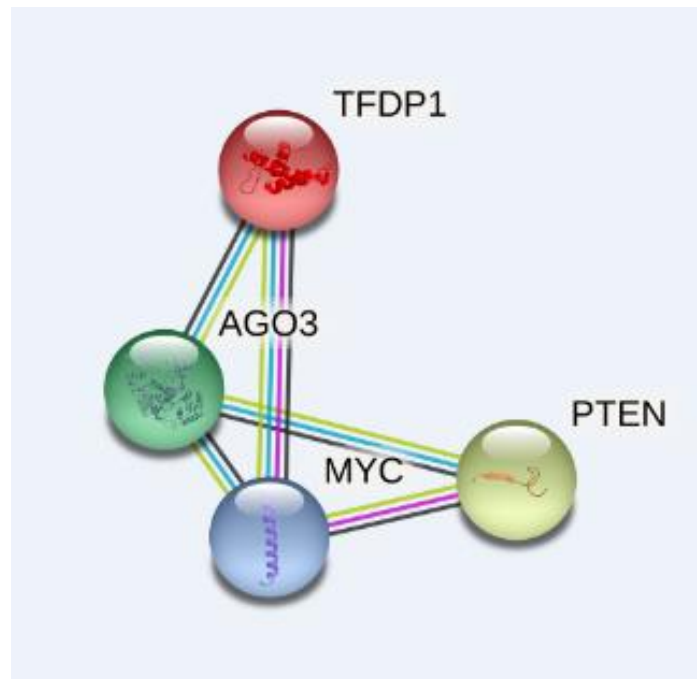


**Figure 4.36: String protein network analysis showing the interaction between AGO3 and MYC from curated databases.** Colored nodes represent proteins, lines represent interactions, light blue represents interactions from curated databases, yellow represents interactions from text mining, purple represents experimentally determined interactions and, black represents co-expression.

#### 4.3.4.2: PP2CA interactor's analysis

Preys recombinant vectors from PP2CA mating were also extracted from bacteria grown on Ampicillin plates and isolated plasmids were analyzed on an agarose gel to test for isolated plasmids (Figure 4.37). Recombinant vectors were sequenced using a T7 sequence primer (source Bio-Science) and compared to databases (NCBI, ensemble) to identify interactor's cDNA. The results of the PP2CA Y2H are novel and new binding partners are identified using this technique. These proteins and their cellular function are listed below (Table 4.3)

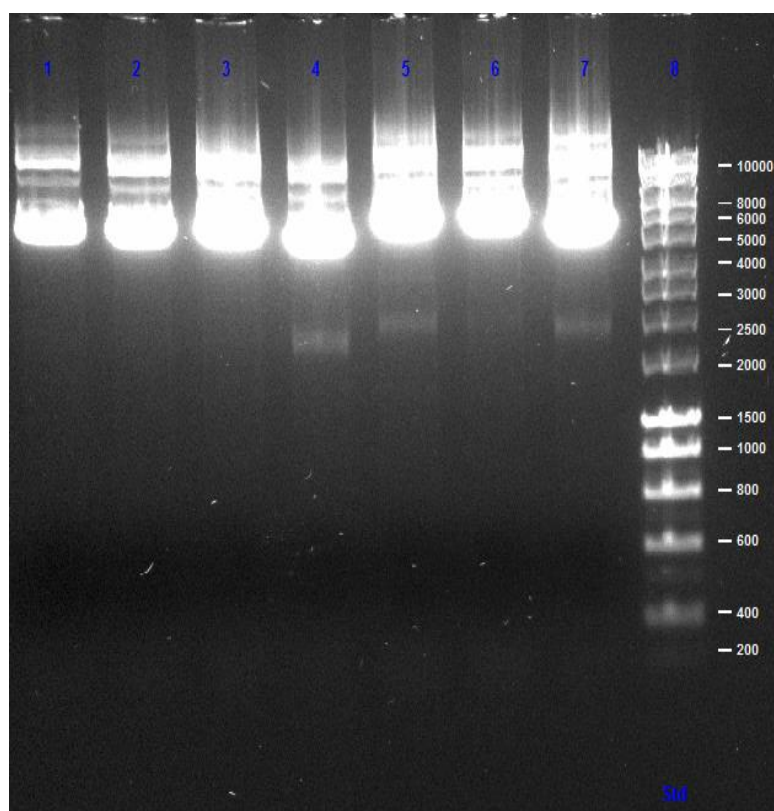


**Figure 4.37: analysis of plasmids isolated from PP2CA Y2H mating.** Lanes 1 to 7 are different samples of prey's plasmids isolated from the mating of PP2CA with a normalized human mate and plate library.

**Table 4.3 PP2CA binding partners identified by yeast two hybrid mating assay**

<b>PP2CA binding partners gene symbol</b>	<b>Protein name</b>	<b>Cellular function by Uniprot</b>
PSMG2	Proteasome assembly chaperone 2	-Mitotic spindle assembly checkpoint. -Negative regulation of apoptotic process. -Proteasome assembly.
MAT2B	Methionine adenosyltransferase 2 subunit beta	Regulatory subunit of S-adenosylmethionine synthetase 2, an enzyme that catalyses the formation of S-adenosylmethionine from methionine and ATP. Regulates MAT2A catalytic activity by changing its kinetic properties, increasing its affinity for L-methionine.
SHANK2	SH3 and multiple ankyrin repeat domains protein 2	Seems to be an adapter protein in the postsynaptic density (PSD) of excitatory synapses that interconnects receptors of the postsynaptic membrane including NMDA-type and metabotropic glutamate receptors, and the actin-based cytoskeleton.

These identified proteins were analyzed using STRING protein interactions tool to scan for any previously reported PP2CA binding partners (Figure 4.38).



**Figure 4.38: STRING protein analysis for PP2CA identified binding partners.** The analysis shows that none of the identified PP2CA binding partners have been reported prior to this study. Colored nodes represent proteins, lines represent interactions

#### **4.4 Discussion**

Choosing this specific approach (Y2H) was based on the fact that it is one of the most widely used protein-protein interaction techniques; it is simple and allows the screening of the candidate protein against a universal library of human proteins (Brückner et al., 2009). The initial yeast two hybrid design was criticized for too many false positives. However; the progress made to this technique and the addition of more reporter genes to be activated for detecting a true positive has made this technique the best candidate for our experimental design. As the system used requires the activation of four different reporter genes which minimizes to a great extent the false positive results. Another motive behind this technique is the novelty of applying the Y2H to study the full sequence complementary DNA of Ambra1 protein. There is one study reported using this technique with Ambra1 DNA encoding only 667 amino acids a bait, Ambra1 fragment was cloned in *EcoR I* and *Bgl II* sites of the pGBKT7 vector, the Y2H screen of this study identified the interaction between Ambra1 and BECLIN1 (Fimia et al., 2007). The same group of researchers identified the interaction of Ambra1 with PP2CA using the same vector (Cianfanelli et al., 2015). Another study has identified the interaction of Ambra1 with DLC1 by the same technique where they cloned a fragment of Ambra towards its C-terminus using *EcoR I* and *Sal I* into the same vector (Di Bartolomeo et al., 2010). Another study has used the same technique to study a protein called RNF2 and Ambra1 was one of the preys picked up by RNF2 (Xia et al., 2014). Mostly Ambra1 protein interaction studies involved other techniques like co-immunoprecipitation and affinity purification of complexes followed by mass spectrometry analysis.

The initial step of performing the Y2H was to clone Ambra1 into the carrier vector (pGBKT7). The restriction enzymes choice was limited to *EcoR* I and *Nde* I (4.3.1). Upon designing these primers few bases were added to the *Nde* I restriction site. Adding few bases to the *Nde* I site end of the PCR product can enhance the efficiency of *Nde* I digestion (Jung et al., 1990).

Few possibilities were considered to identify the reason of initial un-successful cloning of Ambra1. First was the weak efficiency of the restriction enzyme used *Nde* I which is reported to be one of the weakest restriction enzymes used (Chang et al., 2005). Second was the size of the plasmid plus the insert which is more than 11Kbp. However; this possibility was minimized when cloning was unsuccessful upon using Electroporation transformation instead of chemical-transformation. Electroporation can be used to overcome the relatively large size of a recombinant vector (Matsumura, 2015).

Different approaches were applied to overcome the cloning issues. One of which was cloning first into a zero blunt TOPO vector followed by sub-cloning into the desired pGBKT7 plasmid. Using the TOPO vector is reported to be more efficient in cloning PCR products without the use of restriction enzymes (Motohashi, 2019).

Finally, the successful approach was cloning the full length Ambra1 gene using the most recent fusion cloning technique which does not require the use of the restriction enzymes on the DNA fragment to be cloned (Kirchmaier et al., 2013).

This study reports novel Ambra1 binding partners (Table 4.2), that gives more insight into the potential role of Ambra1 in different cellular functions. These interactions with Ambra1 protein have not been reported in literature (Figure 4.35). It is important to highlight that all the reported identified proteins were



picked up more than once by our bait Ambra1 except for AGO3. This shows that these interactions are more likely to be genuine rather than false positives. False positives were also omitted by the use of the highly strict quadrupole dropout plates which allows only the growth of genuine interactions. It is notable that none of the already known Ambra1 binding partners were picked up in this Y2H assay, this can be due to the relatively small number of analyzed positive interactors in this study (approximately 50 colonies), it can also be due to the normalized transcript library used in this assay, which may have picked up less abundant binding partners under physiological conditions, finally in this study and for the first time the full length cDNA of Ambra1 ORF was used in a Y2H assay, considering that Ambra1 is an IDP, the full length protein will have a different conformation compared to just a protein translated by a part of Ambra1 cDNA which was the case in all previous Ambra1 Y2H studies (4.1).

To address the potential novel roles of Ambra1 that can be explored by these results; it is important to review the binding partners identified in terms of their cellular functions and, identify different roles of these proteins that can be mediated or affected by Ambra1.

On top of the list of Ambra1 interactors is Protein argonaute-3 (AGO3). Argonaute proteins (Ago) are essential components of the RNA-induced silencing complex (RISC); they act as binding modules that are highly specialized for small RNA including: microRNAs (miRNAs), small interfering RNAs (siRNAs) and Piwi-interacting RNAs (piRNAs). These RISC binds to complementary sequence and cleave target mRNA with an end result of gene silencing (Ender and Meister, 2010). AGO1, AGO2, AGO3 and AGO4, are the members of the human Ago proteins. AGO3 is reported to show positive and negative regulation of gene expression and, it is also proposed to interact with

MYC (Figure 4.33). Protein Argonaute-3 is essential in regulating stem cell proliferation in human embryos; it acts with DICER protein to generate retinoic acid siRNAs that are essential to modulate the exit from the proliferative stem cell state (Hu et al., 2012).

Second and third Ambra1 identified protein binding partners are: Ankyrin-3 (ANK3) and, Ankyrin repeat domain-containing protein 7 (ANKRD7) respectively. ANK3 is a member of the Ankyrin proteins family, a ubiquitously expressed family of intracellular adaptor proteins; they target proteins to specialized membrane domains. ANK3 also termed ANK-G is expressed in most cell types in the nervous system, they are also the main ankyrin forms in epithelial cells, myocytes, hepatocytes, megakaryocytes, and neurons, its non-canonical isoforms are also expressed in Golgi and lysosomes. Canonical Ankyrins comprise a membrane-binding domain (MBD) of 24 ANK repeats, a spectrin-binding domain, a death domain and a C-terminal domain. Alternative splicing of the Ankyrins gives rise to different subtypes by the insertion of different coils between the spectrin-binding and the death domains. ANK3 also contains a 40 KDa glycosylated serine/threonine-rich domain (Mohler et al., 2002). ANK3 is one of the most consistently repeated and significant schizophrenia and, bipolar risk genes; it has been shown that it can regulate Wnt signaling in neural progenitor cell proliferation in the developing cortex by altering the availability and localization of  $\beta$ -catenin (Durak et al., 2015). It is very interesting that ANK3 has been reported to be able to bind to the LIR motif on different autophagy related proteins resulting in autophagy inhibition, this effect was first reported in neurons. There is a high affinity of interaction of ANK3-LIR to GABARAP (mammalian homologue of yeast Atg8), but not to LC3s (Popelka and Klionsky, 2018).

ANKRD7 is a protein coding gene that contains five ankyrin repeat domains which expression has only been reported in testis. Ankyrin repeat domains are one of the most common protein-protein interaction motifs in nature and, they function exclusively for protein-protein interactions, they consist of 30–34 amino acid residues, they have been found in numerous proteins with diverse cellular functions. For instance; ankyrin repeat domains can be found in INK4 tumor suppressor family. Mutations in these repeats have also been linked to diseases like cancer including melanoma (Mosavi et al., 2004). ANKRD7 has also been reported to be an effector of the endocytic Rab GTPase RAB32 that is involved in autophagy, distribution of mitochondria, trafficking of melanogenic enzymes to melanosomes, and RAB38 which transports tyrosinase to immature melanosomes (Wandinger-Ness and Zerial, 2014).

Next comes DSTN which encodes the protein Destrin; It is widely expressed in different tissues and is ubiquitously expressed in prostate and esophagus. DSTN is an Actin-depolymerizing factor (ADF) which is a component of the highly dynamic cellular cytoskeleton scaffold; it enhances the turnover of actin by slicing actin filaments and binding to actin monomers during cell locomotion, cytokinesis and other forms of cell motility. Destrins are essential for cell viability and, Actin is one of the most abundant proteins in eukaryotic cells and is involved in cell structure and cell motility (Yeoh et al., 2002). Autophagy is a process that involves a lot of proteins trafficking, and autophagosomes transportation to specific cellular locations. Cytoskeleton network plays an essential role in autophagy. However; relatively little is known about this role (Monastyrska et al., 2009). Destrin is also reported to be down regulated as a result of parathyroid hormone mediated autophagy activation in response to dexamethasone damage (Zhu et al., 2017).

The next gene that interacts with Ambra1 is STX7; it encodes the protein Syntaxin-7. Syntaxins also termed as t-SNAREs are key proteins in membrane fusion that assemble a core-trans SNARE complex with v-SNARE. This fusion is essential for communication between cells as well as; intracellular compartments. Unlike v-SNAREs that contains an anchored tail with one SNARE motif; t-SNAREs consist of two to three polypeptides, a member of the Syntaxins subfamily as the heavy chain and members of the SNAP-25 subfamily as the light chains. The function of SNAREs is simply catalyzing the fusion of the membranes of the transport intermediate (vesicles or containers) and the target compartment, v-SNAREs are associated with vesicles while; t-SNAREs are associated with target compartments (Hong, 2005).

SNAREs have long been reported to have a key role in autophagy; by acting as regulators of the precise autophagic fusion process moreover; recently they have been reported to have a role in autophagosome biosynthesis. The role of these proteins in autophagy has been extensively reviewed (Wang et al., 2016). Homotypic fusion of Atg16L1 depends on different SNARE proteins including Syntaxin-7 and, is essential for autophagosome formation. Autophagic precursors are unable to mature into autophagosomes in the absence of these SNARE proteins (Wang et al., 2016). STX7 which forms a SNARE complex with VTI1B, STX8 and VAMP8 which functions in the homotypic fusion of late endosomes; is specifically involved in protein trafficking from plasma membrane to the lysosomes passing through early and late endosomes, which is the last barrier for autophagosome degradation. Lysosomes are the primary protein degradation vesicles for cargos from unrecycled endocytosed proteins, phagocytosed material and autophagized proteins (Mullock et al., 2000).

To add to the list of identified proteins that exerts different roles in protein trafficking; Transmembrane emp24 domain-containing protein 7 (TMED7) is on the list of Ambra1 identified interactors, which is involved in vesicular protein trafficking. It contains a Golgi dynamics (GOLD) domain; it is a  $\beta$ -strand-rich domain found in several proteins involved in Golgi dynamics, as well as intracellular protein trafficking. TMED7 has been proven to show an essential role in inhibiting the toll-like receptor 4 (TLR4) signaling from the endosome (Doyle et al., 2012). TMED7 is also involved in the biosynthesis of secreted cargos by processing and post translational modifications.

Finally we have identified an interaction between Ambra1 and an unnamed protein encoded from clone RP4-789D17 on chromosome 1p34.1-34.3.

After reviewing these proteins and their different roles; we were looking for common properties and functions that can relate these different proteins. Despite the fact that STRING protein analysis did not show a direct interaction between these proteins except for TMED7 that interacts with ANK3, nearly all these proteins are related to protein trafficking. TMED7 is a trans-membrane protein that is involved in vesicular protein trafficking. Moreover; half of the proteins on our list either Bear a SNARE domain or are reported to directly or indirectly interact with SNARE domains. As mentioned before STX7 is a t-SNARE protein, Ankyrin repeat domains have long been reported to form complexes with SNARE domains (Daste et al., 2015). Moreover; ANRD7 is a direct effector of the well-known Snare domain interactor's endocytic Rab Gtpases (Wandinger-Ness and Zerial, 2014), the actin cytoskeleton which is regulated by destrin is also known to interact with SNAREs (Karunakaran et al., 2012).

Ambra1 physical interaction with these proteins and pathways give a whole new insight about Ambra1 roles. Perhaps the most obvious is that Ambra1 is involved extensively in cellular proteins trafficking and, specifically proteins involved in autophagy (Figure 4.39).

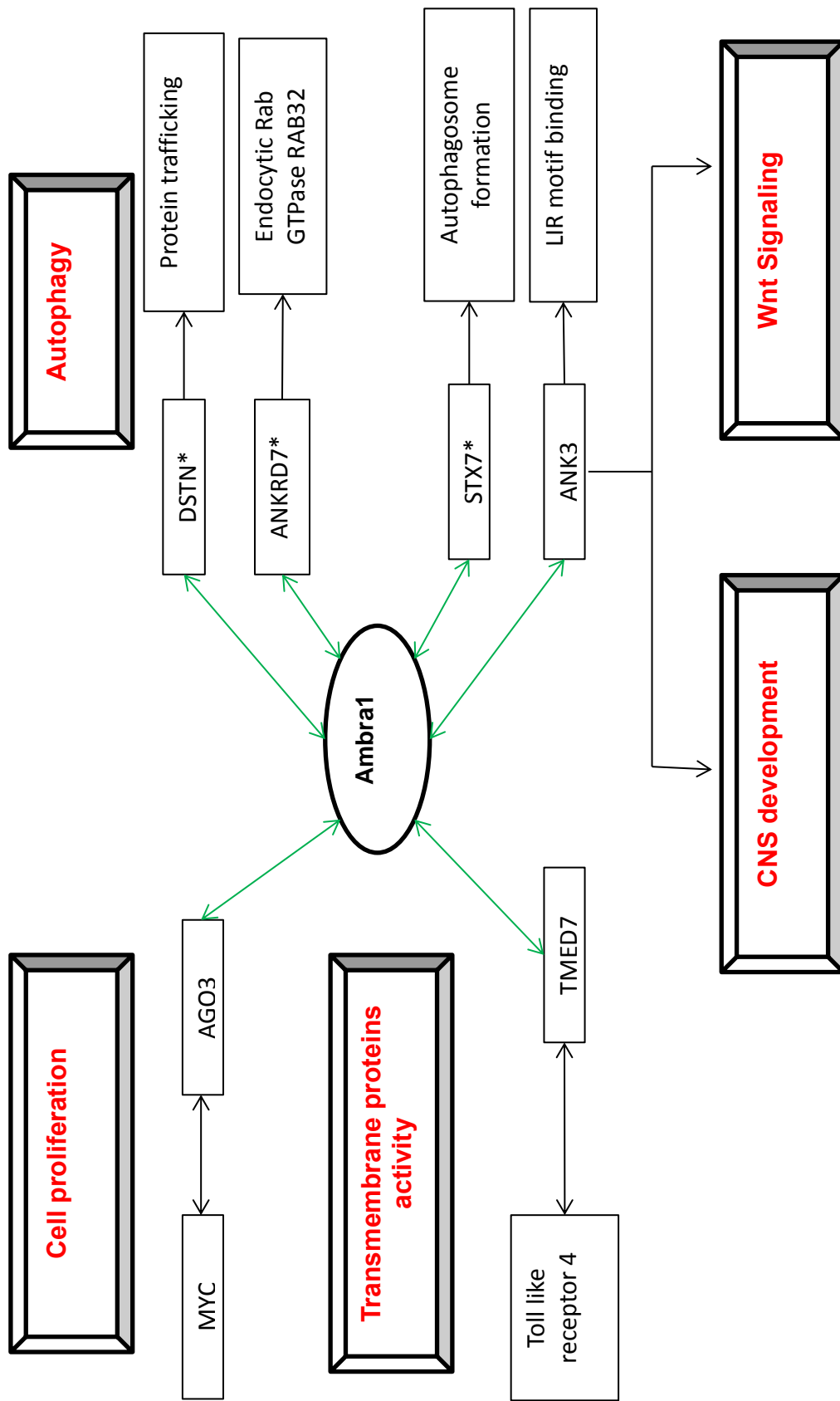


**Figure 4.39: A representative diagram of Ambra1 novel roles identified by yeast two hybrid assays.** Green arrows represent novel interactions identified by the Y2H. Black arrows represent reported roles in literature. Red font is for major pathways that are identified to be affected by Ambra1 in this study. Stared proteins are reported to interact with SNARE domains.

In the context of protein trafficking; STX7, ANKRD7, DSTN and, TMED7 stand out in the list of identified proteins. While most of these proteins are centered on autophagy related transport; some of their roles extend to different cellular processes.

The interaction of Ambra1 with STX7 is of a great importance to explore a new role of Ambra1 in autophagy, Ambra1 is translocated together with Beclin-1 and PI3KIII to the endoplasmic reticulum PAS where the autophagosome formation starts; a process that involves a lot of protein trafficking (1.5). The global network of phagophore formation is not fully discovered, and a lot of members of this process are yet to be identified (Wang et al., 2017). Ambra1 loss results in reduction in the rate of autophagosome formation (Antonioli et al., 2014; Benato et al., 2013). Different proteins including SNAREs and, SNARE complexes roles in the autophagosome maturation and fusion with lysosomes journey are very well explained (Zhao and Zhang, 2019). The interaction between Ambra1 and Syntaxin7 gives a lead to a possible mechanism by which Ambra1 may regulate autophagosome formation. Moreover, this interaction suggests a role of Ambra1 in the journey of trafficking proteins from plasma membrane all the way to lysosomes for degradation; which is a specific role of STX7.

To highlight the role of Ambra1 with SNAREs, ANKRD7, a known effector of RAB32 and RAB38 GTPases is on the list of the identified proteins, Rab GTPases and their effectors act upstream of SNAREs to provide the first layer of specificity in the recognition of membranes compatible for fusion. In addition, they contribute key functions and factors required for SNARE-mediated membrane fusion. This study shows that Ambra1 can interact with SNAREs protein trafficking by binding the GTPase effector ANKRD7. Moreover; it



identifies a second role of Ambra1 in protein trafficking as RAB GTPases and their effectors roles are not limited to SNAREs, but extends to contribute to the structural and functional identity of intracellular organelles. Identified specific roles of ANKRD7 include: autophagy, distribution of mitochondria, trafficking of melanogenic enzymes to melanosomes, transporting tyrosinase to immature melanosomes (Wandinger-Ness and Zerial, 2014). Studying specific roles of ANKRD7 mediated by Ambra1 and vice versa can be of a great importance. However, since both proteins are involved in autophagy therefore, it is more likely that this interaction will be related to their roles in autophagy.

The final addition to SNARE interaction on our list is Destrin, an Actin cytoskeleton depolymerizing factor. Actin cytoskeleton is a very complex network that is required for endocytosis, pinocytosis, phagocytosis, cytokinesis, cell motility and membrane fusion (Karunakaran et al., 2012); its interaction with SNAREs is just one side of this complex network. However; in the context of this study it highlights the role of our protein of interest Ambra1 and, how it can directly and indirectly interacts with SNAREs. The interaction between Ambra1 and Destrin gives a novel insight about the potential role of Ambra1 in different cellular processes. Destrins are essential for cell viability and, Actin is one of the most abundant proteins in eukaryotic cells. An interaction between such protein and Ambra1 broadens the role of Ambra1 in vital and essential cellular functions specifically cell motility. Moreover, it adds to novel roles of Ambra1 in autophagy reported in this study by highlighting a possible role in the link between cytoskeleton and, autophagy. Ambra1 can be of an essential role for protein trafficking during autophagy through its interaction with Destrin.

This study also reports Ambra1 to be a bait for TMED7 which is a transmembrane protein involved in vesicular protein trafficking and Golgi

dynamics. This finding adds to the identified roles of Ambra1 in protein trafficking. It is also interesting that this study shows that Ambra1 upregulation and knockdown in A375 melanoma cell lines result in a non-significant and a significant upregulation of TLR4 respectively (6.3.2) this suggest a role of Ambra1 in TLR4 signaling that might be mediated by TMED7. Further analysis to study the binding site of TMED7 and Ambra1 can potentially be a gate to identify a novel role of Ambra1 in transportation of cargo molecules from the endoplasmic reticulum to the Golgi complex specially, if the binding site is the GOLD domain of TMED7.

The interaction between Ambra1 and ANK3 is novel and of a great importance. Ambra1 is known to be involved in the development of the nervous system and it has been related to different CNS disorders like schizophrenia and, autism. This study shows a great influence of Ambra1 on axon guidance cellular process pathway (6.3 and 6.4). ANK3 plays an essential role in the development of the nervous system and moreover; it is associated with CNS disorders and is of an essential role in establishing neuronal axon initial segment (Leterrier et al., 2017). The physical interaction between Ambra1 and ANK3 provides a proof of a direct link of these two proteins in the development of the nervous system as well as; CNS related disorders. This study have also shown a role of Ambra1 in regulating the Wnt signaling pathway by altering the expression of Wnt5a (6.5), taking this together with the ability of ANK3 in regulating the same pathway in cortex development can contribute to the understanding of Ambra1 effect of the development of the nervous system. The expression of this gene in lysosomes as well can highlight a potential role of ANK3 as a protein adaptor in Ambra1-mediated autophagy. Ambra1 bears LIR

motif which can potentially be the region where an interaction between Ambra1 and ANK3 takes place.

Protein argonaute-3 which shows positive and negative regulation of gene expression comes last on our identified proteins. AGO3 functions are not widely explored in literature. However; curated databases from string propose and interaction of AGO3 with MYC. The few studies that reported AGO3 roles is so important, both AGO3 and Ambra1 are reported to be essential in the embryonic development, AGO3 with DICER are essential to generate retinoic acid sliced siRNAs which modulate the exit of stem cells active proliferative phase during embryonic development, studying if Ambra1 has a role in this context with AGO3 will be essential to explore Ambra1's role in cell proliferation. Perhaps the first approach should be monitoring AGO3 slicer activity on Ambra1 and whether it can promote or limit the activity of Ambra1 during embryogenesis and also if this role is also mediated by MYC or by a different pathway.

Collectively this study reports that Ambra1 interacts with SNARE proteins, Actin cytoskeleton proteins, RAB GTPases proteins and transmembrane proteins. These proteins are widely involved in protein trafficking at different stages, as well as, specific involvement in autophagosome formation, membranes fusion, autophagy, cell proliferation, Wnt signaling, CNS development and pathologies, cell motility and toll like receptor 4 signaling.

The yeast two hybrid control experiment performed using PP2CA have also identified three novel PP2CA binding partners (Table 4.3). Only a small sample of PP2CA was sequenced as it is not the main focus of this study, and it was

only used a control experiment. However, a relation between identified novel Ambra1 and PP2CA binding partners have been identified (7.3).

***Chapter 5- Development of methods for the proteomic and metabolomics analysis of Ambra1 overexpression***

## **5.1 Introduction:**

“Omics” refers to the collective technologies used to explore the roles, relationships, and actions of the various types of molecules that make up the cells of an organism. These technologies include: genomics, proteomics, metabolomics, transcriptomics, glycomics and lipomics.

The study of proteome allows the understanding of how the genes are translated and allows the detection of post-translational modifications (PTM) of the proteins. 2D-electrophoresis (2D-E) was first introduced in 1970s (O’Farrell, 1975) and it is an orthogonal approach which is capable of, simultaneous fractionation, identification, and quantification of proteins when coupled with mass spectrometry (Magdeldin et al., 2014). 2D-E allows the separation of proteins by two dimensions, the first is isoelectric point (pI) and the second is the protein molecular weight. 2D-E is mostly coupled with mass spectrometry (2D-E-MS) this technique is very reproducible and applicable for identifying proteins by MS (Rabilloud and Lelong, 2011). Comparing two samples can give a visual representation of changes in the proteome between them by staining the gels with a chemical stain that will bind to the cysteine groups of the analyzed proteins. 2D-E can also be used to study PTMs that causes change in a protein pI and/or the MW; for example: phosphorylated proteins can show higher molecular weights and different pI to dephosphorylated forms of the same protein. The literature is rich with studies using this technique to compare different *in-vivo* and *in-vitro* samples. For example, one study identified four differentially expressed genes in chemo-therapy resistant melanoma patients using 2D-E-MS (Sinha et al., 2000).

Metabolomics is defined as “the systematic study of all chemical processes concerning metabolites, providing characteristic chemical fingerprints that

specific cellular processes yield, by means of the study of their small-molecule metabolite profiles” (Burgess et al., 2014). Mass spectrometry (MS) associated metabolomics has emerged as a technique for profiling metabolic features associated with clinically relevant aspects of tumor biology (Kaushik and DeBerardinis, 2018). The most commonly used application of metabolomics in cancer is identifying novel biomarkers for diagnosis or predicting prognosis (Gowda et al., 2008).

In this arm, a proteomics and a metabolomics approaches were applied to the two melanoma cell lines rAmbra and rBgal to investigate the change in proteome/metabolome in melanoma cell lines upon over-expressing Ambra1.

## **5.2 Results**

To study the proteome change associated with Ambra1 over-expression, a mass spectrometry-based proteomics approach was designed. rAmbra cells were utilized to study proteomic change upon the over-expression of Ambra1 compared to the matched control rBgal. The same cell lines were also used to apply a mass spectrometry-based metabolomics to study the effect of Ambra1 over-expression.

### **5.2.1 2D gel electrophoresis**

Protein separation using 2D-E is a multi-step process that needs optimization. It involves protein extraction, sonication, purification, quantification, focusing on IEF strips and separation by TGX gels. Protein extraction, quantification and sonication are detailed in section 2.2.2. Protein purification was initially performed using 2D clean-up kit (Bio-Rad, Uk). However protein yield was optimum when TCA protein precipitation protocol was used (2.2.10).

After optimizing the protein extraction step; the study shifted forward towards protein separation by the two dimensions electrophoresis.

#### **5.2.1.1: E-coli standard 2D electrophoresis**

It was important at the beginning to optimize the 2D-E protocol and hence; a standard E-coli protein sample (Bio-Rad, Uk) was focused on different strips using different protocols (2.2.10). Initial runs (n=4) showed poor protein separation (Figure 5.1). However; an optimum protocol was reached after trying different focusing conditions; this protocol involved a “desalting” step in which protein samples were focused at 2K volts for 2 hours followed by replacing the wicks on each side of the focusing strips. A total of 40K volt-hours were set to be the optimum separating protocol (figure 5.2).



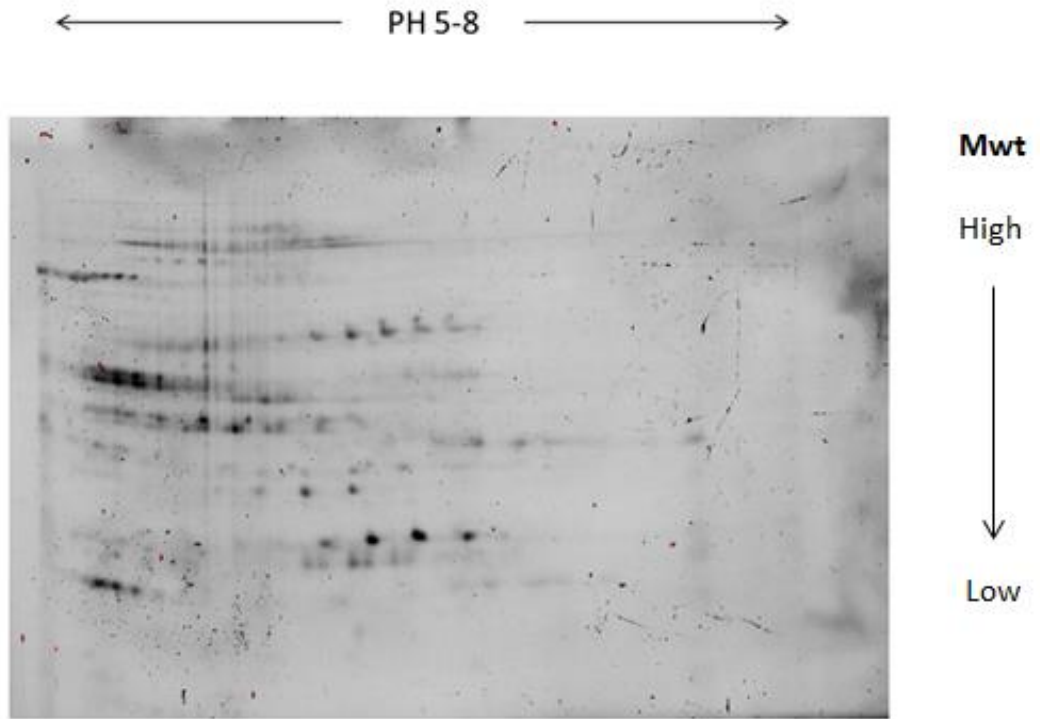


**Figure 5.1 E-coli standard protein sample separation using 2D electrophoresis.** Each dot on the gel represents a protein.

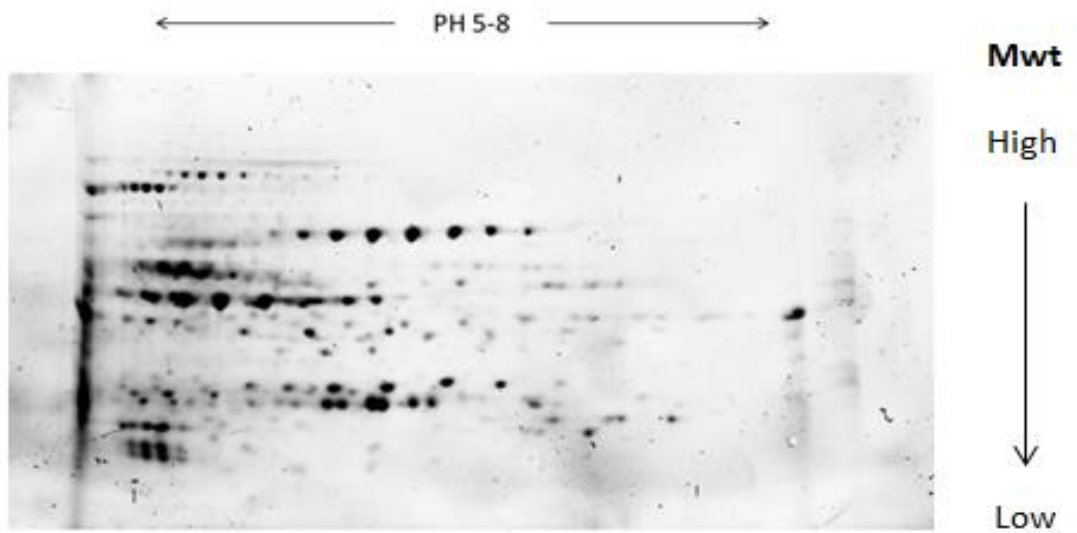


**Figure 5.2: Optimized E-coli standard protein sample separation using 2D electrophoresis.** Each dot on the gel represents a protein. Gel shows successful protein separation by 2D-E.

### **5.2.1.2 rAmbra and rBgal 2D electrophoresis**

Different IEF strips were used for focusing rAmbra and rBgal samples (2.2.10). The first protein separation was performed using a 5-8 11cm. IEF strip, first dimension was overnight separation at 25k volt-hours and the second dimension was gel electrophoresis separation on stain free gels (Figure 5.3). However; separation was optimum when using 40K volt-hours for protein focusing on 11cm IEF strips (Figure 5.4) and 60K volt-hours for 17cm IEF strips (Figure 5.5). Reproducibility of protein separation using the two cell lines (n=12) was very low, and also the few 2D-E runs that did show protein separation did not show any noticeable visual difference between rAmbra and rBgal. Some of the gels were stained by either colloidal coomassie or silver stain (2.2.10) to decide between which stain will be used to proceed to spots excision and mass spectrometry. Despite the fact that silver stains showed much higher sensitivity compared to colloidal coomassie, this was not of a great use as reproducibility of protein separation was very low and therefore; it was useless to stain the gels at this point.

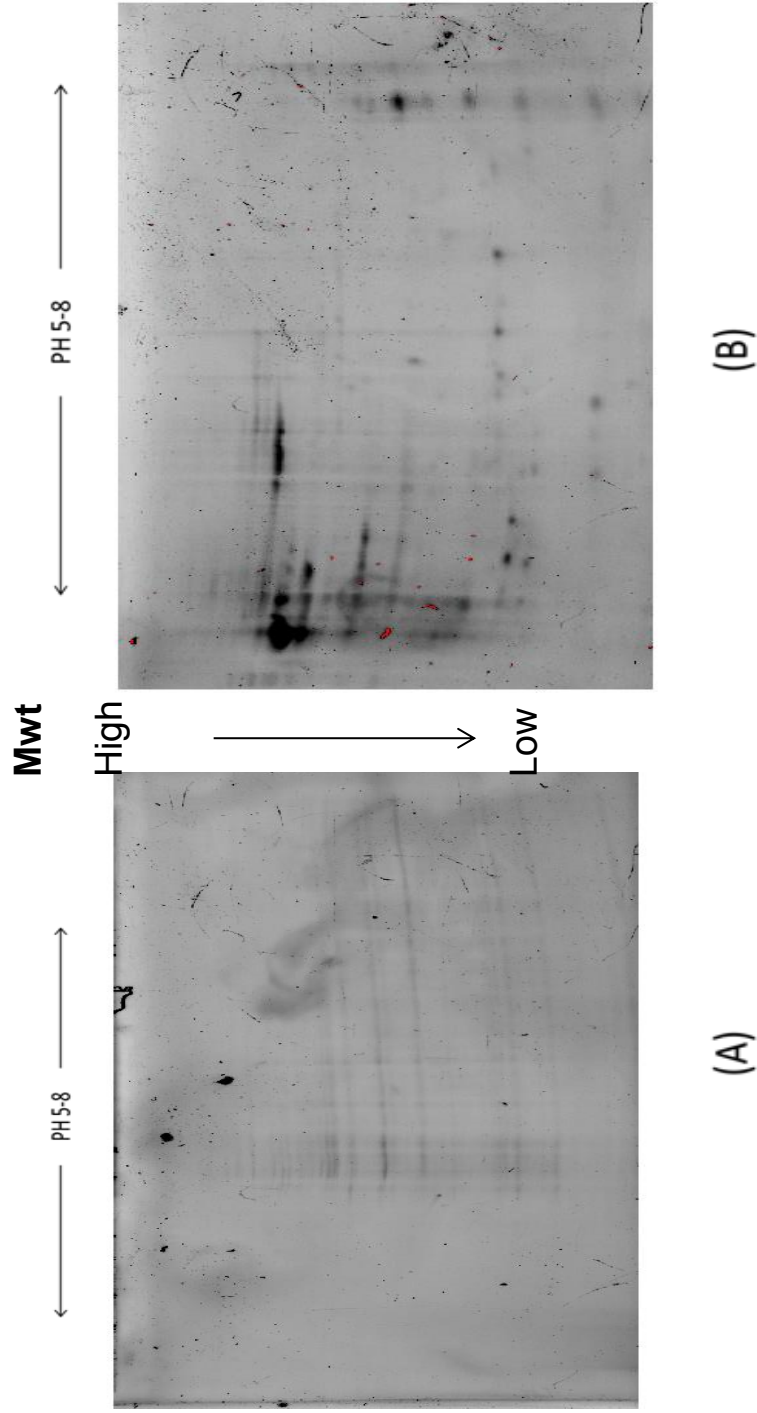


**Figure 5.3: 2D electrophoresis of protein samples on 5-8 11cm IEF strip at 25K volt-hours. (A) rAmbra. (B) rBgal. Poor protein separation was observed by focusing 5-8 IEF strips at 25k volt-hours.**

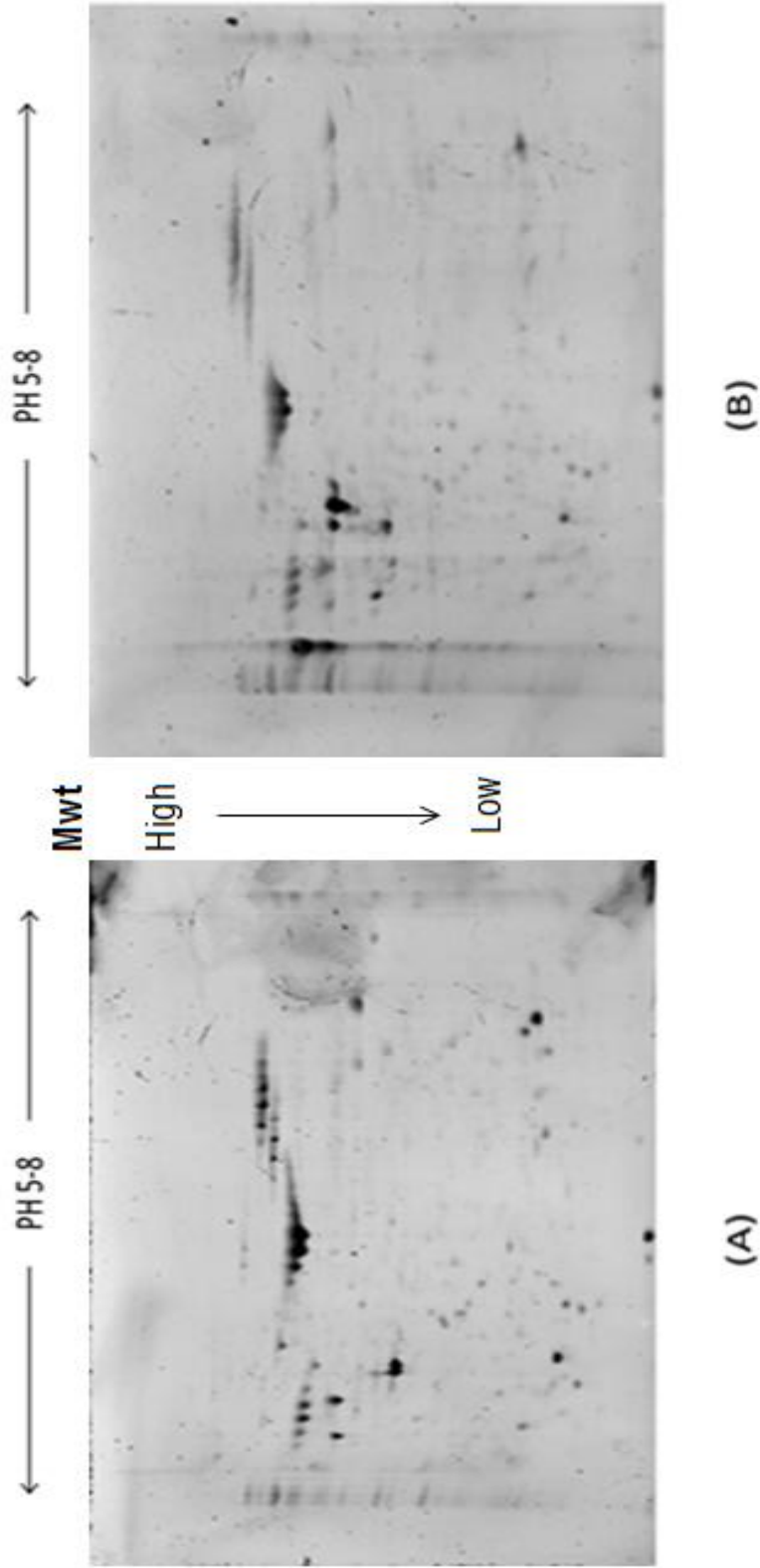


**Figure 5.4: 2d-Electrophoresis of rAmbra and rBgal 11 cm 5-8 IEF strips at 40K volt-hours.** (A) rAmbra. (B) rBgal. Better protein separation was observed when 5-8 IEF strips were focused at 40K volt-hours. No visual difference between rAmbra and rBgal.

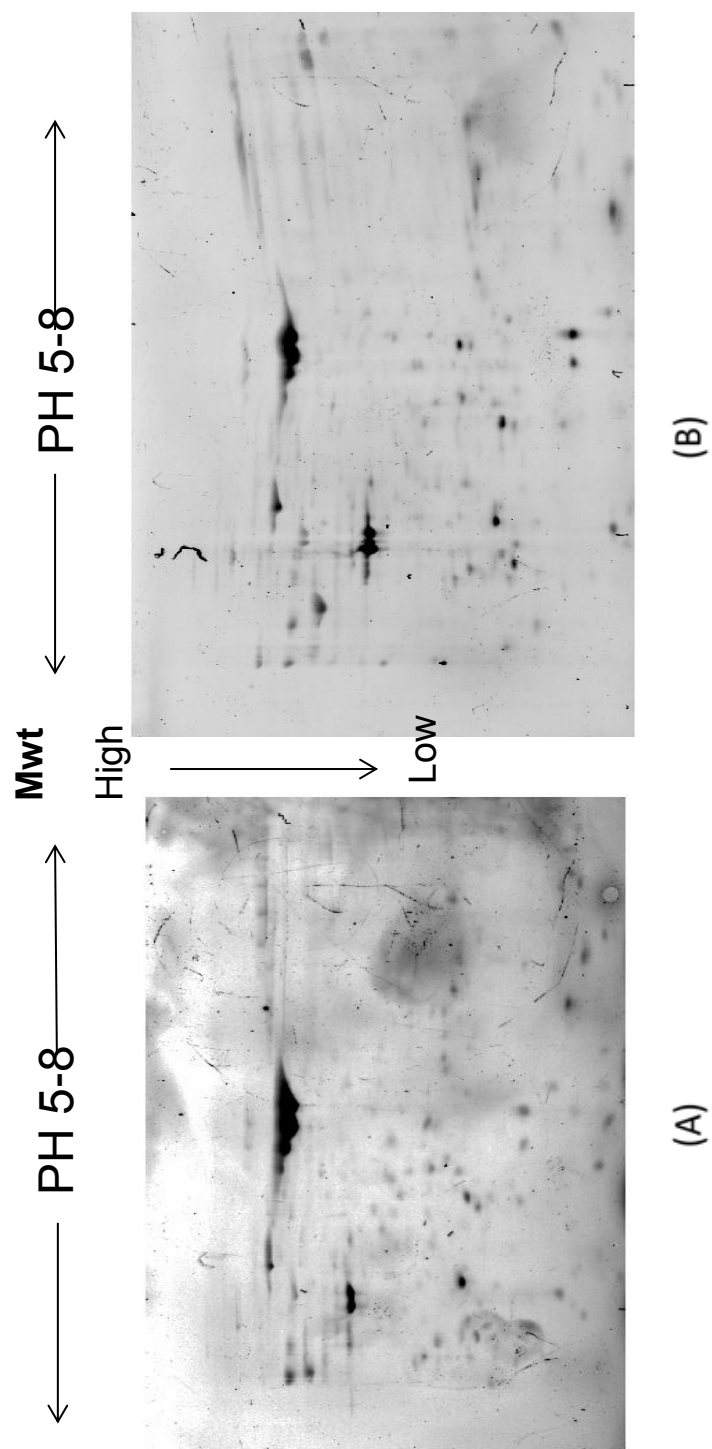


**Figure 5.5: 2d-Electrophoresis of rAmbra and rBGal 17 cm 5-8 IEF strips. (A) rAmbra. (B) rBgal. No visual difference can be observed between rAmbra and rBgal**

### **5.2.1.3 *rAmbra and rBgal 2D western blots***

Visual difference between the gels was not enough to spot significant change in the proteome and further analyze these spots using mass spectrometry. *rAmbra* western blots showed additional bands to the 130KDa band for Ambra1 protein that was not observed in the *rBgal* (Figure 3.1). 2D western blots were performed to try and identify spots for Ambra1 itself, ideally these spots were to be excised and analyzed by mass spectrometry to confirm if they are genuine bands of Ambra and, study the difference between them. To test for Ambra1 spots separated proteins were transferred to the Trans-Blot® Turbo™ Midi PVDF membranes (Bio-Rad, UK) using the Trans-Blot® Turbo™ Blotting System (Bio-Rad, UK), according to manufacturer's instructions. However; protein transfer was poor (Figure 5.5). Using the same Ambra1 antibody and the same protocol used for the 1D western blots was not successful and no spots were observed for Ambra1 on the western blot.

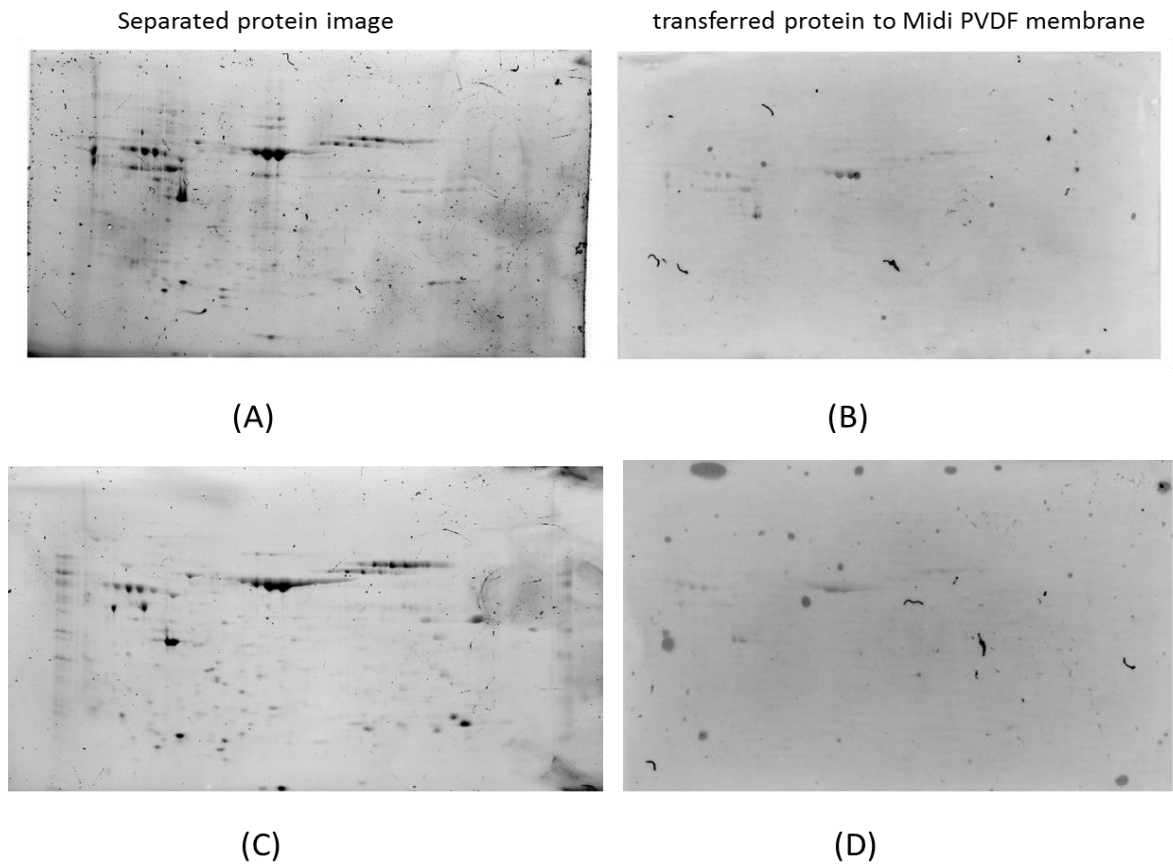
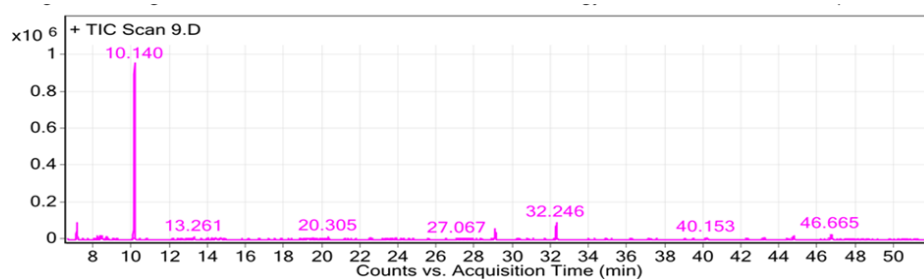


**Figure 5.5 2D-Electrophoresis and stain free blots of rAmbra and rBgal.** Proteins from both cell lines were separated by 2d electrophoresis and transferred to PVDF membranes. (A) rAmbra protein separation. (B) Stain free rAmbra PVDF membrane. (C) rBgal protein separation. (D) Stain free rBgal PVDF membrane. PVDF membranes show poor protein transfer.

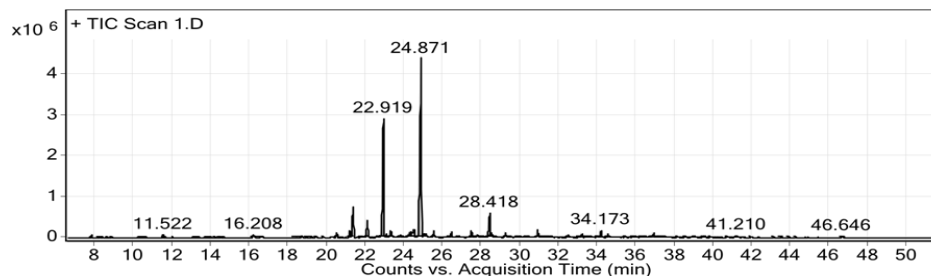
### **5.2.2 GC-MS metabolomics studies:**

This arm of the study was started by metabolite extraction from rAmbra cell lines using methanol followed by metabolites derivatization, separation by GC and finally identification by MS (2.2.11) an Initial run was performed as a control experiment to validate the protocol using rAmbra cell line metabolites derivatised by either BSTFA or MSTFA and a blank derivatised only by BSTFA (2.2.11). Total ion chromatograms (TIC) were generated from the mass spectrometric analysis (Figure 5.6). The blank analysis shows a distinguishable peak at 10.140 for derivatizing agent (BSTFA) itself with little background noise, the same peak at 10.265 was observed for rAmbra analysis using the same derivatizing agent, and was not observed for rAmbra when a different derivatizing agent was used. This means that derivatization and analysis worked well as in the blank BSTFA did not derivatise anything else but the reagent itself. Also the difference in rAmbra identified metabolites upon using two different derivatizing agents (Table 5.1) show that these peaks are genuine metabolites from rAmbra and that different metabolites can be identified upon using two different derivatizing agents. A representative example of MS identification of peaks is included in which a peak from TIC of rAmbra derivatised by BSTFA was analyzed by MS (Figure 5.7).

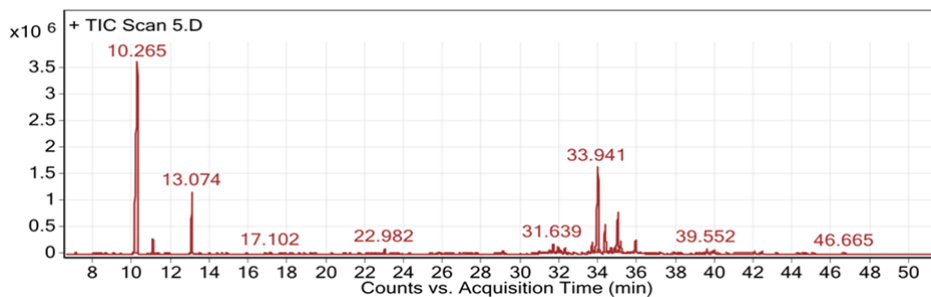




(A)



(B)



(C)

**Figure 5.6: Total ion chromatograms obtained from rAmbra metabolites GC-MS.** (A) Blank derivatised by BSTFA (B) rAmbra metabolites derivatised by MSTFA (C) rAmbra metabolites derivatised by BSTFA. Different peaks can be observed for different derivatizing agents used to derivatise rAmbra.

**Table 5.1: mass spectrometry identified metabolites for rAmbra.** (A) Blank. (B) rAmbra metabolites using MSTFA. (C) rAmbra metabolites using BSTFA.

(A)

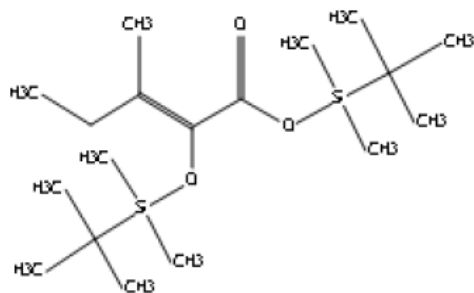
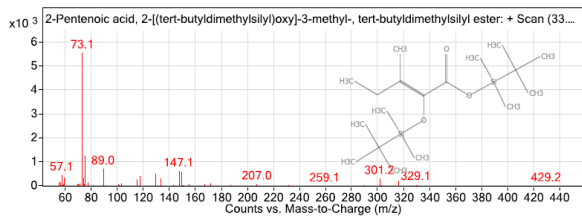
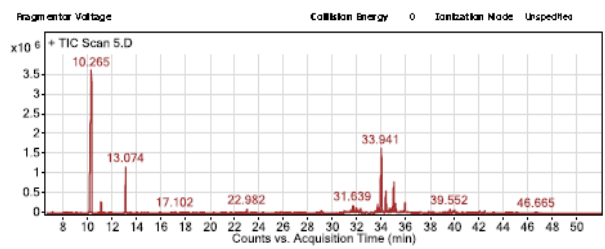
Peak Number	Metabolites
10.140	tert-Butyl-[2-(tert-butyl)dimethylsilyl]oxyethoxy]dimethylsilane

(B)

Peak Number	Metabolite
11.522	Trimethylsilyl ether of glycerol
16.208	Nonadecane
22.919	Glucopyranose, pentakis-O-trimethylsilyl-
24.871	Glucopyranose, 1,2,3,4,6-pentakis-O-(trimethylsilyl)-, D-
28.418	Octadecanoic acid, trimethylsilyl ester
34.173	Hexadecanoic acid, 2,3-bis[(trimethylsilyl)oxy]propyl ester
41.210	3.alpha.-(Trimethylsiloxy)cholest-5-ene
46.646	Dodecane, 1-fluoro-

(C)

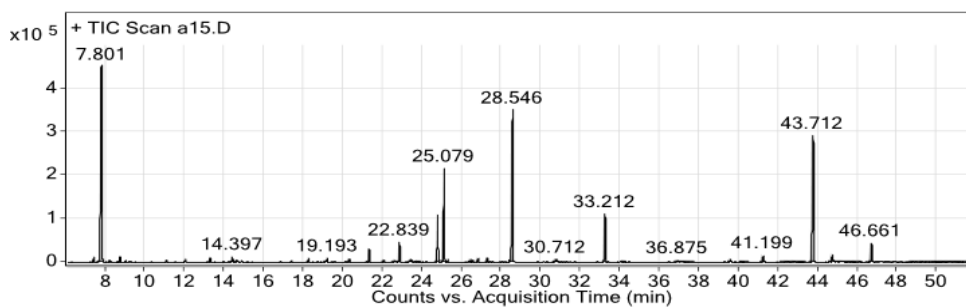
Peak Number	Metabolite
10.265	tert-Butyl-[2-(tert-butyl)dimethylsilyl]oxyethoxy]dimethylsilane
13.074	Lactic acid ditbdms
17.102	tert-Butyl-(2-methoxyethoxy)dimethylsilane
22.982	L-Proline, 1-(tert-butyl)dimethylsilyl-5-oxo-, tert-butyl)dimethylsilyl ester
28.418	2-Propen-1-ol, 1-[(1,1-dimethylethyl)dimethylsilyl]
31.639	4-Hydroxythiophenol, S-trimethylsilyl-, trimethylsilyl ether
33.941	Pentanedioic acid, 3-[(tert-butyl)dimethylsilyl]oxy]-3-methyl-, bis(tert-butyl)dimethylsilyl ester
39.552	Cyclopentanecarboxylic acid, trimethylsilyl ester
46.665	Phenol, 2,6-bis(1,1-dimethylethyl)-



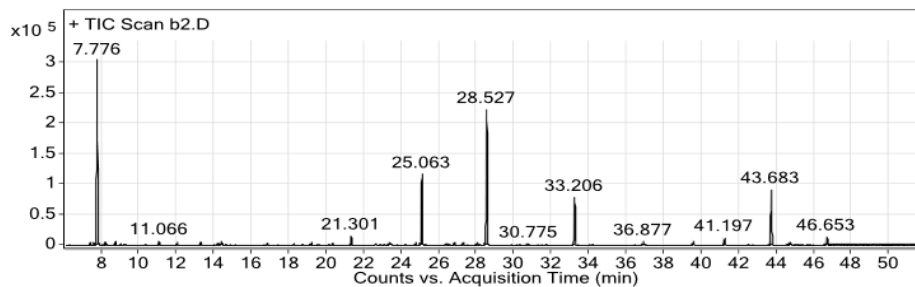
2-Pentenoic acid, 2-[(tert-butyl dimethylsilyl)oxy]-3-methyl-, tert-butyl dimethylsilyl ester

**Figure 5.7: MS analysis of peaks from TIC representative example. Peak identified at 33.941 from TIC of rAmbra metabolites derivatization by MBTSTFA**

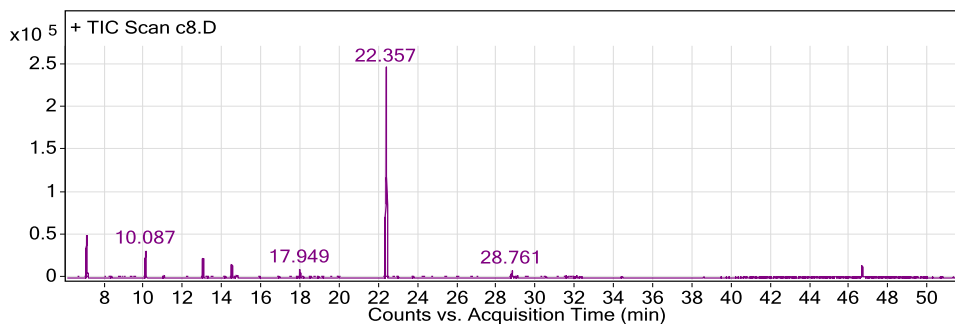
The following runs were designed to compare metabolites from rAmbra and rBgal using both derivatization agents. TICs generated from using MSTFA (Figure 5.8) showed difference between the blank sample used and both rAmbra and rBgal. However; both cell lines showed nearly identical TICs. While TICs generated from using BSTFA (Figure 5.9) showed nearly no difference between the three chromatograms from the blank, rAmbra and rBgal, indicating that derivatization did not work very well and that these peaks on the TICs are more likely to be for contaminants in the samples rather than genuine metabolites from the cell line extractions. To study for the difference between rAmbra and rBgal metabolites, MS identification was applied to individual peaks of the chromatogram. Peaks from both cell lines derivatised by MSTFA were analyzed by MS. Compounds identified from both cell lines were near identical, indicating no difference between rAmbra and rBgal.



(A)

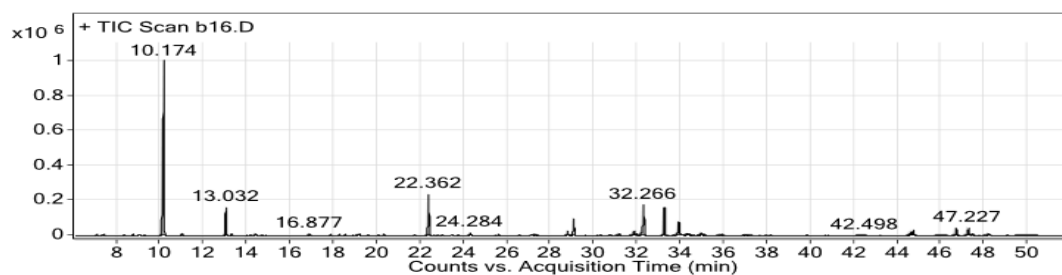


(B)

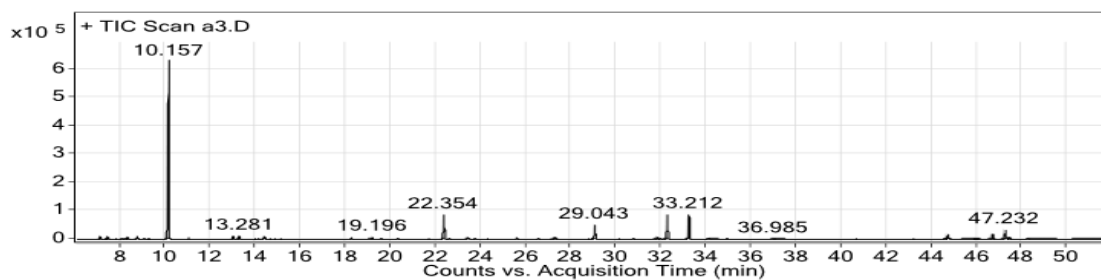


(C)

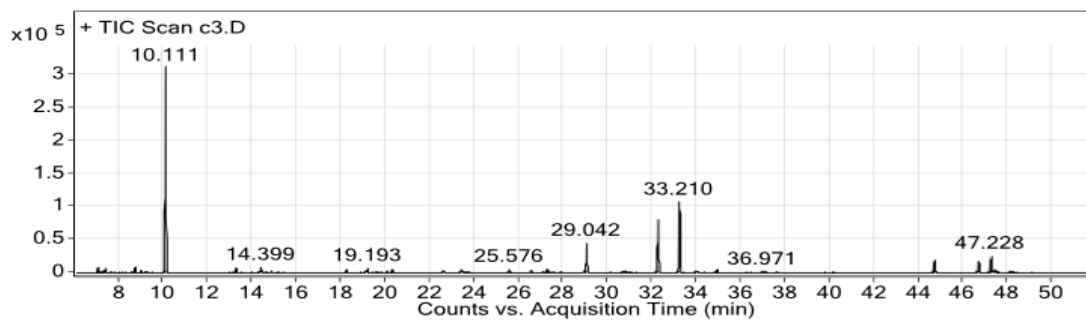
**Figure 5.8: MS total ion chromatograms for metabolites extracted and derivatised using MSTFA. (A) rAmbra. (B) rBgal. (C) Blank. No difference in peaks can be observed for rAmbra and rBgal.**



(A)



(B)



(C)

**Figure 5.9: MS total ion chromatograms for metabolites extracted and derivatised using BSTFA. (A) rAmbra. (B) rBgal. (C) Blank. No difference can be observed between three TICs.**

These runs were repeated few times (n=3) in attempts to identify more metabolites that can allow further comparisons of the cell lines and were not successful, reproducibility at this point was very low and samples separation was not achieved as before. In an attempt to identify and overcome these issues; a technique control experiment was performed using a standard solution of 20 amino acids at three different concentrations and a blank. The GC separation and the MS identification were performed. TIC from a blank and three different dilutions were generated (Figure 5.10). The blank sample showed more than one peak indicating contamination. And the identified metabolites in the amino acid standard used did not relate to all amino acids of the stock solution and also, there was contamination with other materials.

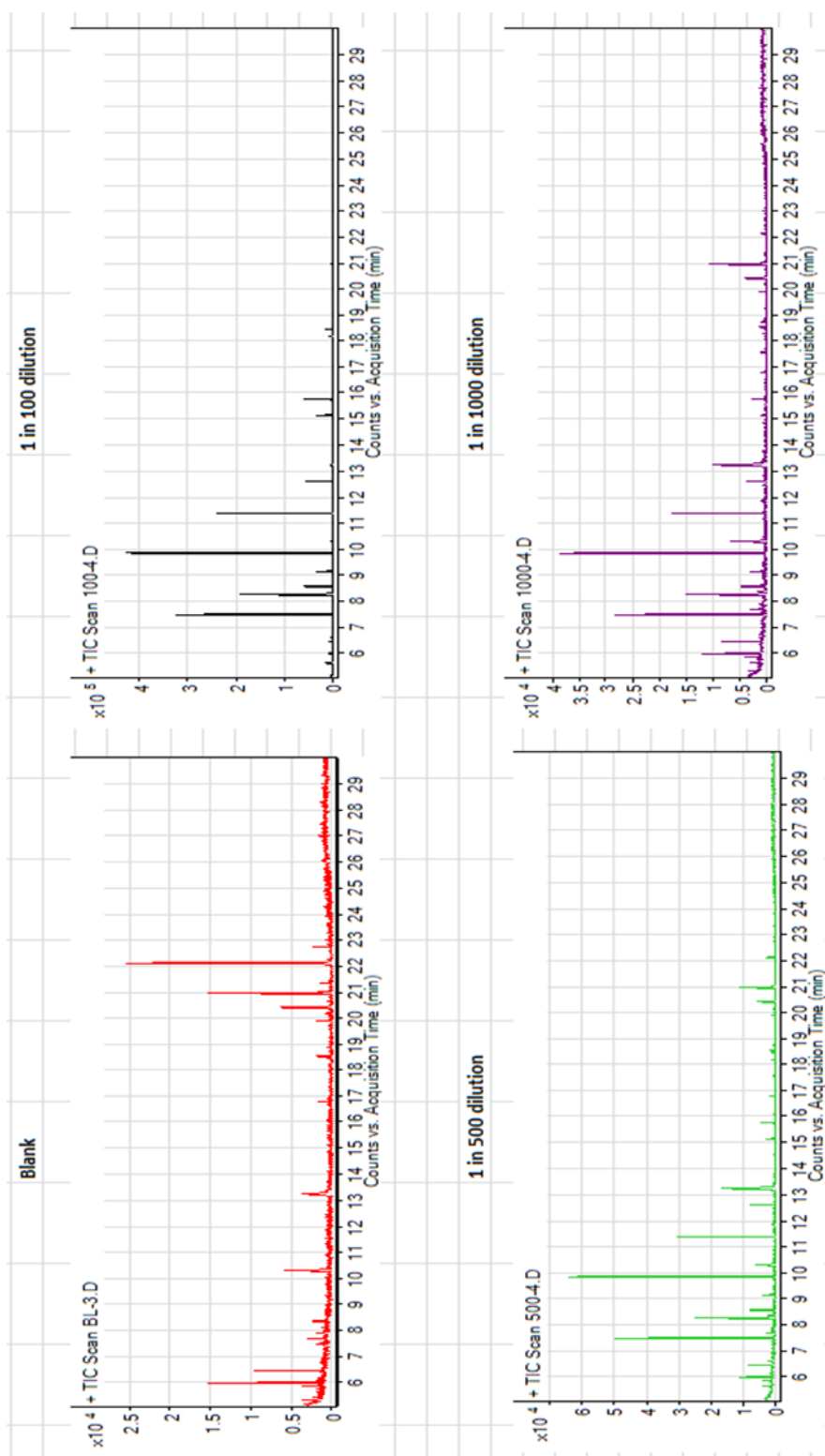


**Figure 5.10: Total Ion Chromatogram (TIC) of a 20 amino acids standard solution. TICs obtained from GC-MS of a blank, a 1 in 100, a 1 in 500 and a 1 in 1000 dilutions showing the peaks of the amino acids separated.**



### **5.3 Discussion:**

The application of proteomics in cancer studies is widely established and is an effective way to identify the change in protein expression between two specimens (Cai et al., 2004). Applications of proteomics in melanoma studies have been a primary method to look for biomarkers (Sabel et al., 2011).

Ambra1 PTMs plays an essential role in the activity of this protein and other proteins during autophagy, Ambra1 is found in an in-active form by its phosphorylation at Ser<sup>52</sup> by mTORC1. Upon nutrient starvation mTORC1 is inhibited and Ambra1 is dephosphorylated (Nazio et al., 2013), Ambra1 activation enhances ULK1 kinase activity which phosphorylates essential autophagic components including Ambra1 itself at sites that are yet to be identified (Botti-Millet et al., 2016). There are more than 20 Ambra1 phosphorylation sites that are reported and yet to be characterized to understand the dynamic role of Ambra1 PTM by phosphorylation (Cianfanelli et al., 2015). A recent study has characterized the phosphorylation of Ambra1 at Ser<sup>1014</sup> by HUWE1 an E3 ubiquitin ligase which enhances Ambra1- LC3B binding during mitophagy (Di Rita et al., 2018).

There are also a number of studies that proved Ambra1 ubiquitylation; it is ubiquitinated by RNF2 which is an ubiquitin E3 ligase at Lysine 45 by Lys48-linked ubiquitin chains to mediate Ambra1 degradation by proteasomes; a process that result in autophagy suppression after it has been induced by starvation (Xia et al., 2014). A study has summarized the ubiquitylation of Ambra1 by Cullin E3 Ubiquitin Ligases during autophagy (Antonioli et al., 2014). Moreover; Ambra1 is not only considered as a substrate for ubiquitylation, but also it is an essential co-factor in the activity of different E3 ligases (Cianfanelli

et al., 2015). It has been shown that Ambra1 and TRAF6 are essential for the ubiquitylation of ULK1 by LYS-63-linked chains during autophagy (Nazio et al., 2013). This study also shows that Ambra1 may affect the acetylation of CDC25A (6.4), as well as a role in PTMs specifically ubiquitination (7.3)

Western blot analyses (3.2) showed Ambra1 band at ~130kDa; as well as different bands in the rAmbra cell lines only. A band is observed at ~150kDa which is approximately 20 kDa higher than the Ambra1 band; this can indicate different changes to the Ambra1 protein including PTM (Larsen et al., 2006). Other bands were observed at ~90 kDa, 50 kDa and 30 kDa which indicates a possibility of Ambra1 protein cleavage. A band is observed in the two cell lines at ~10 kDa which indicates a possible cross-reactive protein. Indeed the study that reported Ambra1 cleavage by Caspases and Calpains showed an N-terminal (~60 kDa=Ambra1 plus myc-tag) and a C-terminal (~100 kDa) cleavage products by western blot analysis (Pagliarini et al., 2012). Another possible explanation to the multiple bands on western blot analysis is Ambra1 transcript variants, which are identified by Uniprot to be at least 6 variants for this protein. Transcript variants can be generated due to alternative splicing of an mRNA. If the epitope that the antibody recognizes is shared between the proteins, then multiple bands will be observed (Ghosh et al., 2014)

Differential expression and PTM studies on these protein samples were started. The visual comparison of the well separated proteins on gels for rAmbra and rBgal indicated that there is not much difference in the proteomic profile at least for the few runs that were successful. However; this arm required a lot of optimization and 2D gel electrophoresis was extensively repeated to reach the point where visual separated proteins can be clearly and reproducibly seen on the gels. Reproducibility of protein separation was not achievable and hence;

further analysis of these gels either by mass spectrometry or PTM using 2D western blotting were not feasible.

2DE technique is deemed to be one of the leading powers in the expansion of proteomics and protein studies (Magdeldin et al., 2014). Despite the wide use of 2DE for proteomics experiments, there are few limitations of protein separation by this technique. These limitations include poor reproducibility of separation, inability to detect low abundant proteins, and moreover; a protein pI has to be between 3 and 10 also a protein size has to be between 10 and 150 KDa to be identified by 2DE, and finally streaking of spots and poor membrane resolutions which result in poor protein separation (Chandramouli and Qian, 2009; Magdeldin et al., 2014). Spot streaking and poor separation was the main limitation of our work, other limitations included poor reproducibility.

Metabolomics studies were initiated and the initial runs showed nearly no difference in the metabolome between rAmbra and rBgal. However; repeating the same steps on a larger scale did not perform the same and this protocol was repeated to identify possible technical errors. A last attempt was designing a control experiment. A 20 amino acid standard solution was prepared and different dilutions were extracted in methanol and underwent derivatization using MSTFA reagent. However the separation of these amino acids was not achievable and the blanks showed a lot of noise and contamination on the columns and hence; metabolomics studies were discontinued.

There can be many reasons during different steps of extraction, derivatization and detection behind the poor quality results of metabolomics. The choice of the quenching reagent is critical to ensure effective metabolism quenching as well as; largely affecting the yield of metabolites, the method used in this study is

direct quenching and extraction by cold methanol after a single wash by PBS which is reported to be one of the most effective methods that result in minimal leakage of intracellular metabolites (Kapooore et al., 2017).

Derivatization is obviously most effective method to improve the detection characteristics of metabolites. It acts by changing an analyte to make it detectable in gas chromatography and enable chromatographic separation. Derivatization either increases or decreases the volatility of the compound and it reduces the absorption of the analyte in the gas chromatography system. The two derivatization agents used in this study BSTFA and MSTFA are the most widely used derivatization agents; they both act by silylation of active hydrogens present in functional groups (Monteiro et al., 2013).

Regarding detection, GC-MS has advantages of a greater chromatographic resolution when compared to LC-MS-based methods (Aretz and Meierhofer, 2016). Our initial work shows that extraction and derivatization approaches used were promising to generate reproducible data. It is more likely that the poor results were due to poor separation resulting from column deterioration.

Results from proteomics and metabolomics indicate that there is not a great difference between the profiles of rAmbra and rBgal. However; a comprehensive conclusion cannot be made due to poor reproducibility of the experiments as well as testing only a fraction of the proteome and metabolome and not the full profiles of the different cell lines.

***Chapter 6- Transcriptomic analysis of differential  
Ambra1 expression***

## **6.1 INTRODUCTION:**

Studying the effect of Ambra1 differential expression has been an attraction for many researchers since its discovery in 2007. The first study that reported the role of Ambra1 in autophagy used the overexpression and the knockdown of Ambra1 to identify its role in autophagy and different cellular processes (Maria Fimia et al., 2007). Literature show more studies that utilized overexpression and/or knockdown of Ambra1 to assess the roles and study the functions of Ambra1, its ability to induce autophagy and inhibit apoptosis as an autophagic pro-survival response has been shown by the overexpression and knockdown of Ambra1 in fibroblasts (Pagliarini et al., 2012) and, the same role was shown in SW620 cells (Gu et al., 2014). In relation to this role the knockdown of Ambra1 in A375 melanoma cell lines was used to show that Tetrahydrocannabinol (THC) induced autophagy was independent of Ambra1 (Armstrong et al., 2015). Furthermore; the downregulation of Ambra1 has also shown: reduced ability of Beclin1 to interact with Vps34 (Sun, 2016), and an increase in basal apoptosis in adult neural stem cells (Yazdankhah et al., 2014). There can be far more studies that have performed the same approach to study this gene; these ones mentioned are to show that the differential expression of Ambra1 is of a great impact on different cellular processes.

Transcriptome can be defined as the sum of all RNA transcripts produced by an organism (Lowe et al., 2017), transcriptome analysis is then the study of the transcriptome, of the complete set of RNA transcripts that are produced by the genome, under specific circumstances or in a specific cell, using high-throughput methods. There are two main techniques applied to study transcriptomes; microarrays and, RNA-Seq. DNA microarrays are discovery type research that can be used as a tool to assess the genetic information or

the gene expression by analyzing mRNA complete set produced by the genome of a specific organism (Govindarajan et al., 2012).

Previous experiments carried out in this study did not indicate that the overexpression of Ambra1 is of a great value in the A375 melanoma cell lines. On the other hand; there was a growing interest in the knockdown of the same gene. As mentioned before the proliferation rate of the ShAmb cell lines was notably different to all other cell lines, the decreased proliferation rate of the ShAmb cell lines was proved by SRB and Incucyte proliferation assays. The effect of Ambra1 knockdown on cell proliferation rate in this model is the opposite of reported Ambra1 role in normal and primary melanoma cells (3.4). In order to study the transcriptome changes related to Ambra1 differential expression; a DNA microarray experiment was designed. Unlike the proteomics and the metabolomics studies which were limited to the overexpression model, the knockdown model was included in the microarray analysis to allow for investigating the outcomes of Ambra1 knockdown as well as overexpression. A workflow of this arm of study is shown in Figure 6.1.

## 6.2 Microarrays analysis workflow

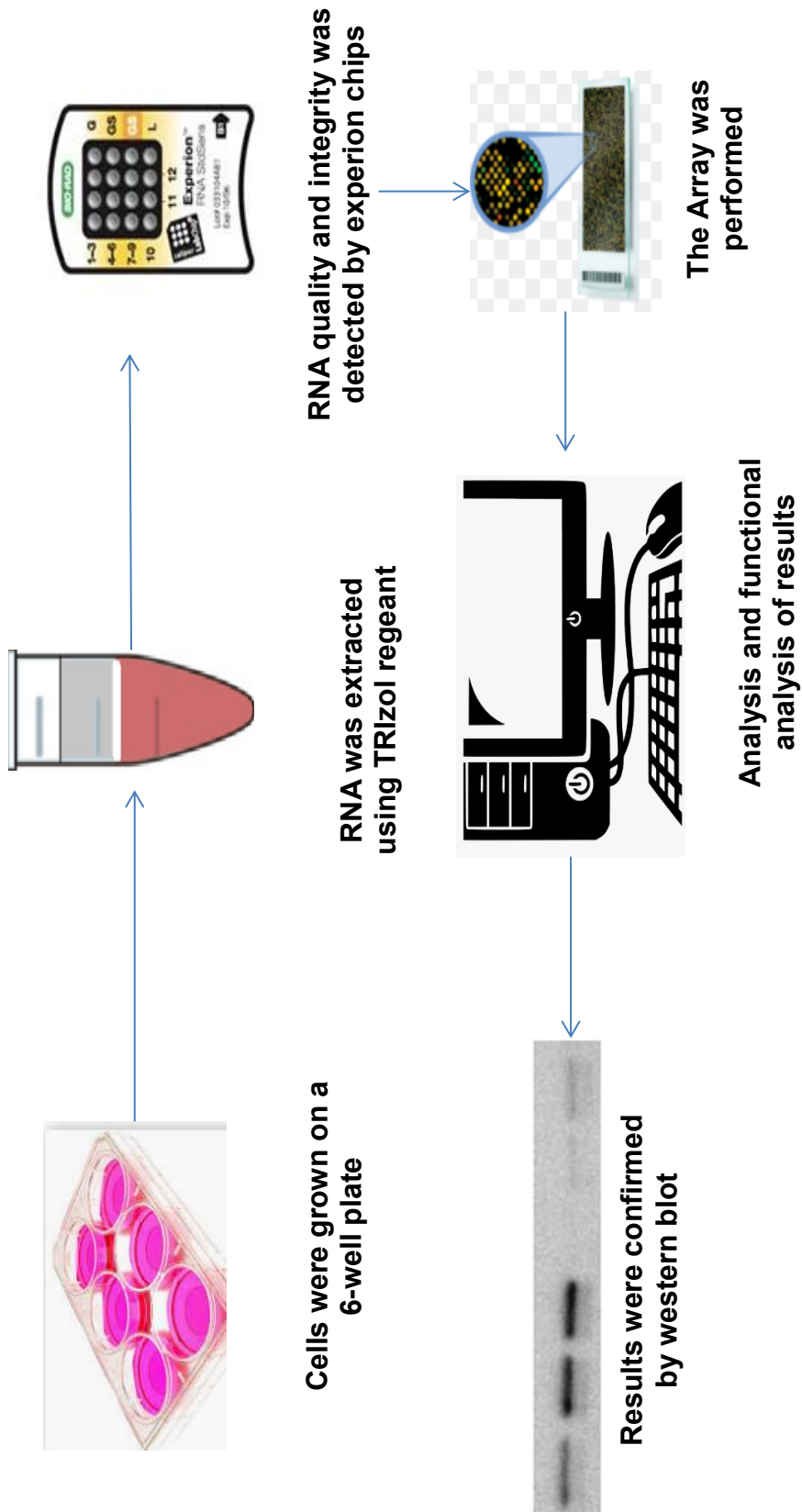


Figure 6.1: Microarray work flow



## **6.3 Results**

To perform a microarray analysis, RNA was extracted using Trizol reagent (2.2.12) from four different passages of each cell line 72 hours after selection antibiotic removal.

### **6.3.1 RNA quality analysis**

Quality analysis of extracted RNA samples from rAmbra, rBgal, ShAmb and ShCon is shown in Figure 6.2. RNA integrity numbers are shown in table 6.1.

3 samples (highlighted on table 6.1) from each cell line were selected to be analyzed

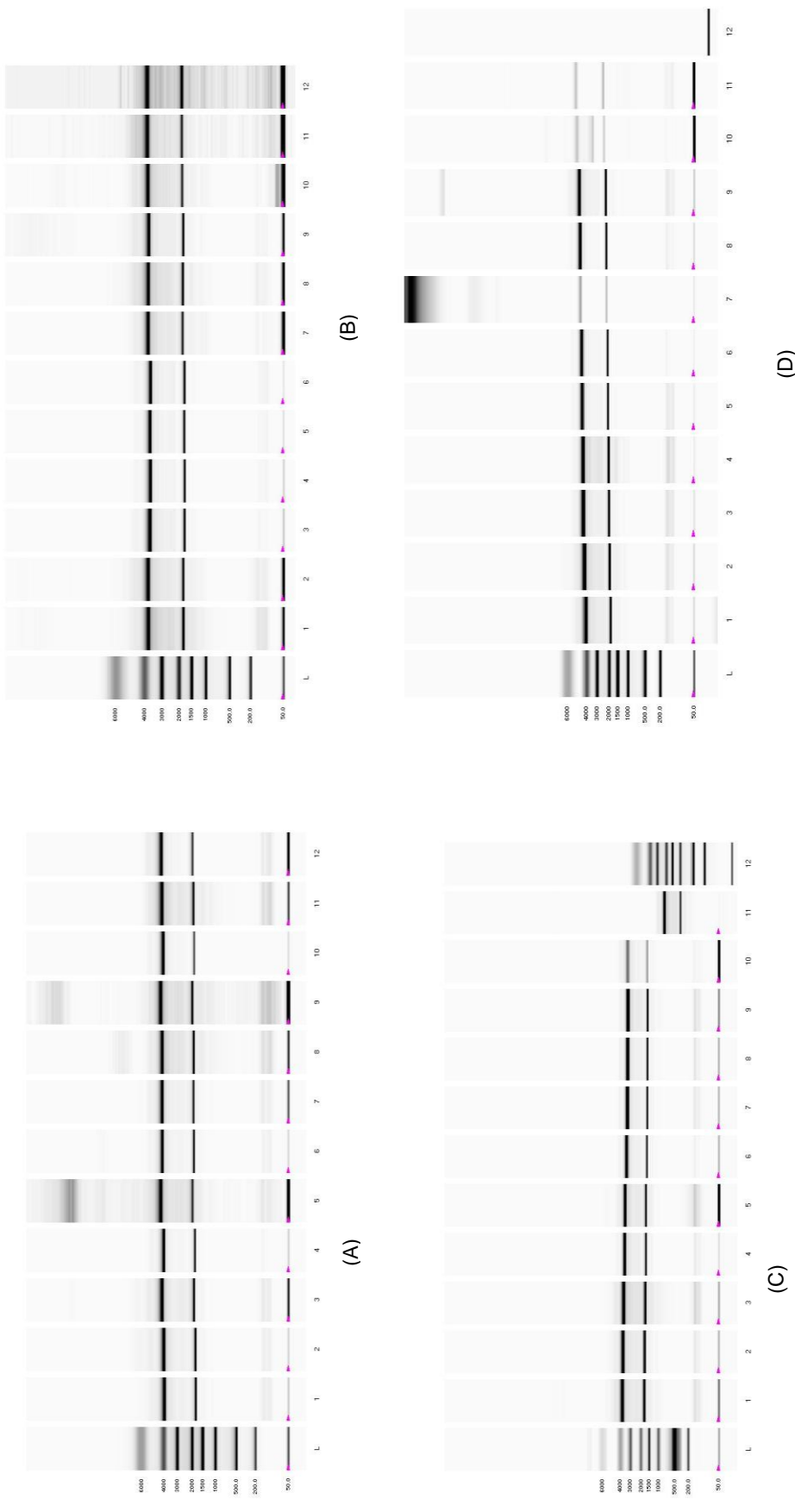


**Figure 6.2: Quality analysis of total RNA using Bio-Rad electrophoresis station.** For each figure there are four biological replicates (1-3, 4-6, 7-9 and 10-12). Where there are 3 technical replicates for each extraction. (A) rAmbra. (B) rBgal. (C) ShAmb. (D) ShCon.

**Table 6.1: RNA integrity numbers for RNA extractions used for microarrays data analyses.** Table shows 12 RNA integrity numbers for the four different cell lines. Highlighted are the samples chosen to be analyzed by Microarray gene chip.

Lane number	1	2	3	4	5	6	7	8	9	10	11	12
rAmbra	9.8	9.8	9.9	9.8	8.8	9.9	9.8	9.4	7.5	10	9.5	10
rBgal	9.5	9.7	9.9	9.8	9.9	9.8	9.7	9.5	9.8	-	-	-
ShAMB	9.7	9.8	9.1	9.8	8.7	9.9	9.6	9.6	9.3	-	-	-
ShCon	9.9	10	10	9.9	10	10	-	10	10	-	--	-

### 6.3.2 Differential expression analysis of the microarray results

In this arm two datasets were analyzed (Table 6.2) using transcriptome analysis suite (2.2.14). In the first dataset rAmbra was compared to the matching control rBgal. While in the second dataset ShAmb was compared to its matching control ShCon. Three samples of each cell line were analysed using an array Type HuGene-2\_0-st, Genome Version hg19 (Homo sapiens) annotated: HuGene-2\_0-st-v1.na36.hg19.transcript.csv. The analysis results (Figure 6.3) showed 107 differentially expressed genes in the first dataset where 60 and 47 genes are up and down regulated respectively, in the second dataset 243 are upregulated and 79 are downregulated to give a total of 322 differentially expressed genes.

**Table 6.2 datasets analyzed from the HUGENE\_2.0 microarray for comparing Ambra1 effect on transcriptome**

Comparison	Group 1	Group 2	Count 1	Count 2	Up	Down
rAmbra vs rBgal	rAmbra	rBgal	3	3	60	47
ShAmb vs ShCon	ShAmb	ShCon	3	3	243	79

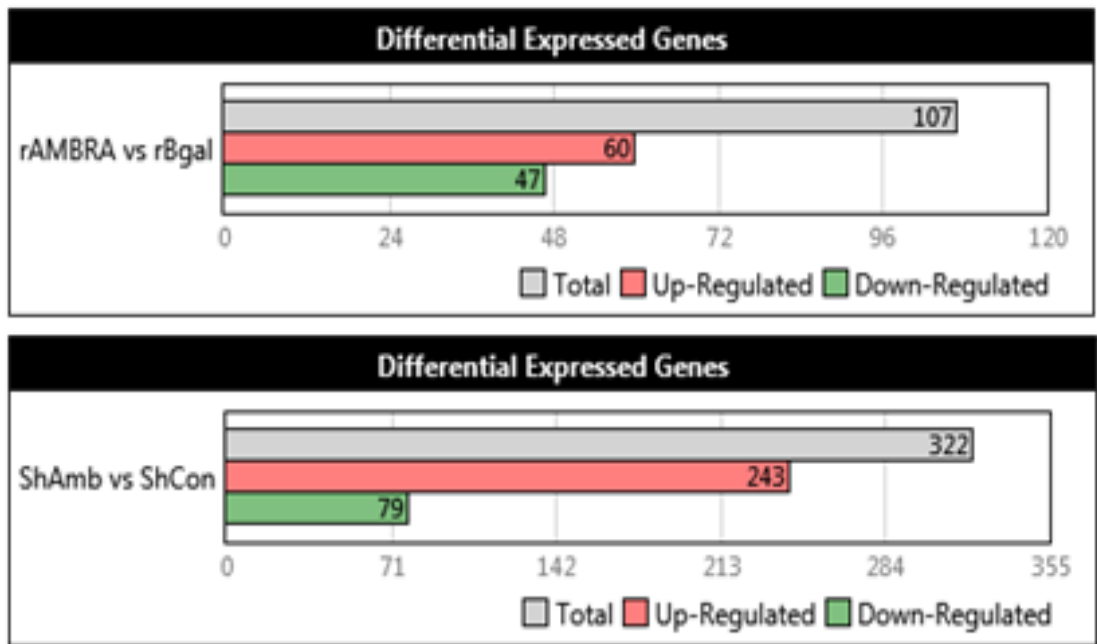


**Figure 6.3: analysis results of the differentially expressed genes in two different datasets showing up and down regulated genes in each dataset. The top dataset is comparing rAmbra vs rBgal. The bottom dataset is comparing ShAmb vs. ShCon.**

Principal components analyses (PCA) mapping for the two datasets were performed to analyze the samples clustering. The first dataset shows a distinct pattern of the rBgal. However; the rAmbra did not show the same clustering (Figure 6.4). On the other hand, the second dataset shows distinct patterns of ShAmb and ShCon clustering (Figure 6.5). To demonstrate the effect of Ambra1 knockdown on the change of transcriptome, a PCA mapping for the four cell lines was performed (Figure 6.6). It is clear that ShAmb cells cluster distinguishably different to all other three cell lines.

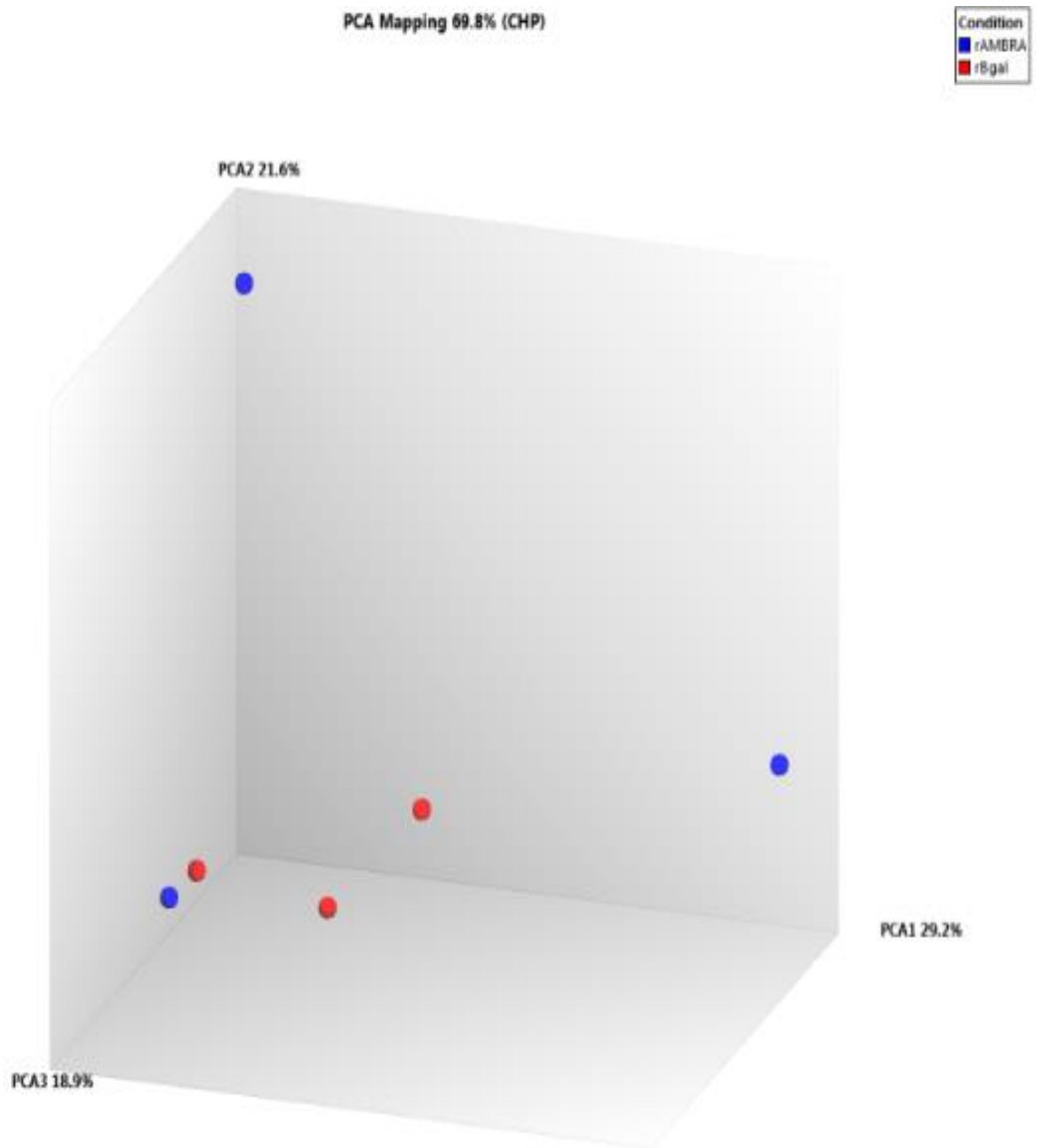


**Figure 6.4: PCA mapping of the Ambra1 overexpression model microarray dataset.** Blue dots represent rAmbra and red dots represent rBgal. A distinct clustering pattern is observed for rBgal and not rAmbra.

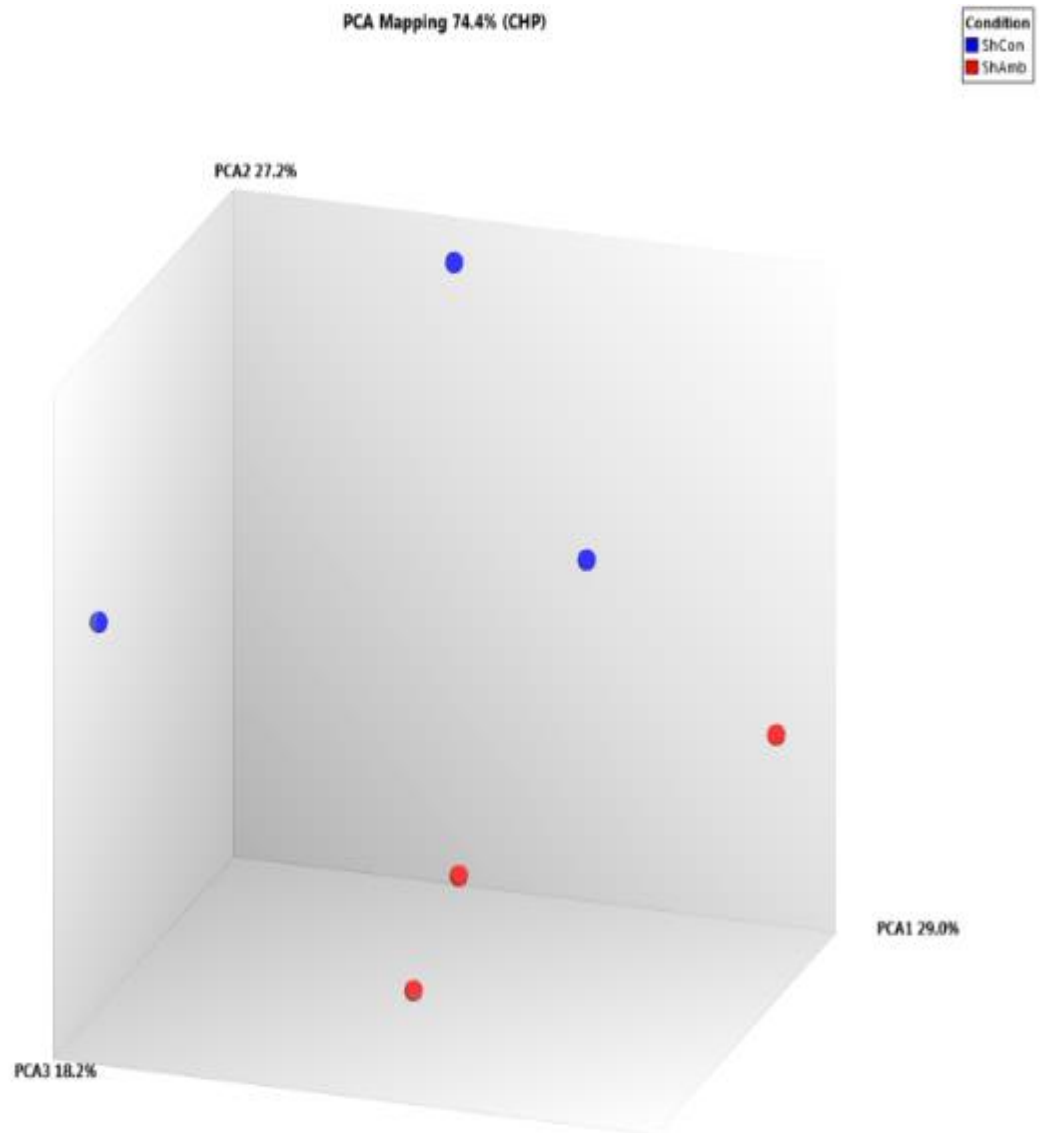


**Figure 6.5: PCA mapping of the Ambra1 knockdown model microarray dataset.** Red dots represent ShAmb and blue dots represent ShCon. A distinct clustering pattern is observed for both ShAmb and ShCon

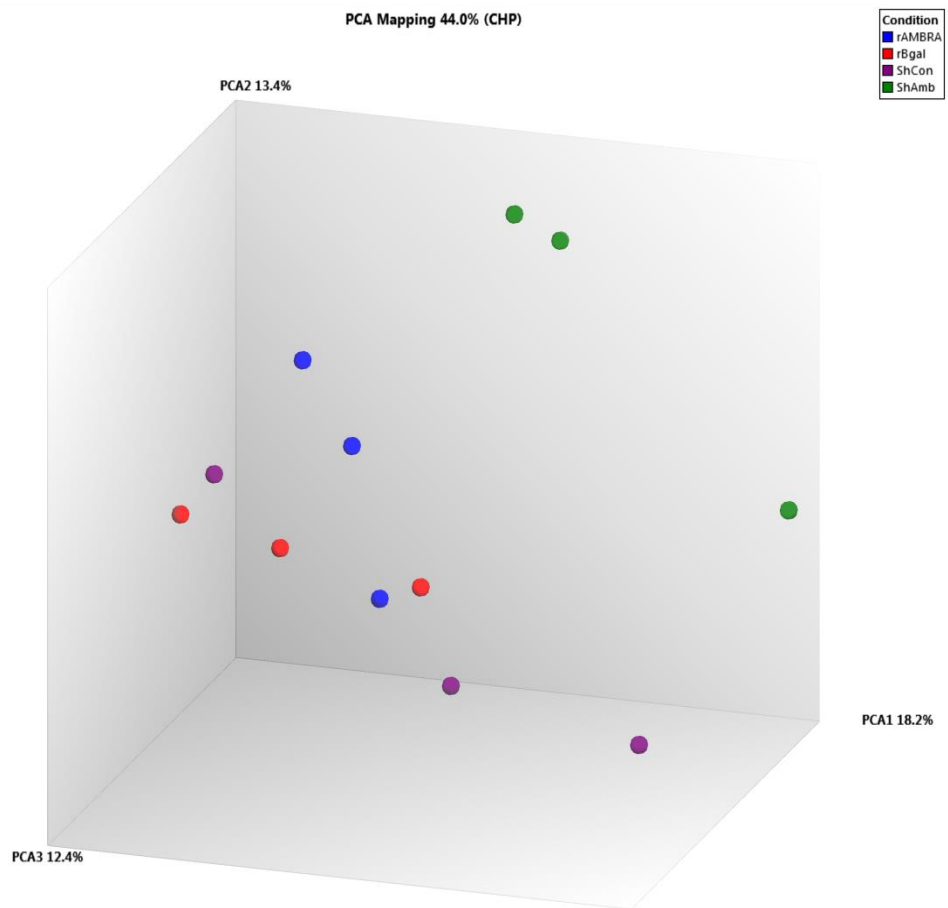
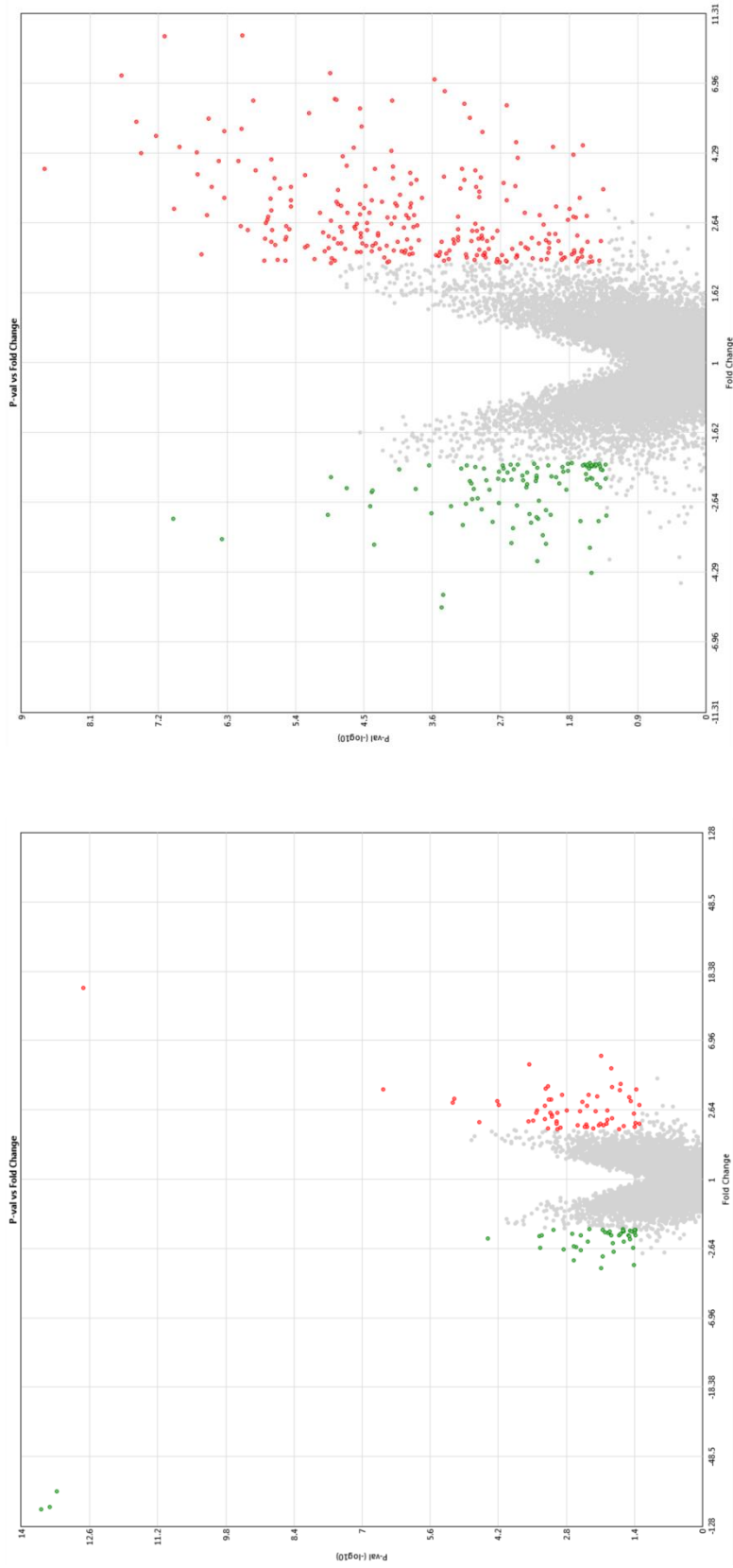


**Figure 6.6: Combined PCA Mapping of the overexpression and knockdown models microarrays datasets.** Blue dots represent rAmbra, red dots represent rBgal, purple dots represent ShCon and, green dots represent ShAmb. It is clear that ShAmb cluster separately to all other cell lines.



Volcano plots were generated for each dataset to summarize the fold change and the ANOVA eBayes method used for performing the analysis (Figure 6.7) this plot can be considered to determine the most significant differentially expressed genes. However; a corrected p-value which in this case is false discovery rate (FDR) can be used instead to determine the significance of each differentially expressed gene.

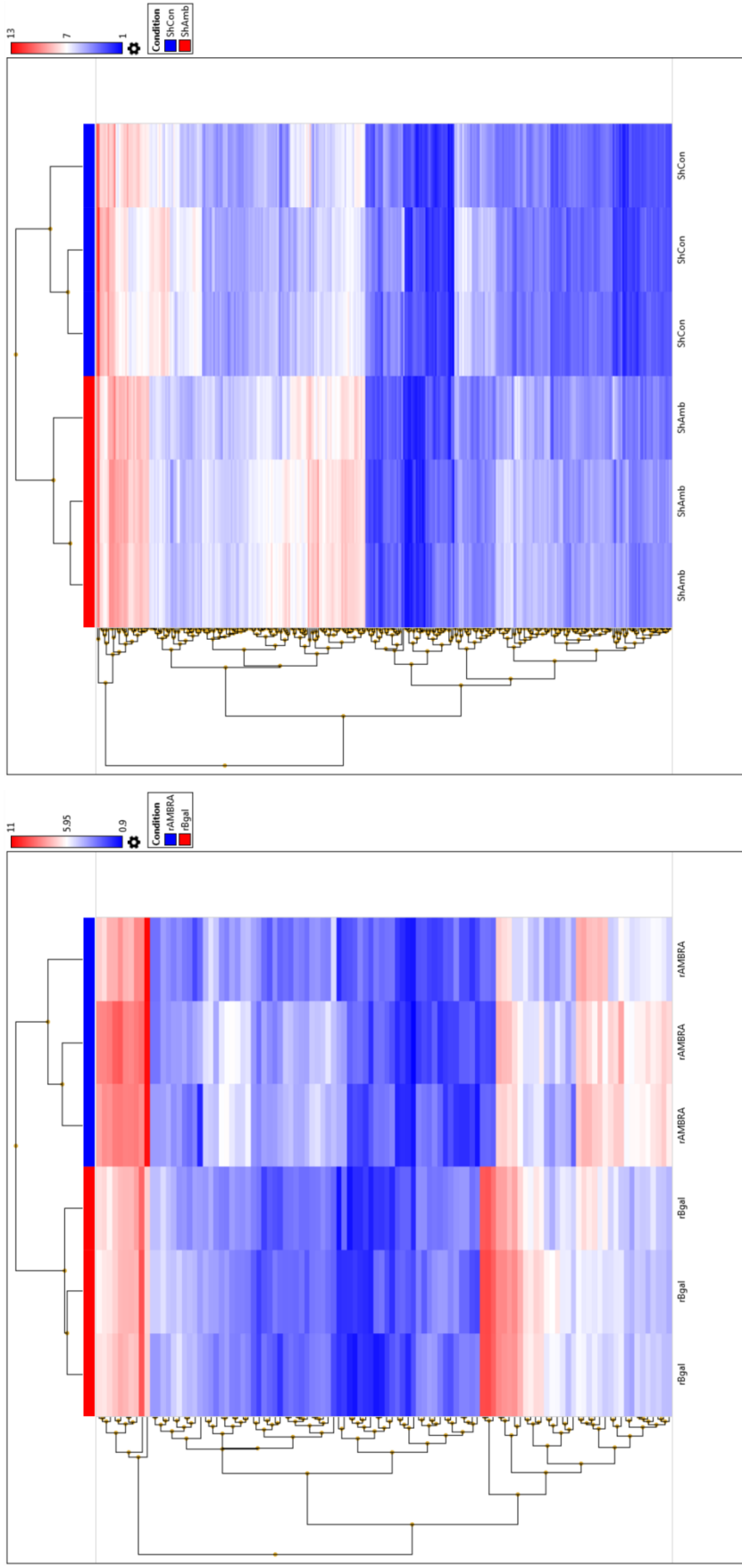


(A)

(B)

**Figure 6.7 volcano plots analysis.** Every gene is represented by a dot in the graph. X-Axis is the fold change and the y-axis is the  $-\log_{10}$  p-value. The red dots represent upregulated genes while the green dots represent downregulated genes and, the grey dots represent the unchanged genes. The further up the spot the more significant the value. (A) rAmbra vs. rBGal. (B) ShAmb vs. ShCon

Hierarchical clustering Heatmaps were generated to visualize the change in the genes expression among the different datasets (Figure 6.8). They were generated to visualize the expression of the significantly differentially expressed genes in the two datasets. Every row represents a gene expression profile across the samples (Rows). Red color refers to upregulated genes; white refers to unchanged and blue represents downregulated genes. A clear clustering within each group for the two datasets can be observed except for the rAmbra where the far right sample shows different clustering to the two other samples.



(A)

(B)

**Figure 6.8: Hierarchical clustering Heatmaps of the microarrays overexpression and knockdown datasets.** Each row represents a single sample and each column represents a single probe. Absolute gene expression is indicated via a color coding. The darker the red the higher expression level, and the darker the blue the lower expression level. (A) rAmbra blue vs rBgal red (B) ShAmb red vs ShCon blue.

Differentially expressed genes were analyzed (2.2.14) and the lists of the significantly differentially expressed genes ( $P < 0.05$ ) were arranged according to the FDR. The first dataset showed higher values of FDR when comparing the differential expression between rAmbra and rBgal which indicates a high rate of false discovery. The overexpression of Ambra1 in the rAmbra cells was confirmed to be 16.37 folds up-regulated compared to the rBgal matching control by this technique. Also N(Alpha)-Acetyltransferase 11 (NAA11) and Cadherin13 (CDH13) were shown to be overexpressed within an acceptable FDR values. A list of the p-value significant differentially expressed genes, the p-values and the FDR values are listed in table 6.3.

**Table 6.3: Differentially expressed genes comparing rAmbra to rBgal.**  
Showing the gene symbol, fold change, p-value and FDR.

Gene Symbol	Fold Change	P-val	FDR P-val
Uncharacterized	-88.18	1.74E-10	3.34E-06
Uncharacterized	-109.49	2.13E-10	3.34E-06
Ambra1	16.37	2.72E-10	3.34E-06
Uncharacterized	-108.15	2.77E-10	3.34E-06
NAA11	4.27	8.47E-07	0.0082
CDH13	3.06	5.78E-06	0.0465

On the other hand, the second dataset showed a great difference in the gene expression profile. Comparing the ShAmbra genome expression to the matched control ShCon confirmed the knockdown of Ambra1 in the ShAmb cell line to be 1.58 folds downregulated compared to the ShCon, and showed that Ambra1 knockdown led to a significant difference in the expression of 322 genes (p-value  $< 0.05$ ), a list of genes with FDR value  $< 0.07$  was generated (table 6.4.) It is notable that only few genes from this list were downregulated leaving the majority of the most significant differentially expressed genes upregulated.

**Table 6.4: genes differential expression in the ShAmb cells compared to the ShCon cells** at a cut of FDR <0.07 showing the gene symbol, fold change, P-value and FDR P-value.

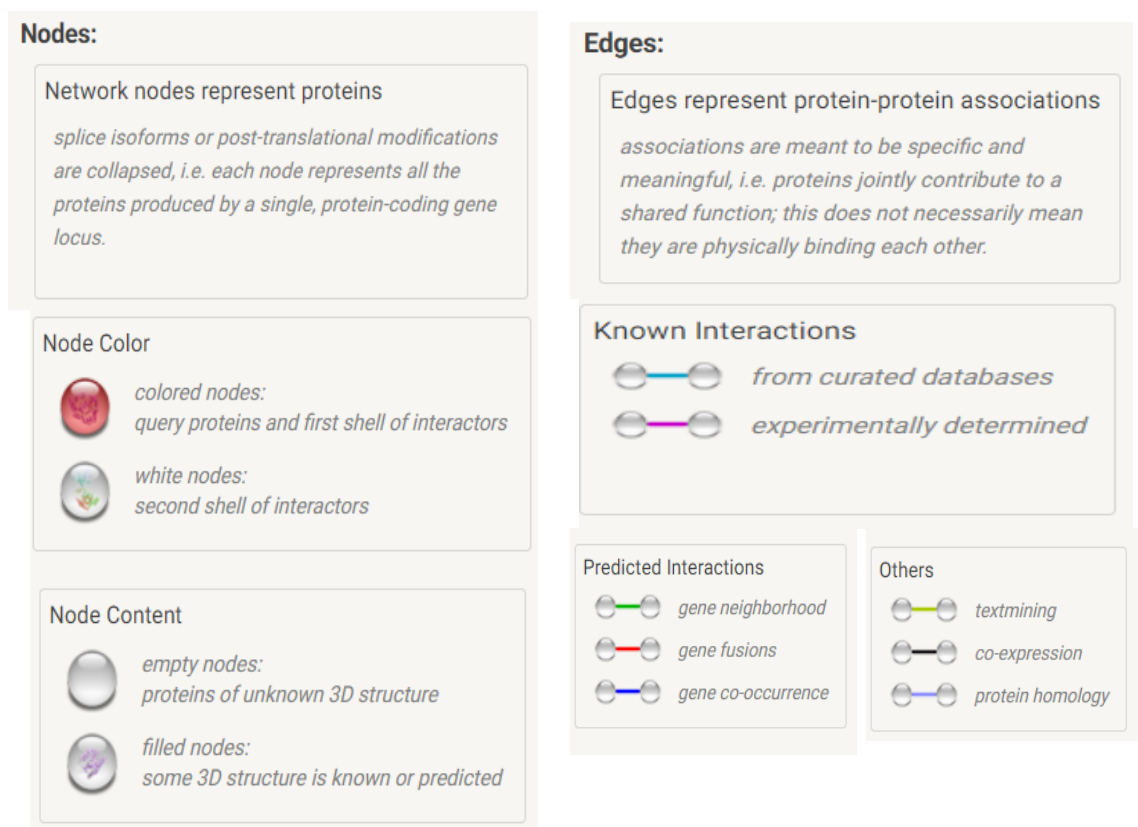
Gene Symbol	Fold Change	P-val	FDR P-val
SEMA3C	3.74	5.93E-07	0.0079
ZNF844	4.2	5.95E-07	0.0079
SEMA3A	3.11	7.65E-07	0.0079
LINC00440	7.05	8.90E-07	0.0079
RUNX1-IT1	3.86	1.11E-06	0.0079
AJAP1	3.94	1.14E-06	0.0079
TCN1	4.94	1.16E-06	0.0079
MEOX2	3.02	1.46E-06	0.0079
GALNT5	3.37	1.47E-06	0.0079
TFPI2	3.6	2.51E-06	0.0113
FAT3	4.41	2.58E-06	0.0113
PLA2G7	8.61	3.33E-06	0.0126
JAG1	3.39	3.45E-06	0.0126
CDH19	3.19	3.65E-06	0.0126
SLC14A1	2.74	4.06E-06	0.0131
IL24	-2.85	4.44E-06	0.0134
ACTBL2	5.51	5.24E-06	0.0143
COL4A1	2.55	5.71E-06	0.0143
NEK10	3.26	5.75E-06	0.0143
TP73	2.63	5.91E-06	0.0143
WNT5A	3.65	7.08E-06	0.0163
EPHA4	2.83	7.82E-06	0.0167
LOC105377108	2.35	7.96E-06	0.0167
Uncharacterized	2.94	9.81E-06	0.0197
NRP1	3.75	1.02E-05	0.0197
GLIPR1	4.1	1.06E-05	0.0197
Uncharacterized	4.1	1.17E-05	0.0209
FLI1	2.26	1.29E-05	0.0222
RAB27B	4.05	1.38E-05	0.023
ADGRF1	3.36	1.48E-05	0.0235
PAPSS2	2.43	1.51E-05	0.0235
COL4A2	2.03	1.58E-05	0.0238
GEM	2.36	1.65E-05	0.0241
NFE2L3	2.26	1.76E-05	0.0244
SLITRK6	9.41	1.77E-05	0.0244
ARNTL2	2.99	2.04E-05	0.0273
NEBL	2.19	2.24E-05	0.0279
IL1RL1	2.33	2.25E-05	0.0279
THSD4	2.42	2.26E-05	0.0279
USP53	2.58	2.37E-05	0.0285
SLIT3	2.06	2.54E-05	0.0299
KYNU	2.95	2.65E-05	0.0299
LOC105379362	2.97	2.72E-05	0.0299
STC1	5.47	2.73E-05	0.0299
CEMIP	3.86	2.99E-05	0.032
IRF4	-3.57	3.10E-05	0.0322
SV2C	2.27	3.14E-05	0.0322
ME3	2.14	3.38E-05	0.0334
CLMP	2.26	3.79E-05	0.0364
FZD8; MIR4683	2.21	3.85E-05	0.0364

NT5E	2.66	3.92E-05	0.0364
TGFB1	2.06	4.02E-05	0.0366
F2RL2	2.7	4.41E-05	0.0394
C15orf54	2.88	4.64E-05	0.0396
PRR9	2.76	4.66E-05	0.0396
PPARG	2.35	4.69E-05	0.0396
ENC1	2.32	5.28E-05	0.0426
Uncharacterized	-2.33	5.31E-05	0.0426
KCNIP4-IT1	2.41	5.39E-05	0.0426
KCNN4	2.56	5.64E-05	0.043
PGM5P2	2.19	5.66E-05	0.043
HACL1	2.23	5.71E-05	0.043
SIRPB1	2.02	6.04E-05	0.0448
PXDN	3.55	6.42E-05	0.0463
GPX1	2.55	6.49E-05	0.0463
CADM4	2.1	6.52E-05	0.0463
ZNF860	2.01	6.95E-05	0.0481
FLT1	2.06	6.98E-05	0.0481
SAMD5	2.73	7.26E-05	0.049
TRIM58; OR2W3	2.82	7.52E-05	0.0497
Uncharacterized	2.82	7.86E-05	0.0512
TGFA	3.54	8.03E-05	0.0512
GLIS3	3.35	8.07E-05	0.0512
TLR4	5.99	8.17E-05	0.0512
LOC105379109	2.56	8.67E-05	0.0536
MIR548XHG	3.18	9.05E-05	0.0553
SULF1	5.03	9.23E-05	0.0556
Uncharacterized	2.41	9.48E-05	0.0561
FAM135B	2.55	9.55E-05	0.0561
SLC24A3	3.76	9.68E-05	0.0563
PTHLH	2.9	9.99E-05	0.0573
MMP2	2.04	0.0001	0.0592
ITGA3	2.24	0.0001	0.0592
SFRP1	2.3	0.0001	0.0592
PMEPA1	2.45	0.0001	0.064
DAPK1	-2.01	0.0001	0.0656
PRDM1	2.88	0.0001	0.0663
ZNF385A	2.17	0.0001	0.0681
Ambra1	-1.58	0.0075	0.3987

### 6.3.3 Differential expression functional analysis of the microarray results:

Functional analysis of the first dataset (rAmbra overexpression) was not considered due to the high false discovery rate. The second data set was analyzed by submitting the 81 characterized differentially expressed genes to STRING protein-protein interaction tool, KEGG pathways tool and Go biological process tool (2.215).

STRING analyses showed that the list of the upregulated genes centers around VEGFA on the protein level (Figure 6.9).



**General String analysis legend**



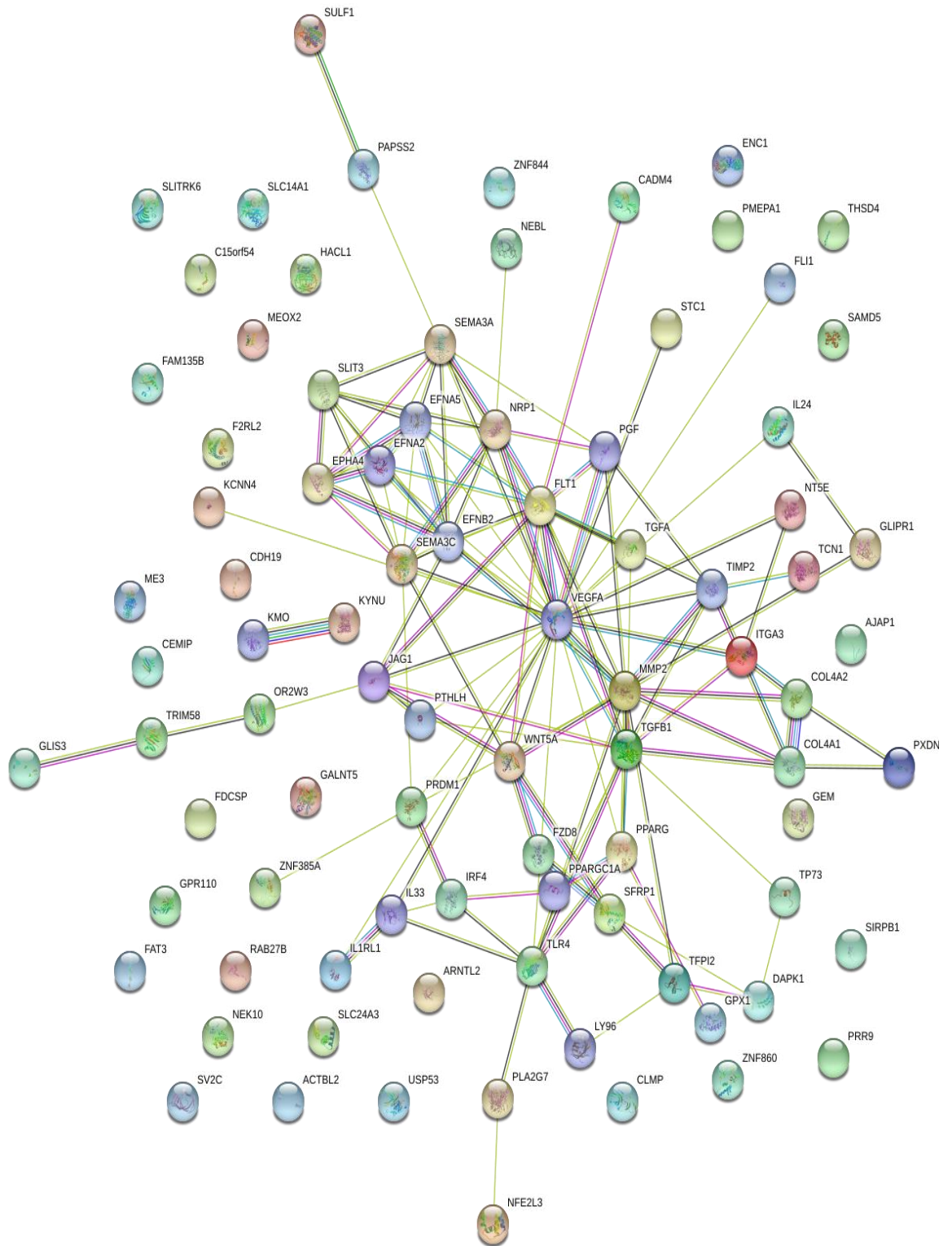


**Figure: 6.9: STRING analysis of the 81 differentially expressed genes resulting from Ambra1 knockdown.** The analysis shows that a large number of the coded proteins of the differentially expressed genes are linked by different interactions and centers on VEGFA.

KEGG pathways were used to detect which pathways are related to the Ambra1 knock-down and the five top pathways are presented in table 6.5. Axon guidance, PI3K-Akt, Ras and MAPK pathways were among the top pathways affected by the knock down of Ambra1.

**Table 6.5: KEGG pathway showing top five pathways affected by Ambra1 knockdown.**

Term ID	Term description	observed gene count	Background gene count	FDR
hsa04360	Axon guidance	12	173	0.00015
hsa05200	Pathways in cancer	18	515	0.0018
hsa04060	Cytokine-cytokine receptor interaction	12	263	0.0024
hsa04151	PI3K-Akt signaling pathway	14	348	0.0024
hsa04014	Ras signaling pathway	9	228	7.59e-05
Hsa04010	MAPK signalong pathway	10	293	7.59e-05

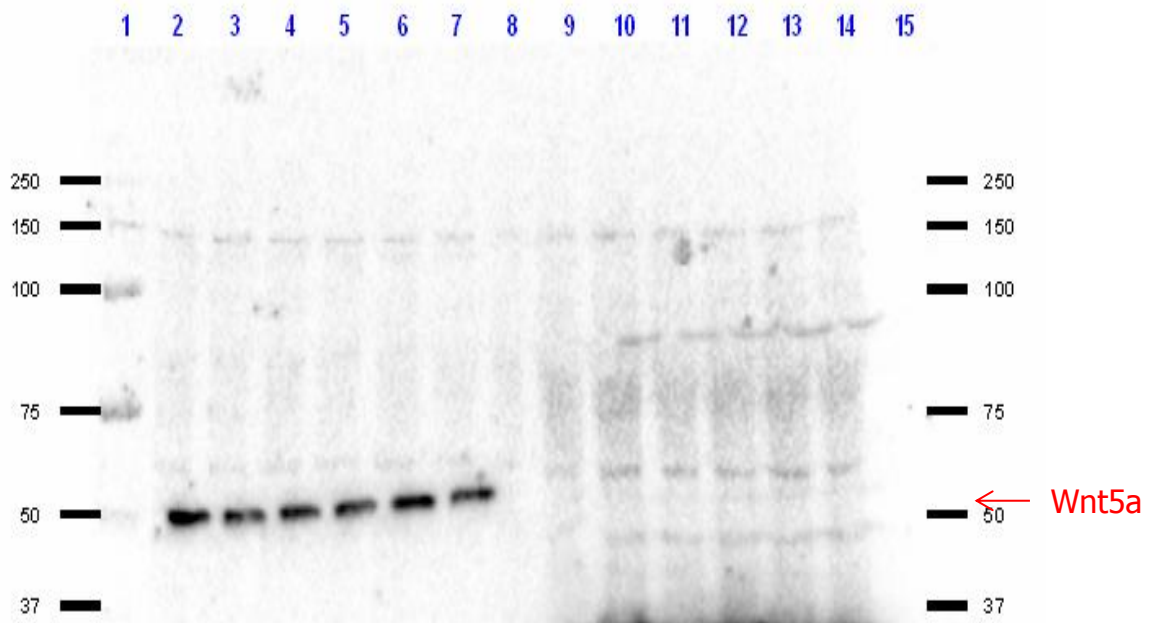
GO biological process was used to detect the top biological processes affected by Ambra1 knock-down (Table 6.6). On top of this list is angiogenesis which support STRING analysis results that the knockdown of Ambra1 largely affects VEGFA. The list also includes axon guidance, as well as MAPK activation

**Table 6.6: GO biological processes showing top biological processes affected by Ambra1 knockdown.**

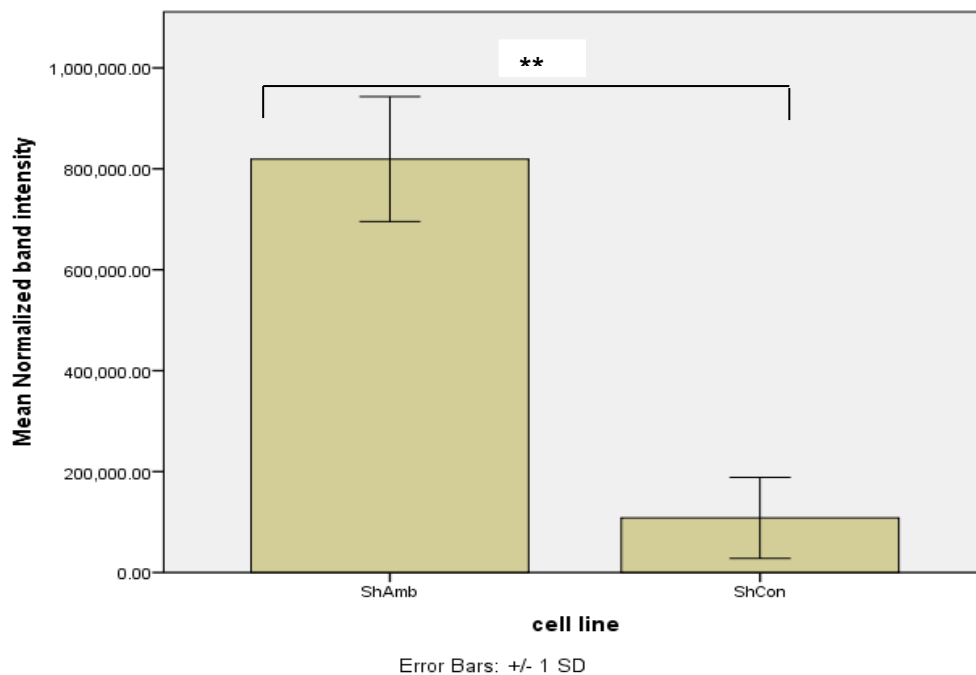
Term	Count	P-Value	FDR
GO:0001525~angiogenesis	8	3.23E-05	0.050532135
GO:0048843~negative regulation of axon extension involved in axon guidance	4	1.54E-04	0.241341287
GO:0071560~cellular response to transforming growth factor beta stimulus	4	0.001024	1.5899426
GO:0048846~axon extension involved in axon guidance	3	0.001039	1.612567923
GO:0007411~axon guidance	5	0.003939	5.986044987
GO:0030336~negative regulation of cell migration	4	0.006741	10.03802224
GO:0071526~semaphorin-plexin signaling pathway	3	0.007868	11.62186571
GO:1900020~positive regulation of protein kinase C activity	2	0.008083	11.92089347
GO:0050919~negative chemotaxis	3	0.008338	12.27447187
GO:0000187~activation of MAPK activity	4	0.009339	13.64974567

#### **6.3.4 Western blot analysis to confirm differential genes overexpression**

To confirm the effect of Ambra1 gene knockdown on the protein level of differentially expressed analysis; two key candidates were selected to confirm their over expression by western blots analysis, Wnt5a and FLT1 (VEGFR-1) (2.2.4). Wnt5a western blot analysis (Figure 6.10) showed a band for Wnt5a at~50 KDa in the ShAmb cell lines only. These results confirmed significant Wnt5a overexpression in the ShAmb cell lines. Statistical analysis was performed by comparing normalized band intensities to normalized adjusted volumes of total proteins loaded. Wnt5a western blots were performed by chemiluminescence using a HRP-conjugated secondary antibody. The FLT1 western blots were unsuccessfully performed using the traditional HRP-conjugated secondary antibody, human protein atlas show that FLT1 expression in skin is less than WNT5A so we considered a more sensitive approach to detect FLT1 and therefore; western blots were performed using a fluorescent Alexa fluor448 conjugated secondary antibody. Western analysis of FLT1 was performed (Figure 6.11), a band was observed in the ShAmb cell lines only for FLT1 at~100 KDa. Bands were normalized against adjusted volume of protein loaded. Results were statistically significant for FLT1 overexpression in the ShAmb.

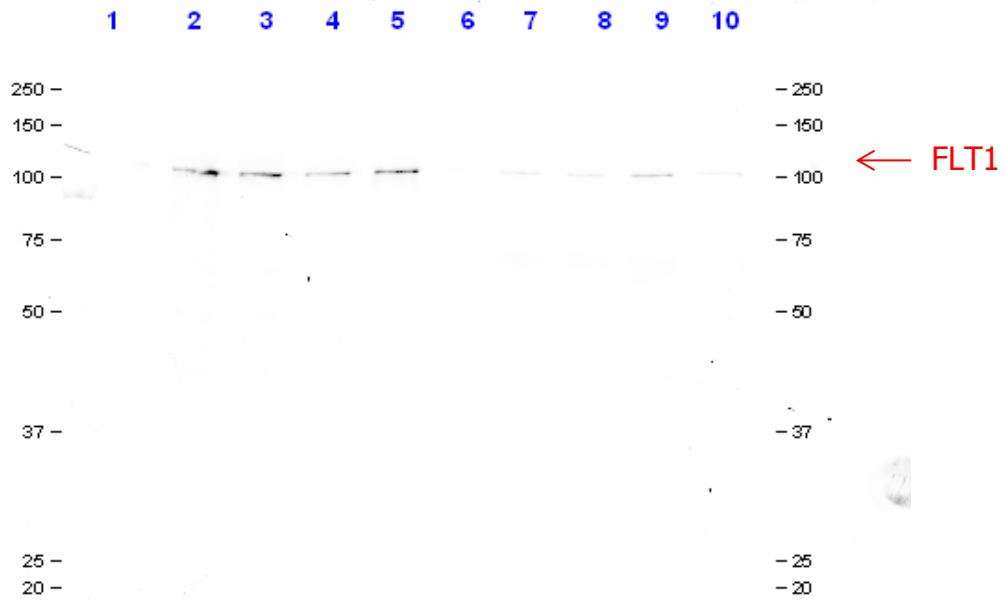


(A)

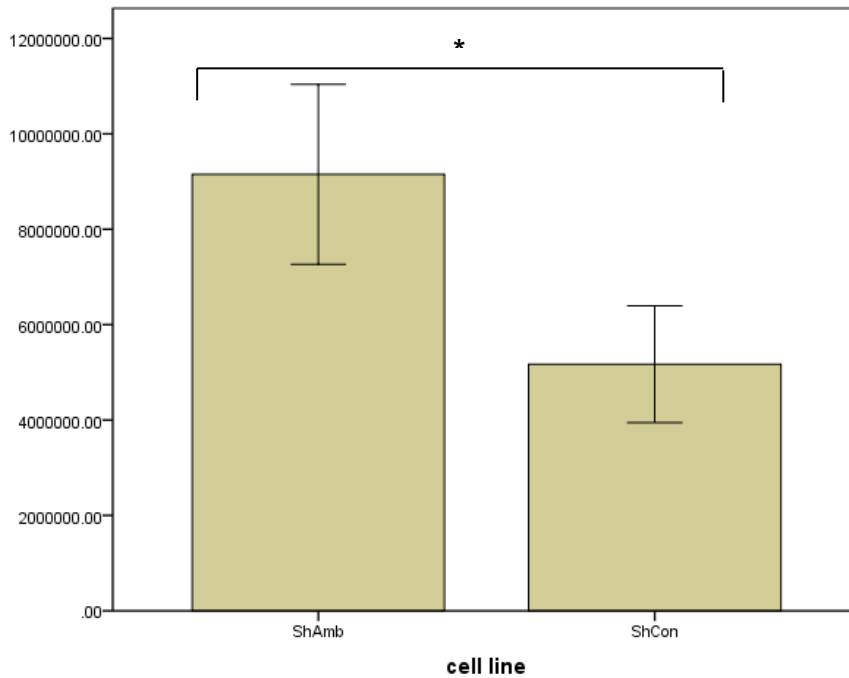


(B)

**Figure 6.10: Western blot analysis of WNT5A from Ambra1 knockdown model.** (A) Lanes 2 to 4 and 5 to 7 are replicates of two ShAmb biological extracts from different passages and, lanes 9 to 11 and 12 to 14 are replicates of two ShCon biological extracts from different passages. A band for Wnt5a is observed at ~50 KDa after 9 seconds exposure for ShAmb cell lines which cannot be observed for the ShCon. (B) Normalized band intensities against adjusted volumes of total proteins loaded. Statistics: Mann-whitney U-test significant Bar chart shows mean +/- SD, n=6, \*\*p<0.01.



(A)



Error bars: +/- 1 SD

(B)

**Figure 6.11: Western blot analysis of FLT1 from Ambra1 knockdown model.** (A) Lanes (2 and 3) and (4 and 5) are replicates of two ShAmb biological extracts from different passages and, lanes (7 and 8) and (9 and 10) are replicates of two ShCon biological extracts from different passages. A band for FLT1 is observed at ~100 KDa for ShAmb cell lines which cannot be observed for the ShCon. (B) Normalized band intensities against adjusted volumes of total proteins loaded. Statistics: Mann-whitney U-test significant Bar chart shows mean +/- SD, n=4, \*p<0.05.

FLT1 and WNT5A differential expression data generated by the microarrays and the western blots as a result of the knockdown of Ambra1 were compared (Table 6.7), the microarray data showed that WNT5a was 3.65 folds overexpressed on the transcription level and western blot analysis showed that it is 5.2 folds overexpressed on the protein level. Both microarrays and western blot analysis showed FLT1 to be about 2 folds upregulated.

**Table 6.7: FLT1 and WNT5A microarrays and western blot analyses differential expression fold change as a result of Ambra1 knockdown.**

<b>Gene/protein name</b>	<b>Gene upregulation fold change detected by Microarray</b>	<b>Protein upregulation fold change detected by Western blot</b>
<b>FLT1</b>	2.06 (p-value 6.98E-05)	2.021 (p-value: 0.043)
<b>WNT5A</b>	3.65 (p-value 7.08E-06)	5.2 (p-value 0.002)

### **6.3.5 Further analyses**

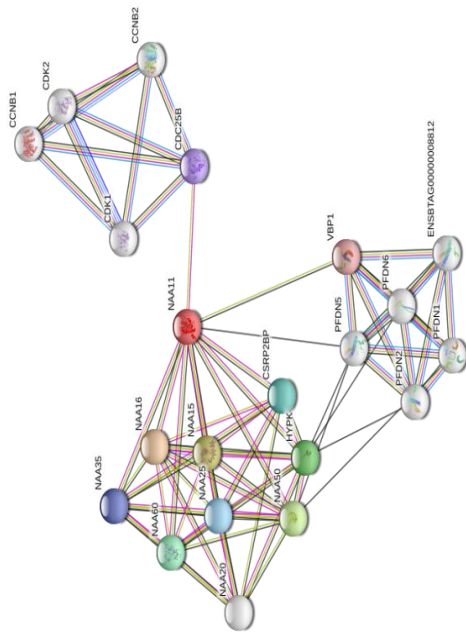
It was important to further analyze the data generated from Ambra1 differential expression to allow investigating roles of the differentially expressed genes and clustering them into groups that can help understand the mechanisms by which Ambra1 can affect different cellular processes.

#### **6.3.5.1 Analyses of differentially expressed genes that may affect cell cycle**

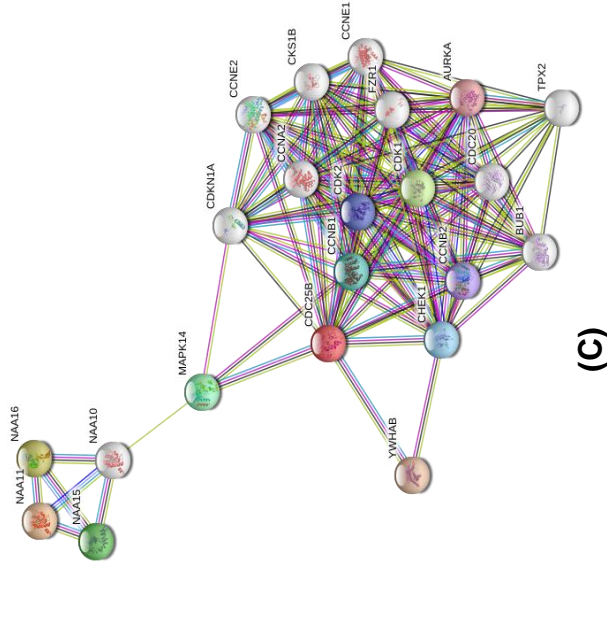
NAA11 is differentially expressed as a result of Ambra1 overexpression, and was found to be of a specific importance in cell proliferation, it can affect the activity of cyclin dependent kinases. To understand its interaction with different cell cycle components a STRING analysis of NAA11 was performed (Figure 6.12), the analysis show that it can interact directly and indirectly with cell cycle components like CDC25A and CDC25B.

In relation to cell cycle, there is also TRIM63 that was found to be differentially expressed in this study, a STRING protein analysis was performed to demonstrate the link between TRIM63 and different cell cycle components (Figure 6.13)

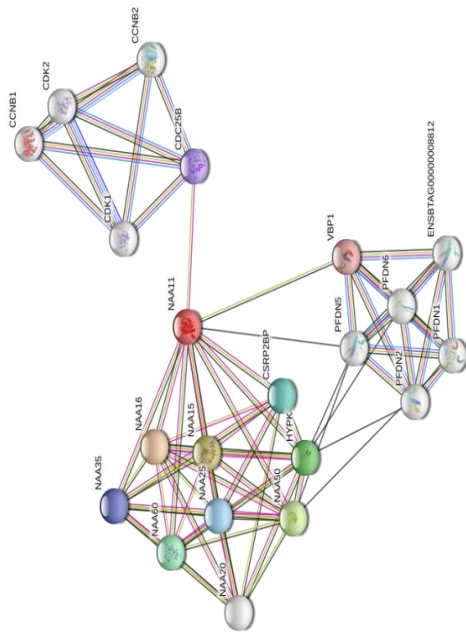




(A)



(B)



(C)

**Figure 6.12 STRING protein analyses showing the interaction between NAA11 and cyclin dependent kinases (A) Homo-sapiens string analysis showing NAA11 interaction with CDC25A. (B) Bos Taurus (C) Homo-sapiens showing NAA11 interaction with CDC25B.**

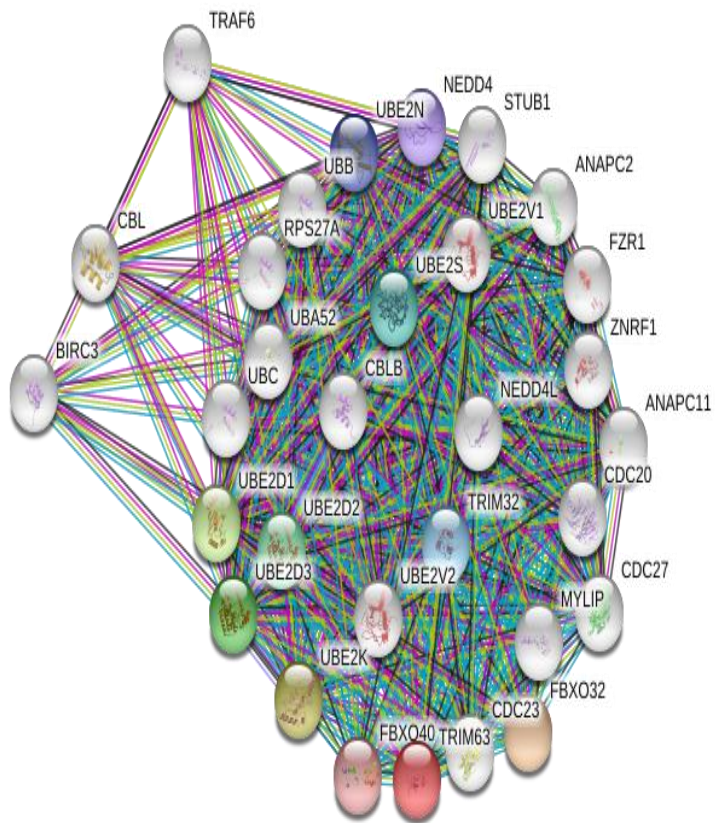


**Figure 6.13 STRING protein analysis of TRIM63.** Analysis show TRIM63 can interact with different cell cycle components like CDC20, CDC23 and CDC27.

### 6.3.5.2 Analyses of differentially expressed genes that may affect angiogenesis

STRING protein analysis performed in figure 6.9 for the whole set of the proteins that are encoded by different genes affected by Ambra1 knockdown show that many of these proteins center on VEGF-A, in order to study and demonstrate this effect, selected genes that may affect angiogenesis (Table 6.8) were analyzed using the STRING tool (Figure 6.14). Analysis shows that at least 21 of the differentially expressed genes can directly and/or indirectly affect VEGF-A including VEGFR-1 (FLT1) and VEGFR-2 (KDR).

**Table 6.8: VEGF related genes differential expression in the Knockdown model**

Gene name	Folds overexpression in ShAmb cells	FDR P-val
SEMA3C	3.74	0.0079
WNT5A	3.65	0.0163
TGFB1	2.06	0.0366
FLT1	2.06	0.0481
TGFA	3.54	0.0512
JAG1	3.39	0.0126
ITGA3	2.24	0.0592
SEMA3A	3.11	0.0079
EPHA4	2.83	0.0167
PRDM1	2.88	0.0663
PPARG	2.35	0.0396
IL1RL1	2.33	0.0279
TLR4	5.33	0.0512
PTHLH	2.9	0.0573
MMP2	2.04	0.0592
NT5E	2.66	0.0364
FLI1	2.26	0.0222
IL24	-2.85	0.0134
STC1	5.47	0.0299
NRP1	3.75	0.0197
KCNN4	2.56	0.043

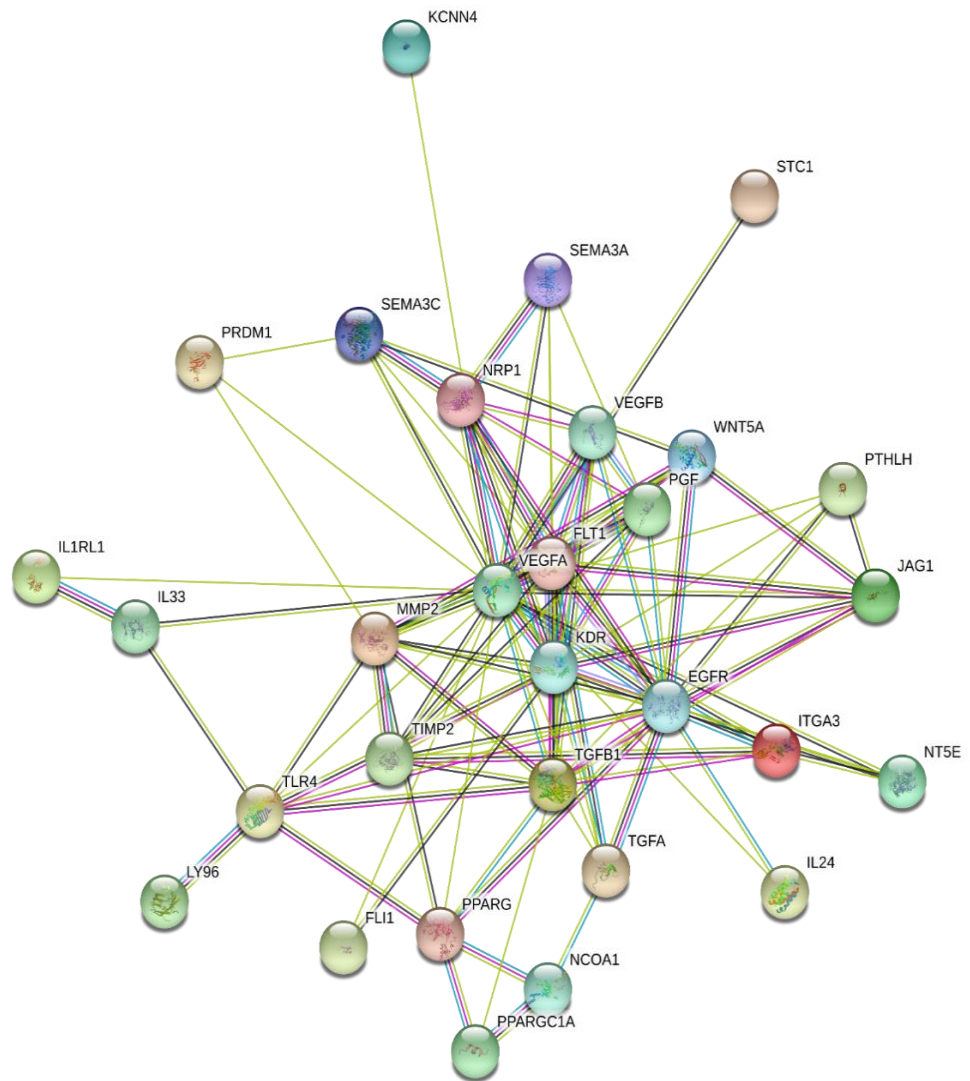


**Figure 6.14: string analysis of selected differentially expressed genes.** Analysis shows a network of interaction that directly affects VEGF-A resulting from the knock-down of Ambra1.

### 6.3.5.3 Analyses of differentially expressed genes that may affect melanoma cell proliferation

Microarray differential expression data was analyzed to search for key genes that can affect the proliferation of melanoma, key melanoma related genes were identified and are listed in table 6.9

**Table 6.9: melanoma progression related genes identified to be differentially expressed upon Ambra1 knockdown.** The table compares ShAmb. Vs. ShCon and it includes the gene name, gene symbol, fold change, P-value and FDR.

Gene name	Gene symbol	Fold change (ShAmb. Vs. ShCon)	P-value	FDR
BRAF-activated non-protein coding RNA	BANCR	-3.46	0.0149	0.5095
growth hormone receptor	GHR	-2.04	0.0036	0.2977
RAB17, member RAS oncogene family	RAB17	-2.03	0.0031	0.2801
RAB38, member RAS oncogene family	RAB38	-2	0.0153	0.5109
RAB27B, member RAS oncogene family	RAB27B	4.05	1.38E-05	0.023
Ras association (RalGDS/AF-6) domain family member 3	RASSF3	-2.06	0.0007	0.1407
secreted frizzled-related protein 1	SFRP1	2.3	0.0001	0.0592
insulin like growth factor binding protein 5	IGFBP5	5.27	0.002	0.2287
inhibin beta A	INHBA	5.57	0.0014	0.19

## **6.4. Discussion**

Microarray studies require careful planning and development of analysis strategies. However, to be most effective it requires a design of a study to answer well-defined questions (Simon et al., 2002). The clear question of this study was what are the effects of Ambra1 differential expression on transcriptomic regulation? Questions also included: What are the possible mechanisms by which Ambra1 can regulate cell proliferation other than its reported activity on c-Myc? And how can Ambra1 knockdown inhibit melanoma cells proliferation?

To answer these questions, microarrays studies were designed to utilize the A375 cell lines that differentially express Ambra1 (rAmbra and ShAmb) and compare the effect of altering Ambra1 levels to a matching control. The Affymetrix Gene Chip Human Gene 2.0 ST Array used in this study includes more than 53,000 probe sets offering a highly comprehensive expression analysis of the entire genome. Also the characterization of the cell lines used in this study (chapter 3) contributed to design an effective microarray analysis, as RNA extractions were performed after 72 hours of seeding the cells with no antibiotic selection, this step was crucial to allow for most of the population of each cell line to be expressing Ambra1 at the desired level. Lastly, four replicates of each cell line were submitted to the array analysis as having replicates for each RNA specimen permits discarding bad arrays (Simon et al., 2002).

Differential expression of Ambra1 in this study shows a great alteration in pathways that are related to cell proliferation and cancer prognosis, reviewing the role of Ambra1 in cancer shows that it is not fully clear and two views predominate. The first is that Ambra1 acts as a tumor suppressor gene as it

decreases cell proliferation (1.6.5 and 3.4), also Ambra1 deficient mice have a higher rate of tumorigenesis compared to the controls (Cianfanelli et al., 2015).

Secondly there is evidence that Ambra1 over expression in cancer is favorable to the tumor in different ways. However, evidence largely relates this effect to autophagy. A study has related the role of Ambra in the cross talk between autophagy and apoptosis to its pro survival role in SW620 colorectal cancer cell line, as it contributes to shifting the cells towards autophagy and survival rather than apoptosis (Gu et al., 2014), another has shown that the overexpression of Ambra1 is significantly correlated with lymph node metastasis and poor survival rate of the patients in cholangiocarcinoma (Nitta et al., 2014).

Data showing levels of Ambra1 expression in cancer cells and its role in tumorigenesis is limited. However; some studies have reported Ambra1 overexpression in the late stages of a variety of cancers. For example: Ambra1 is expressed in ~63.9% of pancreatic ductal adenocarcinoma. However; the exact levels of Ambra1 were not measured neither were related to prognosis of this cancer (Ko et al., 2013), “perineural invasion” a negative prognostic factor for cancer therapy is associated with Ambra1 overexpression in prostate cancer, gastric adenocarcinoma (Qu et al., 2017) and cholangiocarcinoma (Nitta et al., 2014; Sun, 2016). More recently a meta-analysis clearly related Ambra1 up regulation to tumorigenesis and progression of breast cancer using data from 25 microarrays datasets that included 2460 breast cancer samples (He et al., 2018). Also a recent study suggest a role of Ambra1 in cancer cell resistance to therapy by showing that higher levels of Ambra1 are associated with resistance of breast cancer cells to the most currently used breast cancer treatment Epirubicin (Sun et al., 2018). The underlying mechanism of how

Ambra1 can make such a difference in the treatment of cancer remains unknown.

On the other hand, a recent study reported that Ambra1/Loricrin loss in stage I melanomas indicates worse prognosis independent of Breslow depth (Ellis et al., 2019), levels of Ambra1 reported in that study are in the epidermis surrounding tumors and not in the tumor itself. But this gives indications that Ambra1 loss is favorable for tumor in early stages. The role of Ambra1 in cell proliferation and cancer can be explained by different effects of the highlighted gene in different cancer stages from initiation to progression and metastasis. Generally it seems that Ambra1 loss is favored to tumor development. However; its overexpression in a well-developed cancer can contribute to cancer survivability and treatment resistance, this role also appear to be parallel to the role of autophagy in cancer (1.5). However, Ambra1 is also reported to have roles in differentiation, apoptosis, and development in addition to its roles mentioned above (1.6), and more research is required to investigate its role in cell proliferation and cancer and if its role in cancer is related to its well defined role in autophagy..

FDR is an essential statistical tool in “omics” due to the large number of data points and only adjusted P-values are really considered significant. After adjusting the P-values using FDR to account for multiple correction testing there were few significant genes differentially regulated when comparing the rAmbra cell line to its control showing that either Ambra1 overexpression in this cell line model is not of a great effect on the transcriptome or, that Ambra1 is already expressed to a level which exerts its maximum effect in this malignant cell line. Ambra1 was confirmed to be upregulated in the rAmbra cells, also the two significantly upregulated genes in this dataset that lie in an acceptable FDR



value CDH13 and NAA11 are of specific importance. CDH13 is well reported to be down regulated in the malignant melanoma. Loss of this specific gene is reported to have a role in metastasis and the expression of this gene in a different melanoma model reduces the tumor invasiveness (Kuphal et al., 2009), a study has shown that tumor growth was diminished after subcutaneous injection of CDH13 positive melanoma cells compared with CDH13 negative cells in nude mice (Bossert et al., 2014) the same study has reported that the decreased cell proliferation was due to induced apoptosis in the CDH13 positive model, this effect was found to be mediated by the inhibition of AKT signaling as well as, antiapoptotic molecules like BCL-2 and BCL-x . Considering this data supports the evidence that Ambra1 is a tumor suppressor gene. The relationship between the loss of Ambra1 and developing a worse metastatic cancer (Ellis et al., 2019) can be partially explained by our findings that Ambra1 may promote CDH13 expression leading to AKT hypophosphorylation and downregulation of the antiapoptotic molecules BCL-2, BCL-x and Clusterin.

NAA11 is proposed to be an alternative catalytic subunit of the N-terminal acetyltransferase A (NatA) complex.<sup>1</sup> and it displays an alpha (N-terminal) acetyltransferase activity. NAA11 can acetyl different components of the cell cycle and its acetylation of CDC25A can modulate the extent of Cdc25A ubiquitination, diminish its phosphatase activity and disrupts cell cycle (Lozada et al., 2016). Literature lacks enough data about the role of NAA11 or its expression. One study has limited the expression of NAA11 to placenta and testis assuming that they did not find any of the tissue reported expression of NAA11 in previous studies (Pang et al., 2011). In contrast, another study reported that NAA11 was among the top 20 genes with the most altered RNA

expression levels in vitiligo patients, which indicates that NAA11 expression can well be extended in melanocytes (Reimann et al., 2014). STRING protein network shows a direct interaction between NAA11 and cyclin dependent kinases through the acetylation of CDC25A in *homo-sapiens* and CDC25B in *Bos-Taurus*. The interaction with CDC25B is reported in *homo-sapiens* to take place indirectly through MAPK14 (Figure 6.12) which is a key activator of cyclin dependent kinases (Lammer et al., 1998) CDC25A is overexpressed in different types of cancer, its function as stated by UniProt is “Tyrosine protein phosphatase which functions as a dosage-dependent inducer of mitotic progression. Directly dephosphorylates CDK1 and stimulates its kinase activity. Also dephosphorylates CDK2 in complex with cyclin E, *in vitro*”. Similarly, CDC25B directly dephosphorylates CDK1 and stimulates its kinase activity, it is also an inducer of mitotic progression. Data generated by this study suggests Ambra1 functions to upregulate NAA11 which suggests that Ambra1 may have a role in cell proliferation by disrupting cell cycle as a result of the CDC25A acetylation by NAA11. Confirmatory experiments should be carried on to investigate the expression of NAA11 in skin, its role and function in acetylation of the cyclin dependent kinases and the degree of expression in melanoma, also to prove this novel role of Ambra1, levels of NAA11 and ubiquitination of CDC25A should be monitored upon Ambra1 overexpression in normal cells.

To add to the suggested Ambra1 effect on cyclin dependent kinases, this study suggests Ambra1 functions to inhibit TRIM63 (Appendix 2), which is an oncogene that is overexpressed in melanoma and was described as a signature gene in an analysis that used expression profiles for 240 tumor samples from eight cancer types and 63 melanoma cell lines (Rambow et al., 2015). TRIM63 which is an E3 ubiquitin ligase can interact with members of the CDK and MAP

cascades like CDC20, CDC23, CDC27 and FZR1 (Figure 6.13) Ambra1 knockdown results in the downregulation of TRIM63 which may suggest a role of Ambra1 in cell proliferation by decreasing the expression of this oncogene. However, this finding to be valid a confirmatory experiment is required as the false discovery rate of TRIM63 downregulation is relatively high (P-value 0.0009, FDR 0.158).

Results from studying the effect of Ambra1 on differentially expressed genes that can affect cell cycle components in this study, show that Ambra1 may functions to disrupt of cell cycle and subsequently inhibit cell proliferation.

As mentioned before the knockdown of Ambra1 appears to be highly unfavorable to the cancer model used in this study, and result in a significant decrease in cell proliferation, results from this study suggest that in a well-developed metastatic cancer Ambra1 is essential for the survival and proliferation of Cancer cells (3.4).

Analyzing the second dataset (ShAmb vs ShCon) showed more wide ranging effect on the transcriptome as a result of Ambra1 knockdown. Functional analysis of these genes gives more insight about Ambra1 different roles in cellular functions and molecular pathways. Perhaps one of the strongest findings is that Ambra1 knock-down appears to alter the expression levels of angiogenesis related genes. There is differential expression in 8 genes (COL4A2, FLT1, FZD8, JAG1, MMP2, MEOX2, NRP1 and TGFA) that are involved in angiogenesis biological process, and 20 genes that encode proteins which interact with VEGF-A (Figure 6.14), these genes and their fold change in the ShAmb cell lines compared to the ShCon are shown in table 6.8, which shows that all angiogenesis related genes were found to be overexpressed in

the ShAmb cell lines but IL24. It is important to mention that both vascular endothelial growth factor receptors VEGFR-1 (FLT1) and VEGFR-2 (KDR) are up-regulated as a result of Ambra1 knockdown, suggesting that AMBRA1 functions to inhibit their expression. FLT1 levels were confirmed to be higher in the ShAmb cell lines by western blot analysis (Figure 6.11). Although KDR up regulation has an FDR value of 0.11 (Appendix 2), it will be of a specific importance to study KDR levels as a result of Ambra1 inhibition, as if Ambra1 can be proven to inhibit the two VEGF receptors as well as all the previously mentioned angiogenesis related genes, it will prove a novel role of Ambra1 in regulating angiogenesis.

Tumor growth and metastasis largely depend on angiogenesis, angiogenic activators play an important part in the growth and spread of tumors (Nishida et al., 2006). VEGF is defined as one of the major therapeutic targets in melanoma. Studies have shown that there is a direct correlation between the levels of VEGF and the progression of melanoma. Moreover; VEGF is at highest levels in the malignant phase of many tumors (Carmeliet, 2005). The primary functions of VEGF-A are to promote blood vessel dilation and permeability and to induce new blood vessel formation. In one particular study that measured the levels of expression of cancer related genes in primary oral melanoma patients; VEGF was more expressed in the melanocytes of 70% of melanoma patients and this study proved an inverse correlation between VEGF levels and overall survival (Simonetti et al., 2015). VEGF-A is overexpressed by the vast majority of tumors studied, and circulating levels of VEGF-A are elevated in many patients with cancer.

This finding is of a great importance as if Ambra1 can function to decrease angiogenesis in both healthy and primary cancer cells, then this will support the

evidence that it is a tumor suppressor gene. It can also give a possible explanation to the finding that Ambra1 loss in epidermis surrounding melanoma stage I is related to worse prognosis, it may be well due to increased angiogenesis which leads to more aggressive tumor formation. It is of a specific importance to monitor Ambra1 and VEGFs levels during tumorigenesis and metastasis to prove this suggestion. However, this finding does not explain why the proliferation rate is decreased upon the knockdown of Ambra1, if Ambra1 can function to inhibit angiogenesis, then decreasing Ambra1 levels should result in increased angiogenesis, and therefore increased proliferation and malignancy, but results in this study show that cell proliferation is decreased upon Ambra1 inhibition despite increased levels of angiogenesis related genes.

Interestingly on the list of angiogenesis related genes, there are few differentially expressed genes that are reported to be involved in cancer cell proliferation. Perhaps one of the most important genes on the list is WNT5A which is a member of the WNT family that signals through both the canonical and non-canonical WNT pathways. The role of WNT5A in cancer remains under investigation (Asem et al., 2016). WNT5A signaling was strongly correlated to melanoma invasion of metastatic melanoma, and its expression in human melanoma biopsies directly correlated to increasing tumor grade (Weeraratna et al., 2002). WNT5A is most often associated with non-canonical Wnt signalling (McDonald and Silver, 2009).

This study shows that Ambra1 may function to inhibit WNT5A, which can add to the evidence that Ambra1 can act as a tumor suppressor gene. The finding that Ambra1 knockdown result in increased WNT5A levels was confirmed by western blot analysis (Figure 6.10).

Two angiogenesis regulators semaphorin-3A (SEMA3A) and semaphorin-3c (SEMA3C) are also found to be overexpressed in ShAmb cells, which suggest Ambra1 functions to inhibit SEMA3A, and SEMA3C. SEMA3A is potential inhibitors of tumorigenesis and angiogenesis in mice melanoma models (Chakraborty et al., 2012) its overexpression can dramatically decrease tumor vascularization and promote apoptosis, this effect was shown to be mediated through neuropilin1 (NRP1) receptors which are also up-regulated as a result of Ambra1 knock-down. Surprisingly, however, SEMA3A is reported to be secreted by tumor cells and has major functions in regulating the tumor microenvironment (Capparuccia and Tamagnone, 2009). On the other hand, the full length SEMA3C protein can directly inhibit VEGF-A and decrease metastasis (Mumblat et al., 2015), and in an analysis that compared the microarray data from 31 primary melanomas to 52 metastatic melanomas SEMA3C was among the top down regulated genes in metastatic melanoma (Qiu et al., 2015). Not only SEMA3C and SEMA3A but also other semaphorins like SEMA5A and SEMA3B were differentially expressed in the ShAmb (Appendix 2). A summary of the role of these different semaphorins in cancer is shown in table 6.10.

**Table 6.10: differentially expressed semaphorins as a result of Ambra1 knock-down** showing the fold change, the role of each gene in cancer and the references

Gene name	Fold change	Role in cancer	Reference
SEMA3A	3.11	Inhibits angiogenesis and tumorigenesis	Chakraborty et al., 2012
SEMA3C	3.74	Decrease metastasis	Mumblat et al., 2015
SEMA3B	2.44	Tumor suppressor	Neufeld et al., 2012
SEMA5A	-2.38	Angiogenesis inducer	Neufeld et al., 2012

Semaphorins signaling has been reported to be involved in regulating cell adhesion and motility, and tumor progression (Capparuccia and Tamagnone,

2009). While individual semaphorins on the list of the differentially expressed genes appear to have a negative effect on angiogenesis, the end result of semaphorins activation is not necessarily inhibiting tumorigenesis, semaphorins dysregulation has been linked to tumor progression (Neufeld et al., 2012). Moreover, semaphorins seems essential for the cross talk between cancer cells and may play a role in the metastasis process (Capparuccia and Tamagnone, 2009). Semaphorins are also involved in semaphorin-plexin signaling pathway, which is reported to be involved in axon guidance and regulating the morphology and motility in many different cell types (Alto and Terman, 2017). Data generated in this study suggests that Ambra1 functions to inhibit NRP1 as well as PLXNA2, which is a co-receptor for SEMA3A and is involved in a complex with neuropillins (Capparuccia and Tamagnone, 2009).

Results from this study suggest that Ambra1 may function to alter the expression of different semaphorins, while it is hard to assess the net outcome of the differentially expressed semaphorins, it gives an indication that Ambra1 may be a regulator of this pathway and that it may be a new mechanism by which Ambra1 can exert an effect on cell motility and cancer progression. Moreover, axon guidance was among the top pathways identified by KEGG pathways and the top biological processes identified by GO to be affected by the knock-down of Ambra1. The suggested role of Ambra1 in this signaling pathway reported in this study can be supported by the finding of six different components of this pathway to be differentially expressed as a result of Ambra1 knockdown: SEMA3A, SEMA3B, SEMA3C, SEMA5A, NRP1 and PLXNA2.

Further analysis of the Ambra1 knockdown dataset was performed to find key melanoma cell proliferation regulators that can explain the decreased cellular

proliferation in the ShAmb. Few genes were identified that are of known role in melanoma progression (Table 6.10).

On top of the list sits the BRAF-activated non-protein coding RNA (BANCR) which appeared to be down regulated as a result of Ambra1 knockdown. BANCR is upregulated in different types of melanoma and can interact with chemokine CXCL11 to promote melanoma cell migration. It can also activate ERK1/2 and JNK MAPK pathway to promote proliferation (Hulstaert et al., 2017), (Li et al., 2014). The second identified gene was growth hormone receptor (GHR), data suggests that Ambra1 function to increase the expression of this gene. GHR is well known to be an oncogene in many cancers including melanoma. GHR role in melanoma is well established to activate different pathways in the melanoma progression like ERK1/2, STAT1, STAT3, STAT5, AKT and mTOR. The knock-down of GHR in four melanoma cell lines affected the growth and the progression of the tumor cells (Basu et al., 2017).

Three genes from the RAS family appeared to be down-regulated: RAB17, RAB38 and RASSF3. RAB27B appeared to be upregulated. RAB17 has been linked to melanocyte pigmentation (Beaumont et al., 2011). There is not enough data about its role in melanoma. However; the human protein atlas reports that 7 out of 11 melanoma patients have this gene overexpressed. RAB38 mRNA was found to be overexpressed in 80-90% of melanoma patients. It is the only RAB that shows a predominant expression in melanocytes and is related to melanosomal transport and docking (Jäger et al., 2000). The last down-regulated RAS member is RASSF3 which is known to be expressed in melanoma. But if it acts as a tumor suppressor or as an oncogene remains unclear (van der Weyden and Adams, 2007). RASSF3 can interact with PP2CA, the latter is proven to be an Ambra1 binding partner (Cianfanelli et al., 2015).



The only up-regulated gene in the RAS family is RAB27B which role has been shown to regulate the movement of melanosomes and suggested to maintain the dendritic extensions in melanocytes (Chen et al., 2002). This study suggests Ambr1 function to inhibit SFRP1 which is known to interact with the WNT-frizzled signalling pathway. It is suggested that SFRPs can bind different WNTs and massively affect their activity. Data from this study suggests Ambra1 function to inhibit SFRP1 expression, which is the only protein form the frizzled-related proteins family that shows a tumor suppressor activity and its over expression can be beneficial to treat malignancies (Vincent and Postovit, 2017). This study also suggests Ambra1 function to inhibit IGFBP5. This gene is of a particular importance and is proven to be a tumor suppressor gene. The over expression of IGFBP5 in a study that used the same melanoma cell lines A375 showed significant inhibition of cancer cell proliferation, invasion and migration *in vitro*. The capability of this gene to exert this effect was related to the reduction of the phosphorylation of IGF1R, ERK1/2, and p38-MAPK kinases, and decreasing the expression of HIF1 $\alpha$  and its target genes (Wang et al., 2015). Results suggest that Ambra function to inhibit INHBA expression, which is known to be one of the TGF- $\beta$  superfamily. It is strongly related to different cell signaling pathways involved in cell cycle arrest, cell differentiation and cell development, it shows a cytokine activity and is also involved in MAPK pathways (Singh et al., 2018).

Differential expression of these key genes mentioned above can give a possible explanation to how the decreased melanoma cell proliferation can be mediated by the knockdown of Ambra1 in a late stage cancer, it appears that the knockdown of Ambra1 results in a dysregulation of the RAS/RAF/MAPK as well

as PI3K/AKT/mTOR pathways, which are known to be key driver pathways in melanoma (1.4).

The list of the differentially expressed genes also suggests that Ambra1 functions to inhibit TGF $\beta$ 1 and INHBA as mentioned before. What is surprising is that Ambra1 overexpression also resulted in the up-regulation of INHBA (Appendix 1). This means that apparently altering Ambra1 levels either by overexpression or knocking-down may result in the overexpression of components of the TGF- $\beta$  superfamily, if this finding can be confirmed then it will identify a novel role of Ambra1 in cell proliferation as well as, differentiation and migration that can be mediated by this pathway.

In conclusion, results from this study show that Ambra1 role as a tumor suppressor gene may well be extended beyond its effect on c-Myc and can be a result of Ambra1 effect on angiogenesis related genes and WNT signaling. Combining results in this study with what is already known about Ambra1 show that its role in melanoma can indeed be parallel to the role of autophagy, this study suggests that Ambra1 loss is required for tumorigenesis and malignancy and adds to the evidence that Ambra1 is a tumor suppressor gene, but in late stage cancer its expression can help the malignant cells to survive. Despite the parallel roles of autophagy and Ambra1 in cancer, it is still unknown if Ambra1 mediates its effects on tumors by its role in autophagy or by a distinct mechanism. Results from this study suggest that this role can be mediated by pathways other than autophagy.

This study suggests that Ambra1 is essential for melanoma cell proliferation and its knock-down results in decreased cell proliferation *in-vitro*. It also suggest that Ambra1 is a potential interactor with hall mark cell biological processes and

signaling pathways like angiogenesis, Cyclin dependent kinases, semaphoring-plexin signaling, WNT signaling, and transforming growth factor signaling.

## ***Chapter 7- Final discussion***

## ***7.1 prelude to final discussion***

Ambra1 is defined as an important component of the autophagy machinery. Upon autophagic stimuli Ambra1 activates beclin1, an event which is followed by a cascade of interactions that allow autophagy to take place. Since its discovery in 2007 as an autophagy regulator by Beclin1 activation and as a regulator of development of the nervous system (Maria Fimia et al., 2007) Ambra1 has been extensively studied. It is becoming clear that a range of different cellular processes that can be linked to this protein and it appears to play a role in a number of cancers. However, most of Ambra1's identified roles are still focused on autophagy with few other reports on its roles in other cellular processes. The aim of this project was to explore this, initially by looking at its role in cellular proliferation but as the project progressed this broadened out.

Understanding the complex relationship between genotype and phenotype is largely a fundamental goal of molecular research. The systems-based approach is dependent on the detection and precise quantification of the molecular diversity of the cell at the levels of the genome, transcriptome, proteome and interactome (Figure 7.1) (Bludau and Aebersold, 2020). This study attempted to study Ambra1 using every "omic" level except genomics. RNA microarrays were performed to study the change of the transcriptome resulting from Ambra1 differential expression. A number of proteomic approaches were used to study the proteome and interactome level. Of these the yeast two hybrid based approach was most successful and identified potentially novel Ambra1 binding partners. A summary of novel roles and pathways that involve Ambra1 in A375 melanoma cell lines are summarized in Figure 7.2.

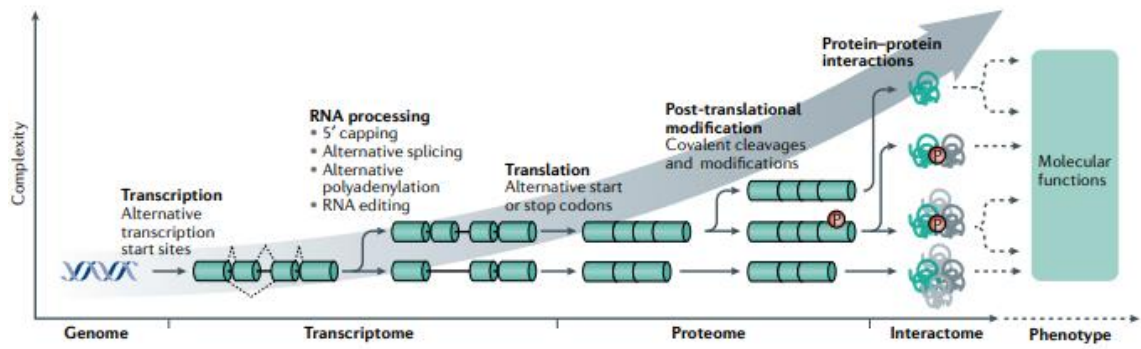


**Figure 7.1: The generation of functional diversity at different molecular levels.** In contrast to the ‘one gene, one protein, one function’ paradigm, cellular complexity arises from many mechanisms that expand molecular diversity beyond that encoded by the protein-coding genome. These mechanisms include an increase in coding potential using alternative transcription start sites as well as 5’ capping, alternative splicing, alternative polyadenylation and RNA editing at the co-transcriptional or post-transcriptional level. The diversity of proteins is further increased using alternative start and stop codons during translation. A high degree of diversification is introduced by post-translational modifications, which include covalent cleavages and covalent modifications (such as phosphorylation (P)). Finally, proteins can interact with each other to form multiple distinct functional units that can potentially perform various downstream functions. Although recent technological advances provide headway towards fully characterizing the transcriptome, proteome and interactome and their relationships in any given state, the assessment of their functional impact and the phenotype is a challenge that still remains to be fully explored (dashed lines). (Bludau and Aebersold, 2020).

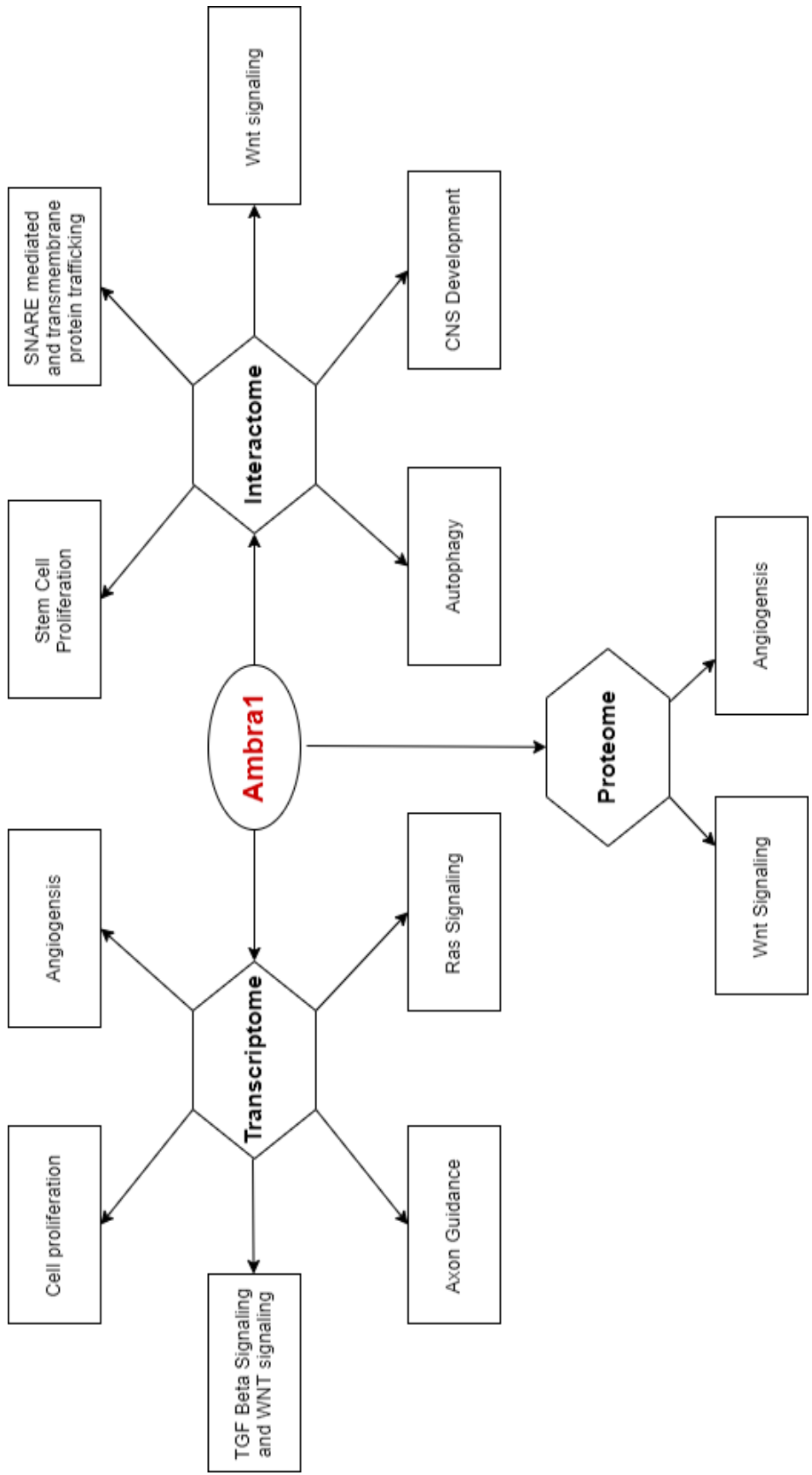


**Figure 7.2: key pathways identified by Ambra1 transcriptome, proteome and interactome analyses.** Hexagons represent the systems based approaches used and rectangles represent identified pathways by each approach.

## ***7.2 Ambra1 role in cell proliferation***

### ***7.2.1 Ambra1 role in melanoma cells proliferation rate***

As discussed in the introduction chapter, Ambra1 has been linked with a role in cell proliferation. In normal cells Ambra1 loss is associated with non-developed hyper-proliferative cells (Benato et al., 2013) and, also associated with higher mRNA levels of cyclins A and B (Cianfanelli et al., 2015). In early stage melanoma the loss of Ambra1 is associated with higher risk tumors (3.4)

In this study we report that in metastatic A375 melanoma cells the overexpression of Ambra1 did not appear to significantly affect the transcriptome, proteome nor metabolome of the A375 cell lines. Growth curve analyses showed that Ambra1 overexpression appears to have no effect on the proliferation rate in an environment where nutrition is not limited. However, knockdown of Ambra1 resulted in decreased cell proliferation, this was shown by both SRB assays and Incucyte live cell imaging. A simple explanation is that the blockage of autophagy by Ambra1 knockdown is essential and that melanoma cells need the autophagy machinery to avoid apoptosis and cell death (Sun, 2016). However, the transcriptional analysis of the Ambra1 knockdown suggests that Ambra1 has a much wider role across a range of cellular processes that are affected by its loss. Are the transcriptional changes directly attributable to the loss of Ambra1 or as a result of defective autophagy? The exact mechanism would require further validation.



### ***7.2.2 Ambra1 interacts with cell cycle components***

There is a relationship between autophagy and cell cycle that has been well reported and reviewed in literature (Mathiassen et al., 2017). The mechanism by which Ambra1 can affect cell cycle components has been reported to be through interaction with C-Myc and PP2CA in a study that demonstrated elevated levels of Cyclins A and B upon Ambra1 depletion (Cianfanelli et al., 2015).

This study provides a possible link between Ambra1 and cell cycle components. It appears that Ambra1 can alter the expression of the N-terminal acetyltransferase, NAA11, which is an alternative catalytic subunit of the N-terminal acetyltransferase A (NatA) complex<sup>1</sup>; NAA11 can modulate the extent of Cdc25A ubiquitination, diminish its phosphatase activity and disrupts cell cycle (Lozada et al., 2016). This study suggests that activation of Ambra1 can inhibit CDC25A by promoting its acetylation by NAA11. It also shows that Ambra1 may function to inhibit TRIM63; a protein that can interact with members of the CDK and MAP cascades like CDC20, CDC23, CDC27 and FZR1 (Rambow et al., 2015). Also in relation to cell proliferation, AGO3 was among the proteins identified to interact with Ambra1 by the Y2H approach, this protein is reported to have a role in stem cell proliferation and also in regulating gene expression. Moreover, AGO3 shows a slicer activity. Can it be an Ambra1 slicer? Answering this question can be done by the knock-down of AGO3 and testing the resulting effect on the levels and activity of Ambra1.

Future studies can also include exploring the role of Ambra1 on cell cycle via CDC25A by NAA11; this can be done by monitoring the degree of CDC25A ubiquitination at Ambra1 and NAA11 different levels.

Confirmatory experiments to prove the alteration in the expression of TRIM63 upon Ambra1 differential expression is also essential to prove that Ambra1 can influence cell proliferation by inhibiting cell cycle.

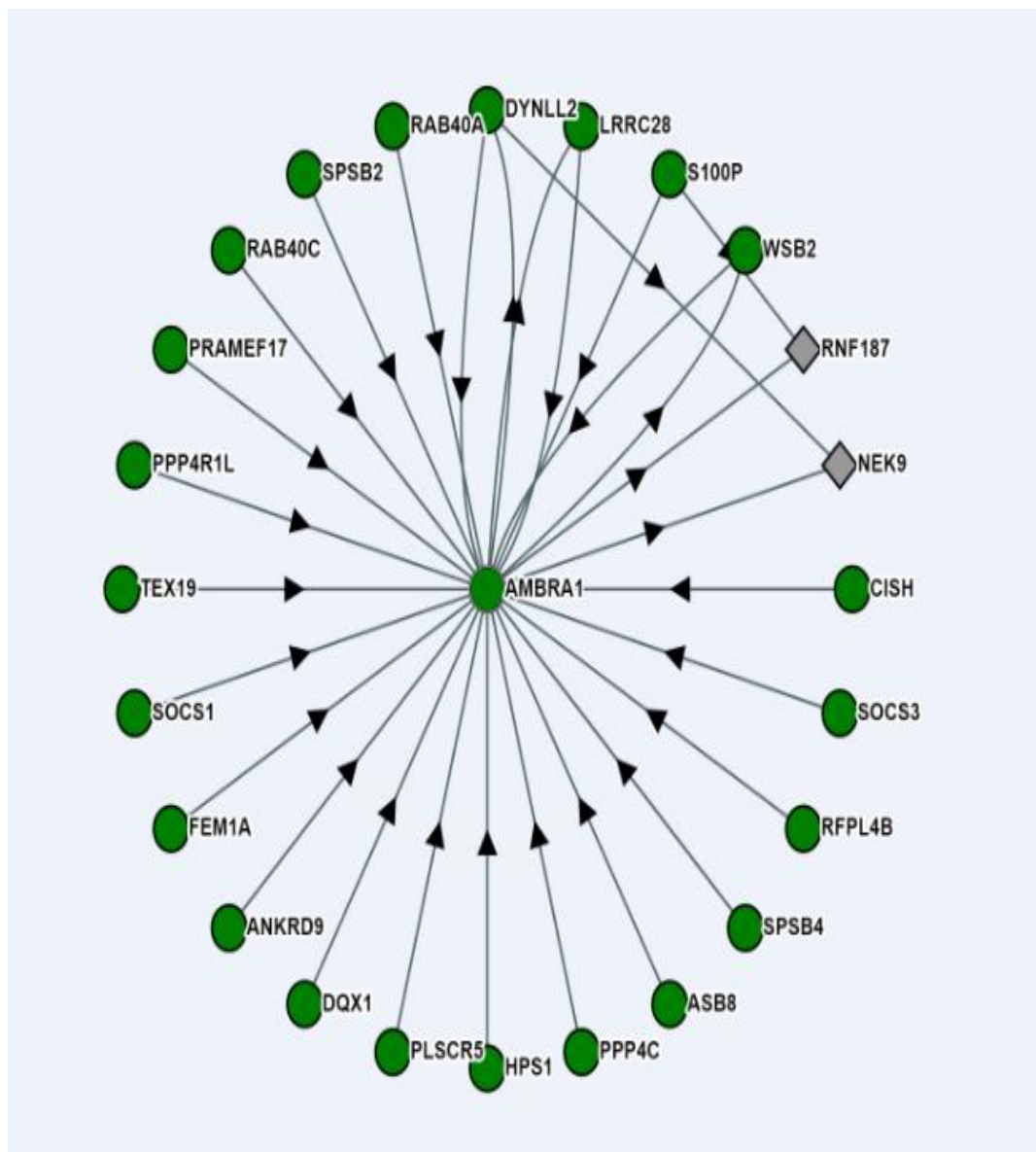
### ***7.2.3 Ambra role in embryogenesis***

At the discovery of Ambra1 in 2007, its role in embryogenesis was reported; its loss was accompanied by unbalanced cell proliferation (Maria Fimia et al., 2007). In this study an interaction between Ambra1 and protein Argonaute-3 was found using Y2H. The protein Argonaute3 is reported to be essential in human embryogenesis specifically regulating stem cell proliferation (Hu et al., 2012). The finding of such an interaction correlates with Ambra1 role reported in embryogenesis and, suggests that this role can be mediated by AGO3 which is reported to have an RNA slicer activity and an ability to regulate gene expression. It will be important to confirm this interaction and monitor the effect of AMBRA1/AGO3 interactions during embryogenesis; and it would be interesting if this interaction could be inhibited experimentally



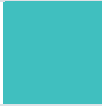


### ***7.3 Ambra1 novel protein binding partners in this and other recent studies***

Ambra binding partners that are already reported in literature are listed in the introduction (1.6.1). Recently a group in Harvard used affinity-purification mass spectrometry to profile protein interactions in human cells and systematically analyze interactions for all accessible human proteins at proteome scale (Huttlin et al., 2015). Searching this database, the BioPlex network, also reported additional Ambra1 novel binding partners (Figure 7.3). It is notable that ANKRD9 is on the list of the interactors as well as ASB8 which bears an ankyrin repeat domain as this study has also found interactions with ankyrin repeat proteins including ANKRD7 and ANK3. Enrichment analysis of these interactions (Figure 7.4) shows that these genes are centered on PTMs like ubiquitination and PI3K activity. Ambra1 has also been reported to be an essential co-factor in the activity of different E3 ligases (Cianfanelli et al., 2015). A combined string protein network analysis of Ambra1 identified protein binding partners reported in literature along with results from this study and BioPlex data (Appendix 3) was performed to explore possible overlapping interactions with the data from this study (Figure 7.5). Figure 7.5(A) shows a string analysis of the previously known interactors with those identified within this study, with the red arrows indicating interactions this study identified in Chapter 4. Figure 7.5 (B) shows a string analysis using the data from the Bioplex database. Figure 7.5(C) shows the string analysis for the combined set of proteins from (a) and (B), again with red arrows noting new interactions from this study. What is clear is the combined data identifies overlapping between Ambra1 different binding partners. For example, this identified an overlap between two identified binding partners in this study (ANK3 and TMED7) and, DYNLL2 which was identified to

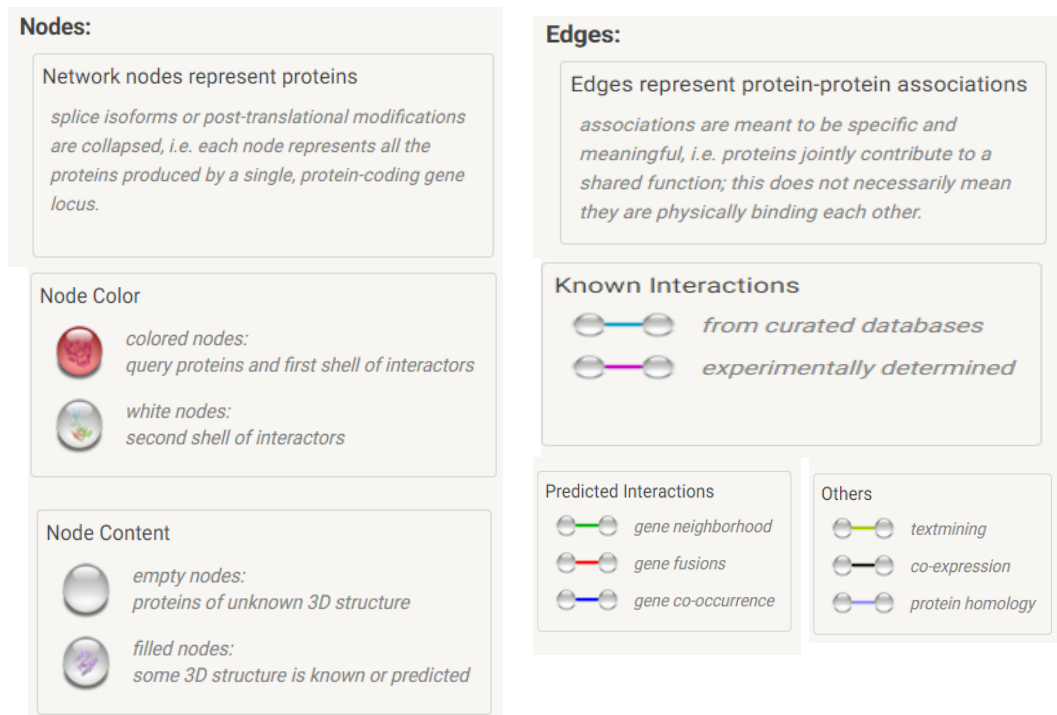
be an Ambra1 binding partner by both BioPlex database and co-immunoprecipitation (Di Bartolomeo et al., 2010). Moreover, an enrichment analysis of Combined Ambra1 identified protein binding partners shows an increasing pattern of networks of proteins that regulate PTMs (Figure 7.6). Importantly, this also provides additional confidence that the interactions identified in Chapter 4 are genuine and biologically meaningful.



**Figure 7.3: BioPlex database analysis of Ambra1 binding partners.**

Category	Color	Hits	Nodes	Hits	Nodes	Adjusted p-value
post-translational protein modification		7	21	343	14543	3.80e-7
1-phosphatidylinositol-3-kinase regulator activity		3	21	14	14543	1.78e-6
protein ubiquitination		7	21	438	14543	2.01e-6
regulation of PDI3-kinase activity		3	21	17	14543	3.14e-6
PDI3-kinase complex		3	21	20	14543	5.01e-6

**Figure 7.4: Gene ontology enrichment analysis of BioPlex Ambra1 binding partners**



**General String analysis legend**

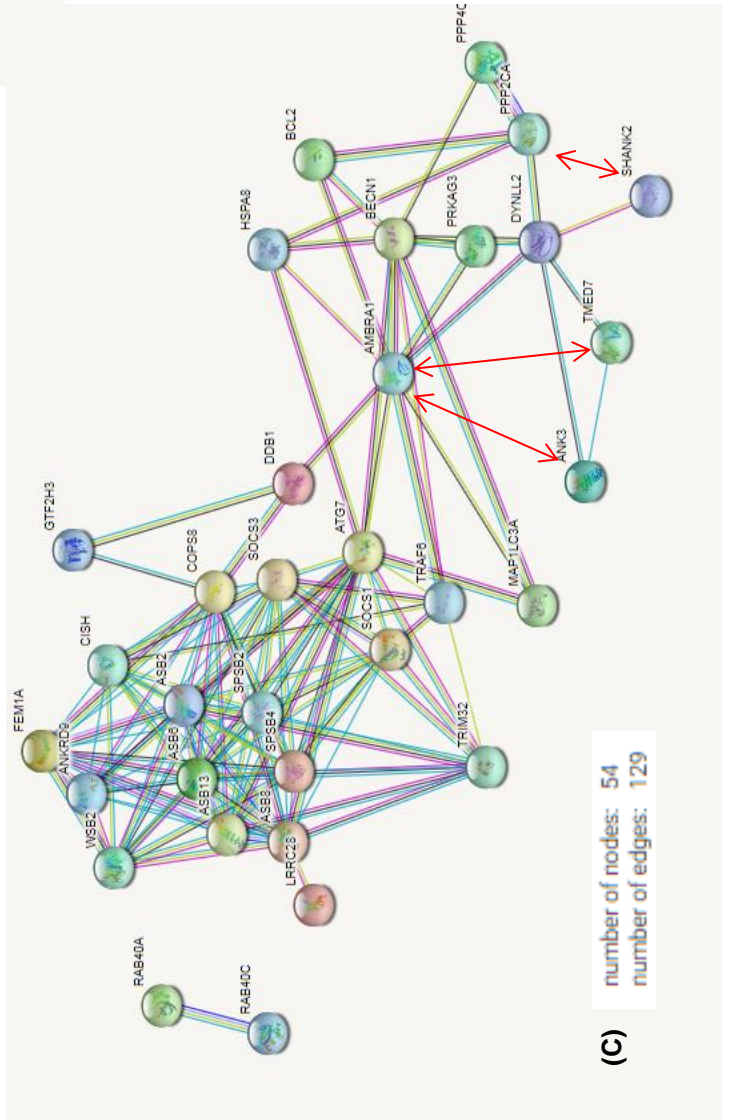
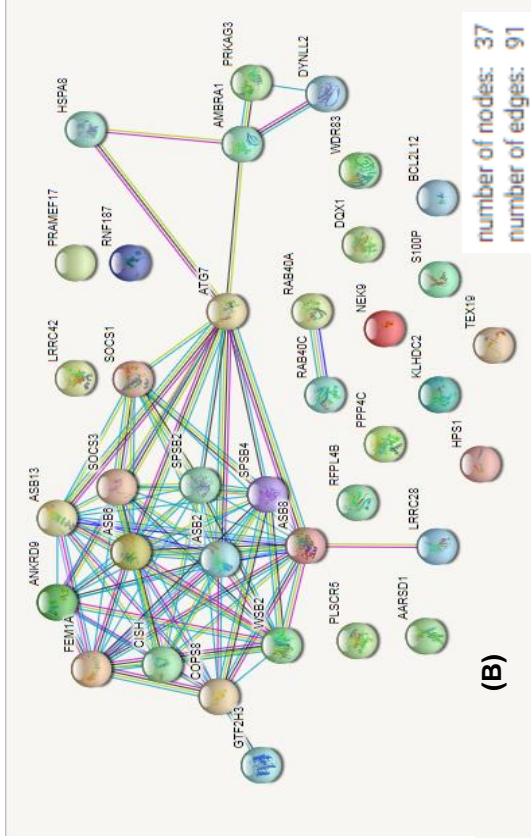
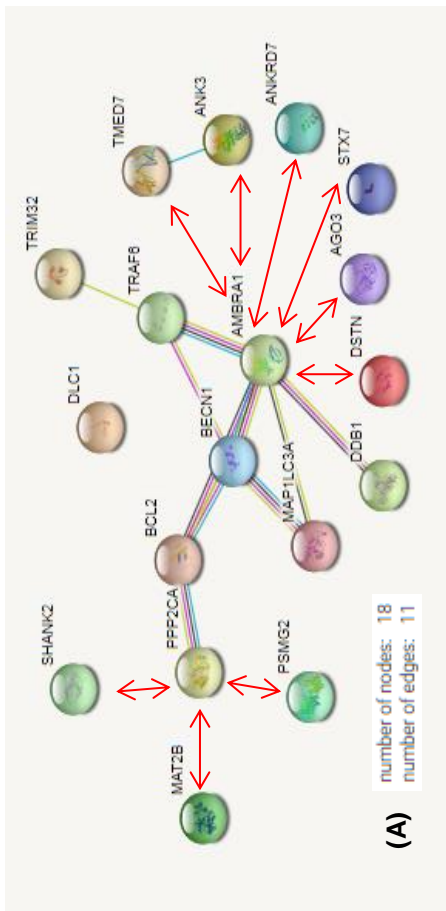


**Figure 7.5: String protein network analyses of Ambra1 protein binding partners.** (A) Combined Ambra1 binding partners reported in literature and identified Ambra1 and PP2CA binding partners in this study. (B) Ambra1 binding partners identified by BioPlex databases. (C) Combined Ambra1 and PP2CA binding partners identified in this study with Ambra1 binding partners reported in literature and, reported by BioPlex databases. Disconnected nodes have been hidden from C for simplifying. Double headed red arrows represent novel interactions identified in this study. All figures show number of nodes and edges for each analysis.

Biological process (GO)			
Goterm	Description	Count in gene set	False discovery rate
GO:0006283	Transcription coupled nucleotide excision repair	13 of 75	9.17e-16
GO:0043687	Post-translational protein modification	18 of 365	4.34e-14
GO:0070647	Protein modification by small protein conjugation or removal	24 of 945	9.84e-14
GO:0006464	Cellular protein modification process	37 of 2999	1.75e-13
GO:0044267	Cellular protein metabolic process	38 of 3603	5.58e-12

**Figure 7.6: Gene ontology biological process enrichment analysis of Ambra1 binding partners.** The list of protein entries is combined from literature, BioPlex and our results.

This study report seven novel Ambra1 binding partners (4.4.1). This not only show new interactions of Ambra1 protein, but suggests that Ambra1 is involved in a range of different cellular pathways and that its role is not limited to autophagy. Identified cellular pathways using this technique appear to show a novel role of Ambra1 in protein trafficking as most interactors identified have roles that are related to protein transport.

Despite elimination of false positives by a two tier screening process in the yeast two hybrid assay confirmation of these interactions by either directed two hybrid assays or co-immunoprecipitations is essential.

A potential novel role of Ambra1 in SNARE mediated protein transport has been identified in this study. Identified binding partners show that Ambra1 is extensively involved in protein trafficking, this role can extend to endless numbers of cellular processes and functions, studying individual interactions between Ambra1 and these proteins involved in cellular transport and the effect



of these interactions on different cellular processes will probably identify a whole set of Ambra1 effects and highlight the role of this core protein that extends well behind autophagy.

This study also shows that Ambra1 interacts with ANKRD7 and ANK3. Combining this study results with BioPlex data which identify that Ambra1 interacts with two other proteins that bear ankyrin repeat domains (ANKRD9 and ASB8) confirm that Ambra1 is likely to be an ankyrin repeat domain binding partner. These interactions are potentially a novel functional role for Ambra1 across a range of different cellular processes. Studying the interaction between Ambra1 and different ankyrin repeat domain proteins could provide a new branch of Ambra1 research.

String analysis shows that the number of edges which represent proteins interactions in the combined string network analysis of Ambra1 and PP2CA binding partners identified in this study with Ambra1 binding partners reported in literature and Ambra1 binding partners identified by BioPlex (Figure 7.5 C) is more than the sum of the edges from string network analysis of Ambra1 and PP2CA binding partners identified in this study and Ambra1 binding partners reported in literature (Figure 7.5 A), and the edges from string network analysis of Ambra1 binding partners identified by BioPlex (Figure 7.5 B). which means that combining novel results from this study with literature and other databases like BioPlex broadens Ambra1 identified network and leads to exploring more novel roles of this protein, the analysis also shows that DYNLL2 which is identified by (Di Bartolomeo et al., 2010) as well as, BioPlex to be an Ambra1 binding partner can mediate the interaction of Ambra1 with two of identified binding partners in this study, ANK3 and TMED7. The analysis shows that DYNLL2 can also mediate the interaction of Ambra1 with PP2CA. It is

interesting that in the PP2CA Y2H control experiment SHANK2 was identified as a novel PP2CA binding partner, which is another DYNLL2 interactor, DYNLL2 is involved in cellular cargo trafficking as well as Macroautophagy (Uniprot) and this analysis adds up to the novel identified role of Ambra1 in protein trafficking. Ambra1 is reported to regulate mammalian autophagy by its interaction with the dynein motor complex (Di Bartolomeo et al., 2010). However, that study focused on DYNLL1 interaction with Ambra1 and the role of this complex in regulating autophagy, they have shown that Ambra1 also interacts with DYNLL2 to regulate autophagy but, their results reported the effect of Ambra1/DYNLL2 in autophagy regulation to be less than that of Ambra1/DYNLL1. The combined string network analysis performed in this study shows ANK3 and TMED7 to be interactors of Ambra1 (novel results) and DYNLL2 (from string analysis), these findings highlight AMBRA1/DYNLL2 complex importance, perhaps not in autophagy regulation as reported by Di Bartolomeo and colleagues but in protein trafficking during autophagy and other cellular processes.

Results from different enrichment analyses show that Ambra1 networks play important roles in different types of PTMS and specifically; ubiquitination. It would be interesting to study the ability of Ambra1 to modify other proteins by ubiquitination. Although Ambra1 is reported to be involved in ULK1 ubiquitylation by LYS-63-linked chains during autophagy (Nazio et al., 2013), these results suggest a deeper role of Ambra1 in the ubiquitination of other cellular proteins. Ambra1's role could be explored by the co-expression of tagged Ubiquitin in different Ambra1 overexpression/knockdown models for the isolation and identification of ubiquitinated proteins.

## ***7.4 Ambra1 role in different cellular processes***

### ***7.4.1 Ambra1 role in angiogenesis***

Angiogenesis is simply the formation of new blood vessels and, is a hall mark of tumors metastasis. It is a process that involves migration, growth, and differentiation of endothelial cells (Nishida et al., 2006). Melanomas show high levels of VEGF, VEGF-R1, VEGF-R2, and VEGF-R3. Studies have shown that there is a direct correlation between the levels of VEGF and the progression of melanoma. Moreover, VEGF is at highest levels in the malignant phase of many tumors (Carmeliet, 2005). Anti-VEGF monoclonal antibody Bevacizumab is used to treat different types of cancer, but it failed to be validated for melanoma treatment after it was tested in clinical trials and used in combination with Temozolomide (TMZ). However; ongoing clinical trials are testing the same anti-VEGF in combination with chemotherapy (Domingues et al., 2018).

This study demonstrates a novel role of Ambra1 in angiogenesis. Ambra1 knock-down in melanoma cell lines may result in an increase in a number of proteins associated with angiogenesis including; COL4A2, VEGF-R1 (FLT1), VEGF-R2 (KDR) FZD8, JAG1, MMP2, MEOX2, NRP1, TGFA, SEMA3C, WNT5A, TGFB1, ITGA3, SEMA3A, EPHA4, PRDM1, PPARG, IL1RL1, TLR4, PTHLH, MMP2, NT5E, FLI1, IL24, STC1, NRP1 and, KCNN4. The over-expression of VEGFR-1 was confirmed by western blot. The findings in this study support the finding that Ambra1 loss in early stage tumors is associated with poor prognosis and suggest this may be a mechanism for driving metastasis.

### **7.4.2 Ambra role in Wnt signaling**

The Wnt family of proteins is involved in the regulation of cell proliferation, cell motility, cell polarity, organogenesis, cell fate and stem cells renewals (Logan and Nusse, 2004). WNT5A is a member of the Wnt family that signals through both the canonical and non-canonical Wnt pathways but, it is most often associated with non-canonical Wnt signaling (McDonald and Silver, 2009). The role of WNT5A in cancer remains under investigation (Asem et al., 2016).

Frizzled receptors (FZDs) are transmembrane receptors that serve as receptors for the WNT ligands. FZDs play crucial roles in regulating cell polarity, embryonic development, cell proliferation, formation of neural synapses (Zeng et al., 2018)

Our results indicate a role for Ambra1 in regulating canonical Wnt signaling via FZD8 and non-canonical Wnt signaling via WNT5A. This study shows that Ambra1 may function to inhibit WNT5A. This was shown by RNA microarrays of the Ambra1 knockdown cell line and confirmed by western blot to monitor the protein levels of WNT5A. Results have shown a significant increase in WNT5A gene expression/protein upon the knockdown of Ambra1. We have also shown by RNA microarray that the knockdown of Ambra1 significantly increases the expression of FZD8 frizzled receptor. Moreover; we have identified ANK3; a regulator of Wnt signaling (Durak et al., 2015) to be an Ambra1 binding partner. This example demonstrates the advantage of “multi-omic” approach taken in this study.

It may be of interest to study the regulation of cell cycle by Ambra1 through WNT signaling, monitoring the level of destruction of the  $\beta$ -catenin complex upon Ambra1 activation may give a new insight about the role of Ambra1 in cell

proliferation. ANK3 could also be blocked or down regulated to better understand if Ambra1 role in Wnt signaling is mediated by ANK3.

### **7.4.3 Ambra1 role in axon guidance**

Axon guidance can be defined as the rules by which the neuronal axons grow to reach their target and establish appropriate connections, a process which is essential during the development of the nervous system. Semaphorins are one of the major soluble proteins that can affect this pathway by binding to their receptor proteins which are known as plexins (Alto and Terman, 2017). The first study that identified Ambra1 protein stated that Ambra1 plays an essential role in developing the nervous system during embryogenesis. They have shown high levels of Ambra1 in neuroepithelium, spinal cord, dorsal root ganglia, neural retina and encephalic vesicles (Fimia et al., 2007).

This study reports a novel role of Ambra1 in the regulation of axon guidance signaling by changing the expression profile of hall mark genes in this pathway. Axon guidance was among the top pathways affected by Ambra1 knockdown and genes from this pathway were differentially expressed and, include: SEMA3A, SEMA3B, SEMA3C, SEMA5A, NRP1 and PLXNA2. Moreover, ANK3 is also involved in axon guidance specifically in axon segment initiation (Durak et al., 2015)

Monitoring axon guidance as well as; ANK3 levels in different Ambra1 expression levels can be a direct step towards identifying the mechanism by which Ambra1 is involved in the development of the nervous system.

#### **7.4.5 Ambra1 role in RAS signaling pathway**

RAS signaling pathway have been reviewed in the introduction chapter and it is a major pathway in cellular growth. Ambra1 has previously linked to this pathway through its ability to enhance the degradation of C-Myc (Cianfanelli et al., 2015).

This study reports a novel role of Ambra1 in this signaling pathway. The knock-down of Ambra1 appear to result in the down regulation of BANCR, GHR, RAB17, RAB38 and RASSF3 and also, the up-regulation of RAB27B, SFRP1, IGFBP5, and INHBA. All these genes are regulators of the RAS signaling in melanoma. It is also important that we have identified an interaction between Ambra1 and ANKRD7, the latter is an effector of the small RAB GTPases RAB32 and RAB38.

#### **7.4.6 Ambra1 role in (TGF- $\beta$ ) signaling pathways**

TGF- $\beta$  receptor plays an important role in tissue homeostasis. It is also a trans-membrane receptor and it is a serine/threonine kinase. This pathway signaling end result is arresting cell cycle and promoting cell entry to G0 (Massagué et al., 2000).

This study suggests that Ambra1 can be part of TGF- $\beta$  signaling pathways. Results obtained by transcriptomics show that altering the expression of Ambra1 whether by overexpression or knockdown result in a change in the expression of TGF- $\beta$  superfamily components including INHBA and TGF $\beta$ 1. The FDR obtained from Ambra1 overexpression effect on these components is relatively high but, obtaining the same differential expression of these components within a significant FDR value upon Ambra1 knockdown is a strong evidence that Ambra1 is related to the TGF-  $\beta$  signaling pathways.

Future studies of Ambra1 role in TGF- $\beta$  signaling pathway is of a great interest, it can open a new window on how Ambra1 is involved in hall mark cell signaling pathways. Assays to identify motifs of Ambra1 that can interact with these family members and carrying out assays to identify these interactions as well as; monitoring the levels of Ambra1 effect on this pathway will help identify a central role of Ambra1 in tumor progression.



### ***7.5 Limitations of the study***

This study could have reported more novel roles of the highlighted protein Ambra1 but, this was not possible due to some limitations that are listed below:

- Technical limitations: The GC-MS analysis was performed by a different team.
- Financial limitations: complete 2D-E gels analyses were considered during this study but was not performed due to financial limitations
- Time limitations: this study was suddenly stopped due to the situation of the COVID-19 pandemic that broke out in UK in March 2020, the main effect on this study is that it would have been possible to isolate and identify more Y2H Ambra1 binding partners if the study was not stopped.

## **7.6 final remarks**

This study has also demonstrated that the role of Ambra1 extends beyond autophagy and may be pivotal in a range of cellular processes. We also demonstrate that taking a multi-omics approach is a good way to identify networks of gene/proteins involved in cellular processes, despite the fact that some strands of the research were not fully realized. The findings indicate that Ambra1 could play a key role in metastasis in malignant melanomas, treatments targeting Ambra1 in metastatic melanoma may be of importance in driving the development of future. This role was shown only in melanoma A375 derived cell lines and may not be universal. However, it adds to the evidence that show that Ambra1 loss appears to upregulate metastatic genes/proteins and is associated with poor prognosis.

## ***Chapter 8- Appendices***

**Appendix 1: full list of differentially expressed genes resulting from Ambra1 overexpression ( $P < 0.05$ )**

Gene Symbol	Fold Change	P-val	FDR P-val
AMBRA1	16.37	2.72E-10	3.34E-06
NAA11	4.27	8.47E-07	0.0082
CDH13	3.06	5.78E-06	0.0465
MIR548AN	-2.55	3.07E-05	0.1853
TFPI2	3.26	3.93E-05	0.2096
NRG1	2.57	4.77E-05	0.2096
FAT3	2.24	6.88E-05	0.2389
CYGB	-2.59	6.94E-05	0.2389
PDE3A	2.66	0.0001	0.3703
NPR2	2.34	0.0001	0.3836
MIR3689D2	3.09	0.0002	0.3836
NOX4	2.9	0.0002	0.3836
CEMIP	2.29	0.0002	0.3882
FAM105A	3.49	0.0002	0.3882
TLR4	2.85	0.0002	0.4051
ABCB5	-2.43	0.0003	0.4322
SLC24A5	-2.54	0.0003	0.4495
FAM167B	-2.32	0.0005	0.6231
PPARGC1A	-2.34	0.0006	0.626
PLA2G7	4.7	0.0009	0.626
LINC00707	3.26	0.0009	0.626
GALNT5	2.13	0.001	0.641
AXL	2.05	0.0011	0.641
LINC01602	-2.15	0.0011	0.641
NOV	-2.6	0.0011	0.641
LHFPL3-AS1	-2.8	0.0012	0.6596
LOC105376382	2.16	0.0012	0.6596
P2RX7	-2.61	0.0013	0.6928
TAC1	3.15	0.0015	0.7253
MIR3689A	2.56	0.0018	0.7253
XYLT1	-2.28	0.0019	0.7253
HELLPAR	-2.09	0.0022	0.7568
MT1A	3.24	0.0023	0.7568
CLMP	2.39	0.0027	0.7641
MIR4486	-2.2	0.0028	0.7641
BEST1	-2.45	0.003	0.7641
MIR3689E	2.64	0.0032	0.7641
INHBA	3.41	0.0032	0.7641
MIR3689B	2.79	0.0038	0.7641
SBF1P1	2.02	0.0038	0.7641
PRICKLE4; TOMM6	-2.3	0.0047	0.7641
ACAN	-2.01	0.0049	0.7641
SULF1	2.2	0.0062	0.7641
SNRPN; IPW	-2.07	0.0063	0.7641
MIR3189	-3.46	0.0071	0.7641
RUNX1-IT1	5.3	0.0073	0.7641
CNTN3	2.65	0.0079	0.7641
FOXR2	2.65	0.0093	0.7641
LOC105374524	2.49	0.0093	0.7641
PPIP5K1	-3.18	0.0094	0.7641

LINC00383	5.32	0.0102	0.7641
TRAV8-6	-2.11	0.0108	0.7641
MPV17L	2.41	0.0126	0.7641
PWAR6	-2.06	0.0138	0.7641
PDZD2	2.99	0.0144	0.7641
OR2M3	2.08	0.0153	0.7652
MIR4518	-2.14	0.0158	0.7652
IGHV3OR16-12	-2.08	0.0181	0.7737
GRAMD1B	3.52	0.0183	0.7737
MRGPRX3	3.9	0.0206	0.7767
GOLGA2P6; MTPAP	-2.04	0.0219	0.7783
TNFRSF14	-2.57	0.0221	0.7783
TGFA	2.04	0.0243	0.7858
SLC24A3	2.18	0.025	0.7876
RTL1	3.88	0.0293	0.8061
STK32A	-2.02	0.0336	0.8086
PRDM7	-2.51	0.0339	0.8086
LINC00597	-2.41	0.0381	0.8185
CXCL8	2.94	0.0406	0.8243
NID1	3.02	0.0446	0.8251
ENPP2	-2.71	0.0468	0.8251

**Appendix 2: full list of differentially expressed genes resulting from Ambra1 Knockdown ( $P < 0.05$ )**

Gene Symbol	Fold Change	P-val	FDR P-val
SEMA3C	3.74	5.93E-07	0.0079
ZNF844	4.2	5.95E-07	0.0079
SEMA3A	3.11	7.65E-07	0.0079
LINC00440	7.05	8.90E-07	0.0079
RUNX1-IT1	3.86	1.11E-06	0.0079
AJAP1	3.94	1.14E-06	0.0079
TCN1	4.94	1.16E-06	0.0079
MEOX2	3.02	1.46E-06	0.0079
GALNT5	3.37	1.47E-06	0.0079
TFPI2	3.6	2.51E-06	0.0113
FAT3	4.41	2.58E-06	0.0113
PLA2G7	8.61	3.33E-06	0.0126
JAG1	3.39	3.45E-06	0.0126
CDH19	3.19	3.65E-06	0.0126
SLC14A1	2.74	4.06E-06	0.0131
IL24	-2.85	4.44E-06	0.0134
ACTBL2	5.51	5.24E-06	0.0143
COL4A1	2.55	5.71E-06	0.0143
NEK10	3.26	5.75E-06	0.0143
TP73	2.63	5.91E-06	0.0143
WNT5A	3.65	7.08E-06	0.0163
EPHA4	2.83	7.82E-06	0.0167
LOC105377108	2.35	7.96E-06	0.0167
NRP1	3.75	1.02E-05	0.0197
GLIPR1	4.1	1.06E-05	0.0197
FLI1	2.26	1.29E-05	0.0222
RAB27B	4.05	1.38E-05	0.023
ADGRF1	3.36	1.48E-05	0.0235
PAPSS2	2.43	1.51E-05	0.0235
COL4A2	2.03	1.58E-05	0.0238
GEM	2.36	1.65E-05	0.0241
NFE2L3	2.26	1.76E-05	0.0244
SLITRK6	9.41	1.77E-05	0.0244
ARNTL2	2.99	2.04E-05	0.0273
NEBL	2.19	2.24E-05	0.0279
IL1RL1	2.33	2.25E-05	0.0279
THSD4	2.42	2.26E-05	0.0279
USP53	2.58	2.37E-05	0.0285
SLIT3	2.06	2.54E-05	0.0299
KYNU	2.95	2.65E-05	0.0299
LOC105379362	2.97	2.72E-05	0.0299
STC1	5.47	2.73E-05	0.0299
CEMIP	3.86	2.99E-05	0.032
IRF4	-3.57	3.10E-05	0.0322
SV2C	2.27	3.14E-05	0.0322
ME3	2.14	3.38E-05	0.0334
CLMP	2.26	3.79E-05	0.0364
FZD8; MIR4683	2.21	3.85E-05	0.0364
NT5E	2.66	3.92E-05	0.0364

TGFB1	2.06	4.02E-05	0.0366
F2RL2	2.7	4.41E-05	0.0394
C15orf54	2.88	4.64E-05	0.0396
PRR9	2.76	4.66E-05	0.0396
PPARG	2.35	4.69E-05	0.0396
ENC1	2.32	5.28E-05	0.0426
KCNIP4-IT1	2.41	5.39E-05	0.0426
KCNN4	2.56	5.64E-05	0.043
PGM5P2	2.19	5.66E-05	0.043
HACL1	2.23	5.71E-05	0.043
SIRPB1	2.02	6.04E-05	0.0448
PXDN	3.55	6.42E-05	0.0463
GPX1	2.55	6.49E-05	0.0463
CADM4	2.1	6.52E-05	0.0463
ZNF860	2.01	6.95E-05	0.0481
FLT1	2.06	6.98E-05	0.0481
SAMD5	2.73	7.26E-05	0.049
TRIM58; OR2W3	2.82	7.52E-05	0.0497
TGFA	3.54	8.03E-05	0.0512
GLIS3	3.35	8.07E-05	0.0512
TLR4	5.99	8.17E-05	0.0512
LOC105379109	2.56	8.67E-05	0.0536
MIR548XHG	3.18	9.05E-05	0.0553
SULF1	5.03	9.23E-05	0.0556
FAM135B	2.55	9.55E-05	0.0561
SLC24A3	3.76	9.68E-05	0.0563
PTHLH	2.9	9.99E-05	0.0573
MMP2	2.04	0.0001	0.0592
ITGA3	2.24	0.0001	0.0592
SFRP1	2.3	0.0001	0.0592
PMEPA1	2.45	0.0001	0.064
DAPK1	-2.01	0.0001	0.0656
PRDM1	2.88	0.0001	0.0663
ZNF385A	2.17	0.0001	0.0681
FDCSP	6.4	0.0001	0.0697
MIR432	4.06	0.0001	0.0724
ANPEP	2.21	0.0002	0.073
EFEMP1	2.92	0.0002	0.073
FAM20C	2.23	0.0002	0.073
HSPA2	-2.4	0.0002	0.0748
ZC4H2	2.32	0.0002	0.0748
LOC105375451	2.2	0.0002	0.075
PARM1	2.57	0.0002	0.0787
MET	2.22	0.0002	0.0809
CHAC1	-2.77	0.0002	0.083
MUC13	2.98	0.0002	0.083
MAB21L1; MIR548F5	2.67	0.0002	0.083
PLXNA2	2.11	0.0002	0.083
LOC105376382	3.24	0.0002	0.0857
MYO10	-2.22	0.0002	0.0857
MIR708	2.02	0.0002	0.0857
DEPDC7	2.57	0.0002	0.0857
FAM105A	5.69	0.0002	0.0857
SCML1	-2.43	0.0003	0.0884

ESM1	3.53	0.0003	0.0884
LINC01433	-2.08	0.0003	0.0885
PTGS2	2.74	0.0003	0.091
LAMA1	-2.4	0.0003	0.091
MGAM2	2.03	0.0003	0.091
TSHZ3	2.12	0.0003	0.0919
SNORD114-28	3.37	0.0003	0.0925
GRAMD1B	2.33	0.0003	0.0946
CADPS	2.46	0.0003	0.0994
SLIT2	3.35	0.0003	0.0994
SEL1L3	2.49	0.0004	0.1016
COL9A3	2.11	0.0004	0.1083
IKZF2	2.7	0.0004	0.1083
RTL1	5	0.0004	0.1105
LCTL	3.89	0.0004	0.1116
BCAR3	2.01	0.0004	0.1166
TGFA-IT1	3.58	0.0004	0.1167
PLAUR	2.4	0.0004	0.1167
KDR	2.41	0.0004	0.1171
ELL2	2.55	0.0005	0.1191
FLRT2	2.19	0.0005	0.1191
OSBPL10	2.02	0.0005	0.1192
EPHB1	2.04	0.0005	0.1198
PXYLP1	2.22	0.0005	0.1203
TENM4	2.77	0.0005	0.1241
CDYL2	2.17	0.0005	0.1293
CYGB	-2.31	0.0005	0.13
LHFPL3-AS1	-3.93	0.0006	0.1319
GRAMD1B	3.93	0.0006	0.1319
DTNA	2.07	0.0006	0.1319
XYLT1	-2.57	0.0006	0.1319
IL37	3.93	0.0006	0.1327
ASTN1	2.16	0.0006	0.1327
CLU; MIR6843	2.44	0.0006	0.1332
MIR433	3.19	0.0006	0.1336
ZNF704	-2.35	0.0006	0.1336
LOC105374003	2.4	0.0007	0.1406
RASSF3	-2.06	0.0007	0.1407
SLAMF9	3.23	0.0007	0.1422
FLRT3	2.54	0.0007	0.1422
FAM19A3	3.96	0.0007	0.1477
SPATS1	-2.4	0.0007	0.1477
MYOZ2	2.02	0.0008	0.1485
SH3PXD2A	2.29	0.0008	0.1504
MIR127	3.83	0.0008	0.1504
GALM	-2.26	0.0009	0.1578
MIR136	5.48	0.0009	0.1578
TRIM63	-3.92	0.0009	0.158
CXCL8	4.12	0.0009	0.1598
KIAA0040	2	0.0009	0.1605
TMEM171	2.24	0.001	0.1613
LOC100506257	2.05	0.001	0.1613
KDELC1	2.66	0.001	0.1716
P2RX7	-2.09	0.0011	0.1732



PDE8B	2.12	0.0011	0.1773
LOC105376617	2.14	0.0011	0.1788
TIAM2	2.65	0.0011	0.1788
ABI3BP	3.41	0.0012	0.1788
PDE5A	2.27	0.0012	0.1828
SPP1	-2.6	0.0012	0.1831
DKK1	2.42	0.0012	0.1836
MRGPRX3	2.13	0.0013	0.1849
LOC105369559	2.7	0.0013	0.1873
SYTL5	2.18	0.0013	0.1897
INHBA	5.57	0.0014	0.19
NRG1	4.49	0.0014	0.19
SULT1B1	6.44	0.0014	0.1923
LOC102724542	2.23	0.0014	0.1927
LINC00410	-2.18	0.0017	0.209
STRIP2	-2.01	0.0017	0.213
ANKH	2.31	0.0018	0.2152
TAC1	2.45	0.0018	0.2163
KCNE4	2.03	0.0018	0.2183
ERO1B	2.2	0.0019	0.2209
MIR548O2	-2	0.0019	0.2209
IGFBP5	5.27	0.002	0.2287
BIRC3	4.81	0.0021	0.2287
PRDM7	-3.26	0.0021	0.2321
Mar-02	2.02	0.0022	0.2332
ZP4	2.22	0.0023	0.2408
XAGE3	-2.89	0.0024	0.2494
DCT	-2.61	0.0024	0.2509
EHF	3.24	0.0027	0.2643
VGf	-2.25	0.0028	0.2669
SRPX2	2.17	0.0028	0.2671
RUNX1T1	2.93	0.0029	0.2706
TMEM47	3.56	0.0029	0.2714
MGAM2	3.11	0.003	0.2761
RAB17	-2.03	0.0031	0.2801
CA14	-2.53	0.0034	0.2883
KIAA1644	2.08	0.0035	0.2919
SERPINB7	2.04	0.0035	0.2934
SNORD70	2.12	0.0036	0.296
CACNA2D3	2.48	0.0036	0.2977
LINC01186	2.3	0.0036	0.2977
GHR	-2.04	0.0036	0.2977
SSX2B; SSX2	2.44	0.0037	0.2977
SSX2B; SSX2	2.44	0.0037	0.2977
MIR431	6.62	0.0038	0.3037
GPM6B	-2.88	0.0039	0.3069
LOC105376425	-2.78	0.0039	0.3069
SEMA5A	-2.38	0.0043	0.3232
KRTAP2-3	3.27	0.0046	0.3328
LRIG3	2.16	0.0053	0.3506
TXNIP	-2.12	0.0056	0.3551
SNORD1B	-2.24	0.0062	0.3686
GMCL1	-2.01	0.0063	0.3699
KCNN2	-2.85	0.0063	0.3705

TDRD7	-2.06	0.0063	0.3707
RORB	2.22	0.0065	0.3749
PCDH7	-2.47	0.0069	0.3839
MIR4500	2.46	0.0074	0.3986
TTYH2	-2.49	0.0074	0.3986
LOC105372845; LOC105378172	-2.08	0.0075	0.3987
CTLA4	2.41	0.0081	0.4106
ACPP	3.07	0.0082	0.4112
NID1	2.17	0.0083	0.4144
GABRG3	2.32	0.0083	0.4147
BEST1	-2.07	0.009	0.4297
VAT1L	4.18	0.0092	0.4346
DPYD	2.12	0.0097	0.4426
FAM21C	-2.24	0.01	0.4442
CXCL14	6.23	0.0102	0.4477
MIR221	2.64	0.0102	0.4482
LOC105377747; LOC105379684	-2.58	0.0102	0.4484
CASC21	2.12	0.012	0.4724
ALS2CR12	-2.44	0.0121	0.4751
SERTAD4	2.02	0.0124	0.4757
HAPLN1	2.54	0.0125	0.4772
CCL2	3.4	0.013	0.4834
TRPM1	-2.95	0.0133	0.486
FGF14	2.02	0.0135	0.4892
BANCR	-3.46	0.0149	0.5095
RAB38	-2	0.0153	0.5109
CDH13	2.28	0.0154	0.512
SNORD115-45	-2.04	0.0156	0.5146
MAP3K14	2.29	0.0159	0.517
IL7R	3.29	0.0168	0.5238
CHRNA6	-3.45	0.0169	0.5239
MIR548X	3.03	0.0179	0.5309
LINC01372	-2.01	0.0184	0.5365
DIRC3-AS1	4.83	0.0188	0.5394
B3GALT2	2.29	0.0191	0.5434
PLA1A	-2.97	0.0193	0.5458
TBC1D7	-3.29	0.0201	0.5538
NF2	2.58	0.0203	0.5538
LINC00383	3.68	0.0204	0.5538
MIR544A	2.23	0.0205	0.5548
SLC24A5	-3.04	0.0211	0.5586
NAV3	-2.33	0.0214	0.5592
CAPN3	-3.87	0.0216	0.5596
ADAM19	2.41	0.022	0.5619
MGAM2	2.21	0.0221	0.5627
LOC105373730	-2.03	0.0234	0.5683
COL12A1	2.39	0.0249	0.5775
CTGF	2.77	0.0254	0.58
MIR873	2.42	0.0309	0.599
PLEKHH1	-2.29	0.0313	0.6009
LCE1F	2.16	0.0318	0.6024
TNFRSF12A	2.95	0.0336	0.6117

PKNOX2	-2.15	0.0337	0.6121
MIR222	2.97	0.035	0.6144
GNG11	2.07	0.0378	0.6266
LOC105376694	2.06	0.0381	0.6266
LINC00707	4.49	0.0397	0.6327
LINC01419	2.78	0.0397	0.6327
SEMA3B	2.44	0.0399	0.6336
GYG2	-2.29	0.0416	0.6379
FAM167B	-3.51	0.0478	0.6534

**Appendix 3: Ambra binding partners identified in this study, by BioPlex data bases and reported in literature.**

Ambra1 binding partner	Reference
ANK3	This study
ANKRD7	This study
AGO3	This study
STX7	This study
TMED7	This study
DSTN	This study
DDB1	Antonioli et al., 2014
TRIM32	Rienzo et al., 2019
TRAF6	Nazio et al., 2013
DLC1	Di Bartolomeo et al., 2010
BECN1	Fimia et al., 2007
BCL2	Strappazon et al., 2011
LC3	Strappazon et al., 2015
PP2CA	Cianfanelli et al., 2015
SPSB2	BioPlexHCT_1_0
RAB40C	BioPlexHCT_1_0
FEM1A	BioPlex_3_0, BioPlexHCT_1_0
RNF187	BioPlex_3_0
DYNLL2	BioPlex_3_0
DYNLL2	BioPlex_3_0
RFPL4B	BioPlex_3_0, BioPlexHCT_1_0
WSB2	BioPlex_3_0, BioPlexHCT_1_0
WSB2	BioPlex_3_0
LRRC28	BioPlex_3_0
LRRC28	BioPlex_3_0
SOCS3	BioPlex_3_0, BioPlexHCT_1_0
RAB40A	BioPlexHCT_1_0
HPS1	BioPlex_3_0, BioPlexHCT_1_0
SOCS1	BioPlex_3_0
SPSB4	BioPlex_3_0, BioPlexHCT_1_0
PPP4C	BioPlex_3_0
CISH	BioPlex_3_0, BioPlexHCT_1_0
PLSCR5	BioPlex_3_0
DQX1	BioPlex_3_0
NEK9	BioPlex_3_0
TEX19	BioPlex_3_0, BioPlexHCT_1_0
S100P	BioPlex_3_0
ASB8	BioPlex_3_0, BioPlexHCT_1_0
PRAMEF17	BioPlexHCT_1_0
PPP4R1L	BioPlex_3_0
ANKRD9	BioPlex_3_0, BioPlexHCT_1_0
LRRC42	BioPlexHCT_1_0

GTF2H3	BioPlex_3_0
ASB6	BioPlexHCT_1_0
ATG7	BioPlexHCT_1_0
ASB13	BioPlexHCT_1_0
ASB2	BioPlex_3_0
PRKAG3	BioPlexHCT_1_0
NSUN5P1	BioPlexHCT_1_0
AARSD1	BioPlex_3_0
COPS8	BioPlexHCT_1_0
BCL2L12	BioPlexHCT_1_0
KLHDC2	BioPlex_3_0
WDR83	BioPlexHCT_1_0
HSPA8	BioPlex_3_0

## ***Chapter 9- References***

- Abdullah, C., Wang, X., and Becker, D. (2011). Expression analysis and molecular targeting of cyclin-dependent kinases in advanced melanoma. *Cell Cycle* 10, 977–988.
- Aita, V.M., Liang, X.H., Murty, V.V.V.S., Pincus, D.L., Yu, W., Cayanis, E., Kalachikov, S., Gilliam, T.C., and Levine, B. (1999). Cloning and Genomic Organization of Beclin 1, a Candidate Tumor Suppressor Gene on Chromosome 17q21. *Genomics* 59, 59–65.
- Alto, L.T., and Terman, J.R. (2017). Semaphorins and their Signaling Mechanisms. *Methods Mol Biol* 1493, 1–25.
- Antonoli, M., Albiero, F., Nazio, F., Vescovo, T., Perdomo, A.B., Corazzari, M., Marsella, C., Piselli, P., Gretzmeier, C., Dengjel, J., et al. (2014). AMBRA1 Interplay with Cullin E3 Ubiquitin Ligases Regulates Autophagy Dynamics. *Developmental Cell* 31, 734–746.
- Aretz, I., and Meierhofer, D. (2016). Advantages and pitfalls of mass spectrometry based metabolome profiling in systems biology. *International Journal of Molecular Sciences* 17, 632.
- Armstrong, J.L., Hill, D.S., McKee, C.S., Hernandez-Tiedra, S., Lorente, M., Lopez-Valero, I., Eleni Anagnostou, M., Babatunde, F., Corazzari, M., Redfern, C.P.F., et al. (2015). Exploiting Cannabinoid-Induced Cytotoxic Autophagy to Drive Melanoma Cell Death. *Journal of Investigative Dermatology* 135, 1629–1637.
- Asem, M.S., Buechler, S., Wates, R.B., Miller, D.L., and Stack, M.S. (2016). Wnt5a Signaling in Cancer. *Cancers (Basel)* 8.
- Aslantürk, Ö. (2018). In Vitro Cytotoxicity and Cell Viability Assays: Principles, Advantages, and Disadvantages. p.
- Axe, E.L., Walker, S.A., Manifava, M., Chandra, P., Roderick, H.L., Habermann, A., Griffiths, G., and Ktistakis, N.T. (2008). Autophagosome formation from membrane compartments enriched in phosphatidylinositol 3-phosphate and dynamically connected to the endoplasmic reticulum. *J Cell Biol* 182, 685–701.
- Basu, R., Wu, S., and Kopchick, J.J. (2017). Targeting growth hormone receptor in human melanoma cells attenuates tumor progression and epithelial mesenchymal transition via suppression of multiple oncogenic pathways. *Oncotarget* 8, 21579–21598.
- Beaumont, K.A., Hamilton, N.A., Moores, M.T., Brown, D.L., Ohbayashi, N., Cairncross, O., Cook, A.L., Smith, A.G., Misaki, R., Fukuda, M., et al. (2011). The recycling endosome protein Rab17 regulates melanocytic filopodia formation and melanosome trafficking. *Traffic* 12, 627–643.
- Becher, J., Simula, L., Volpe, E., Procaccini, C., La Rocca, C., D’Acunzo, P., Cianfanelli, V., Strappazon, F., Caruana, I., Nazio, F., et al. (2018). AMBRA1 Controls Regulatory T-Cell Differentiation and Homeostasis Upstream of the FOXO3-FOXP3 Axis. *Developmental Cell* 47, 592-607.e6.
- Beer, S., Zetterberg, A., Ihrie, R.A., McTaggart, R.A., Yang, Q., Bradon, N., Arvanitis, C., Attardi, L.D., Feng, S., Ruebner, B., et al. (2004). Developmental

- Context Determines Latency of MYC-Induced Tumorigenesis. *PLOS Biology* 2, e332.
- Behrends, C., Sowa, M.E., Gygi, S.P., and Harper, J.W. (2010). Network organization of the human autophagy system. *Nature* 466, 68–76.
- Benato, F., Skobo, T., Giocchini, G., Moro, I., Ciccocanti, F., Piacentini, M., Fimia, G.M., Carnevali, O., and Dalla Valle, L. (2013). Ambra1 knockdown in zebrafish leads to incomplete development due to severe defects in organogenesis. *Autophagy* 9, 476–495.
- Beroukhi, R., Mermel, C.H., Porter, D., Wei, G., Raychaudhuri, S., Donovan, J., Barretina, J., Boehm, J.S., Dobson, J., Urashima, M., et al. (2010). The landscape of somatic copy-number alteration across human cancers. *Nature* 463, 899–905.
- Bludau, I., and Aebersold, R. (2020). Proteomic and interactomic insights into the molecular basis of cell functional diversity. *Nature Reviews Molecular Cell Biology*.
- Boissy, R.E. (2003). Melanosome transfer to and translocation in the keratinocyte. *Experimental Dermatology* 12, 5–12.
- Bonaventure, J., Domingues, M.J., and Larue, L. (2013). Cellular and molecular mechanisms controlling the migration of melanocytes and melanoma cells. *Pigment Cell & Melanoma Research* 26, 316–325.
- Bosserhoff, A.K., Ellmann, L., Quast, A.S., Eberle, J., Boyle, G.M., and Kuphal, S. (2014). Loss of T-cadherin (CDH-13) regulates AKT signaling and desensitizes cells to apoptosis in melanoma. *Molecular Carcinogenesis* 53, 635–647.
- Botti-Millet, J., Nascimbeni, A.C., Dupont, N., Morel, E., and Codogno, P. (2016). Fine-tuning autophagy: from transcriptional to posttranslational regulation. *American Journal of Physiology-Cell Physiology* 311, C351–C362.
- Boya, P., Reggiori, F., and Codogno, P. (2013). Emerging regulation and functions of autophagy. *Nature Cell Biology* 15, 713.
- Broustas, C.G., and Lieberman, H.B. (2014). DNA Damage Response Genes and the Development of Cancer Metastasis. *Radiation Research* 181, 111–130.
- Brückner, A., Polge, C., Lentze, N., Auerbach, D., and Schlattner, U. (2009). Yeast Two-Hybrid, a Powerful Tool for Systems Biology. *International Journal of Molecular Sciences* 10, 2763–2788.
- Burgess, K., Rankin, N., and Weidt, S. (2014). Chapter 10 - Metabolomics. In *Handbook of Pharmacogenomics and Stratified Medicine*, S. Padmanabhan, ed. (San Diego: Academic Press), pp. 181–205.
- Cai, Z., Chiu, J.-F., and He, Q.-Y. (2004). Application of Proteomics in the Study of Tumor Metastasis. *Genomics, Proteomics & Bioinformatics* 2, 152–166.
- Cancer Research UK (2015). Melanoma skin cancer statistics.
- Capparuccia, L., and Tamagnone, L. (2009). Semaphorin signaling in cancer cells and in cells of the tumor microenvironment – two sides of a coin. *J. Cell Sci.* 122, 1723.



- Cappellen, D., Schlange, T., Bauer, M., Maurer, F., and Hynes, N.E. (2007). Novel c-MYC target genes mediate differential effects on cell proliferation and migration. *EMBO Rep* 8, 70–76.
- Carmeliet, P. (2005). VEGF as a key mediator of angiogenesis in cancer. *Oncology* 69 Suppl 3, 4–10.
- CHAFFEY, N. (2003). Alberts, B., Johnson, A., Lewis, J., Raff, M., Roberts, K. and Walter, P. *Molecular biology of the cell*. 4th edn. Ann Bot 91, 401.
- Chakraborty, G., Kumar, S., Mishra, R., Patil, T.V., and Kundu, G.C. (2012). Semaphorin 3A Suppresses Tumor Growth and Metastasis in Mice Melanoma Model. *PLoS One* 7.
- Chandramouli, K., and Qian, P.-Y. (2009). Proteomics: challenges, techniques and possibilities to overcome biological sample complexity. *Hum Genomics Proteomics* 2009, 239204.
- Chang, E., Ge, B., Lee, M., So, M., and Wang, W. (2005). Investigation of the Ligation Efficiency of NdeI Digested Fragments. 7, 5.
- Chen, H.-Z., Tsai, S.-Y., and Leone, G. (2009). Emerging roles of E2Fs in cancer: an exit from cell cycle control. *Nat Rev Cancer* 9, 785–797.
- Chen, Y., Samaraweera, P., Sun, T.-T., Kreibich, G., and Orlow, S.J. (2002). Rab27b Association with Melanosomes: Dominant Negative Mutants Disrupt Melanosomal Movement. *Journal of Investigative Dermatology* 118, 933–940.
- Cheng, L., Lopez-Beltran, A., Massari, F., MacLennan, G.T., and Montironi, R. (2018). Molecular testing for BRAF mutations to inform melanoma treatment decisions: a move toward precision medicine. *Mod Pathol* 31, 24–38.
- Chien, C.T., Bartel, P.L., Sternglanz, R., and Fields, S. (1991). The two-hybrid system: a method to identify and clone genes for proteins that interact with a protein of interest. *Proc Natl Acad Sci U S A* 88, 9578–9582.
- Chin, L., Merlino, G., and DePinho, R.A. (1998). Malignant melanoma: modern black plague and genetic black box. *Genes & Development* 12, 3467–3481.
- Cianfanelli, V., De Zio, D., Di Bartolomeo, S., Nazio, F., Strappazzon, F., and Cecconi, F. (2015a). Ambra1 at a glance. *J. Cell Sci.* 128, 2003.
- Cianfanelli, V., Fuoco, C., Lorente, M., Salazar, M., Quondamatteo, F., Gherardini, P.F., De Zio, D., Nazio, F., Antonioli, M., D’Orazio, M., et al. (2015b). AMBRA1 links autophagy to cell proliferation and tumorigenesis by promoting c-MYC dephosphorylation and degradation. *Nat Cell Biol* 17, 20–30.
- Cianfanelli, V., Nazio, F., and Cecconi, F. (2015c). Connecting autophagy: AMBRA1 and its network of regulation. *Mol Cell Oncol* 2.
- Cichorek, M., Wachulska, M., Stasiewicz, A., and Tymińska, A. (2013). Skin melanocytes: biology and development. *Postepy Dermatol Alergol* 30, 30–41.
- Conacci-Sorrell, M., McFerrin, L., and Eisenman, R.N. (2014). An overview of MYC and its interactome. *Cold Spring Harb Perspect Med* 4, a014357–a014357.

- Csizmok, V., Follis, A.V., Kriwacki, R.W., and Forman-Kay, J.D. (2016). Dynamic Protein Interaction Networks and New Structural Paradigms in Signaling. *Chem Rev* 116, 6424–6462.
- Dang, C.V. (2012). MYC on the Path to Cancer. *Cell* 149, 22–35.
- Daste, F., Galli, T., and Tareste, D. (2015). Structure and function of longin SNAREs. *Journal of Cell Science* 128, 4263–4272.
- Davies, H., Bignell, G.R., Cox, C., Stephens, P., Edkins, S., Clegg, S., Teague, J., Woffendin, H., Garnett, M.J., Bottomley, W., et al. (2002). Mutations of the BRAF gene in human cancer. *Nature* 417, 949–954.
- Dere, E., Dahm, L., Lu, D., Hammerschmidt, K., Ju, A., Tantra, M., Kästner, A., Chowdhury, K., and Ehrenreich, H. (2014). Heterozygous ambra1 deficiency in mice: a genetic trait with autism-like behavior restricted to the female gender. *Front Behav Neurosci* 8, 181–181.
- Dergham, S.T., Dugan, M.C., Kucway, R., Du, W., Kamarauskiene, D.S., Vaitkevicius, V.K., Crissman, J.D., and Sarkar, F.H. (1997). Prevalence and clinical significance of combined K-ras mutation and p53 aberration in pancreatic adenocarcinoma. *Int. J. Pancreatol.* 21, 127–143.
- Dhillon, A.S., Hagan, S., Rath, O., and Kolch, W. (2007). MAP kinase signalling pathways in cancer. *Oncogene* 26, 3279–3290.
- Di Bartolomeo, S., Corazzari, M., Nazio, F., Oliverio, S., Lisi, G., Antonioli, M., Pagliarini, V., Matteoni, S., Fuoco, C., Giunta, L., et al. (2010). The dynamic interaction of AMBRA1 with the dynein motor complex regulates mammalian autophagy. *J Cell Biol* 191, 155–168.
- Di Rita, A., Peschiaroli, A., D'Acunzo, P., Strobbe, D., Hu, Z., Gruber, J., Nygaard, M., Lambrugh, M., Melino, G., Papaleo, E., et al. (2018). HUWE1 E3 ligase promotes PINK1/PARKIN-independent mitophagy by regulating AMBRA1 activation via IKK $\alpha$ . *Nature Communications* 9, 3755.
- Dimova, D.K., and Dyson, N.J. (2005). The E2F transcriptional network: old acquaintances with new faces. *Oncogene* 24, 2810–2826.
- Ding, W.-X., and Yin, X.-M. (2012). Mitophagy: mechanisms, pathophysiological roles, and analysis. *Biol Chem* 393, 547–564.
- Domingues, B., Lopes, J.M., Soares, P., and Pópulo, H. (2018). Melanoma treatment in review. *Immunotargets Ther* 7, 35–49.
- Downward, J. (2003). Targeting RAS signalling pathways in cancer therapy. *Nature Reviews Cancer* 3, 11–22.
- Doyle, S.L., Husebye, H., Connolly, D.J., Espevik, T., O'Neill, L.A.J., and McGettrick, A.F. (2012). The GOLD domain-containing protein TMED7 inhibits TLR4 signalling from the endosome upon LPS stimulation. *Nature Communications* 3, 707.
- Durak, O., de Anda, F.C., Singh, K.K., Leussis, M.P., Petryshen, T.L., Sklar, P., and Tsai, L.-H. (2015). Ankyrin-G regulates neurogenesis and Wnt signaling by altering the subcellular localization of  $\beta$ -catenin. *Mol Psychiatry* 20, 388–397.

- Duronio, R.J., and Xiong, Y. (2013). Signaling Pathways that Control Cell Proliferation. *Cold Spring Harb Perspect Biol* 5.
- El-Deiry, W.S., Tokino, T., Velculescu, V.E., Levy, D.B., Parsons, R., Trent, J.M., Lin, D., Mercer, W.E., Kinzler, K.W., and Vogelstein, B. (1993). WAF1, a potential mediator of p53 tumor suppression. *Cell* 75, 817–825.
- Elledge, S.J., and Harper, J.W. (1994). Cdk inhibitors: on the threshold of checkpoints and development. *Current Opinion in Cell Biology* 6, 847–852.
- Ellis, R., Tang, D., Nasr, B., Greenwood, A., McConnell, A., Anagnostou, M.E., Elias, M., Verykiou, S., Bajwa, D., Ewen, T., et al. (2019). Epidermal autophagy and beclin 1 regulator 1 and loricrin: a paradigm shift in the prognostication and stratification of the American Joint Committee on Cancer stage I melanomas. *Br. J. Dermatol.*
- Elmore, S. (2007). Apoptosis: a review of programmed cell death. *Toxicol Pathol* 35, 495–516.
- Ender, C., and Meister, G. (2010). Argonaute proteins at a glance. *J. Cell Sci.* 123, 1819.
- Felix, C.C., Hyde, J.S., Sarna, T., and Sealy, R.C. (1978). Interactions of melanin with metal ions. Electron spin resonance evidence for chelate complexes of metal ions with free radicals. *J. Am. Chem. Soc.* 100, 3922–3926.
- Fimia, G.M., Stoykova, A., Romagnoli, A., Giunta, L., Di Bartolomeo, S., Nardacci, R., Corazzari, M., Fuoco, C., Ucar, A., Schwartz, P., et al. (2007). Ambra1 regulates autophagy and development of the nervous system. *Nature* 447, 1121–1125.
- Fimia, G.M., Corazzari, M., Antonioli, M., and Piacentini, M. (2013). Ambra1 at the crossroad between autophagy and cell death. *Oncogene* 32, 3311–3318.
- Galluzzi, L., Pietrocola, F., Bravo-San Pedro, J.M., Amaravadi, R.K., Baehrecke, E.H., Cecconi, F., Codogno, P., Debnath, J., Gewirtz, D.A., Karantza, V., et al. (2015). Autophagy in malignant transformation and cancer progression. *EMBO J* 34, 856–880.
- Garber, K. (2011). Inducing Indigestion: Companies Embrace Autophagy Inhibitors. *JNCI: Journal of the National Cancer Institute* 103, 708–710.
- Ghosh, R., Gilda, J.E., and Gomes, A.V. (2014). The necessity of and strategies for improving confidence in the accuracy of western blots. *Expert Rev Proteomics* 11, 549–560.
- Glick, D., Barth, S., and Macleod, K.F. (2010). Autophagy: cellular and molecular mechanisms. *J Pathol* 221, 3–12.
- Gordan, J.D., Thompson, C.B., and Simon, M.C. (2007). HIF and c-Myc: sibling rivals for control of cancer cell metabolism and proliferation. *Cancer Cell* 12, 108–113.
- Govindarajan, R., Duraiyan, J., Kaliyappan, K., and Palanisamy, M. (2012). Microarray and its applications. *J Pharm Bioallied Sci* 4, S310–S312.

Gowda, G.A.N., Zhang, S., Gu, H., Asiago, V., Shanaiah, N., and Raftery, D. (2008). Metabolomics-based methods for early disease diagnostics. *Expert Rev Mol Diagn* 8, 617–633.

Graef, M., Friedman, J.R., Graham, C., Babu, M., and Nunnari, J. (2013). ER exit sites are physical and functional core autophagosome biogenesis components. *Mol Biol Cell* 24, 2918–2931.

Gu, W., Wan, D., Qian, Q., Yi, B., He, Z., Gu, Y., Wang, L., and He, S. (2014). Ambra1 Is an Essential Regulator of Autophagy and Apoptosis in SW620 Cells: Pro-Survival Role of Ambra1. *PLOS ONE* 9, e90151.

Haass, N.K., and Herlyn, M. (2005). Normal Human Melanocyte Homeostasis as a Paradigm for Understanding Melanoma. *Journal of Investigative Dermatology Symposium Proceedings* 10, 153–163.

Hafner, A., Bulyk, M.L., Jambhekar, A., and Lahav, G. (2019). The multiple mechanisms that regulate p53 activity and cell fate. *Nature Reviews Molecular Cell Biology* 20, 199–210.

Hailey, D.W., Rambold, A.S., Satpute-Krishnan, P., Mitra, K., Sougrat, R., Kim, P.K., and Lippincott-Schwartz, J. (2010). Mitochondria supply membranes for autophagosome biogenesis during starvation. *Cell* 141, 656–667.

Hall, M., and Peters, G. (1996). Genetic Alterations of Cyclins, Cyclin-Dependent Kinases, and Cdk Inhibitors in Human Cancer. In *Advances in Cancer Research*, G.F. Vande Woude, and G. Klein, eds. (Academic Press), pp. 67–108.

Hamasaki, M., Furuta, N., Matsuda, A., Nezu, A., Yamamoto, A., Fujita, N., Oomori, H., Noda, T., Haraguchi, T., Hiraoka, Y., et al. (2013). Autophagosomes form at ER–mitochondria contact sites. *Nature* 495, 389.

Hannink, M., and Donoghue, D.J. (1989). Structure and function of platelet-derived growth factor (PDGF) and related proteins. *Biochim. Biophys. Acta* 989, 1–10.

Hara, T., Takamura, A., Kishi, C., Iemura, S.-I., Natsume, T., Guan, J.-L., and Mizushima, N. (2008). FIP200, a ULK-interacting protein, is required for autophagosome formation in mammalian cells. *J Cell Biol* 181, 497–510.

Hartman, M.L., and Czyz, M. (2015). MITF in melanoma: mechanisms behind its expression and activity. *Cell. Mol. Life Sci.* 72, 1249–1260.

He, R.-Q., Xiong, D.-D., Ma, J., Hu, X.-H., Chen, G., and Sun, W.-L. (2018). The Clinicopathological Significance and Correlative Signaling Pathways of an Autophagy-Related Gene, Ambra1, in Breast Cancer: a Study of 25 Microarray RNA-Seq Datasets and in-House Gene Silencing. *Cell. Physiol. Biochem.* 51, 1027–1040.

Heichman, K.A., and Roberts, J.M. (1994). Rules to replicate by. *Cell* 79, 557–562.

Hinds, P.W., Mittnacht, S., Dulic, V., Arnold, A., Reed, S.I., and Weinberg, R.A. (1992). Regulation of retinoblastoma protein functions by ectopic expression of human cyclins. *Cell* 70, 993–1006.

- Hong, W. (2005). SNAREs and traffic. *Biochimica et Biophysica Acta (BBA) - Molecular Cell Research* 1744, 120–144.
- Hosokawa, N., Hara, T., Kaizuka, T., Kishi, C., Takamura, A., Miura, Y., Iemura, S., Natsume, T., Takehana, K., Yamada, N., et al. (2009). Nutrient-dependent mTORC1 association with the ULK1-Atg13-FIP200 complex required for autophagy. *Mol Biol Cell* 20, 1981–1991.
- Hsu, C.-Y., Bristow, R., Cha, M.S., Wang, B.G., Ho, C.-L., Kurman, R.J., Wang, T.-L., and Shih, I.-M. (2004). Characterization of Active Mitogen-Activated Protein Kinase in Ovarian Serous Carcinomas. *Clin Cancer Res* 10, 6432.
- Hu, Q., Tanasa, B., Trabucchi, M., Li, W., Zhang, J., Ohgi, K.A., Rose, D.W., Glass, C.K., and Rosenfeld, M.G. (2012). DICER- and AGO3-dependent generation of retinoic acid-induced DR2 Alu RNAs regulates human stem cell proliferation. *Nat Struct Mol Biol* 19, 1168–1175.
- Hulstaert, E., Brochez, L., Volders, P.-J., Vandesompele, J., and Mestdagh, P. (2017). Long non-coding RNAs in cutaneous melanoma: clinical perspectives. *Oncotarget* 8, 43470–43480.
- Huttlin, E.L., Ting, L., Bruckner, R.J., Gebreab, F., Gygi, M.P., Szpyt, J., Tam, S., Zarraga, G., Colby, G., Baltier, K., et al. (2015). The BioPlex Network: A Systematic Exploration of the Human Interactome. *Cell* 162, 425–440.
- Jäger, D., Stockert, E., Jäger, E., Güre, A.O., Scanlan, M.J., Knuth, A., Old, L.J., and Chen, Y.-T. (2000). Serological Cloning of a Melanocyte rab Guanosine 5'-Triphosphate-binding Protein and a Chromosome Condensation Protein from a Melanoma Complementary DNA Library. *Cancer Res* 60, 3584–3591.
- Jaiswal, B.S., Durinck, S., Stawiski, E.W., Yin, J., Wang, W., Lin, E., Moffat, J., Martin, S.E., Modrusan, Z., and Seshagiri, S. (2018). ERK Mutations and Amplification Confer Resistance to ERK-Inhibitor Therapy. *Clin. Cancer Res.* 24, 4044–4055.
- Jung, V., Pestka, S.B., and Pestka, S. (1990). Efficient cloning of PCR generated DNA containing terminal restriction endonuclease recognition sites. *Nucleic Acids Research* 18, 6156–6156.
- Kabeya, Y., Mizushima, N., Ueno, T., Yamamoto, A., Kirisako, T., Noda, T., Kominami, E., Ohsumi, Y., and Yoshimori, T. (2000). LC3, a mammalian homologue of yeast Apg8p, is localized in autophagosome membranes after processing. *EMBO J* 19, 5720–5728.
- Kang, R., Zeh, H.J., Lotze, M.T., and Tang, D. (2011). The Beclin 1 network regulates autophagy and apoptosis. *Cell Death Differ* 18, 571–580.
- Kapoor, R.V., Coyle, R., Staton, C.A., Brown, N.J., and Vaidyanathan, S. (2017). Influence of washing and quenching in profiling the metabolome of adherent mammalian cells: a case study with the metastatic breast cancer cell line MDA-MB-231. *Analyst* 142, 2038–2049.
- Karbowniczek, M., Spittle, C.S., Morrison, T., Wu, H., and Henske, E.P. (2008). mTOR is activated in the majority of malignant melanomas. *J. Invest. Dermatol.* 128, 980–987.

- Karimkhani, C., Green, A.C., Nijsten, T., Weinstock, M.A., Dellavalle, R.P., Naghavi, M., and Fitzmaurice, C. (2017). The global burden of melanoma: results from the Global Burden of Disease Study 2015. *Br J Dermatol* 177, 134–140.
- Karunakaran, S., Sasser, T., Rajalekshmi, S., and Fratti, R.A. (2012). SNAREs, HOPS and regulatory lipids control the dynamics of vacuolar actin during homotypic fusion in *S. cerevisiae*. *J. Cell Sci.* 125, 1683.
- Kaufman, C.K., Mosimann, C., Fan, Z.P., Yang, S., Thomas, A.J., Ablain, J., Tan, J.L., Fogley, R.D., van Rooijen, E., Hagedorn, E.J., et al. (2016). A zebrafish melanoma model reveals emergence of neural crest identity during melanoma initiation. *Science* 351, aad2197–aad2197.
- Kaur, A., Webster, M.R., and Weeraratna, A.T. (2016). In the Wnt-er of life: Wnt signalling in melanoma and ageing. *Br J Cancer* 115, 1273–1279.
- Kaushik, A.K., and DeBerardinis, R.J. (2018). Applications of metabolomics to study cancer metabolism. *Biochim Biophys Acta Rev Cancer* 1870, 2–14.
- Keegan, L., Gill, G., and Ptashne, M. (1986). Separation of DNA binding from the transcription-activating function of a eukaryotic regulatory protein. *Science* 231, 699.
- Kelly, K., Cochran, B.H., Stiles, C.D., and Leder, P. (1983). Cell-specific regulation of the c-myc gene by lymphocyte mitogens and platelet-derived growth factor. *Cell* 35, 603–610.
- Khan, K.H., Yap, T.A., Yan, L., and Cunningham, D. (2013). Targeting the PI3K-AKT-mTOR signaling network in cancer. *Chin J Cancer* 32, 253–265.
- Kimura, T., Takabatake, Y., Takahashi, A., and Isaka, Y. (2013). Chloroquine in Cancer Therapy: A Double-Edged Sword of Autophagy. *Cancer Res* 73, 3.
- Kirchmaier, S., Lust, K., and Wittbrodt, J. (2013). Golden GATEway Cloning – A Combinatorial Approach to Generate Fusion and Recombination Constructs. *PLOS ONE* 8, e76117.
- Knudsen, E.S., and Wang, J.Y.J. (2010). Targeting the RB-pathway in Cancer Therapy. *Clin Cancer Res* 16, 1094.
- Ko, Y.H., Cho, Y.-S., Won, H.S., Jeon, E.K., An, H.J., Hong, S.U., Park, J.H., and Lee, M.A. (2013). Prognostic Significance of Autophagy-Related Protein Expression in Resected Pancreatic Ductal Adenocarcinoma. *Pancreas* 42, 829.
- Koepp, D.M., Harper, J.W., and Elledge, S.J. (1999). How the Cyclin Became a Cyclin: Regulated Proteolysis in the Cell Cycle. *Cell* 97, 431–434.
- Köhler, C., Nittner, D., Rambow, F., Radaelli, E., Stanchi, F., Vandamme, N., Baggiolini, A., Sommer, L., Berx, G., van den Oord, J.J., et al. (2017). Mouse Cutaneous Melanoma Induced by Mutant BRAf Arises from Expansion and Dedifferentiation of Mature Pigmented Melanocytes. *Cell Stem Cell* 21, 679–693.e6.
- Komiya, Y., and Habas, R. (2008). Wnt signal transduction pathways. *Organogenesis* 4, 68–75.

Kormos, B., Belső, N., Bebes, A., Szabad, G., Bacsa, S., Széll, M., Kemény, L., and Bata-Csörgő, Z. (2011). In Vitro Dedifferentiation of Melanocytes from Adult Epidermis. *PLOS ONE* 6, e17197.

Krantz, S.B. (1991). Erythropoietin. *Blood* 77, 419–434.

Kuphal, S., Martyn, A.C., Pedley, J., Crowther, L.M., Bonazzi, V.F., Parsons, P.G., Bosserhoff, A.K., Hayward, N.K., and Boyle, G.M. (2009). H-Cadherin expression reduces invasion of malignant melanoma. *Pigment Cell & Melanoma Research* 22, 296–306.

Kwong, L.N., and Davies, M.A. (2013). Navigating the therapeutic complexity of PI3K pathway inhibition in melanoma. *Clin. Cancer Res.* 19, 5310–5319.

Lammer, C., Wagerer, S., Saffrich, R., Mertens, D., Ansorge, W., and Hoffmann, I. (1998). The cdc25B phosphatase is essential for the G2/M phase transition in human cells. *Journal of Cell Science* 111, 2445–2453.

Laplante, M., and Sabatini, D.M. (2009). mTOR signaling at a glance. *J Cell Sci* 122, 3589–3594.

Larsen, M.R., Trelle, M.B., Thingholm, T.E., and Jensen, O.N. (2006). Analysis of posttranslational modifications of proteins by tandem mass spectrometry. *BioTechniques* 40, 790–798.

Leterrier, C., Clerc, N., Rueda-Boroni, F., Montersino, A., Dargent, B., and Castets, F. (2017). Ankyrin G Membrane Partners Drive the Establishment and Maintenance of the Axon Initial Segment. *Frontiers in Cellular Neuroscience* 11, 6.

Levine, B., and Abrams, J. (2008). p53: The Janus of autophagy? *Nat Cell Biol* 10, 637–639.

Li, R., Zhang, L., Jia, L., Duan, Y., Li, Y., Bao, L., and Sha, N. (2014). Long Non-Coding RNA BANC1 Promotes Proliferation in Malignant Melanoma by Regulating MAPK Pathway Activation. *PLoS One* 9.

Liang, X.H., Jackson, S., Seaman, M., Brown, K., Kempkes, B., Hibshoosh, H., and Levine, B. (1999). Induction of autophagy and inhibition of tumorigenesis by beclin 1. *Nature* 402, 672–676.

Link, A.J., and LaBaer, J. (2011). Trichloroacetic Acid (TCA) Precipitation of Proteins. *Cold Spring Harbor Protocols* 2011, pdb.prot5651.

Liu, J., Chen, Z., Guo, J., Wang, L., and Liu, X. (2019). Ambra1 induces autophagy and desensitizes human prostate cancer cells to cisplatin. *Bioscience Reports* 39.

Logan, C.Y., and Nusse, R. (2004). THE WNT SIGNALING PATHWAY IN DEVELOPMENT AND DISEASE. *Annu. Rev. Cell Dev. Biol.* 20, 781–810.

Lowe, R., Shirley, N., Bleackley, M., Dolan, S., and Shafee, T. (2017). Transcriptomics technologies. *PLOS Computational Biology* 13, e1005457.

Lozada, E.M., Andrysiak, Z., Yin, M., Redilla, N., Rice, K., and Stambrook, P.J. (2016). Acetylation and deacetylation of Cdc25A constitutes a novel mechanism for modulating Cdc25A functions with implications for cancer. *Oncotarget* 7, 20425–20439.

Ma, X.-H., Piao, S.-F., Dey, S., McAfee, Q., Karakousis, G., Villanueva, J., Hart, L.S., Levi, S., Hu, J., Zhang, G., et al. (2014). Targeting ER stress-induced autophagy overcomes BRAF inhibitor resistance in melanoma. *J Clin Invest* 124, 1406–1417.

Magdeldin, S., Enany, S., Yoshida, Y., Xu, B., Zhang, Y., Zureena, Z., Lokamani, I., Yaoita, E., and Yamamoto, T. (2014). Basics and recent advances of two dimensional- polyacrylamide gel electrophoresis. *Clin Proteomics* 11, 16–16.

Massagué, J. (2008). TGFbeta in Cancer. *Cell* 134, 215–230.

Massagué, J., Blain, S.W., and Lo, R.S. (2000). TGFβ Signaling in Growth Control, Cancer, and Heritable Disorders. *Cell* 103, 295–309.

Mathew, R., Karantza-Wadsworth, V., and White, E. (2007). Role of autophagy in cancer. *Nat Rev Cancer* 7, 961–967.

Mathiassen, S.G., De Zio, D., and Cecconi, F. (2017). Autophagy and the Cell Cycle: A Complex Landscape. *Frontiers in Oncology* 7, 51.

Matsumura, I. (2015). Why Johnny can't clone: Common pitfalls and not so common solutions. *BioTechniques* 59, IV–XIII.

McDonald, S.L., and Silver, A. (2009). The opposing roles of Wnt-5a in cancer. *Br. J. Cancer* 101, 209–214.

Mei, Y., Su, M., Soni, G., Salem, S., Colbert, C.L., and Sinha, S.C. (2014). Intrinsically disordered regions in autophagy proteins. *Proteins: Structure, Function, and Bioinformatics* 82, 565–578.

MelanomaUK STATISTICS.

Mizushima, N. (2007). Autophagy: process and function. *Genes & Development* 21, 2861–2873.

Mizushima, N., Yamamoto, A., Matsui, M., Yoshimori, T., and Ohsumi, Y. (2004). In vivo analysis of autophagy in response to nutrient starvation using transgenic mice expressing a fluorescent autophagosome marker. *Mol Biol Cell* 15, 1101–1111.

Mohler, P.J., Gramolini, A.O., and Bennett, V. (2002). Ankyrins. *J. Cell Sci.* 115, 1565.

Monastyrska, I., Rieter, E., Klionsky, D.J., and Reggiori, F. (2009). Multiple roles of the cytoskeleton in autophagy. *Biol Rev Camb Philos Soc* 84, 431–448.

Monteiro, M., Carvalho, M., Bastos, M., and Guedes de Pinho, P. (2013). Metabolomics analysis for biomarker discovery: advances and challenges. *Current Medicinal Chemistry* 20, 257–271.

Moon, H., Donahue, L.R., Choi, E., Scumpia, P.O., Lowry, W.E., Grenier, J.K., Zhu, J., and White, A.C. (2017). Melanocyte Stem Cell Activation and Translocation Initiate Cutaneous Melanoma in Response to UV Exposure. *Cell Stem Cell* 21, 665-678.e6.

Morgan, D.O. (1995). Principles of CDK regulation. *Nature* 374, 131–134.



- Mosavi, L.K., Cammett, T.J., Desrosiers, D.C., and Peng, Z.-Y. (2004). The ankyrin repeat as molecular architecture for protein recognition. *Protein Sci* 13, 1435–1448.
- Motohashi, K. (2019). A novel series of high-efficiency vectors for TA cloning and blunt-end cloning of PCR products. *Scientific Reports* 9, 1–11.
- Mullock, B.M., Smith, C.W., Ihrke, G., Bright, N.A., Lindsay, M., Parkinson, E.J., Brooks, D.A., Parton, R.G., James, D.E., Luzio, J.P., et al. (2000). Syntaxin 7 is localized to late endosome compartments, associates with Vamp 8, and is required for late endosome-lysosome fusion. *Mol Biol Cell* 11, 3137–3153.
- Mumblat, Y., Kessler, O., Ilan, N., and Neufeld, G. (2015). Full-Length Semaphorin-3C Is an Inhibitor of Tumor Lymphangiogenesis and Metastasis. *Cancer Research* 75, 2177–2186.
- Nair, U., Jotwani, A., Geng, J., Gammoh, N., Richerson, D., Yen, W.-L., Griffith, J., Nag, S., Wang, K., Moss, T., et al. (2011). SNARE proteins are required for macroautophagy. *Cell* 146, 290–302.
- Nazio, F., and Cecconi, F. (2013). mTOR, AMBRA1, and autophagy: an intricate relationship. *Cell Cycle* 12, 2524–2525.
- Nazio, F., Strappazon, F., Antonioli, M., Bielli, P., Cianfanelli, V., Bordi, M., Gretzmeier, C., Dengjel, J., Piacentini, M., Fimia, G.M., et al. (2013). mTOR inhibits autophagy by controlling ULK1 ubiquitylation, self-association and function through AMBRA1 and TRAF6. *Nature Cell Biology* 15, 406.
- Ndoye, A., and Weeraratna, A.T. (2016). Autophagy- An emerging target for melanoma therapy. *F1000Res* 5, F1000 Faculty Rev-1888.
- Neel, J.-C., Humbert, L., and Lebrun, J.-J. (2012). The Dual Role of TGF $\beta$  in Human Cancer: From Tumor Suppression to Cancer Metastasis. *ISRN Molecular Biology* 2012, 381428.
- Neufeld, T.P. (2012). Autophagy and cell growth--the yin and yang of nutrient responses. *J Cell Sci* 125, 2359–2368.
- Neufeld, G., Sabag, A.D., Rabinovicz, N., and Kessler, O. (2012). Semaphorins in Angiogenesis and Tumor Progression. *Cold Spring Harb Perspect Med* 2.
- Nevins, J. (1998). Toward an understanding of the functional complexity of the E2F and retinoblastoma families. *Cell Growth Differ* 9, 585–593.
- Nishida, N., Yano, H., Nishida, T., Kamura, T., and Kojiro, M. (2006). Angiogenesis in cancer. *Vasc Health Risk Manag* 2, 213–219.
- Nitta, T., Sato, Y., Ren, X.S., Harada, K., Sasaki, M., Hirano, S., and Nakanuma, Y. (2014). Autophagy may promote carcinoma cell invasion and correlate with poor prognosis in cholangiocarcinoma. *Int J Clin Exp Pathol* 7, 4913–4921.
- Normanno, N., De Luca, A., Bianco, C., Strizzi, L., Mancino, M., Maiello, M.R., Carotenuto, A., De Feo, G., Caponigro, F., and Salomon, D.S. (2006). Epidermal growth factor receptor (EGFR) signaling in cancer. *Gene* 366, 2–16.
- O'Farrell, P.H. (1975). High resolution two-dimensional electrophoresis of proteins. *J Biol Chem* 250, 4007–4021.

- Olayioye, M.A., Neve, R.M., Lane, H.A., and Hynes, N.E. (2000). The ErbB signaling network: receptor heterodimerization in development and cancer. *EMBO J* 19, 3159–3167.
- Orellana, E.A., and Kasinski, A.L. (2016). Sulforhodamine B (SRB) Assay in Cell Culture to Investigate Cell Proliferation. *Bio Protoc* 6, e1984.
- Osthus, R.C., Shim, H., Kim, S., Li, Q., Reddy, R., Mukherjee, M., Xu, Y., Wonsey, D., Lee, L.A., and Dang, C.V. (2000). Deregulation of Glucose Transporter 1 and Glycolytic Gene Expression by c-Myc. *J. Biol. Chem.* 275, 21797–21800.
- Pagliarini, V., Wirawan, E., Romagnoli, A., Ciccocanti, F., Lisi, G., Lippens, S., Cecconi, F., Fimia, G.M., Vandenabeele, P., Corazzari, M., et al. (2012). Proteolysis of Ambra1 during apoptosis has a role in the inhibition of the autophagic pro-survival response. *Cell Death Differ* 19, 1495–1504.
- Paluncic, J., Kovacevic, Z., Jansson, P.J., Kalinowski, D., Merlot, A.M., Huang, M.L.-H., Lok, H.C., Sahni, S., Lane, D.J.R., and Richardson, D.R. (2016). Roads to melanoma: Key pathways and emerging players in melanoma progression and oncogenic signaling. *Biochimica et Biophysica Acta (BBA) - Molecular Cell Research* 1863, 770–784.
- Pang, A.L., Clark, J., Chan, W.-Y., and Rennert, O.M. (2011). Expression of human NAA11 (ARD1B) gene is tissue-specific and is regulated by DNA methylation. *Epigenetics* 6, 1391–1399.
- Paquette, M., El-Houjeiri, L., and Pause, A. (2018). mTOR Pathways in Cancer and Autophagy. *Cancers (Basel)* 10, 18.
- Pardee, A.B. (1974). A restriction point for control of normal animal cell proliferation. *Proc Natl Acad Sci U S A* 71, 1286–1290.
- Parzych, K.R., and Klionsky, D.J. (2014). An overview of autophagy: morphology, mechanism, and regulation. *Antioxid Redox Signal* 20, 460–473.
- Perri, F., Pisconti, S., and Della Vittoria Scarpati, G. (2016). P53 mutations and cancer: a tight linkage. *Ann Transl Med* 4, 522–522.
- Polakis, P. (2012). Wnt signaling in cancer. *Cold Spring Harb Perspect Biol* 4, a008052.
- Popelka, H., and Klionsky, D.J. (2018). Structural basis for extremely strong binding affinity of giant ankyrins to LC3/GABARAP and its application in the inhibition of autophagy. *Autophagy* 14, 1847–1849.
- Puri, C., Renna, M., Bento, C.F., Moreau, K., and Rubinsztein, D.C. (2013). Diverse autophagosome membrane sources coalesce in recycling endosomes. *Cell* 154, 1285–1299.
- Qiu, T., Wang, H., Wang, Y., Zhang, Y., Hui, Q., and Tao, K. (2015). Identification of genes associated with melanoma metastasis. *The Kaohsiung Journal of Medical Sciences* 31, 553–561.
- Qu, B., Yao, L., Ma, H., Chen, H., Zhang, Z., and Xie, J. (2017). Prognostic significance of autophagy-related proteins expression in resected human gastric adenocarcinoma. *J. Huazhong Univ. Sci. Technol. [Med. Sci.]* 37, 37–43.

- Qu, X., Yu, J., Bhagat, G., Furuya, N., Hibshoosh, H., Troxel, A., Rosen, J., Eskelinen, E.-L., Mizushima, N., Ohsumi, Y., et al. (2003). Promotion of tumorigenesis by heterozygous disruption of the beclin 1 autophagy gene. *J Clin Invest* 112, 1809–1820.
- Rabilloud, T., and Lelong, C. (2011). Two-dimensional gel electrophoresis in proteomics: A tutorial. *Journal of Proteomics* 74, 1829–1841.
- Rambow, F., Job, B., Petit, V., Gesbert, F., Delmas, V., Seberg, H., Meurice, G., Van Otterloo, E., Dessen, P., Robert, C., et al. (2015). New Functional Signatures for Understanding Melanoma Biology from Tumor Cell Lineage-Specific Analysis. *Cell Rep* 13, 840–853.
- Rastogi, R.P., Richa, Kumar, A., Tyagi, M.B., and Sinha, R.P. (2010). Molecular mechanisms of ultraviolet radiation-induced DNA damage and repair. *J Nucleic Acids* 2010, 592980–592980.
- Ravikumar, B., Imarisio, S., Sarkar, S., O’Kane, C.J., and Rubinsztein, D.C. (2008). Rab5 modulates aggregation and toxicity of mutant huntingtin through macroautophagy in cell and fly models of Huntington disease. *J Cell Sci* 121, 1649–1660.
- Ravikumar, B., Futter, M., Jahreiss, L., Korolchuk, V.I., Lichtenberg, M., Luo, S., Massey, D.C.O., Menzies, F.M., Narayanan, U., Renna, M., et al. (2009). Mammalian macroautophagy at a glance. *J Cell Sci* 122, 1707–1711.
- Reimann, E., Kingo, K., Karelson, M., Reemann, P., Vasar, E., Silm, H., and Kõks, S. (2014). Whole Transcriptome Analysis (RNA Sequencing) of Peripheral Blood Mononuclear Cells of Vitiligo Patients. *Dermatopathology (Basel)* 1, 11–23.
- Rienzo, M., Antonioli, M., Liu, Y., Mari, M., Orhon, I., Refolo, G., Germani, F., Corazzari, M., Romagnoli, A., Ciccocanti, F., et al. (2019). Autophagy induction in atrophic muscle cells requires ULK1 activation by TRIM32 through unanchored K63-linked polyubiquitin chains. *Science Advances* 5, eaau8857.
- Rietschel, M., Mattheisen, M., Degenhardt, F., GROUP Investigators, Genetic Risk and Outcome in Psychosis (GROUP Investigators), Kahn, R.S., Linszen, D.H., Os, J. van, Wiersma, D., Bruggeman, R., et al. (2011). Association between genetic variation in a region on chromosome 11 and schizophrenia in large samples from Europe. *Molecular Psychiatry* 17, 906.
- Rubinsztein, D.C., Gestwicki, J.E., Murphy, L.O., and Klionsky, D.J. (2007). Potential therapeutic applications of autophagy. *Nature Reviews Drug Discovery* 6, 304.
- Rubinsztein, D.C., Codogno, P., and Levine, B. (2012). Autophagy modulation as a potential therapeutic target for diverse diseases. *Nat Rev Drug Discov* 11, 709–730.
- Sabel, M.S., Liu, Y., and Lubman, D.M. (2011). Proteomics in Melanoma Biomarker Discovery: Great Potential, Many Obstacles. *International Journal of Proteomics* 2011, 181890.
- Saftig, P., Beertsen, W., and Eskelinen, E.-L. (2008). LAMP-2: A control step for phagosome and autophagosome maturation. *Autophagy* 4, 510–512.

- Salazar, M., Carracedo, A., Salanueva, I.J., Hernández-Tiedra, S., Lorente, M., Egia, A., Vázquez, P., Blázquez, C., Torres, S., García, S., et al. (2009). Cannabinoid action induces autophagy-mediated cell death through stimulation of ER stress in human glioma cells. *J Clin Invest* 119, 1359–1372.
- Sarkar, S., Floto, R.A., Berger, Z., Imarisio, S., Cordenier, A., Pasco, M., Cook, L.J., and Rubinsztein, D.C. (2005). Lithium induces autophagy by inhibiting inositol monophosphatase. *J Cell Biol* 170, 1101–1111.
- Saxton, R.A., and Sabatini, D.M. (2017). mTOR Signaling in Growth, Metabolism, and Disease. *Cell* 168, 960–976.
- Scherz-Shouval, R., Shvets, E., Fass, E., Shorer, H., Gil, L., and Elazar, Z. (2007). Reactive oxygen species are essential for autophagy and specifically regulate the activity of Atg4. *EMBO J* 26, 1749–1760.
- Schweppe, D.K., Huttlin, E.L., Harper, J.W., and Gygi, S.P. (2018). BioPlex Display: An Interactive Suite for Large-Scale AP–MS Protein–Protein Interaction Data. *J. Proteome Res.* 17, 722–726.
- Sepe, S., Nardacci, R., Fanelli, F., Rosso, P., Bernardi, C., Cecconi, F., Mastroberardino, P.G., Piacentini, M., and Moreno, S. (2014). Expression of Ambra1 in mouse brain during physiological and Alzheimer type aging. *Neurobiology of Aging* 35, 96–108.
- Serrano, M., Lin, A.W., McCurrach, M.E., Beach, D., and Lowe, S.W. (1997). Oncogenic ras Provokes Premature Cell Senescence Associated with Accumulation of p53 and p16INK4a. *Cell* 88, 593–602.
- Sherr, C.J. (1996). Cancer Cell Cycles. *Science* 274, 1672.
- Shim, H., Dolde, C., Lewis, B.C., Wu, C.S., Dang, G., Jungmann, R.A., Dalla-Favera, R., and Dang, C.V. (1997). c-Myc transactivation of LDH-A: implications for tumor metabolism and growth. *Proc Natl Acad Sci U S A* 94, 6658–6663.
- Simiczyjew, A., Pietraszek-Gremplewicz, K., Dratkiewicz, E., Podgórska, M., Matkowski, R., Ziętek, M., and Nowak, D. (2019). Combination of Selected MET and EGFR Inhibitors Decreases Melanoma Cells' Invasive Abilities. *Front. Pharmacol.* 10.
- Simon, R., Radmacher, M.D., and Dobbin, K. (2002). Design of studies using DNA microarrays. *Genetic Epidemiology* 23, 21–36.
- Simonetti, O., Lucarini, G., Rubini, C., Lazzarini, R., Primio, R.D., and Offidani, A. (2015). Clinical and Prognostic Significance of Survivin, AKT and VEGF in Primary Mucosal Oral Melanoma. *Anticancer Res* 35, 2113–2120.
- Singh, P., Jenkins, L.M., Horst, B., Alers, V., Pradhan, S., Kaur, P., Srivastava, T., Hempel, N., Győrffy, B., Broude, E.V., et al. (2018). Inhibin Is a Novel Paracrine Factor for Tumor Angiogenesis and Metastasis. *Cancer Res* 78, 2978–2989.
- Sinha, P., Kohl, S., Fischer, J., Hütter, G., Kern, M., Köttgen, E., Dietel, M., Lage, H., Schnölzer, M., and Schadendorf, D. (2000). Identification of novel proteins associated with the development of chemoresistance in malignant melanoma using two-dimensional electrophoresis. *ELECTROPHORESIS* 21, 3048–3057.

- Skobo, T., Benato, F., Grumati, P., Meneghetti, G., Cianfanelli, V., Castagnaro, S., Chrisam, M., Di Bartolomeo, S., Bonaldo, P., Cecconi, F., et al. (2014). Zebrafish *ambra1a* and *ambra1b* Knockdown Impairs Skeletal Muscle Development. *PLOS ONE* 9, e99210.
- Soto, J.L., Cabrera, C.M., Serrano, S., and López-Nevot, M.Á. (2005). Mutation analysis of genes that control the G1/S cell cycle in melanoma: TP53, CDKN1A, CDKN2A, and CDKN2B. *BMC Cancer* 5, 36.
- Souroullas, G.P., and Sharpless, N.E. (2015). mTOR signaling in melanoma: oncogene-induced pseudo-senescence? *Cancer Cell* 27, 3–5.
- Strappazzon, F., Vietri-Rudan, M., Campello, S., Nazio, F., Florenzano, F., Fimia, G.M., Piacentini, M., Levine, B., and Cecconi, F. (2011). Mitochondrial BCL-2 inhibits AMBRA1-induced autophagy. *The EMBO Journal* 30, 1195–1208.
- Strappazzon, F., Nazio, F., Corrado, M., Cianfanelli, V., Romagnoli, A., Fimia, G.M., Campello, S., Nardacci, R., Piacentini, M., Campanella, M., et al. (2015). AMBRA1 is able to induce mitophagy via LC3 binding, regardless of PARKIN and p62/SQSTM1. *Cell Death Differ* 22, 419–432.
- Su, M., Mei, Y., and Sinha, S. (2013). Role of the Crosstalk between Autophagy and Apoptosis in Cancer. *J Oncol* 2013, 102735–102735.
- Sun, W.-L. (2016). Ambra1 in autophagy and apoptosis: Implications for cell survival and chemotherapy resistance (Review). *Oncology Letters* 12, 367–374.
- Sun, W., Wang, L., Luo, J., Zhu, H., and Cai, Z. (2018). Ambra1 modulates the sensitivity of breast cancer cells to epirubicin by regulating autophagy via ATG12. *Cancer Sci* 109, 3129–3138.
- Sviderskaya, E.V., Hill, S.P., Balachandar, D., Barsh, G.S., and Bennett, D.C. (2001). Agouti signaling protein and other factors modulating differentiation and proliferation of immortal melanoblasts. *Developmental Dynamics* 221, 373–379.
- Tan, H., Moad, A., and Tan, M. (2014). The mTOR Signalling Pathway in Cancer and the Potential mTOR Inhibitory Activities of Natural Phytochemicals. *Asian Pacific Journal of Cancer Prevention : APJCP* 15, 6463–6475.
- Tian, T., Li, X., and Zhang, J. (2019). mTOR Signaling in Cancer and mTOR Inhibitors in Solid Tumor Targeting Therapy. *Int J Mol Sci* 20, 755.
- Tomic, T., Botton, T., Cerezo, M., Robert, G., Luciano, F., Puissant, A., Gounon, P., Allegra, M., Bertolotto, C., Bereder, J.-M., et al. (2011). Metformin inhibits melanoma development through autophagy and apoptosis mechanisms. *Cell Death Dis* 2, e199–e199.
- van Tonder, A., Joubert, A.M., and Cromarty, A.D. (2015). Limitations of the 3-(4,5-dimethylthiazol-2-yl)-2,5-diphenyl-2H-tetrazolium bromide (MTT) assay when compared to three commonly used cell enumeration assays. *BMC Res Notes* 8, 47–47.
- Tsao, H., Chin, L., Garraway, L.A., and Fisher, D.E. (2012). Melanoma: from mutations to medicine. *Genes Dev* 26, 1131–1155.
- Uttamsingh, S., Bao, X., Nguyen, K.T., Bhanot, M., Gong, J., Chan, J.L.-K., Liu, F., Chu, T.T., and Wang, L.-H. (2007). Synergistic effect between EGF and

- TGF- $\beta$ 1 in inducing oncogenic properties of intestinal epithelial cells. *Oncogene* 27, 2626.
- Uversky, V.N., and Dunker, A.K. (2010). Understanding protein non-folding. *Biochim Biophys Acta* 1804, 1231–1264.
- van der Vaart, A., Griffith, J., and Reggiori, F. (2010). Exit from the Golgi is required for the expansion of the autophagosomal phagophore in yeast *Saccharomyces cerevisiae*. *Mol Biol Cell* 21, 2270–2284.
- Van Humbeeck, C., Cornelissen, T., Hofkens, H., Mandemakers, W., Gevaert, K., De Strooper, B., and Vandenberghe, W. (2011). Parkin interacts with Ambra1 to induce mitophagy. *J Neurosci* 31, 10249–10261.
- Vázquez, P., Arroba, A.I., Cecconi, F., de la Rosa, E.J., Boya, P., and De Pablo, F. (2012). Atg5 and Ambra1 differentially modulate neurogenesis in neural stem cells. *Autophagy* 8, 187–199.
- Vincent, K.M., and Postovit, L.-M. (2017). A pan-cancer analysis of secreted Frizzled-related proteins: re-examining their proposed tumour suppressive function. *Sci Rep* 7.
- Wandinger-Ness, A., and Zerial, M. (2014). Rab proteins and the compartmentalization of the endosomal system. *Cold Spring Harb Perspect Biol* 6, a022616–a022616.
- Wang, J., Ding, N., Li, Y., Cheng, H., Wang, D., Yang, Q., Deng, Y., Yang, Y., Li, Y., Ruan, X., et al. (2015). Insulin-like growth factor binding protein 5 (IGFBP5) functions as a tumor suppressor in human melanoma cells. *Oncotarget* 6, 20636–20649.
- Wang, J., Davis, S., Zhu, M., Miller, E.A., and Ferro-Novick, S. (2017). Autophagosome formation: Where the secretory and autophagy pathways meet. *Autophagy* 13, 973–974.
- Wang, L., Chen, H., Wang, C., Hu, Z., and Yan, S. (2018). Negative regulator of E2F transcription factors links cell cycle checkpoint and DNA damage repair. *Proc Natl Acad Sci USA* 115, E3837.
- Wang, Y., Li, L., Hou, C., Lai, Y., Long, J., Liu, J., Zhong, Q., and Diao, J. (2016). SNARE-mediated membrane fusion in autophagy. *Semin Cell Dev Biol* 60, 97–104.
- Weeraratna, A.T., Jiang, Y., Hostetter, G., Rosenblatt, K., Duray, P., Bittner, M., and Trent, J.M. (2002). Wnt5a signaling directly affects cell motility and invasion of metastatic melanoma. *Cancer Cell* 1, 279–288.
- Weinberg, R.A. (1995). The retinoblastoma protein and cell cycle control. *Cell* 81, 323–330.
- van der Weyden, L., and Adams, D.J. (2007). The Ras-association domain family (RASSF) members and their role in human tumorigenesis. *Biochim Biophys Acta* 1776, 58–85.
- White, E. (2015). The role for autophagy in cancer. *J Clin Invest* 125, 42–46.
- WHO Cancer. <https://www.who.int/news-room/fact-sheets/detail/cancer>

Williams, A., Sarkar, S., Cuddon, P., Ttofi, E.K., Saiki, S., Siddiqi, F.H., Jahreiss, L., Fleming, A., Pask, D., Goldsmith, P., et al. (2008). Novel targets for Huntington's disease in an mTOR-independent autophagy pathway. *Nat Chem Biol* 4, 295–305.

Wu, X., Yu, J., Yan, J., Dai, J., Si, L., Chi, Z., Sheng, X., Cui, C., Ma, M., Tang, H., et al. (2018). PI3K/AKT/mTOR pathway inhibitors inhibit the growth of melanoma cells with mTOR H2189Y mutations in vitro. *Cancer Biol. Ther.* 19, 584–589.

Xia, P., Wang, S., Huang, G., Du, Y., Zhu, P., Li, M., and Fan, Z. (2014). RNF2 is recruited by WASH to ubiquitinate AMBRA1 leading to downregulation of autophagy. *Cell Res* 24, 943–958.

Xiong, Y., Zhang, H., and Beach, D. (1993). Subunit rearrangement of the cyclin-dependent kinases is associated with cellular transformation. *Genes & Development* 7, 1572–1583.

Xu, C., and Min, J. (2011). Structure and function of WD40 domain proteins. *Protein & Cell* 2, 202–214.

Yang, H., Rudge, D.G., Koos, J.D., Vaidialingam, B., Yang, H.J., and Pavletich, N.P. (2013). mTOR kinase structure, mechanism and regulation. *Nature* 497, 217–223.

Yang, Z.J., Chee, C.E., Huang, S., and Sinicrope, F.A. (2011). The Role of Autophagy in Cancer: Therapeutic Implications. *Mol Cancer Ther* 10, 1533–1541.

Yarden, Y., and Sliwkowski, M.X. (2001). Untangling the ErbB signalling network. *Nature Reviews Molecular Cell Biology* 2, 127–137.

Yazdankhah, M., Farioli-Vecchioli, S., Tonchev, A.B., Stoykova, A., and Cecconi, F. (2014). The autophagy regulators Ambra1 and Beclin 1 are required for adult neurogenesis in the brain subventricular zone. *Cell Death Dis* 5, e1403–e1403.

Yeoh, S., Pope, B., Mannherz, H.G., and Weeds, A. (2002). Determining the differences in actin binding by human ADF and cofilin1 Edited by J. Karn. *Journal of Molecular Biology* 315, 911–925.

Yorimitsu, T., and Klionsky, D.J. (2005). Autophagy: molecular machinery for self-eating. *Cell Death Differ* 12 Suppl 2, 1542–1552.

Zeng, C.-M., Chen, Z., and Fu, L. (2018). Frizzled Receptors as Potential Therapeutic Targets in Human Cancers. *Int J Mol Sci* 19, 1543.

Zhao, Y.G., and Zhang, H. (2019). Autophagosome maturation: An epic journey from the ER to lysosomes. *J Cell Biol* 218, 757–770.

Zhu, L., Chen, J., Zhang, J., Guo, C., Fan, W., Wang, Y.-M., and Yan, Z. (2017). Parathyroid Hormone (PTH) Induces Autophagy to Protect Osteocyte Cell Survival from Dexamethasone Damage. *Med Sci Monit* 23, 4034–4040.

Stages and types | Melanoma skin cancer | Cancer Research UK.  
<https://www.cancerresearchuk.org/about-cancer/melanoma/stages-types>

The Cell that Caused Melanoma | Harvard Medical School.  
<https://hms.harvard.edu/news/cell-caused-melanoma>